SEDIMENT CONTROL AT RIVER ABSTRACTION WORKS IN SOUTH AFRICA – VOLUME 1 (2006)

CJ BRINK, GR BASSON & F DENYS

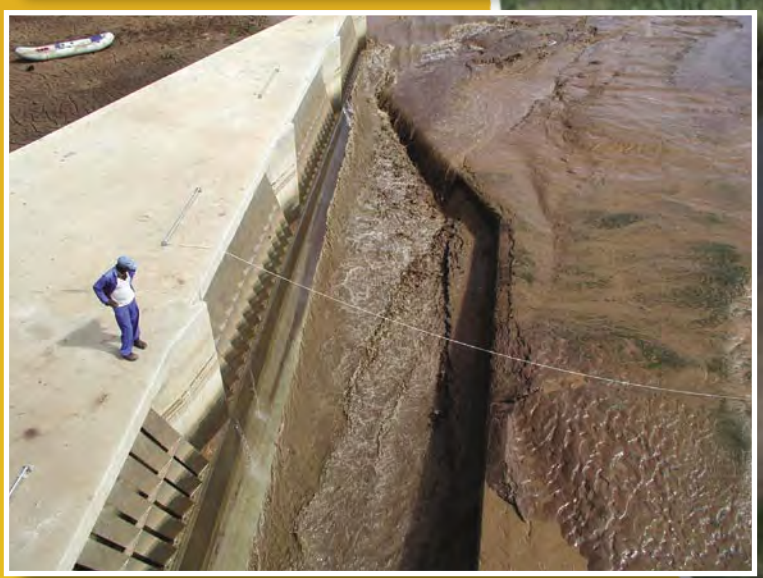

TT 259/06

Water Research Commission

Sediment Control at River Abstraction Works in South Africa

Report to the

Water Research Commission

by

CJ Brink, GR Basson and F Denys

WRC Report No. TT 259/06

NINHAM SHAND
CONSULTING SERVICES

In association with

UNIVERSITEIT·STELLENBOSCH·UNIVERSITY
jou kennisvennoot • your knowledge partner

Obtainable from:

Water Research Commission
Private Bag X03
Gezina
0031

The publication of this report emanates from a project entitled: *Development of guidelines for the design and operation of river diversion structures*

(WRC Project No. K5/1302)

ISBN No 1-77005-410-3
SET No 1-77005-409-X
Printed in South Africa

EXECUTIVE SUMMARY

The South African climate oscillates between drought and flood. This leads to extremes in river flow and sediment transport. While storms last for minutes to days, the hydrological critical low flows can last for years during droughts. The strong variation in river flow associated with even higher variability in sediment loads make the design of river pumpstations and abstraction works highly complex in South Africa, especially if the water supply should have a low risk of failure.

Several handbooks have been written on the topic of control of sediment extraction at river diversions, such as Raudkivi (1993) and Bouvard (1992) and the question can be asked why is yet another study needed? It seems that even though international guidelines are available in the literature, many of the South African abstraction works are experiencing serious problems with sedimentation control.

The typical sediment related problem experienced at South African extraction works are:

a) Changes in the river plan form and geomorphology (which could be natural), with a meandering low flow channel during droughts.
b) Sediment deposition at pump intakes where low velocities are part of the pump sump design. This could lead to damage at start-up of the pump and cause abrasion in the pipeline.
c) Build-up of cohesive sediment in the intake which could be difficult to flush out.
d) High sediment load abstraction which is mainly fine and difficult to settle out.
e) Sediment deposition in pools due to an upstream dam causing flood peak attenuation and narrowing of the river.
f) Increased sediment yields due to land degradation.
g) Sediment build-up caused by a dam downstream, which could be higher than the full supply level of the dam.
h) Wrongly positioned abstraction works on the inside of a river bend.
i) Sediment flushing facilities are in most cases not provided.
j) Incorrect pump selection which cannot deal with the coarse sediment.

k) Underestimation of the operational and maintenance costs that will be incurred with a relatively cheap initial design which does not cater for sediment control.

Most of international studies were however based on:

- Large rivers with high base flow due to snow melt
- Relatively coarse sediment
- Relatively steep rivers
- Relatively low sediment concentrations
- Expensive hydraulic structures and controls

This research project commenced in 2002 with a duration of 2 years. The aim of the study was to research and develop guidelines for the planning and design of river abstraction works in South Africa to limit the impacts of sedimentation. This report covers theoretical hydraulic aspects while more practical design aspects are addressed in an accompanying WRC report: "Considerations for the Design of River Abstraction Works in South Africa".

This study focused on the following aspects of sediment control at abstraction works:

a) Review of international state of the art technologies to control the sediment.
b) Investigation of optimum abstraction location on a river bend.
c) Review of typical South African abstraction case studies.
d) Assessment of flushing channels in abstraction works with field testing.
e) Development of guidelines for the planning and design of river abstraction works in South Africa.

Conclusions

The semi-arid conditions in South Africa create highly variable flows and sediment load variations are large, which makes the design of river diversion works very complex. Furthermore the sediment transported during floods is relatively fine and the sediment concentrations high. Methods developed in Western Europe for example to control sediment extraction are less effective in South Africa due to the different climatic conditions and sediment characteristics.

A review of various diversion control measures to limit sediment diversion was carried out. Most international diversion layouts focus on river bend flow to exclude coarse sediment. Several South African case studies were also reviewed and the conclusion was made that allowance has to be made in the design of control measures for fine sediment entering the diversion. This can be done by using canals that can be flushed through gates under gravity, by selecting pumps that can handle solids and/or by using a sand-silt trap or settler.

The hydraulics of secondary flow currents at a river bend that create a deep scour hole at the outside of the bend was investigated in this study to determine the best location of diversion works to limit sediment diversion. Laboratory tests of a 0.3 m wide and a 0.6 m wide rectangular channel, with various radii, flows and flow depths, and with movable bed conditions, were carried out. These test results were analysed and also used for mathematical model (3D and 2D) calibration, in order to apply the model for river simulations with more confidence. The movable bed conditions observed in the laboratory could be simulated accurately (Figure 1).

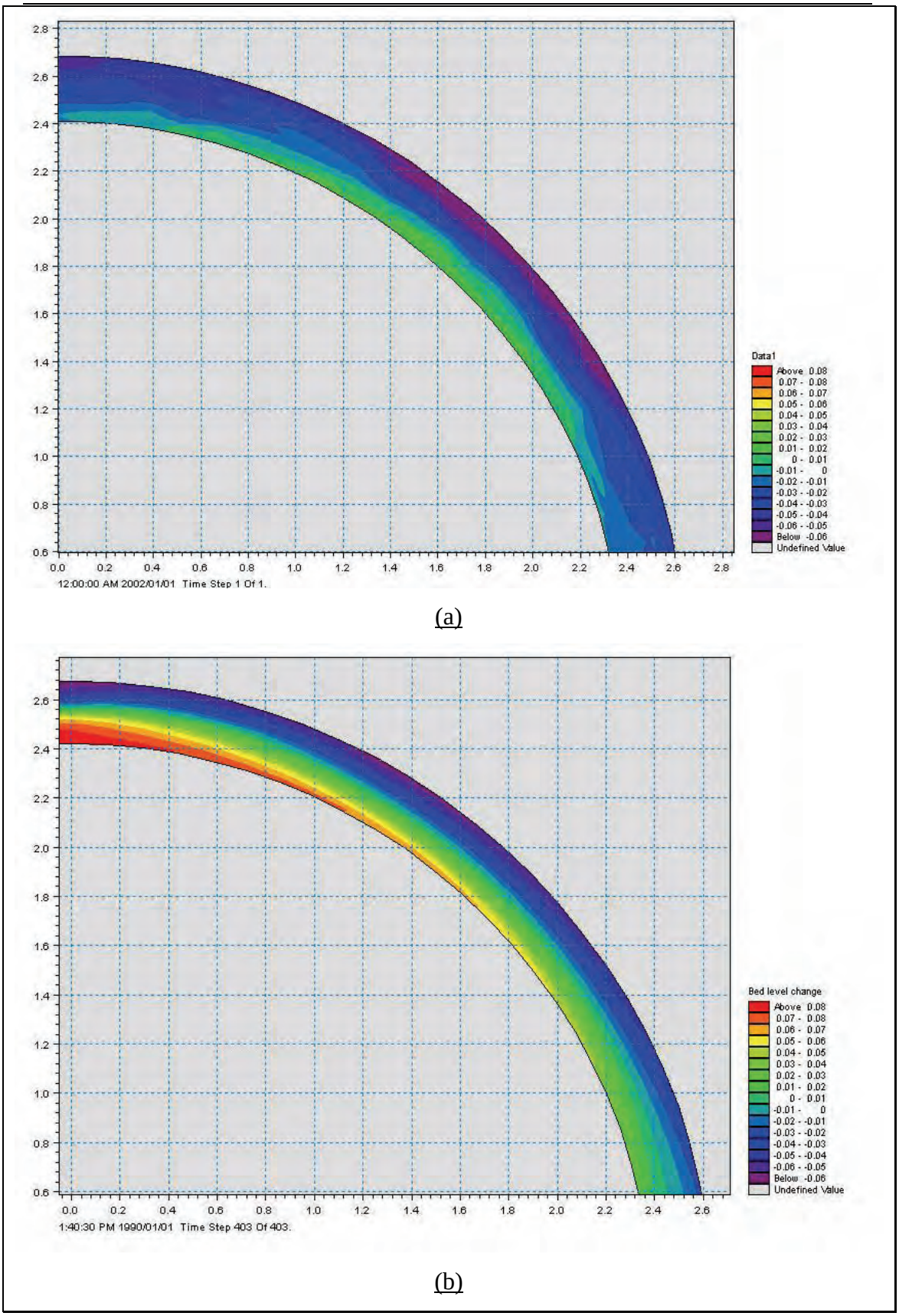

Figure 1 (a) Measured and (b) Simulated sediment bed level changes (m)

Simulations of river bends with 20 m and 70 m width trapezoidal channels, a bed slope of 1:333, a range of steady flows, sediment sizes and different sinuosity of the channel were carried out. The results show that with a wider channel the deepest scour hole forms further downstream. Higher sinuosity also created deeper scour holes (Figure 2).

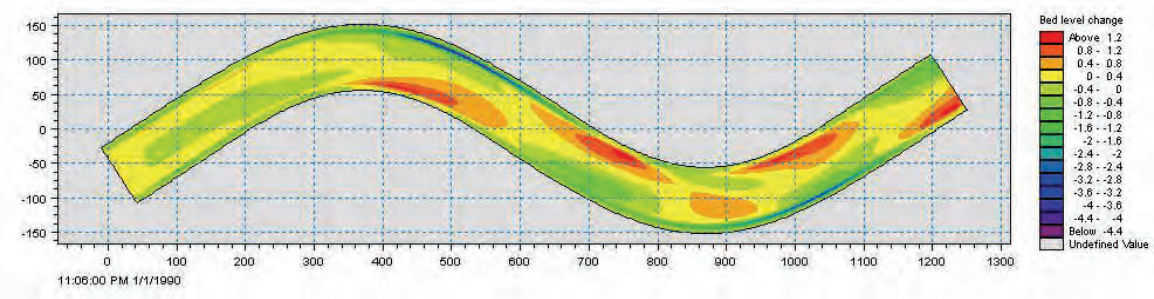

Figure 2 Simulated bed level changes: Sin1.1 Q=300m^3/s d=0.5mm

Laboratory tests were also carried out on the orientation of the diversion works to induce spiral flow along the intake wall. Most of the scour was found at the downstream end of the wall and it was the deepest in the channel with the most sudden contraction, with the diversion wall forming a 45 degree angle with the flow. 2D mathematical model simulations of the movable bed in the flume was carried out with the scour hole position predicted accurately. Further simulations were carried out with a diversion positioned in a river bend and deep scour was found against the structure, but the diversion structure actually inhibits the full development of spiral flow and scour around the river bend.

Mathematical models can be used to determine river bend fluvial processes for the optimum location of diversion works. It was found that empirical rules to determine the deepest scour hole position on a bend are not reliable.

Field tests were carried out at the Lebalelo pumpstation on the Olifants River during 2003. The gravel trap and pump canals were flushed and sediment concentrations recorded. The canals flushed quickly and effectively due to large gates and steep

gradients in the canals. The sediment concentrations of flushed water was extremely high, but the duration very short (Figure 3).

Figure 3 Flushing of gravel trap looking downstream

A review of sand abstraction systems indicated that they often have a low yield (lower than the design and reducing with time), flood damage is a high risk, as is clogging of screens and pipes by biological fouling. When backwash systems are installed and operated on a daily bases, the performance of these systems are better than those systems that are not backwashed. Backwashing removes fine sediment and associated biological fouling. Backwash systems using air and water seem to be effective (Figure 4).

Figure 4 Magudu suction pipe system under construction (Burger du Plessis)

Guidelines for the design of abstraction works to control sedimentation have been prepared as a separate document and give practical guidance on several aspects such as: weir and energy dissipation design, flushing of canals, pump sump design, inclusion of fishways, etc.

Recommendations

It is recommended that the design of a river abstraction works is based on the design guidelines developed in this study. The following are some of the key aspects to consider:

- Assess river stability from aerial photos
- Consider low flow conditions and flood flows and the variability in sediment loads. The environmental flow requirement must be released downstream during low flow periods and the diversion must operate during floods.
- Locate the abstraction on the outside curve of a river bend to limit coarse sediment diversion and to create a deep pool at the intake during floods.

- Use a mathematical model or physical hydraulic model to simulate the sediment dynamics to select the best position and orientation of the diversion at important diversion works
- Fine sediment will enter the diversion, therefore allow for flushing under gravity back to the river. Even the pump canals can be flushed.
- A gravel trap should be provided upstream of the pump/diversion canals.
- Robust pumps, preferably submersible, should be selected to handle the coarse sediments.

The following aspect could be researched in future:

- The ecological impact of sediment flushing of the abstraction works, with field measurements

ACKNOWLEDGEMENTS

The study team wishes to thank the South African Water Research Commission for sponsoring this research project.

Several Water Boards such as Amatola Water played an instrumental role in providing case study information and especially the fieldwork would not have been possible without their contribution.

Finally the Steering Committee members (listed below in no particular order) need to be commended for their role in steering this project from its start in 2002 to its successful completion in 2005:

Mr R Dube	SA Water Research Commission (WRC)
Prof N Armitage	University of Cape Town
Mr NJ van Deventer	Dept. of Water Affairs and Forestry
Mr JK Hauman	PD Naidoo and Associates
Prof CS James	University of Witwatersrand

CAPACITY BUILDING

The following students worked on the project:

• CJ Brink	MScEng	University of Stellenbosch (Lab, analysis & computational modelling)
• Ms O Mngambi	BTech	Pentech (Lab tests)
• B Barr	BEng	University of Stellenbosch (Lab tests)
• SC van der Walt	MScEng	University of Stellenbosch (Lab tests)
• Ms JS Beck	PhD	University of Stellenbosch (Diversion efficiency)
• F Denys	MScEng	University of Stellenbosch (Mathematical modelling)
• N Ma	MScEng	University of Stellenbosch (Laboratory tests)

Ms Makhosazana Princess Mseleku has a BTech National Diploma in Civil Engineering, and is employed by Ninham Shand (Field work, survey and data analysis).

The proposed guidelines developed in this study for sediment control have already been implemented at several newly planned pumpstations and river abstraction works in South Africa.

TABLE OF CONTENTS

NOTE: THE FOLLOWING APPENDICES ARE ENCLOSED ON CD IN THIS DOCUMENT

LIST OF FIGURES

LIST OF TABLES

List of Symbols

Δh	= change in water level
ξ	= coefficient
ϕ	= flow deviation angle
σ_g	= standard deviation of the bed material
θ	= diversion angle
θ_{sec}	= angle for fully developed secondary flow
θ_{bend}	= central bend angle
$\theta_{v,max}$	= the angle where the maximum velocity is located
$\overline{u}$	= radial velocity (xy plane)
b	= bed width of the diversion
w	= channel width
C	= Chezy coefficient
D	= flow depth
d	= water depth
fr	= froude number
g	= acceleration due to gravity
G_0	= incoming sediment load from river
G_b	= sediment concentration in the branch channel
G_d	= diverted sediment load
G_m	= sediment concentration in the main channel
h	= flow depth
H	= water level above V-notch
K	= constant
K	= diversion angle [rad]
L	= distance to optimum diversion location
L_{tot}	= length of the diversion bend
$L_{v,max}$	= location of the maximum velocity
$\overline{Q}$	= long-term average river flow
Q_c	= the critical discharge for the beginning of sediment movement

Q	= river flow
$Q_{\%}$	= frequency of the project's water demand
Q_0	= incoming discharge from river
Q_d	= diverted discharge
r	= distance from the centre of the bend
r_c / w	= radius of curvature to width ratio
r	= radius of curvature
r_c	= average radius of curvature
r_o	= outer radius
r_i	= inner radius
R	= mean radius of curvature
R	= radius of curvature of the local streamline
$R1$	= inner radius
$R2$	= outer radius
R_c	= average radius of curvature
S	= slope of the river
S_{xy}	= strength of the spiral
T	= total length affected by secondary flow
V	= average velocity
V_o	= Q/A (mean velocity)
w	= channel width
w/d	= width-to-depth ratio
y	= depth of water in channel
y_o	= depth of flow [m]

1 INTRODUCTION

The South African climate oscillates between drought and flood. This leads to extremes in river flow and sediment transport. While storms last for minutes to days, the hydrological critical low flows can last for years during droughts. The strong variation in river flow associated with even higher variability in sediment loads make the design of river pumpstations and diversions highly complex in South Africa, especially if the water supply should have a low risk of failure.

River abstraction structures serve to divert water from river streams as well as to limit the sediment load that enters the diversion system. One of the key features of a diversion structure is the location. By ensuring that the structure is properly located i.e. on a stable bank in a stable river reach, the reliability of the delivered water can be enhanced. The effect of the diversion structure on the morphology of the river can also be limited by ensuring that sediment transport is maintained through the structure. This can be achieved by limiting the sediment that enters the diversion structure and by removing the coarse sediments from the diverted water and returning them to the river.

River bends prove to be ideal for abstraction works and a diversion structure should be on the outside of the bend to take advantage of secondary (spiral or curvilinear) flow which creates a deep pool on the outside which is very important during droughts. Secondary (spiral) flow has the tendency to direct the heavy sediment laden bottom layers away from the diversion structure and to allow the top layers, with lower sediment concentration, to be directed towards the diversion structure. If the diversion structure can take advantage of the spiral flow, less sediment will be diverted. This is important in minimising sedimentation in the diversion structure. Hydraulic theory can be used to establish the optimum location of abstraction works at a river bend.

One of the first descriptions of curvilinear flow was provided in the 19th century by *Thompson (1876)*. Thompson stated that the bend flow phenomenon will only occur if there is a horizontal pressure greater on the outside of a curved path than on the inside. The result is that the water surface is super-elevated at the outer (concave) bank. Along any vertical

section the pressure gradient acting towards the centre of the curvature has to be the same, since the cross slope of the water surface at the top determines it. Thus, the centrifugal acceleration has to be the same down any vertical section. This implies that the velocity is smaller near the bottom and the bottom filaments have to move in curves of smaller radii than the top ones thus giving rise to secondary (spiral) flow. The secondary (spiral) flow is directed towards the centre of curvature of the channel and will tend to move the bed sediment away from the outer (concave) bank towards the centre. For continuity there must exist an opposite cross flow at the surface that tend to push the filaments at the top to the outer (concave) bank. Figure 1-1 shows the developed secondary (spiral) flow. This fact being the explanation for diverting water from the outside of river bends. The remains of such diversion schemes date back to ancient Mediterranean civilizations.

Figure 1-1 Secondary (Spiral) flow (Thompson, 1876)

Various classifications of intakes were found in the literature. Intakes are generally classified according to hydraulic or sediment principles. *Scheuerlein (1984)* classified intake types according to their hydraulic and sediment control principles. According to hydraulic principles the intakes were classified as lateral intakes, frontal intakes, bottom intakes and suction intakes. For sediment control a different classification seemed appropriate and the classification with respect to the mechanism of sediment transport is the control of bed load; sediment rejection; sediment extraction; sediment ejection; and the control of suspended load.

Raudkivi (1993) classified the different types of intakes according to their hydraulic and sediment control aspects as follows: intakes on river bends, intakes with dividing walls, intakes with under sluices, intakes with excluder tunnels, intakes with baffles, guide vanes and deflectors. According to the above classification there is no clear subdivision apart from

the hydraulic and sediment aspects. A clearer subdivision would distinguish between separate intakes and intakes connected to dams, weirs or barrages.

Vanoni (1977) stated that water should be diverted according to the following three principles: direct only water into the diversion structure and return the sediment to the river, design the canal system hydraulically so that the water with its sediment will be transported out onto the land with a minimum of sediment deposited in the diversion structure, design the diversion structure to direct as little sediment as practically possible into the diversion channel and remove the deposited sediment by the most inexpensive available method. Of the above-mentioned diversion principles, the third principle is recommended.

Scheuerlein (1984) recommended that the principle of sediment rejection be applied to diversion structures. The principle of sediment rejection is based on allowing the upper, clearer layers of the flow to enter the intake while the lower sediment laden layers are prevented from entering the intake. Advantage can be taken of the river bend phenomenon where the developed secondary current provides favourable flow patterns at the intake. Thus intakes should be located on the outer (concave) bank of a bend to take advantage of this phenomenon. When the intake does not operate in combination with a diversion dam or weir the sediment rejection technique can be applied to divert up to 50% of the total river flow without experiencing bed load problems *(Scheuerlein, 1984)*.

In summary, the principle of sediment rejection, where as little sediment as possible is abstracted from the main channel, is recommended. This can be achieved with the aid of the secondary flow that develops in bends and creates spiral motion. The spiral motion moves the sediment laden bottom flow towards the inside of the bend, while the upper flow with less suspended sediment moves towards the outside of the bend where the diversion is located.

In South African rivers 60 to 80 % of the transported sediment does not consist of sand ("bed load"), but of silt and clay. These fine fractions (often called wash-load) have a near uniform vertical and lateral distribution and therefore it is difficult to apply the sediment rejection principle, using secondary currents at a bend or elevated intakes. Diverted fine sediments could lead to sedimentation in the structure, but is often not harmful to pumps and pipelines.

Pumps and pipelines are however generally sensitive to sand transport and bed load sediment rejection is an important consideration in South African river abstraction designs.

Several handbooks have been written on the topic of control of sediment extraction at river diversions, such as by Raudkivi (1993) and Bouvard (1992) and the question could rightfully be asked why is yet another study needed? The fact is that even though international guidelines are available in the literature, many of the South African abstraction works and pumpstations are experiencing serious problems with sedimentation control.

The typical sediment related problem experienced at South African abstraction works are:

a) Changes in the river plan form and geomorphology (which could be natural), with a shallow shifting low flow channel during droughts.
b) Sediment deposition at pump intakes where low velocities are part of the pump sump design. This could lead to damage at start-up of the pump and cause abrasion in the pipeline.
c) Build-up of cohesive sediment in the intake which could be difficult to flush out.
d) High sediment load diversion which is mainly fine and difficult to settle out.
e) Sediment deposition in pools due to a dam upstream causing flood peak attenuation and narrowing of the river.
f) Increased sediment yields due to land degradation.
g) Sediment build-up caused by a downstream dam, which could be higher than the full supply level of the dam.
h) Wrongly positioned abstraction works on the inside of the bend.
i) Flushing facilities are in most cases not provided
j) Incorrect pump selection which cannot deal with the coarse sediment.
k) Underestimation of the operational and maintenance costs that will be incurred with a relatively cheap initial design which does not cater for sediment control.
l) Weirs have to be constructed to dam the water to provide positive suction heads at pumps during droughts, but this leads to slower flow velocities and a rapid rate of sediment deposition upstream of the weir. In Europe barrages are constructed across the river with large gates that allow floods to pass freely with little damming and therefore sedimentation

is limited. These structures are expensive, requires high maintenance and are not always practical considering the large variation in flow depths from droughts to major floods which could be from 0 m to 15 m depth.

Most of international literature are based on:

- Large rivers with high base flows due to snow melt
- Relatively coarse sediment
- Relatively steep rivers
- Relatively small sediment concentrations
- Expensive hydraulic structures and controls

This research project commenced in 2002 and had a duration of 2 years. The project was carried out by Ninham Shand (Pty) Ltd who has had extensive design experience of abstraction Works in Southern Africa, in association with the Department of Civil Engineering, University of Stellenbosch.

2 OBJECTIVES

The aims of this study were to research and develop guidelines for the planning, design and operation of river abstraction works in South Africa to limit the impacts of sedimentation. The location and orientation of the abstraction works are two aspects investigated in this study.

3 SCOPE OF WORK

This study focused on the following aspects of sediment control at river abstraction works:

a) Review of international state-of-the-art technologies to control the sediment.
b) Investigation of optimum diversion location and orientation on a river bend.
c) Review of typical South African diversion case studies.
d) Assessment of flushing channels as part of abstraction works, with field testing.
e) Development of guidelines for the planning and design of river abstraction works in South Africa.

4 METHODOLOGY

A literature survey was first carried out to evaluate available diversion sediment exclusion technologies, internationally and in South Africa (Chapter 5).

River bend hydraulics and sediment dynamics were studied in the Hydraulic Laboratory of the University of Stellenbosch. This data were used for calibration and verification of three and two dimensional mathematical models. The mathematical models were also used to simulate typical river flow and sediment transport patterns. Assessment of the deepest scour hole on the outside of the bend considered discharge, river width, sediment diameter, diversion orientation and channel sinuosity.

Guidelines for the planning and design of river abstraction works to control the relatively fine sediment found in South African alluvial rivers were developed based on the experience from co-workers, evaluation of case studies and research carried out in this study.

These guidelines are published in a separate WRC report: "Considerations for the design of River Abstraction Works in South Africa".

5 ABSTRACTION WORKS

5.1 INTRODUCTION

Abstraction work intakes can be grouped into the following categories:

a) Intakes without a weir or barrage

- artificial bend intakes
- bank intakes
- bottom intakes
- submerged intakes

b) Intakes with a weir or barrage

- bend intakes
- bank intakes
- frontal intakes

- tiered intakes
- bottom grate-type intakes

c) Sand abstraction systems

It is possible to improve the efficiency (to divert less sediment) of intakes (categories (a) and (b)) by using groynes, guide banks and walls, guide vanes, dividing walls, sand guiding sills and sediment intercepting galleries.

Design details, benefits and disadvantages, and some case studies of the above intake types are discussed in this Chapter.

5.2 INTAKES WITHOUT A WEIR OR BARRAGE

5.2.1 ARTIFICIAL BEND INTAKES

Flow curvature can also be created with man-made bends if there is not sufficient curvature in the natural river reach (Raudkivi, 1993). The intake is usually built on the concave bank at the end of a bend to divert water by meeting the main current and to release sediment towards the side under the effect of secondary flow in the bend (Tan, 1996).

Figure 5-1 shows a typical artificial bend-type intake on the Karshi River in the Xinjiang Region of China. The intake structure consists of an upper flood escape, a diversion bend as well as a water intake and sediment sluice at the end of the diversion bend. The effect of using the secondary flow and the principle of diverting water by meeting the main current and releasing sediment towards the side are applied twice. The first time is in the combination of the inlet of the bend and the flood escape where most of the incoming sediment are flushed downstream through the flood escape. The second time is in the combination of the intake and the sediment sluice where most of the sediment that enters the bend is released through the sediment sluice.

The bend-type intake is commonly suitable for mountainous rivers carrying bed load of gravel, cobbles and coarse sand and have been widely constructed in Middle-Asia, West China and other countries. Table 5-1 list the characteristics of some bend-type intakes in the

Xinjiang Region of China. They cover the following range: irrigation areas of 13 000 to 167 000 ha, designed diversion discharges of 25 to 140 m^3/s, composition of bed material with d_{50} of 20 to 60 mm and river slopes of $\frac{1}{60}$ to $\frac{1}{167}$. (Tan, 1996) is another example of a diversion dam with an artificial bend (Raudkivi, 1993).

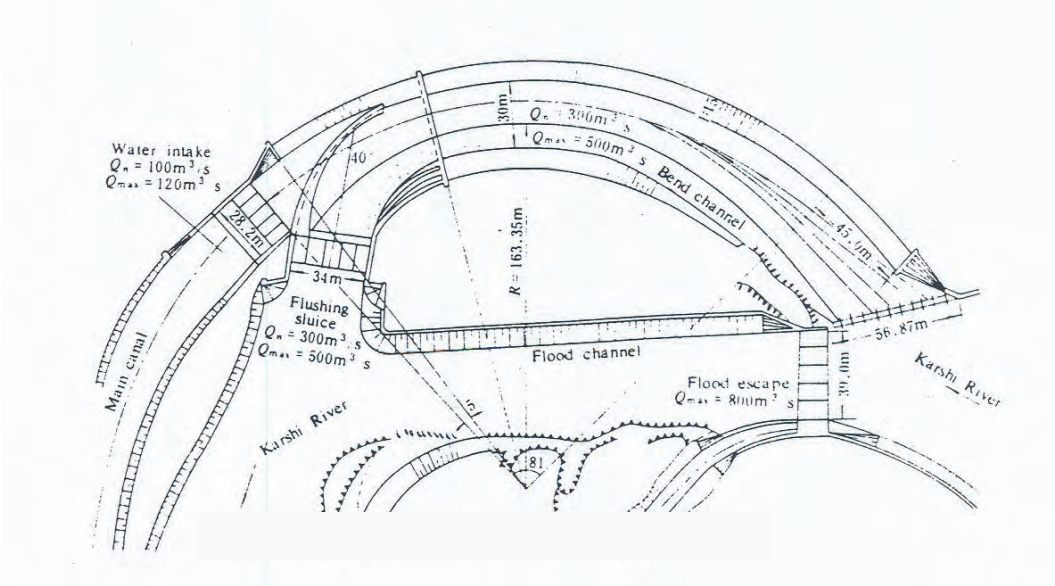

Figure 5-1 Bend-type intake on the Karshi River in Chian (Tan, 1996)

Table 5-1 Artificial bend-type intake in the Xinjiang Region, China (Tan, 1996)

Name of intake	River				Canal		Artificial bend			
	Average runoff (10^6m^3/yr)	Slope	Size of bed material (mm) d_{50}	d_{max}	Design discharge (m^3/s)	Irrigation area (10^3ha)	Length L (m)	Ave. radius R (m)	L/R	Slope
Qingnian	215	1/60		800	25	13.3	186	176.2	1.05	1/67
Santunhe	235	1/80	20	300	65	43.3	180	150	1.2	1/150
Bayingouhe	328	1/80	20	400	60	32.0	450	430	1.04	1/80
Awati	1990	1/167		150	40	28.0	154	161	0.96	1/167
Manasihe	1317	1/132	60	600	140	166.7	218	295.5	0.74	1/132
Jingouhe	321	1/100		300	52.5	35.3	148.5	190	0.78	1/100
Kashihe	4012	1/150		650	100	80.0	200	162.5	1.36	1/150

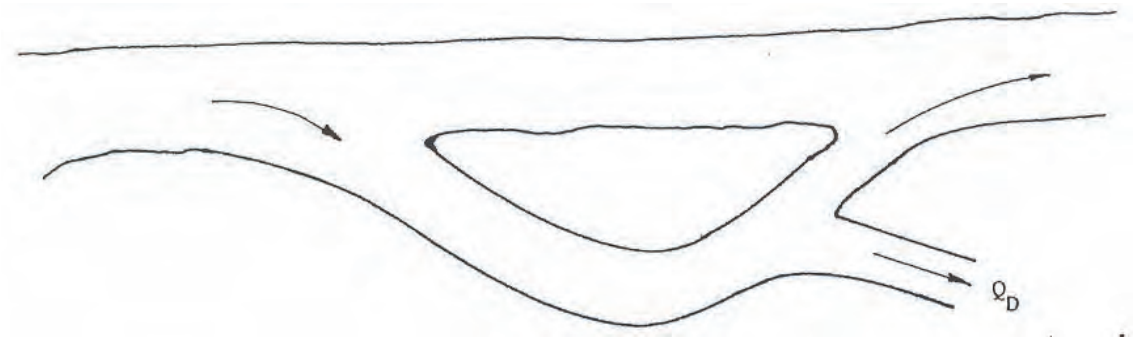

Figure 5-2 Diversion with a man made bend (Raudkivi, 1993)

5.2.2 BANK INTAKES

Bank intakes are located on a river or canal bank, side of reservoir or a coastal site. These structures are generally adopted for locations where only a small portion of the passing flow is abstracted and where the fluctuations in water level are not large. Figure 5-3 shows a typical river bank intake for a water supply pumping station, where the sediment transport in the river is not significant. The face of the intake is aligned with the bank and the intakes, at the bed level, have coarse screens, bulkhead gates and fish electrodes. Behind the coarse screens there are settling chambers to trap coarse material that might enter followed by band screens and finally the pump chambers (Avery, 1989).

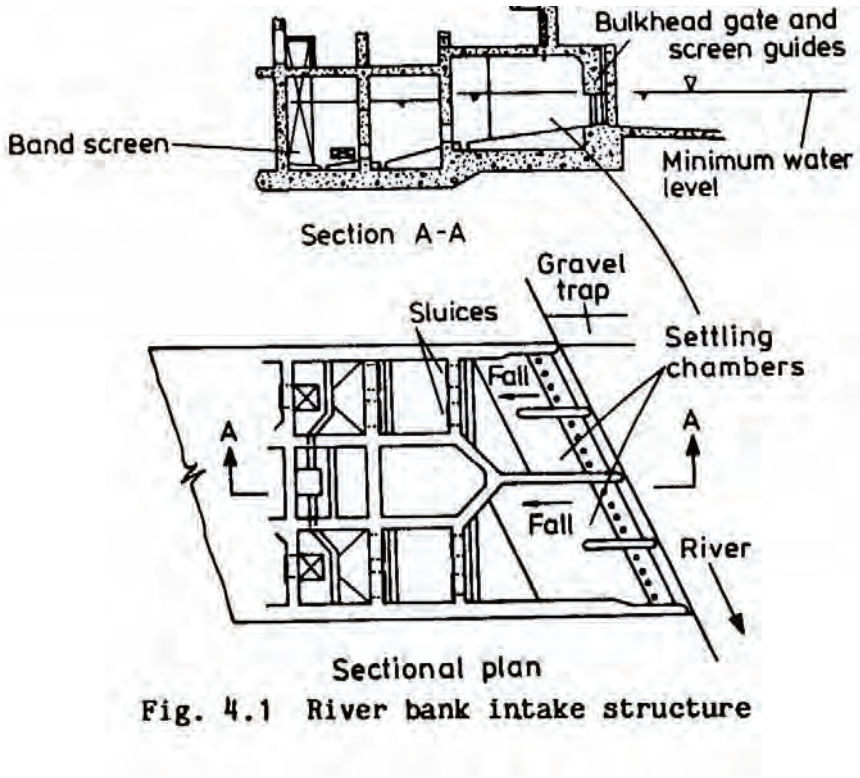

Fig. 4.1 River bank intake structure

Figure 5-3 River bank intake structure (Avery, 1989)

Muller (1955) found that in rivers transporting large sediment loads, only half of the river discharge can be diverted without letting solid materials enter at the same time. This is shown in Figure 5-4. Various types of lateral intakes are shown in Figure 5-5.

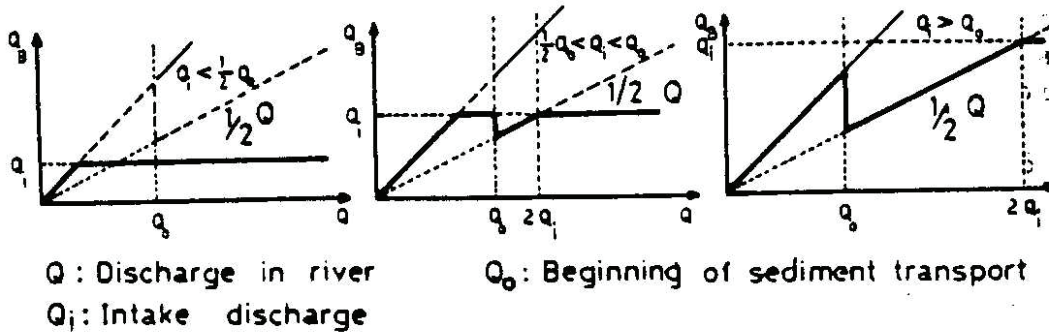

Figure 5-4 Water intake restricted by the percentage of sediment (Muller, 1955)

a) Water intake from curved stream

b) Water intake from an artificial bend

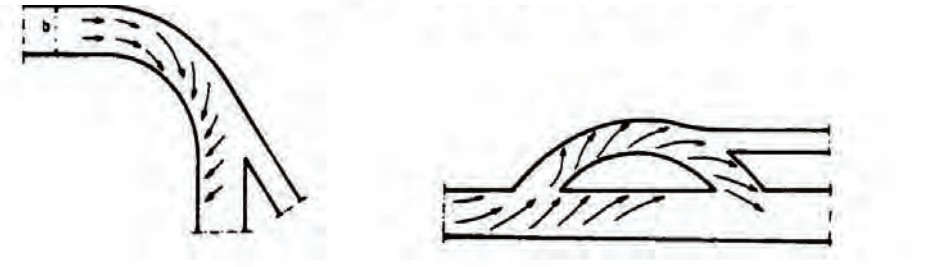

c) Water intake according to GRISHIN

d) Narrowing of stream cross section.

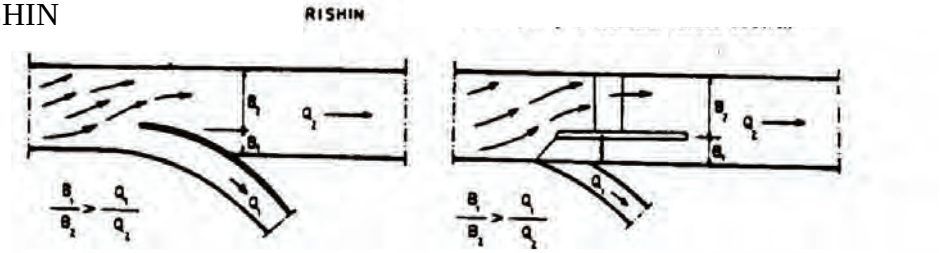

e) Spurs according to R MULLER

f) Creation of secondary flow by means of sluice gates

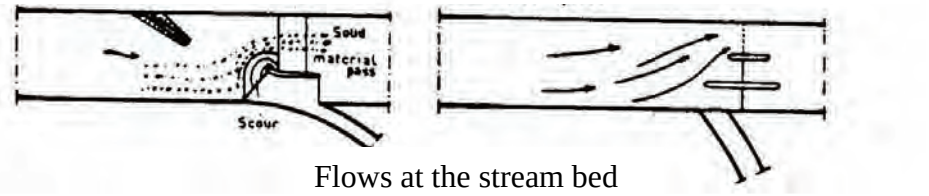

Flows at the stream bed

Figure 5-5 Various alternatives of lateral type water intakes (Muller, 1955)

5.2.3 BOTTOM INTAKES

Bottom intakes have been developed for steep glaciers and mountain torrents where site conditions may be extremely difficult for access and construction and where boulders and rock debris have to be passed with minimum obstruction. Figure 5-6 shows the arrangement for a Tyrolean type of bottom intake for a hydropower scheme in the french Alps. It comprises of a collecting chamber across the bed of the stream covered by a coarse screen. The total stream flow passes over the chamber and the screen admits fine debris with the water entering the chamber. Excess inflow is spilled at the downstream sill. The conduit from the collecting chamber is designed for debris that has entered to be carried with the flow

to a settling basin constructed a short distance downstream. Clean water is skimmed off for the hydropower scheme and arrangements made for periodic scouring of settled debris, for which a relatively high hydraulic head is required. Typical intercepted discharge is 3 m^3/s. Another example of a bottom type intake structure is shown in Figure 5-7.

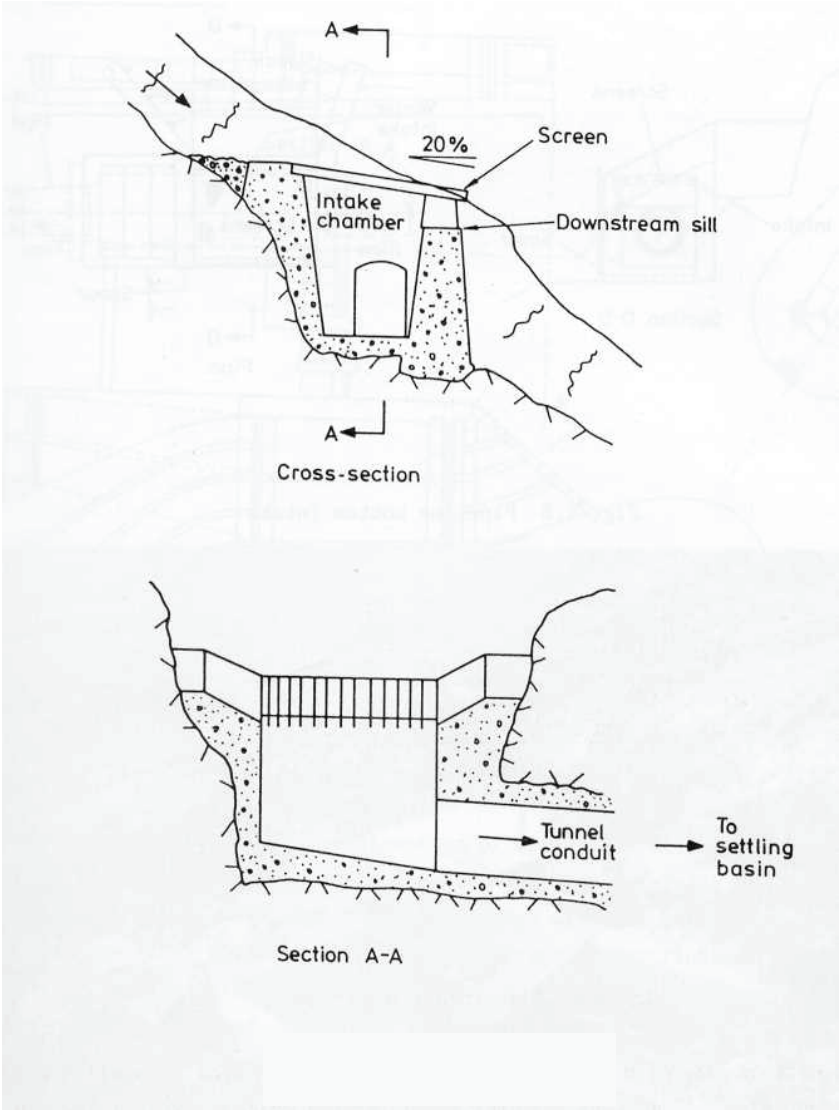

Figure 5-6 Tyrolean intake (Avery, 1989)

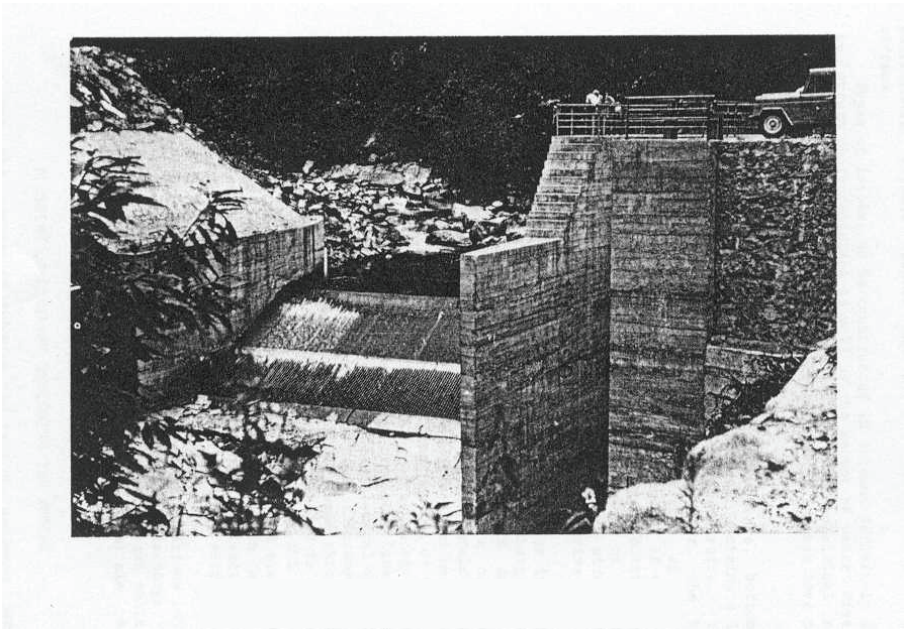

Figure 5-7 Bottom type intake at Kavraz, Turkey (Cecen, 1988)

Smaller versions of bottom intakes have been developed and are shown in Figure 5-8 and Figure 5-9. These were developed for diversions of side streams to hydropower reservoirs. Steeply sloping screens with round bars were found beneficial in minimising blockage and loss of water. Lightweight debris may be carried through the aqueduct to the reservoir and a hand-operated valve scours heavier material trapped in the screen chamber. The maximum design intake flow of the above mentioned examples are 150 ℓ/s and 750 ℓ/s respectively (Avery, 1989).

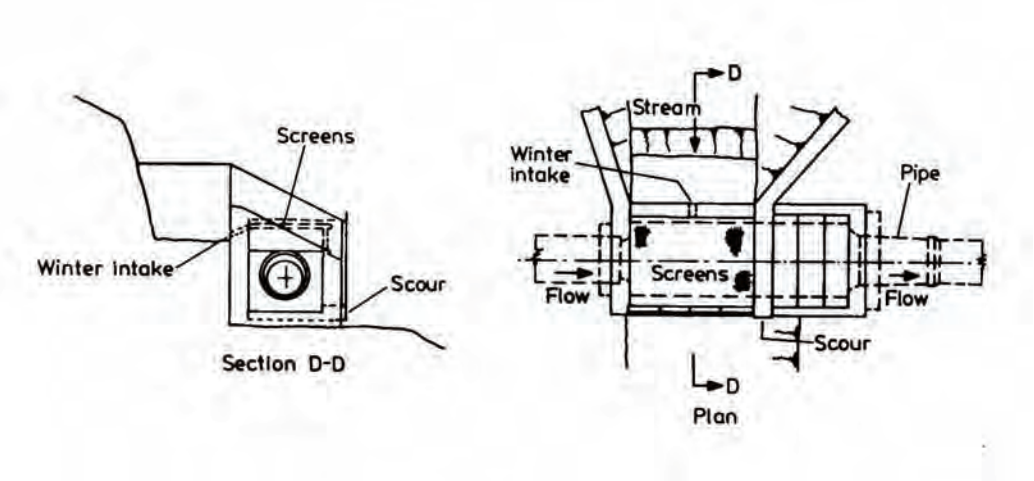

Figure 5-8 Pipeline bottom intake (Avery, 1989)

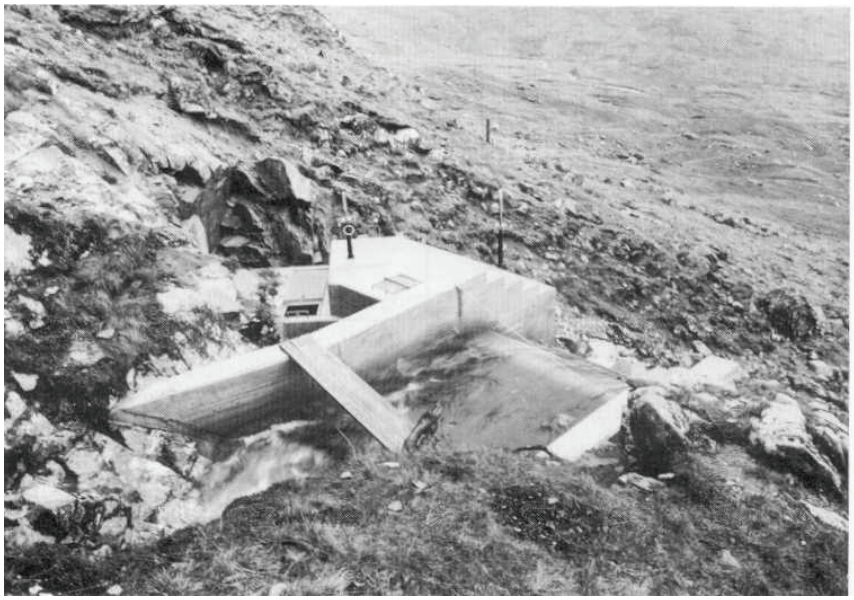

Figure 5-9 Bottom intake to tunnel (Avery, 1989)

The disadvantage of this system is that it is a closed system and if the river does not only convey coarse sediments, the fine sediment could deposit inside the diversion and block the flow completely.

5.2.4 SUBMERGED INTAKES

A submerged intake used in rivers or for the drainage of small reservoirs is shown in Figure 5-10. The intake comprises of a bell mouth and bend set in a block of concrete on the bed of a river or reservoir with a connecting draw-off pipe. The inlet is protected with a bar screen and is set high enough above the bed to allow sediments to pass on either side of it if used in a reservoir (Avery, 1989).

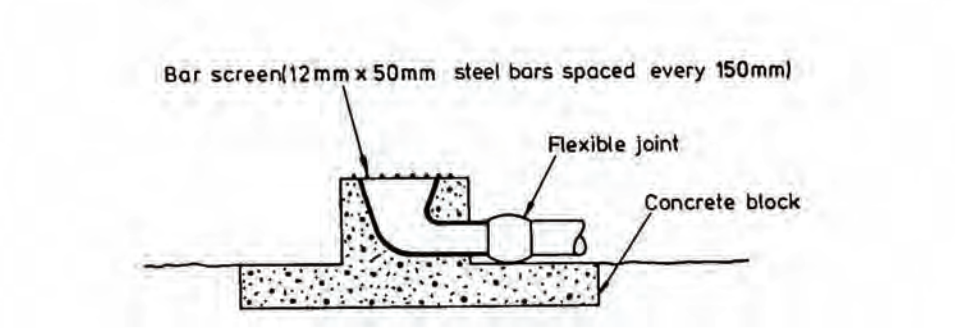

Figure 5-10 Submerged intake (Avery, 1989)

A more elaborate concept for larger flows with a vertical shaft is shown in Figure 5-11. A framed structure extends above the top of the water level allowing access for maintenance to the screens and shaft. The structure was planned as a cooling water intake in a shallow estuary to provide 36 m^3/s of cooling water. The screen sills must be set above the highest level to which the estuarial sediments might be expected to rise (Avery, 1989).

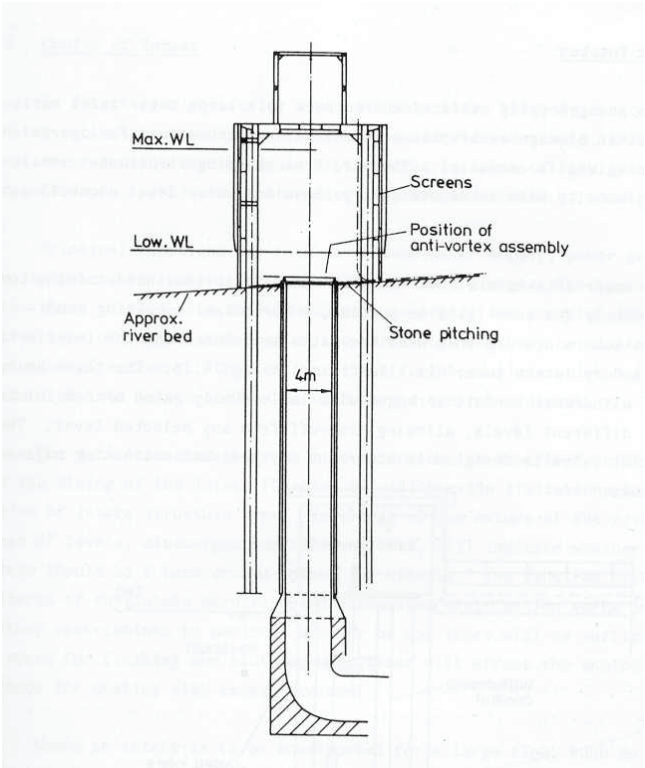

Figure 5-11 Submerged shaft intake (Avery, 1989)

5.3 INTAKES WITH A WEIR OR BARRAGE

5.3.1 BEND INTAKES

Many intakes with a barrage rely on the bend effect to minimise sediment diversion. In the case of intakes on the outer side of the bend, the curvature effect can be amplified by structural means by the so-called Fergana-type of intakes. The concept is illustrated in Figure 5-12 where the sill or barrage amplifies the spiral flow and creates both a strong surface current towards the diversion intake and a bottom current that carries the sediment towards the sill or sluices. The guide bank on the left hand side is at an angle of 45-50° (Raudkivi, 1993).

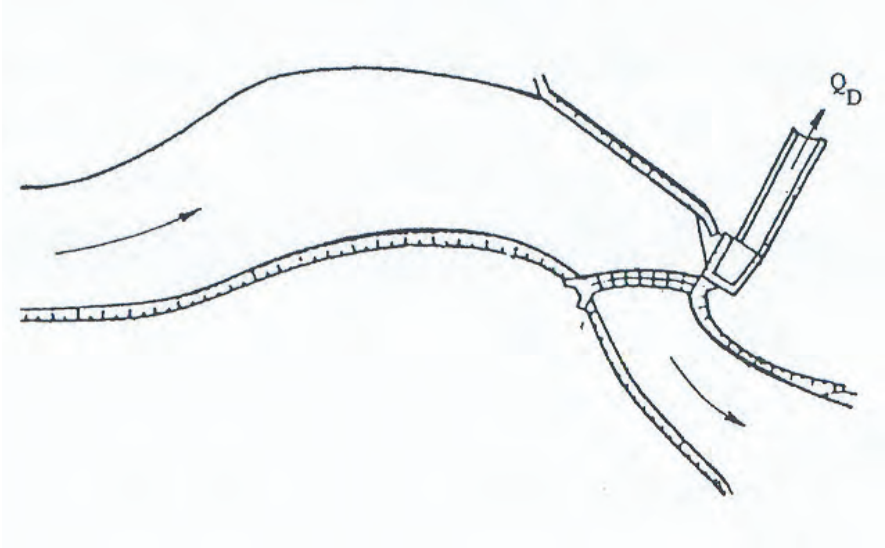

Figure 5-12 The concept of the Fergana-type diversion intake (Raudkivi, 1993)

Figure 5-13 shows the general plan arrangement of the Woodstock Diversion Dam on the South Fork, Solomon River, Pick-Sloan Missouri Basin Program, USBR. The inlet to the canal headworks consists of a 1.52 m wide channel protected by a 3.05 m high pier inside of the curve and away from the headgates. The velocity of flow in the channel between the two walls sweeps the bed load entering that channel by the canal headgate at an elevation below the intake sill and out through the sluice gate. The result is that only the relative clear upper part of the water prism is being diverted into the canal. The design of the diversion structure was based on an average riverflow of 2.18 m^3/s with a diverted flow of 1.19 m^3/s. The ratio

($C_r = C_s / C_h$) is defined as the ratio of sediment concentration passing through the sluiceway (C_s) to the concentration passing through the canal headworks (C_h). The diversion structure was designed for a C_r of 4.76. For low flow conditions when there is no flow over the weir, most of the sediment load is carried into the channel between the headgates. Then a velocity of 2.4 to 3.0 m/s in the channel needs to be maintained in the channel to ensure that most of the bed load is flushed through the sluice gate. (United States Bureau of Reclamation, 1959). Depending on the Froude number, oscillations could occur in the diverted canal due to the high flow velocities in the main channel, based on physical model studies for South African abstraction works.

The curved channel sediment excluder uses the established practise of relying on the favourable effects of the curvature of a channel to reduce the amount of sediment entering the headworks of the canal system.

Figure 5.13 shows the layout of the Osborne Canal diversion works where the flow from the curved channel into the canal is through a relatively short gate-controlled inlet and Figure 5-14 is a diversion structure where the flow from the curved channel into the canal is over a relatively long skimming weir. The main characteristics of some curved channel sediment excluders are given in Table 5-2 (Avery, 1989).

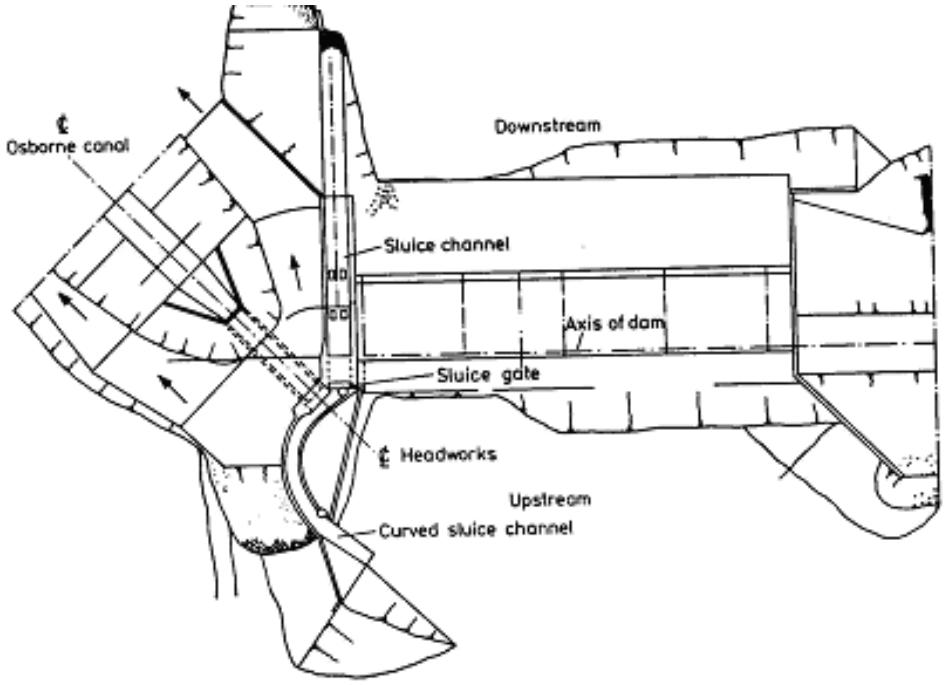

Figure 5.13 Separate curved sluice channel for sediment exclusion, Woodstock Diversion (USBR, 1959) (Avery, 1989)

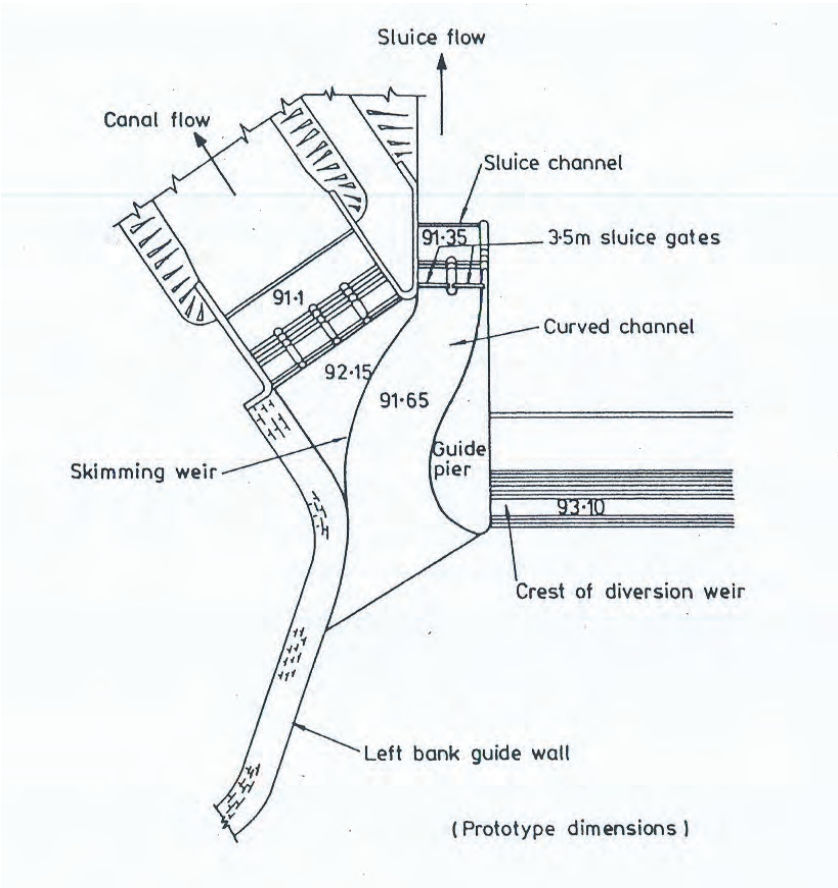

Figure 5-14 Separate curved sluice channel for sediment exclusion with a skimming weir (Avery, 1989)

Table 5-2 Leading characterics of some curved sediment excluders (Avery, 1989)

Headworks	Canal flow m^3/s	Sluice flow m^3/s	Sluice width m	Centreline radius m	Depth m	Average Angle to intake centreline
Courtland	11.3	5.66	6.0	-		
Superior	2.26	1.13	7.0	-		
Republic	3.39	1.69		-		
Bartley	1.70	1.06	3.6	11.0	1.73	60º
Woodston	1.19	0.99	1.5	7.6	2.59	90º

Attempts are sometimes made to produce a curvilinear flow ahead of an intake when the upstream bed is absolutely straight. The idea is to locate the intake on the outside of the curve

that is created. Figure 5-15 shows the layout of the Lavey Dam diversion structure with a design flow of 200 m^3/s.

Another example of a bend-type diversion structure is shown in Figure 5-1. The design discharge is 1530 m^3/s with a design flood of 12 000 m^3/s. The diversion structure embodies an upstream saw tooth over-hang on the intake weir and the combined effect with the horizontal roller formed just below the lip, the teeth generate a useful amount of local scour. This adds to the bend effect and further restricts the transport of material into the off take channel (Bouvard, 1992).

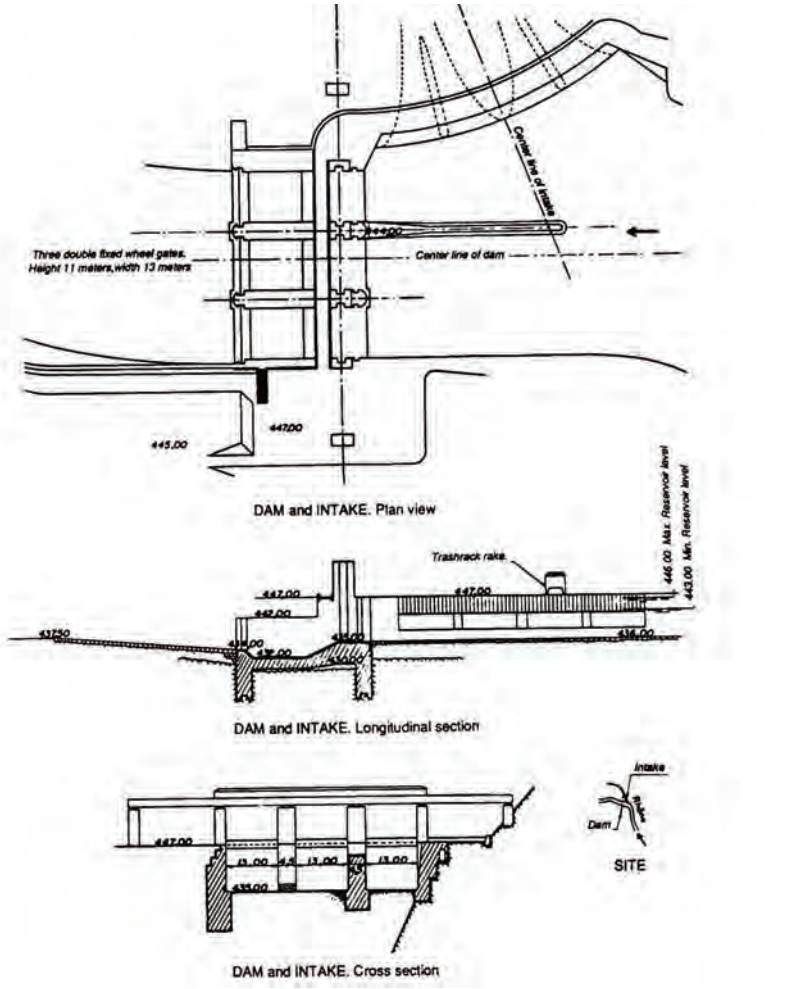

Figure 5-15 Lavey Dam and water intake on the Rhône River, Switzerland (Bouvard, 1992)

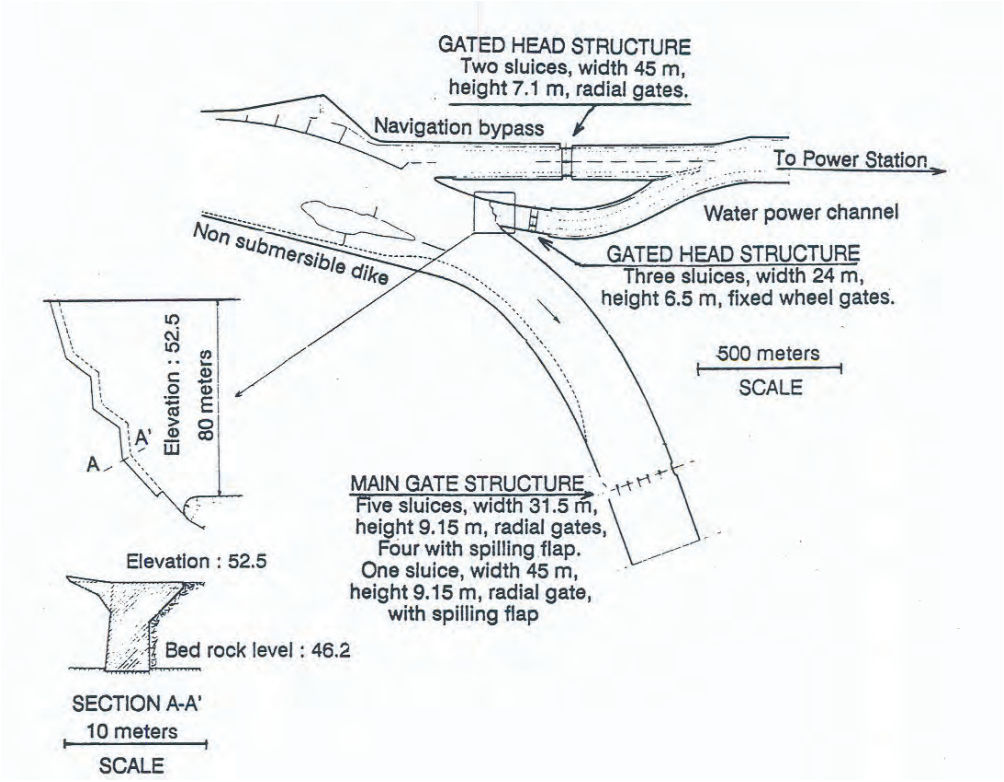

Figure 5-16 Donzere-Mondragon Dam on the Rhône River, France (Bouvard, 1992)

5.3.2 BANK INTAKES

A lateral intake is defined as releasing sediment in the direction of main flow and diverting water sideways. In order to improve the efficiency of lateral intakes the approaching flow may be regulated to be directed towards the intakes by river training works such as guide walls, spurs, vanes, etc or by enhancing the sediment carrying capacity of the flow in front of the intake by facilities such as a circulation sluicing flume and a sediment releasing gallery, etc. (Tan, 1996).

A layout of a side intake with a cross weir that supplies a free flowing pipeline is shown in Figure 5-17. The arrangements work well provided that solid and floating debris are not present in large quantities and if regularly screen cleaning can be undertaken. The average stream flow is 50 ℓ/s and the design intake flow is 250 ℓ/s (typically five times the average). There is about 10 m^3 of sediment storage available in the head pond that requires shovelling

to clear and in turn may require suitable access arrangements. The sediment sizes encountered are in the range of coarse sand to gravel plus a few cobbles (Avery, 1989).

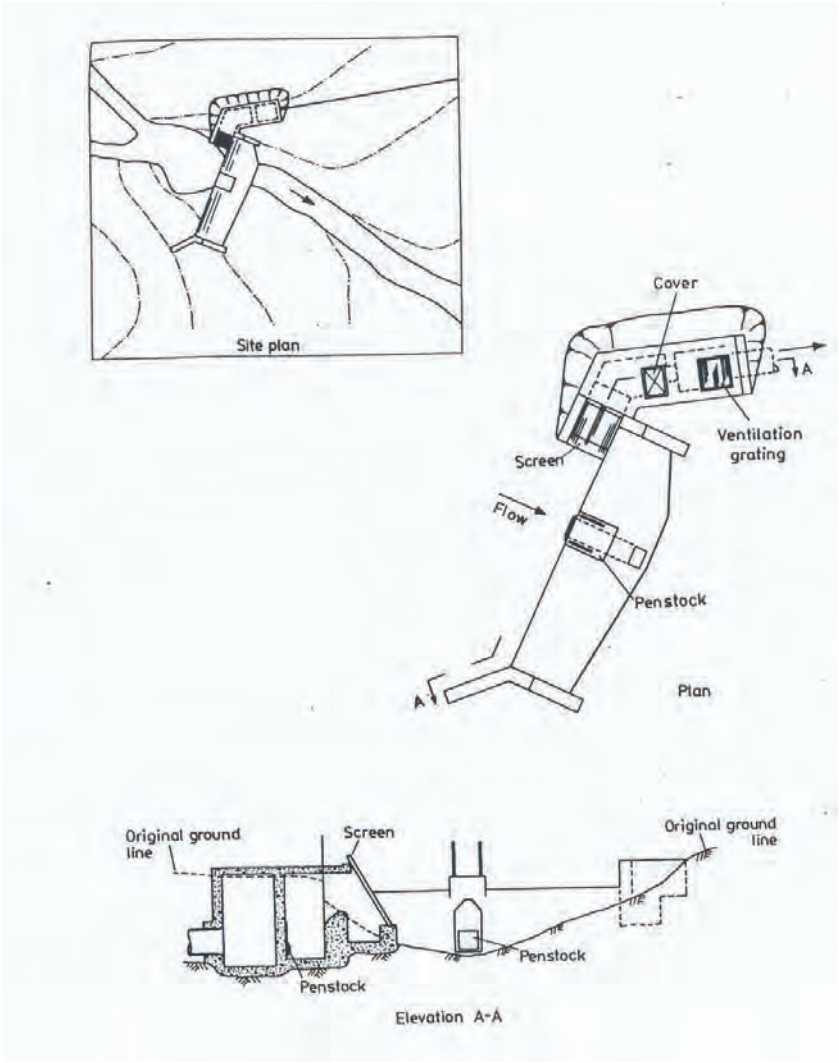

Figure 5-17 Side intake with a cross weir (Avery, 1989)

A modified version of the side intake with a cross weir is shown in Figure 5-18. The screens have been eliminated and a skimmer wall excludes floating debris. Typical flow rates are an average stream flow of 110 l/s with the intake designed at 1000 l/s with sediment sizes that are in the coarse sand and gravel range (Avery, 1989).

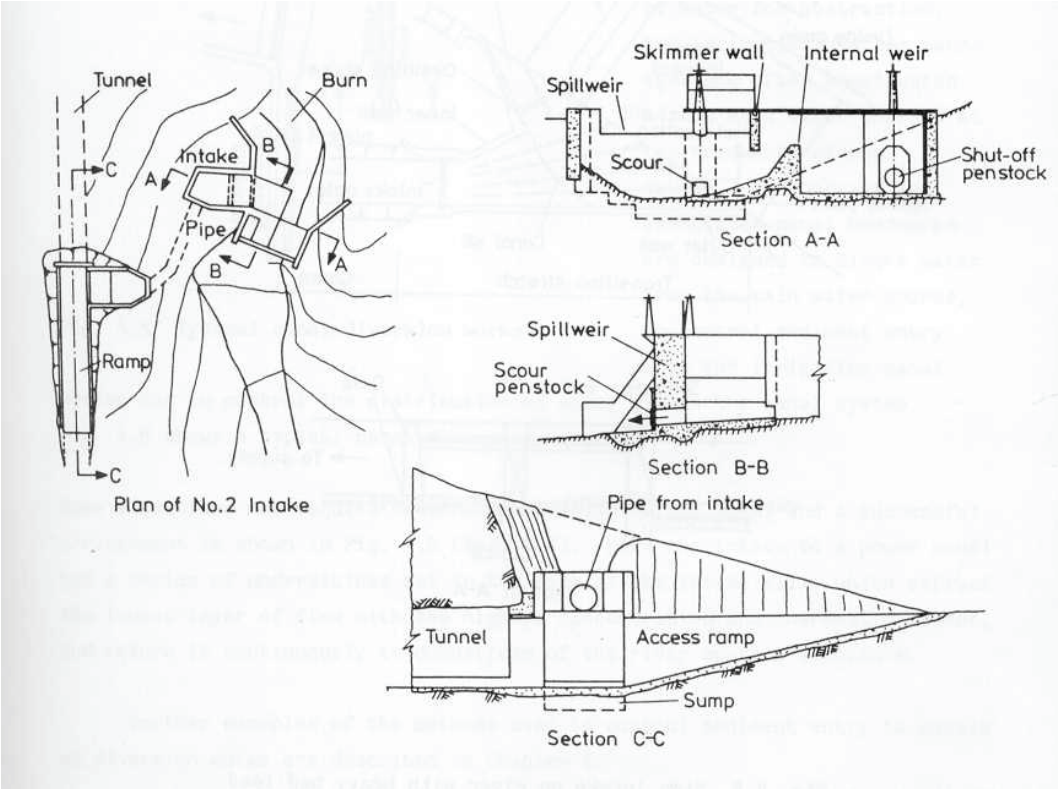

Figure 5-18 Screenless side intake with a cross weir (Avery, 1989)

Additional arrangements may be necessary to minimise sediment influx and to prevent blockage of the intake by shoaling in the river if the river carries a heavy sediment load in suspension or near the river bed. Figure 5-19 shows such an arrangement where the desilting canal is used for intermittent return of desilting flow to the river (Avery, 1989).

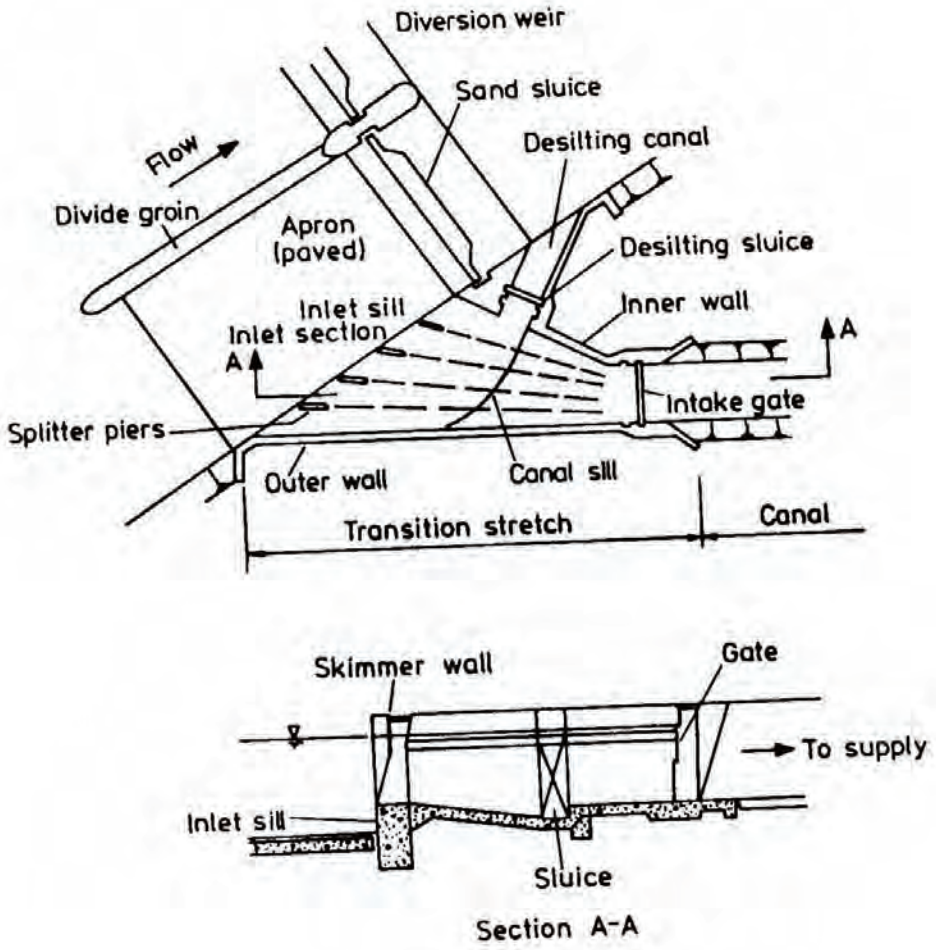

Figure 5-19 Side intake with a cross weir on a river with heavy bed load (Avery,1989)

For irrigation systems barrages are often constructed across main watercourses at the headworks of new canals as is shown in Figure 5-20. The barrage and associated canal headworks are designed to divert water from the main water course, to control sediment entry into the canal system and to control the distribution of water within the canal system (Avery, 1989).

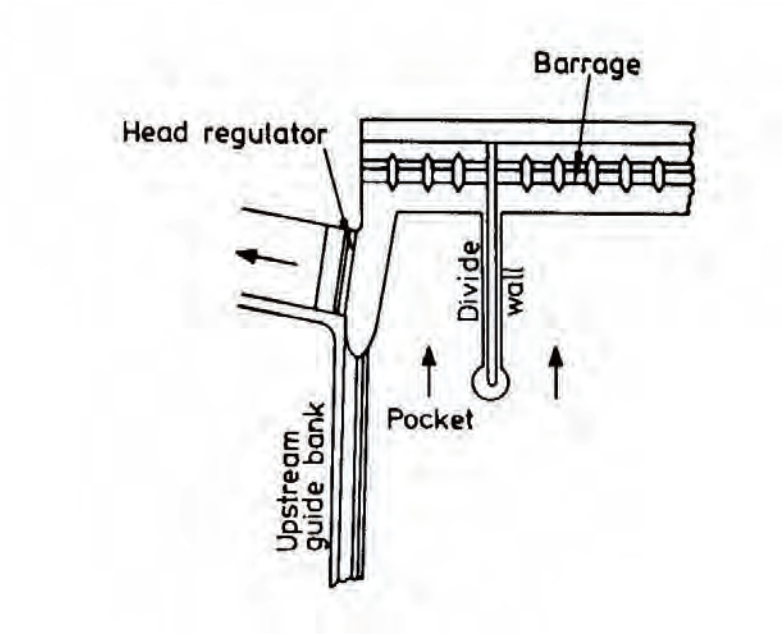

Figure 5-20 Low head river or canal abstraction works (Avery, 1989)

This diversion works are generally composed of flood sluice gates, desilting sluice gates, intakes and other structures. A typical example is shown in Figure 5-21. The intake is usually located in the vicinity of the desilting sluices and flood sluices to keep the main flow as close as possible to the intake. The axis of the intake may be parallel, oblique or perpendicular to the river flow, i.e. the angle of the axis of the intake with the approaching flow can vary from 0° to 90°. In general a smaller angle is favoured for decreasing the sediment entering the intake. The Diverted Sediment Ratio (DSR) of a frontal intake is generally smaller than that of a lateral intake (Tan, 1996).

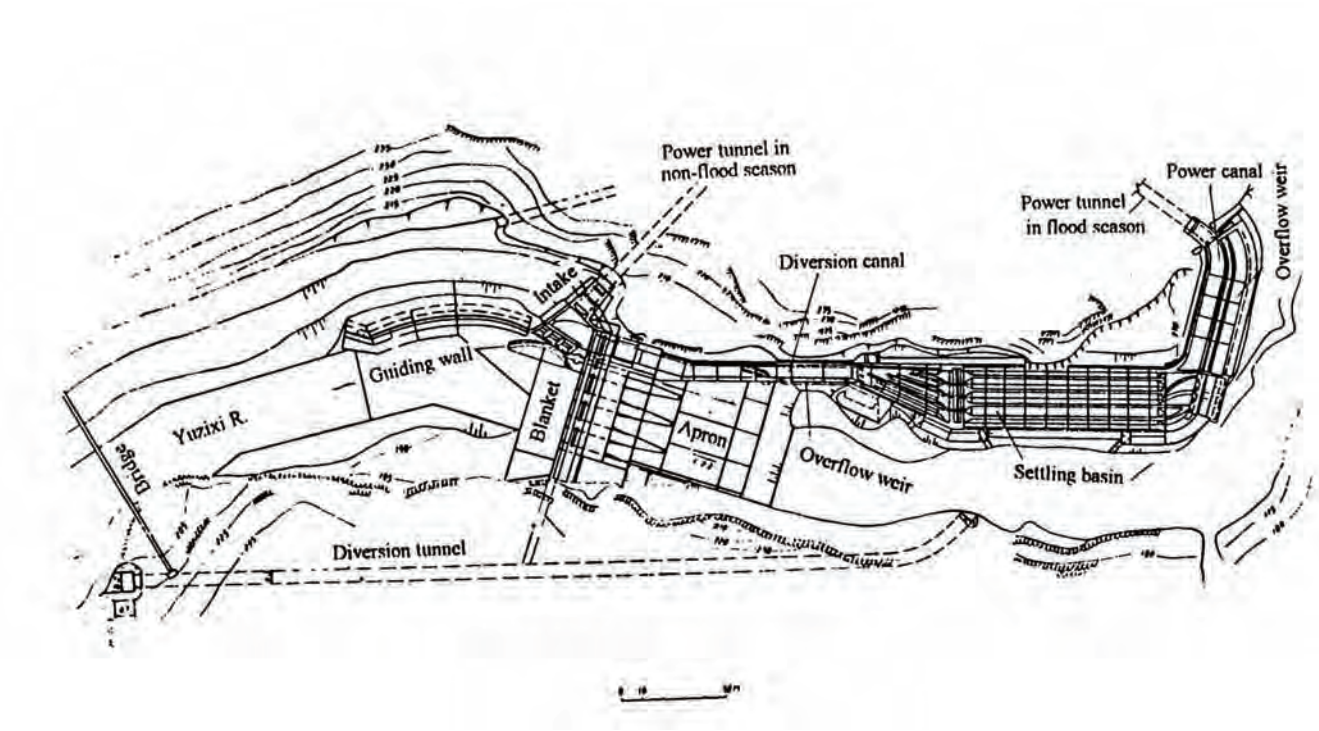

Figure 5-21 Headworks of the Yuzixiki-1 hydropower station (Tan, 1996)

Another form of a bank-type diversion structure is when overpour-channel gravel sluices are incorporated into the system. It is used for intermittent flushing and comprise of an overpour wall in the river. The crest of the wall is below the static water level in the reservoir. The wall continues back upstream until it meets the wall extending from the trashrack panels, thus delineating a closed basin. Material first deposits in the reservoir from where it can be flushed out periodically or continuously. Later, when sediment deposited in the reservoir reaches the crest of the overpour wall, it spills over into the basin from where it can be flushed by opening the sluice gate. The water pours over the crest in a separate nappe that quickly removes the deposited material by the force of its impact. Figure 5-22 shows the layout of the intake structure on the Breda and Figure 5-23 is a photo of the flushing process in progress (Bouvard, 1992). The upstream weir is submerged during normal operation.

Figure 5-24 is another example of a bank intake with a weir (Shen, 1971).

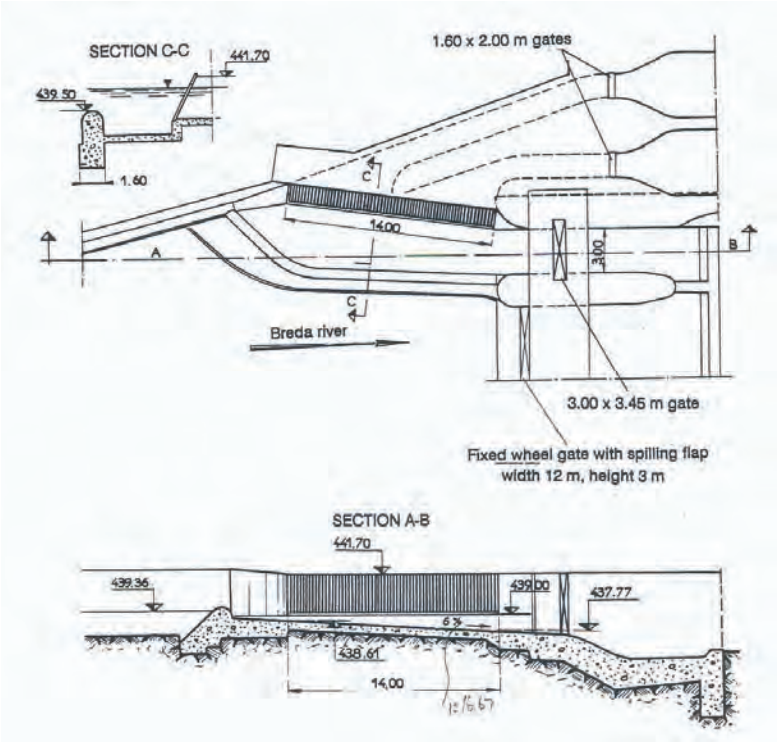

Figure 5-22 Overpour-channel gravel sluice at the water intake on the Breda (Bouvard, 1992)

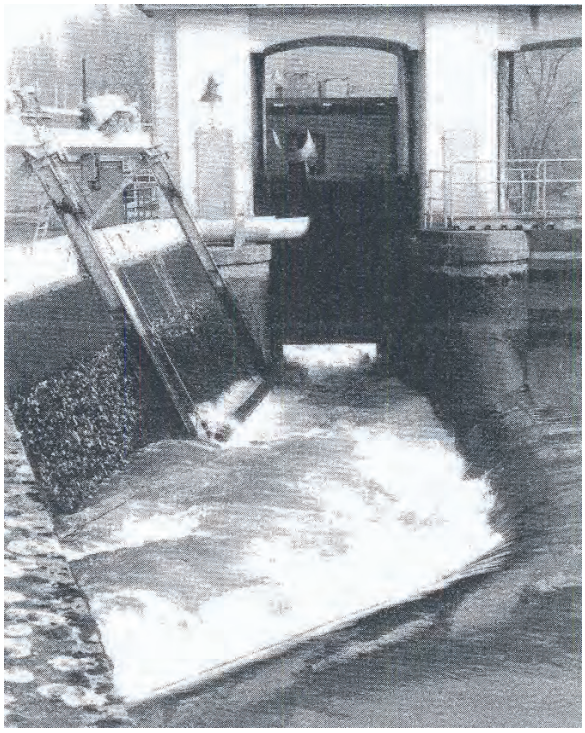

Figure 5-23 Water intake on the Breda with sediment flushing in progress through the gravel sluice (Bouvard, 1992)

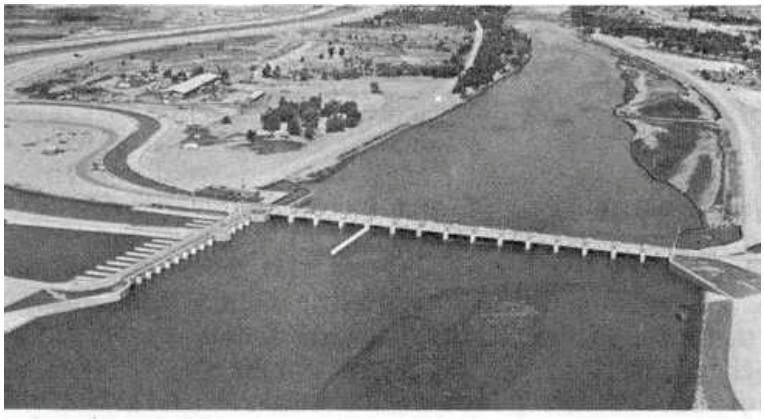

Figure 5-24 Arial view of a barrage and canal headworks in West Pakistan (Shen, 1971)

Rooseboom (2002) recommended a basic diversion/pumpstation layout containing the following components (Figure 5-25):

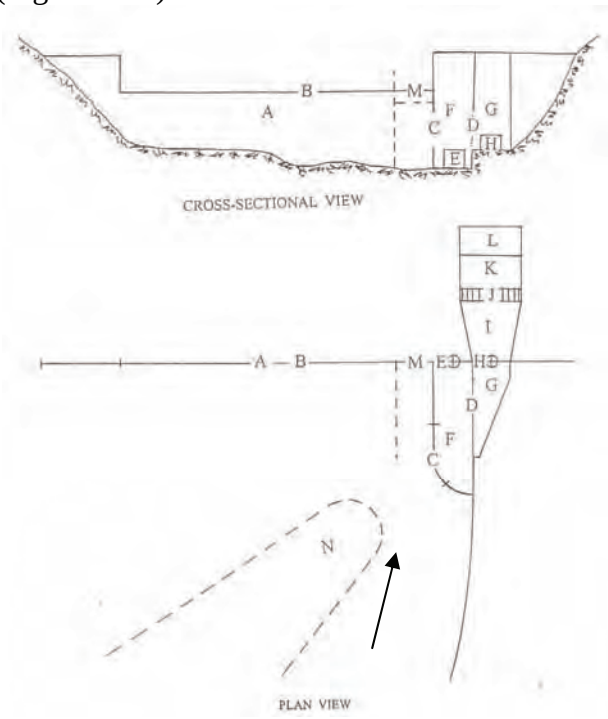

Figure 5-25 Proposed diversion layout (Rooseboom, 2002)

Figure 5-25 Legend:

Weir	A	Control gate(s)	H
Spillway	B	Transition channel(s)	I
Open intake	C	Vortex suppressor	J
Screen intake	D	Settling basin	K
Scour gates	E	Pumps	L
Scour chamber	F	Low notch weir	M
Collection channel	G	Groyne	N

The open intake (C) should keep floating debris out by placing the soffit of the intake below water level. Flow velocities through the opening must also be low enough to prevent objects from being sucked through. The bottom of the opening must be high enough to create sufficient gradient to flush out sediments from the scour basin and to allow for sediment deposition between flushings.

The screen (D) stops suspended debris. The screen openings are determined by the sediment diameter the pumps can deal with. The upper edge of the screen should be below the water surface to limit the entanglement of floating debris.

The scour gate (E) must be low enough to keep sediment levels down and must discharge freely.

The scour chamber traps sediment, but is also shaped to induce scour along its outside perimeter, similar to a bridge pier, to limit sediment build-up around the intake during floods. The outer wall of the scour chamber should be streamlined and its downstream section should run parallel with the flow direction (in plan) to pass floating debris over the spillway.

In the collection channel (G) the velocities should be relatively high and constant to limit sediment deposition. The channel floor is therefore raised and it widens downstream.

Control gates (H) should be kept as small as possible due to their high cost, but this leads to high downstream velocities which should be dissipated to have smooth uniform flow conditions at the pumps.

A settling basin (K) can be used to settle out sand.

The pump layout (L) can be either a wet well or drywell installation.

The low notch weir (M) serves two purposes in that it maintains the low flow channel near the intake and it passes floating debris. A guide wall upstream of the low notch will further help to pass the floating debris.

Groynes (N) can be used to concentrate the flow at the intake and to increase the curvature of the flow lines to create an outside of bend pattern at the intake.

5.3.3 FRONTAL INTAKES

A frontal intake is defined as diverting water in the direction of main flow and releasing sediment sidewise (Tan, 1996). Figure 5-26 shows a frontal intake designed for the abstraction of water from mountain streams. This design has been used successfully in major systems mainly in Turkey. The abstracted water is taken from the upper layers of the river while the lower layer is continually flushed past the intake. This is particularly applicable where the majority of sediment carried by the river is bed load and where a large proportion of the flow continues down the original water coarse (Avery, 1989).

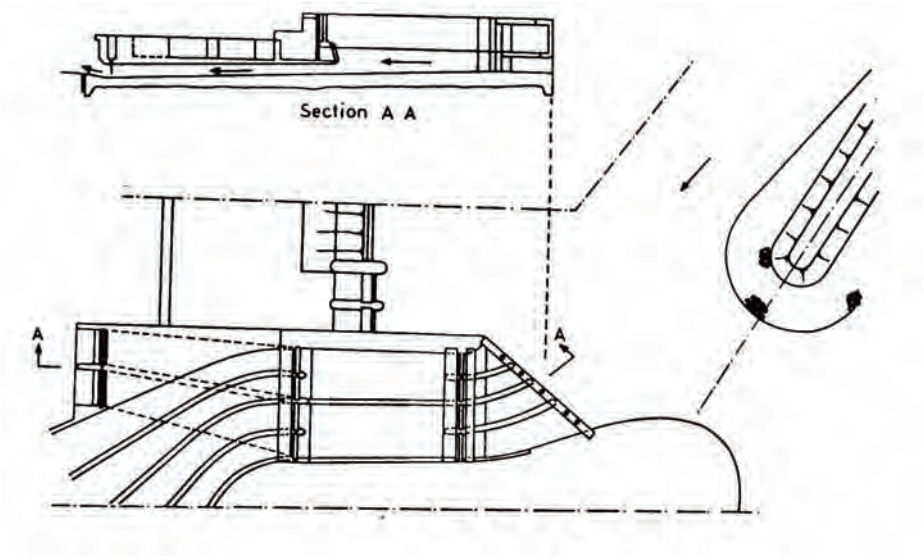

Figure 5-26 Frontal intake (Avery, 1989)

Pier type intakes (Figure 5-27) are a form of frontal intakes and are best suited in mountain streams with moderate slopes (<0.01). These streams are characterised by the fine sediment that they tend to carry. Usually more than 25% of the sediment is finer than 5 mm. The velocity through the screens should preferably be less than 0.5 m/s. This is much less than the average velocities in the stream that is usually of the order 2 to 2.5 m/s. Substantial flow rates can be diverted by pier intakes. For example, on Rio Nahualate (Guatemala) 29 m^3/s is

diverted through screens on four piers and abutments and 4 m^3/s is used for flushing (Raudkivi, 1993).

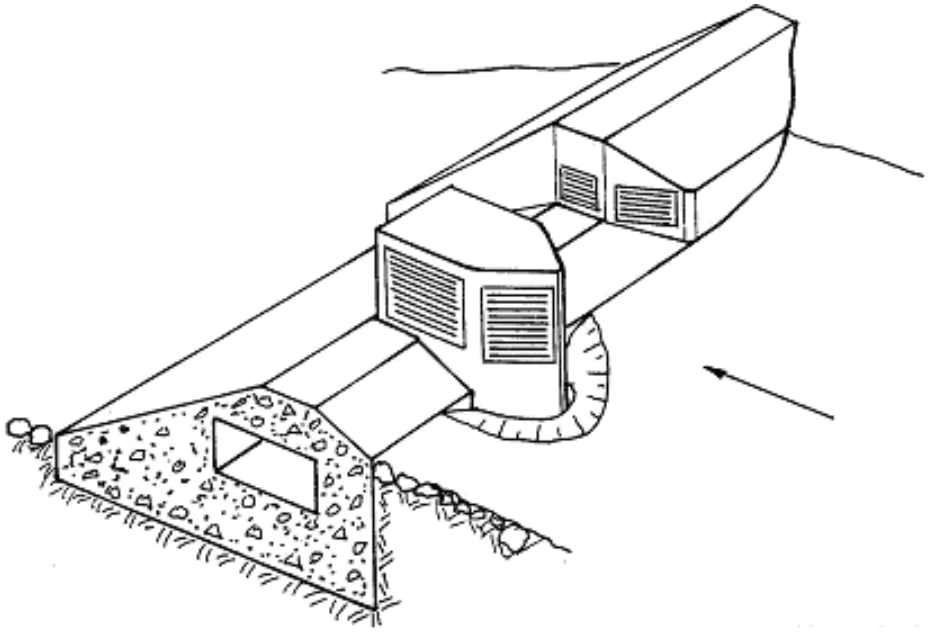

Figure 5-27 Illustration of a pier-type intake (Raudkivi, 1993)

In the case of frontal intakes, it is important to keep the sluice gates underneath the intake sufficiently raised so as to return the sediment to the main stream with only a small amount of flushing water. Continuous flushing is used in this system. The sluice gate is kept open to such an extent that the largest particle entering the gravel sluice may pass safely through it. From Figure 5-28 it is seen that the sediment particles are continuously flushed along the sloped surface of the deposited material in front of the sluice gate. The bottom layers with a large concentration of solids are therefore sucked towards the gate opening. An advantage of frontal intakes is that up to 90 % of the river flow can be diverted sediment free. Figure 5-29 and Figure 5-30 show the frontal type intake structure in Goksu, Turkey (Cecen, 1988).

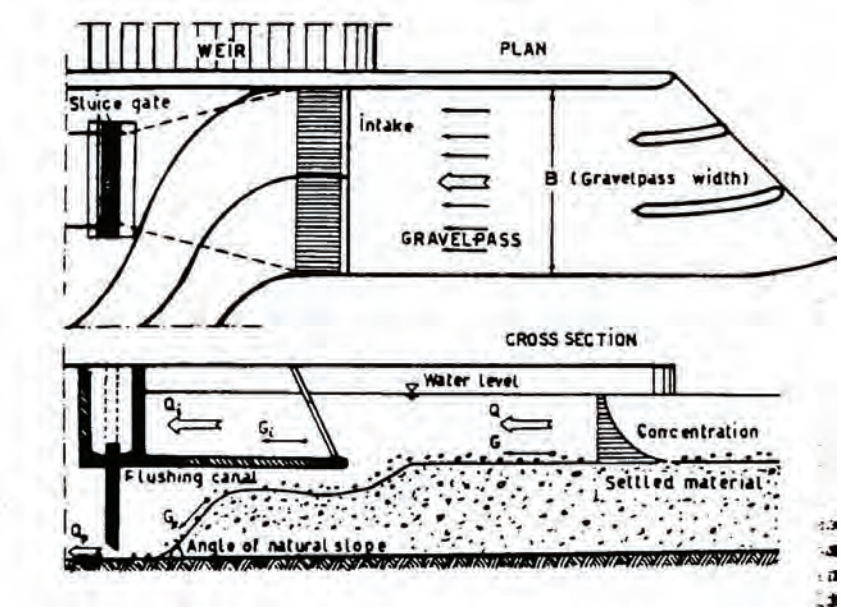

Figure 5-28 Frontal type of intake developed at the Technical University of Istanbul (Cecen, 1988)

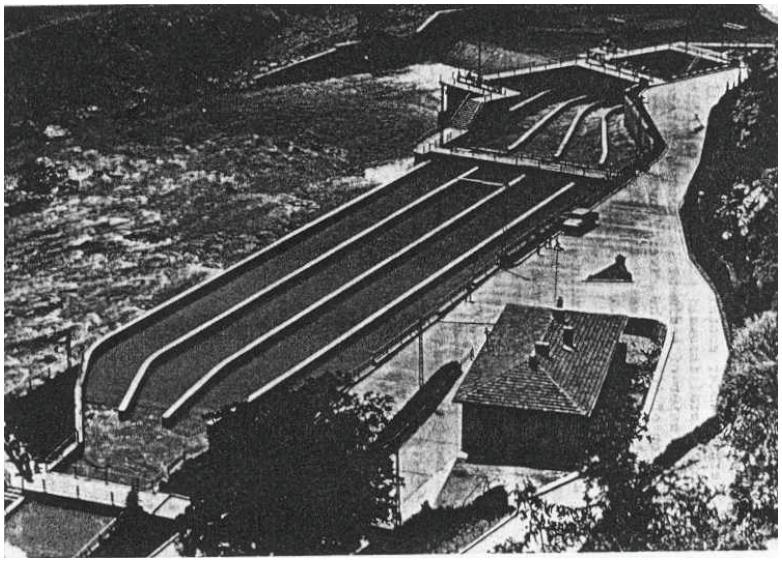

Figure 5-29 General view of the Goksu frontal intake structure in Turkey (Cecen, 1988)

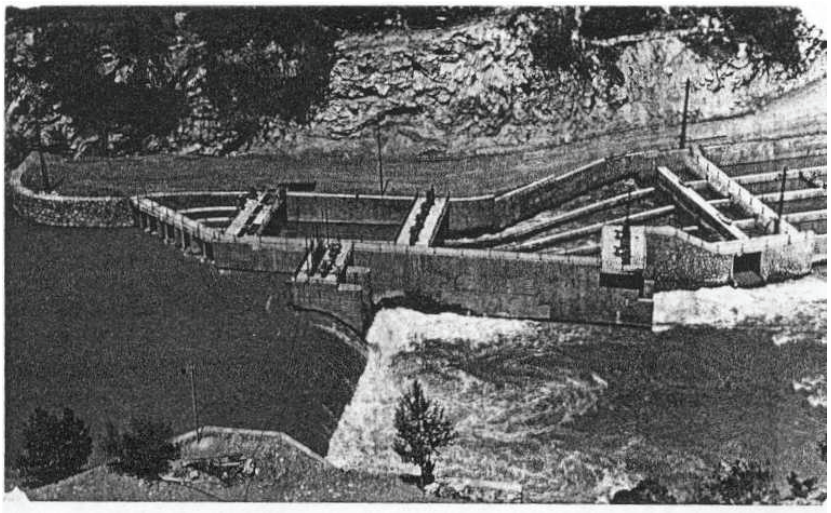

Figure 5-30 Frontal type intake structure in Goksu plant, Turkey (Cecen, 1988)

5.3.4 TIERED INTAKES

A tiered intake consists of a double stairs of gate-openings separated by a horizontal diaphragm. The upper openings are for water diversion and the lower ones for sediment flushing. The basic layout of a tiered intake is shown in Figure 5-31. Generally the tiered intake is applicable for conditions of a small watershed and a large river discharge that is much more than the diversion discharge. The widespread application in practice is limited by the relative complicated nature of a tiered intake, the large water consumption needed for sediment releasing and the difficulty in preventing flotsam and jetsam (timber, ice and garbage etc.) from entering the intake.

The tiered type intake has been used in some mountainous rivers in Middle Asia that are characterised by a steep slope (0.8-1.7 %), coarse sediment and a large seasonal variation in discharge. Figure 5-32 shows the layout of the Sangzhu tiered-type intake in the Xinjiang Uygur Autonomous Region of China that was constructed in 1965. The average discharge during the flood seasons (June to August) is 24.9 m^3/s with a sediment concentration of 1.25 kg/m^3. The median size of the riverbed material (d_{50}) is 57 mm and the designed diversion discharge (Q_d) is 25 m^3/s. The intake is operated by an intermittent sluicing mode; when the incoming flow (Q_0) is smaller than 25 m^3/s the lower sluicing gates are closed and all the flow is diverted into the canal through the upper gate-openings and the sediment is deposited in the

pocket above the sluice gates. When Q_o > 25 m^3/s the sluice gates are opened or partially opened to release sediment. Field observations indicate that the diverted discharge ratio (DDR) during the flood seasons was up to 76 % with no bed load entering the canal (Tan, 1996).

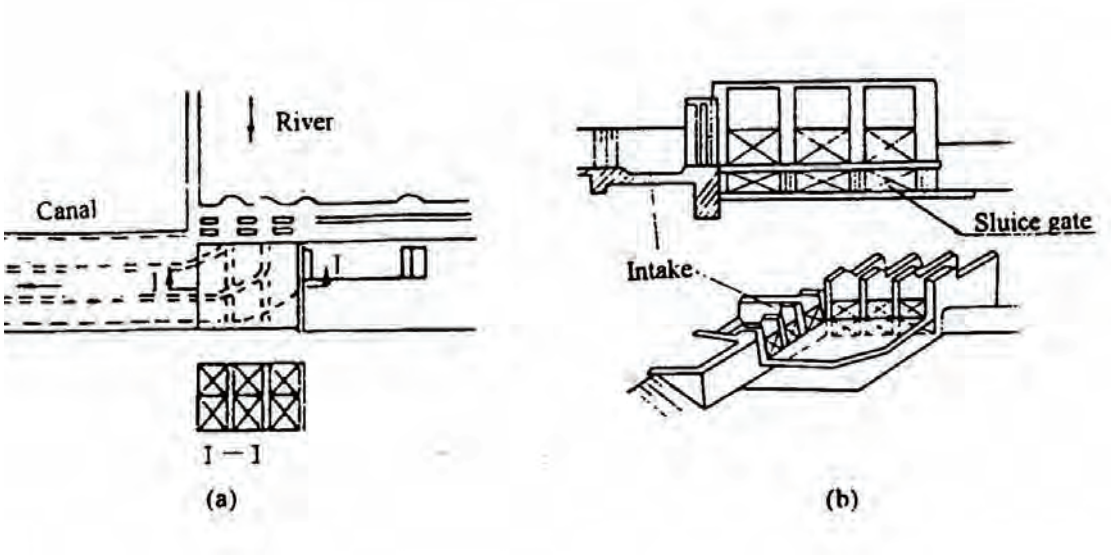

Figure 5-31 Typical layout of a tiered intake (Tan, 1996)

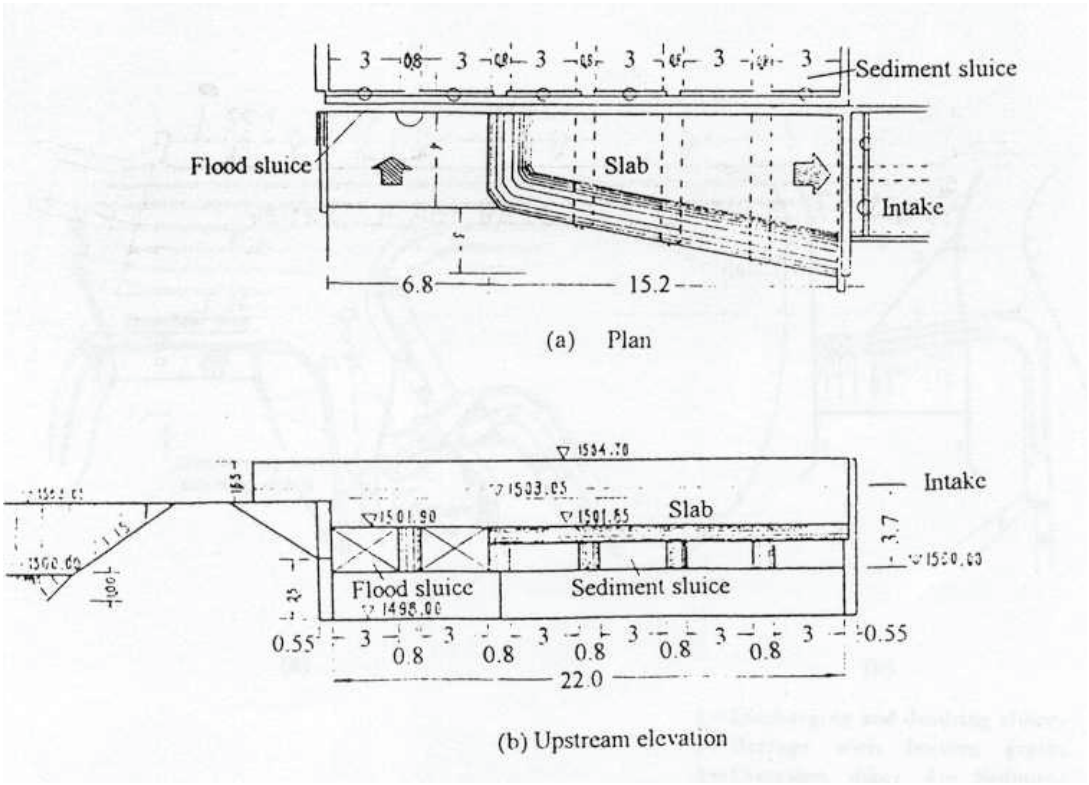

Figure 5-32 Sangzhu tiered intake (Tan, 1996)

5.3.5 BOTTOM GRATE-TYPE INTAKES

The bottom-type intake is usually built on medium and small mountainous creeks with a steep slope and torrential currents that carries a great amount of large sized bed load, such as gravels, pebbles and cobbles. Figure 5-33 shows the layout of two diversion works with bottom grate intakes. They mainly consist of a weir with a bottom grate intake, diversion gallery or canal, sluice and spillway. When the sediment carrying current overflows the bottom grate on top of the weir, sediment coarser than the grate bar spacing is trapped by the bars and is carried downstream by the flow while water drops down through the grate spacing into the diversion gallery. The bottom grate-type intake is usually characterised by small diversion discharges. However, it is still widely used in mountainous areas due to the simple nature of the structure, easy construction, low cost, convenience of management and high efficiency of rejecting coarse material. In recent years over 70 intakes of this type were built in Northwest China that covers diversion discharges of 5 to 35 m^3/s and flood discharges of 100 to 400 m^3/s.

Figure 5-34 shows the layout of the bottom grate intake on the Toutun River in the Xinjiang Region of China with an annual runoff of 240 million m^3. The designed discharge capacity of the intake is 30 m^3/s with the height of the weir 2.66 m above the river bed. Two rows of grates are installed on top of the weir with each row of grate being 20 m in length in the direction perpendicular to the flow. The grate bars are inclined in the downstream direction with a slope of $\frac{1}{10}$ with 6 mm spacing between the bars that is equivalent to the d_{75} of the bed load. The intake has been operational for the past 30 years and it diverts 160 to 220 million m^3 of runoff annually (Tan, 1996).

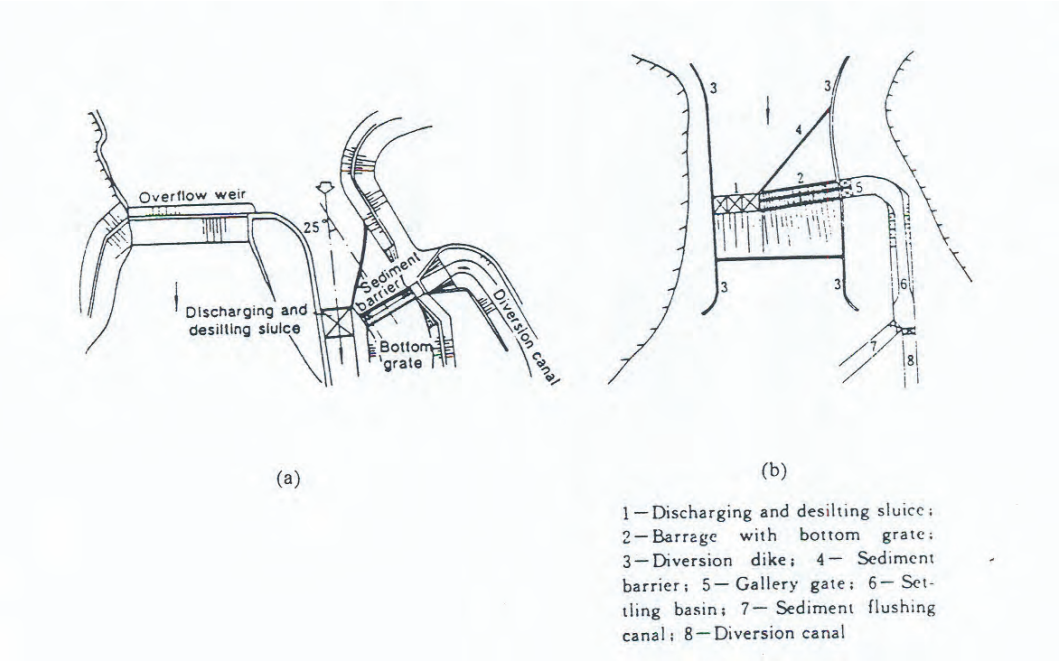

Figure 5-33 Typical layout of bottom –type intake (Tan, 1996)

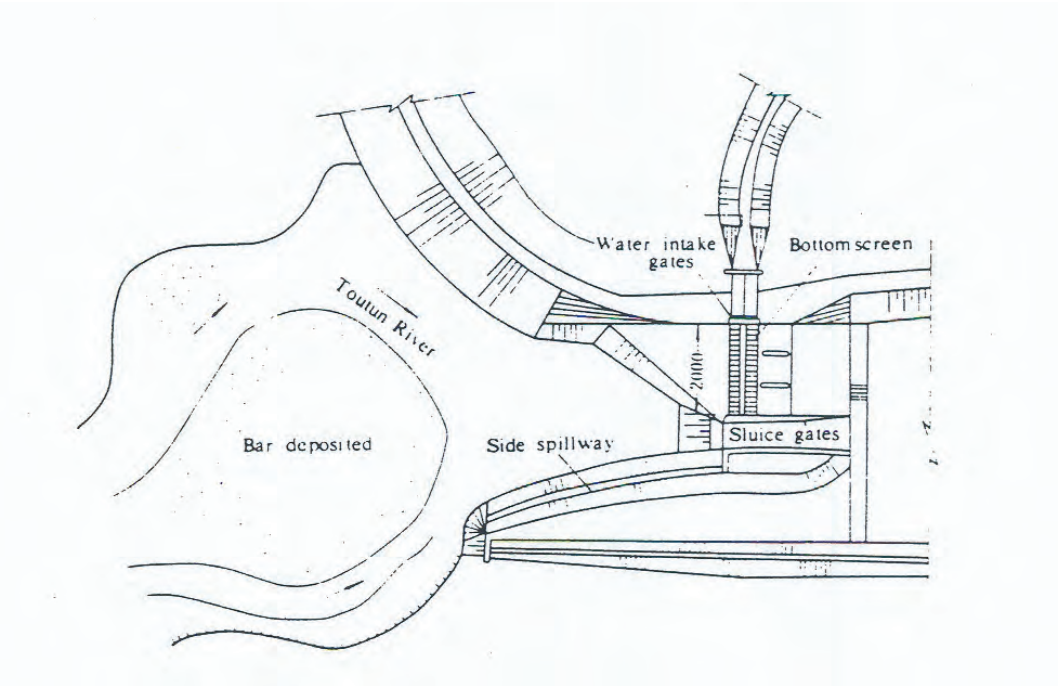

Figure 5-34 Bottom-type intake on the Toutun River, China (Tan, 1996)

5.4 ASPECTS TO IMPROVE THE EFFICIENCY OF INTAKES

5.4.1 GROYNES

Curvature can be created with the aid of groynes in bends with small angles or in straight river reaches. This principle is indicated in Figure 5-35 (Raudkivi, 1993).

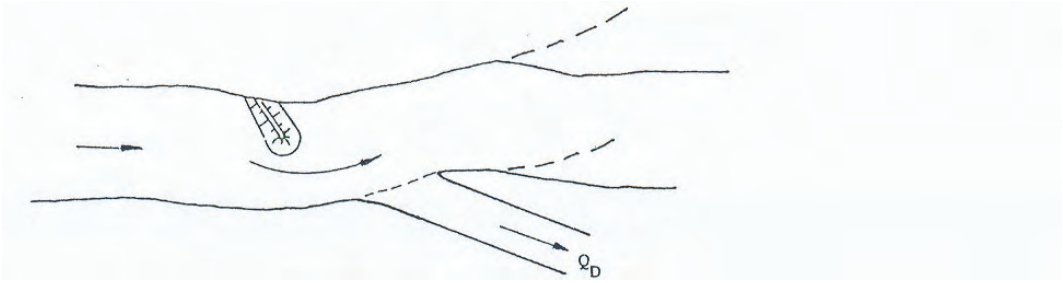

Figure 5-35 Diversion with the aid of a current deflecting groyne (Raudkivi, 1993)

5.4.2 GUIDE BANKS AND WALLS

A guide wall is sometimes called a contraction wall since the upstream portion is usually a curved shape to form a bell mouth for a basin and creates a gradually accelerated current in front of the intake for washing sediment in a sluicing flume. This is illustrated in Figure 5-36 and Figure 5-37. The length of the guide walls is usually equal to 1.1 to 3.0 times the width of the intake or about 5-10 m longer than the width although a length of 2/3 of the width was also found satisfactory by Sharma et al (1973).

The position of the guide wall is very important to ensure the proper functioning of the wall for reducing the sediment entering into the intake. The width mainly depends on the designed discharge of the sluicing flume that should be close to the annual average flood discharge of the river and should also be larger than the sum of the diversion discharge and the scouring discharge. The scouring discharge is often calculated as 0.5 to 1.0 times the diversion discharge. The velocity in the sluicing flume under normal operating conditions should be large enough to pick up the deposits in the flume and to transport them downstream, usually about 2-4 m/s (Tan, 1996).

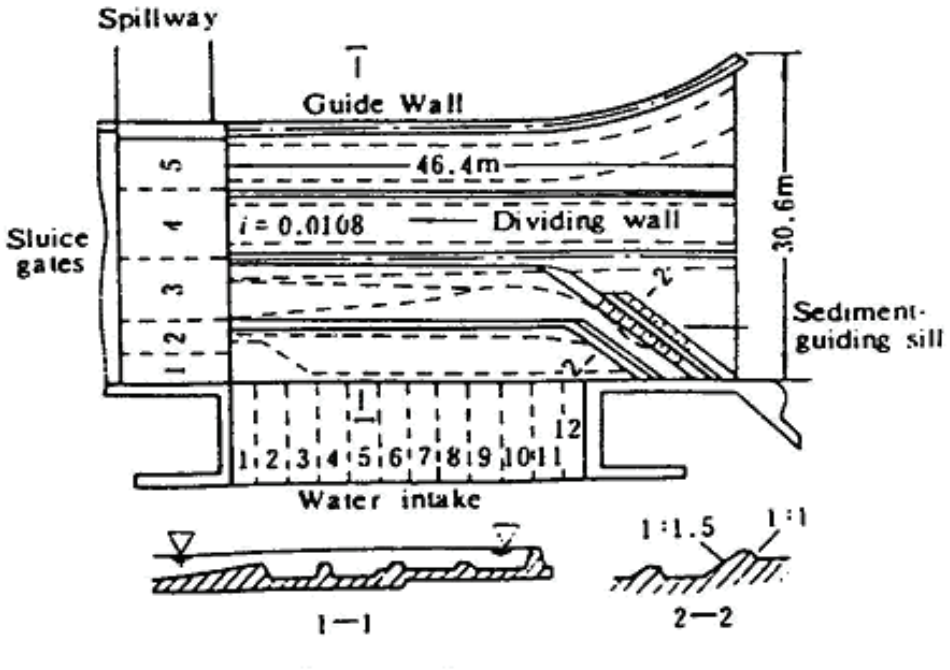

Figure 5-36 Circulation sluicing flume in Weihuiqu diversion works, China (Tan, 1996)

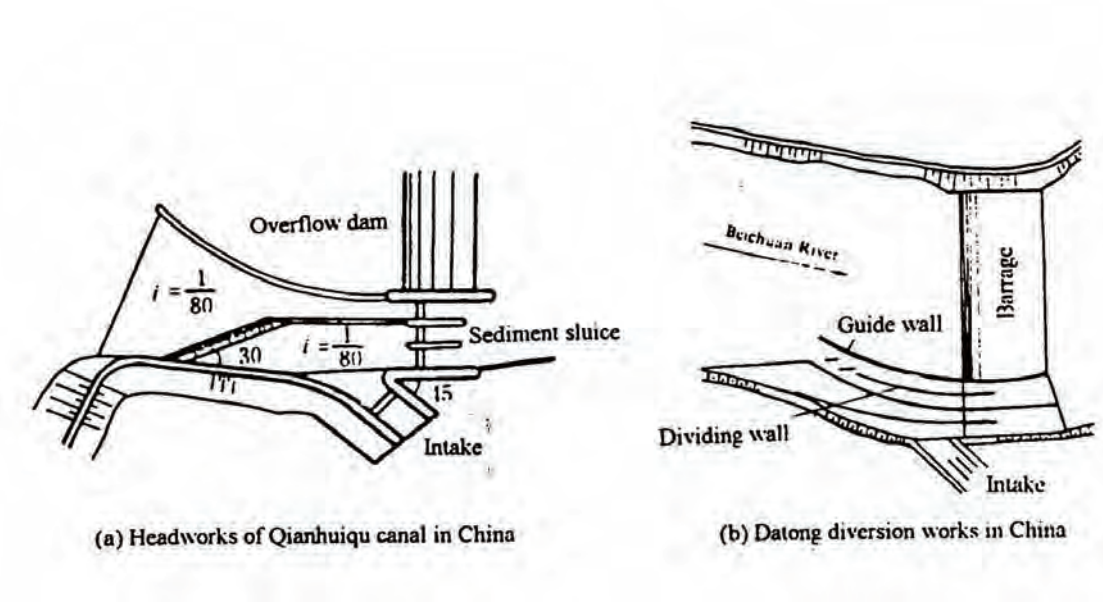

Figure 5-37 Curved sluicing flumes at (a) Headworks of Qianhuiqu canal, China and (b) Datong diversion works, China (Tan, 1996)

The model of the Kotri Dam, Pakistan, is shown in Figure 5-38. The diversion structure was designed to take advantage of a natural island to provide a concave curvature on each side of

the river. Water is diverted on the left bank at the Fuleli Canal and on the right bank at the Pinyari Feeder Canal. Figure 5-39 shows the layout of the Kotri Diversion Dam as it was constructed (Vanoni, 1977).

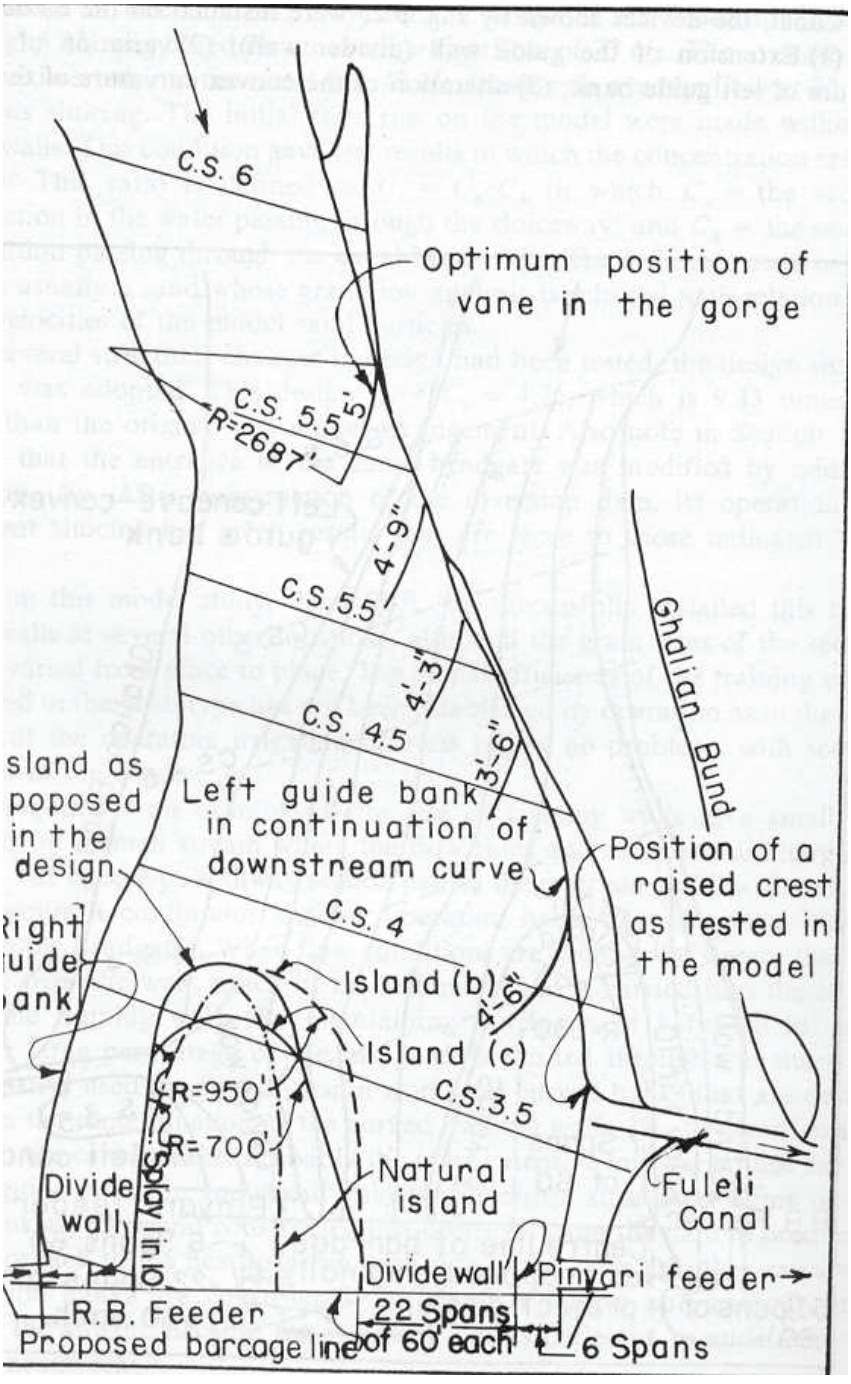

Figure 5-38 Guide Banks and Central Island in Model of the Kotri Diversion Dam, Pakistan (Joglekar, et al., 1951)

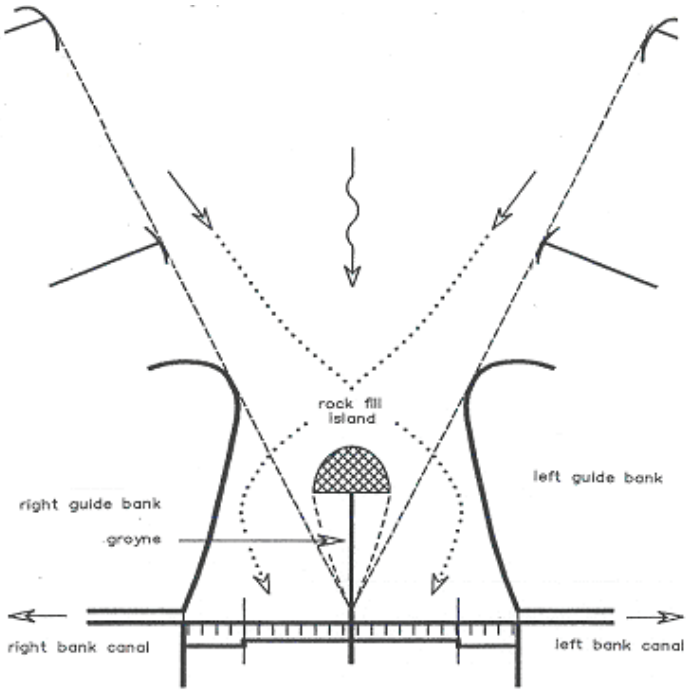

Figure 5-39 Layout of the Kotri Diversion Dam, Pakistan (Ahmad, 1973)

Guide walls can also be used to divert water from both banks of the river as were done on the Indus River in Pakistan (Figure 5-40). The diversion on the left bank was designed to utilise the natural curvature of the river while the diversion on the inner (right) bank made use of curved guiding walls to induce the curvature effect (Raudkivi, 1993).

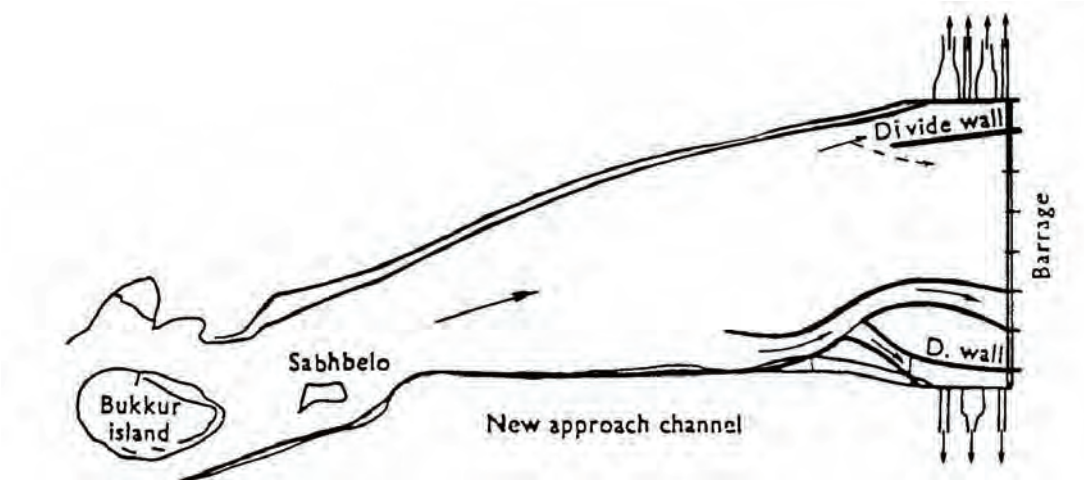

Figure 5-40 Schematic layout of the inner bank diversion with curved guide walls at Sukkur barrage on the Indus river, Pakistan (Raudkivi, 1993)

The Osborne canal diversion (Figure 5-41) at the Woodston diversion dam, Missouri River basin, Kansas, U.S.A. is another example where guide walls were used to create localised curved flow. The dam is less than 4 m high with an ogee-shaped sill made of concrete. The diversion intake is from a rectangular curved channel 1.5 m wide with a radius of 6.86 m. At normal water level the depth in the channel is 2.9 m and the intake sill is 1.35 m above the channel floor. The velocity in the channel is maintained at 2.5 to 3.5 m/s by adjusting the sluice gate at the end of the channel (Raudkivi, 1993).

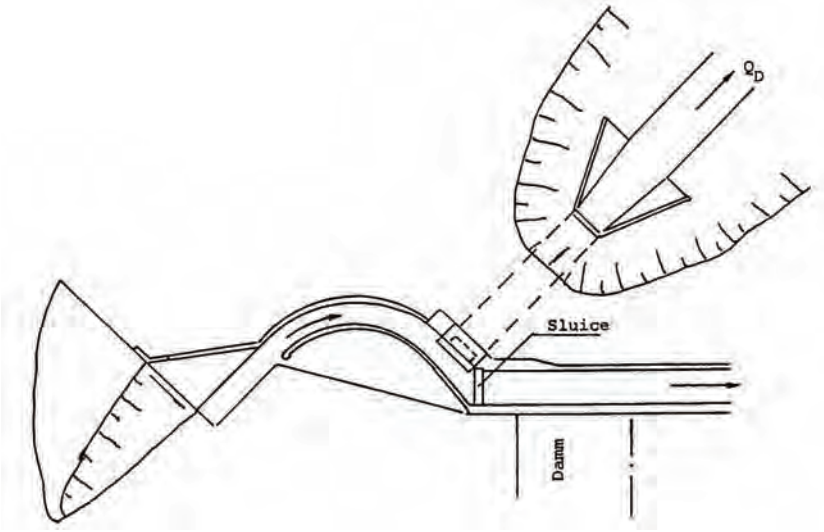

Figure 5-41 Woodston Dam diversion with the aid of guide walls (Raudkivi, 1993)

5.4.3 GUIDE VANES

Guide vanes on the bed as well as on the surface have been mainly used in the former USSR according to Shawmyan (1948). Bottom vanes that impose a transverse component of the flow are particularly effective in keeping the coarse sediment away from the diversion intake (Figure 5-42). In the case of the Cocorro Main Canal intake at San Acacia diversion dam, the use of such vanes reduced the diverted sediment to less than 5% of that without the vanes.

Surface vanes are angled to create a spiral flow in the upper layers of the flow towards the intake. The aim is to impose the spiral current features of bend-flow in the straight channel. The vanes are supported by a raft aligned at an angle $\beta = 20°$ to the river or canal bank. The vanes extend down to not more than half depth and are set at an angle $\alpha = 30°$ to the flow.

The arrangement extends into the channel a distance $b_g = 0.72(Q_D/Q + 0.07)B_D$ and the angle $\theta = 0.974(V_D/V + 69.5)$. This is illustrated in Figure 5-43. In India these vanes are known as King's vanes (Figure 5-4). Design parameters are given in Table 5-3.

The King's vanes have been in use for about sixty years and are functioning well where the discharges of the main and diversion canal are fairly constant. However, they are not recommended if the Q_D / Q ratio fluctuates strongly, or if the bed of the diversion structure is substantially above the river bed or if diversion flow is greater than one third of the main river flow. (Raudkivi, 1993)

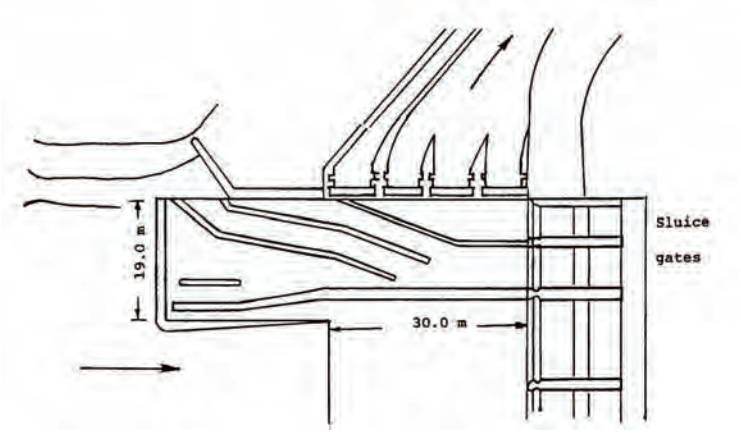

Figure 5-42 Guide vanes at the bed at the Sun-Kosi river intake in Nepal (Raudkivi, 1993)

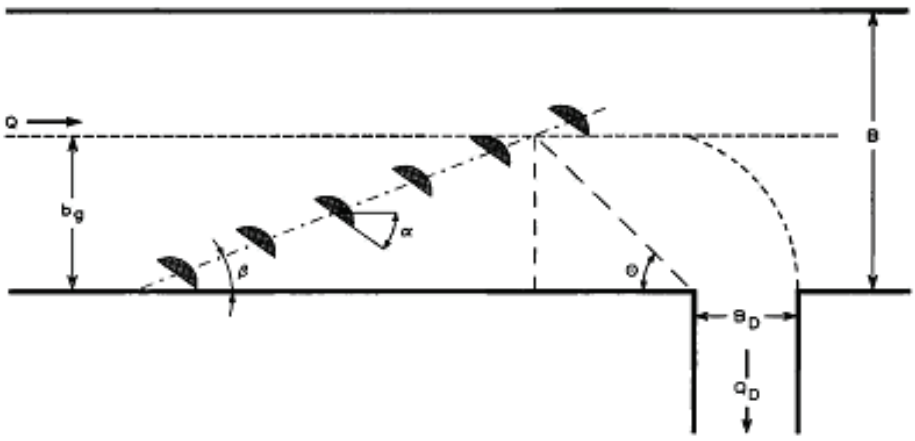

Figure 5-43 Layout of floating guide vanes (Raudkivi, 1993)]

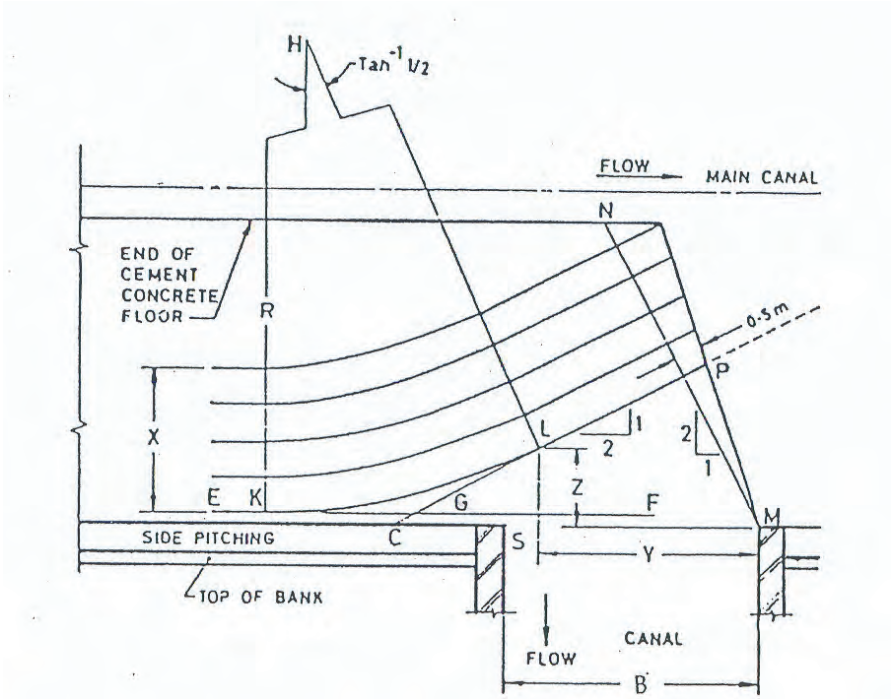

Figure 5-44 Illustration of King's vanes (Raudkivi, 1993)

Table 5-3 Design parameters of King's vanes (Raudkivi, 1993)

B	0.60	1.2	1.8	2.4	3.0	3.6	4.6	6.0	7.6	9.0	10.6	12.0
X	1.2	1.5	2.1	2.4	3.0	3.6	4.6	5.4	6.0	7.0	7.8	8.5
Y	0.6	1.2	1.5	1.8	2.4	2.7	3.0	4.0	5.2	6.0	6.6	7.6
Z	1.2	1.2	1.5	1.8	2.4	2.7	3.0	3.6	4.2	5.2	5.8	6.6
R	9.0	9.0	10.0	12.0	18.0	21.0	24.0	30.0	35.0	44.0	50.0	57.0

5.4.4 DIVIDING WALL

The dividing wall is parallel to the guide wall and is similar in length as the sluicing flume. The interval between adjacent walls is equal to the width of the sluicing gate. The top of the dividing wall is flush with the bottom sill of the intake and the rest of the wall is submerged in water while the height of the wall is generally 1 to 2 m or higher above the bed of the sluicing flume. The dividing walls divide the pocket basin into a number of narrow channels where the number is equal to the number of sluicing gates. The flow under the action of the dividing walls can be separated into two layers; the upper layers spill over the top of the walls and are attracted into the intake where the lower currents are confined by the walls and form spiral

flows, that can carry more bed load and coarse sediment throughout the sluicing gates (Tan, 1996).

Another method of creating flow curvature is by means of dividing walls and/or sluice gates that is illustrated in Figure 5-45. An essential feature of this method is that the flow rate per unit width of diversion flow is smaller than that in the river, i.e. $Q_D/B_D < Q/B < (Q-Q_D)/(B-B_D)$ where Q = discharge in the river, Q_D = diverted discharge, B = river width and B_D = diversion width (Raudkivi, 1993).

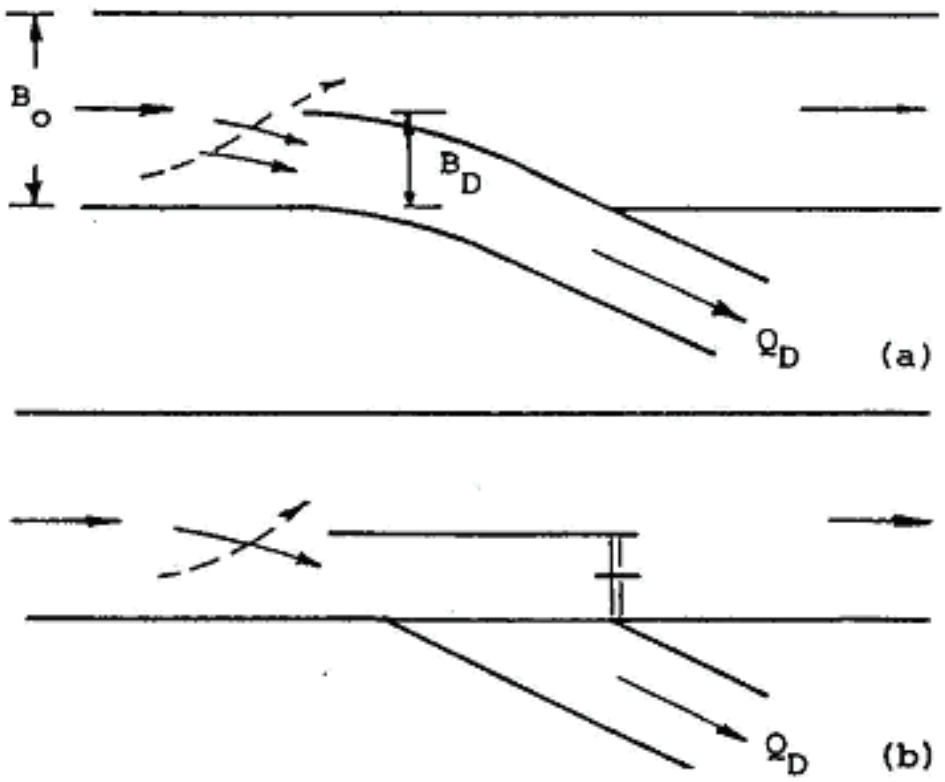

Figure 5-45 Creation of flow curvature with the aid of dividing walls and/or sluices (Raudkivi, 1993)

5.4.5 SAND GUIDING SILLS

The sand-guiding sill is a submerged sill installed just upstream of an intake and intersects the main flow with an appropriate angle to create a spiral flow near the bottom behind the sill.

The bed load can then be directed downstream under the action of the spiral flow. The sand-guiding sills can be in the form of a straight line, a broken line or a curve. The height of the sill is usually between a $\frac{1}{3}$ to $\frac{1}{10}$ of the local water depth. The higher the sill, the more intensive is the spiral flow that develops that is favourable for sediment releasing. However, care must be taken to ensure that the sill is not too high which would lead to the disruption of the spiral flow and therefore increase the sediment entry into the intake. The optimal intersection angle between the sill and main flow is usually between 20° to 40°. A smaller angle will lead to stronger longitudinal sediment delivery but will weaken the secondary flow. Table 5-4 lists the effects of dividing walls and sand guiding sills on the diverted sediment ratio (DSR) of the intakes in three irrigation canals in China. The diverted discharge ratio is depicted by DDR.

The layout of the sluicing flume of the intake at the Tanxiuwan Hydropower Station in China is showed in Figure 5-46. The intake is located on the upper reach of the Minjiang River that transports a large amount of bed load during flood periods. The intake consists of 4 gates (12 m wide) that is situated on the concave bank of the river. In front of the intake is a 50 m guide wall and together with the sill a sluicing flume is formed towards the 12 m sediment-sluicing gate. The average annual discharge of the river is 381 m^3/s with a designed diversion discharge of 240 m^3/s. The DSR of the intake in flood seasons is less than 2 %.

Figure 5-47 shows the layout of the Sunkosi Hydropower Station on the Sunkosi River in Nepal. The intake consists of five sand-guiding sills that are constructed in front of the intake. A model test indicated that the DSR is less than 1 %. Table 5-5 is a list of main features of intakes and sluicing flumes in some completed headworks (Tan, 1996).

Table 5-4 The effect of dividing walls and sand guiding sills on the diverted sediment ratio (DSR) of some diversion structures in China (Tan, 1996)

Intake	DDR (%)	DSR (%) Without the walls and sills	DSR (%) with the walls and sills
Weihuiqu	43	80	<1
Changmahe	50	36.8	<2.6
Yongdeng	50	32.7	~ 0

Note: DDR - diverted discharge ratio

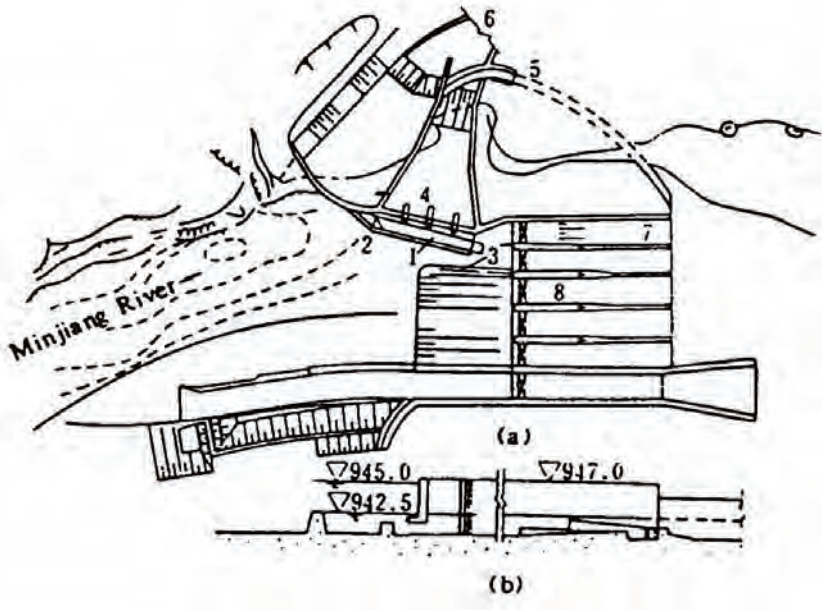

Figure 5-46 Intake of the Tanxiuwan hydropower station in China (Tan, 1996)

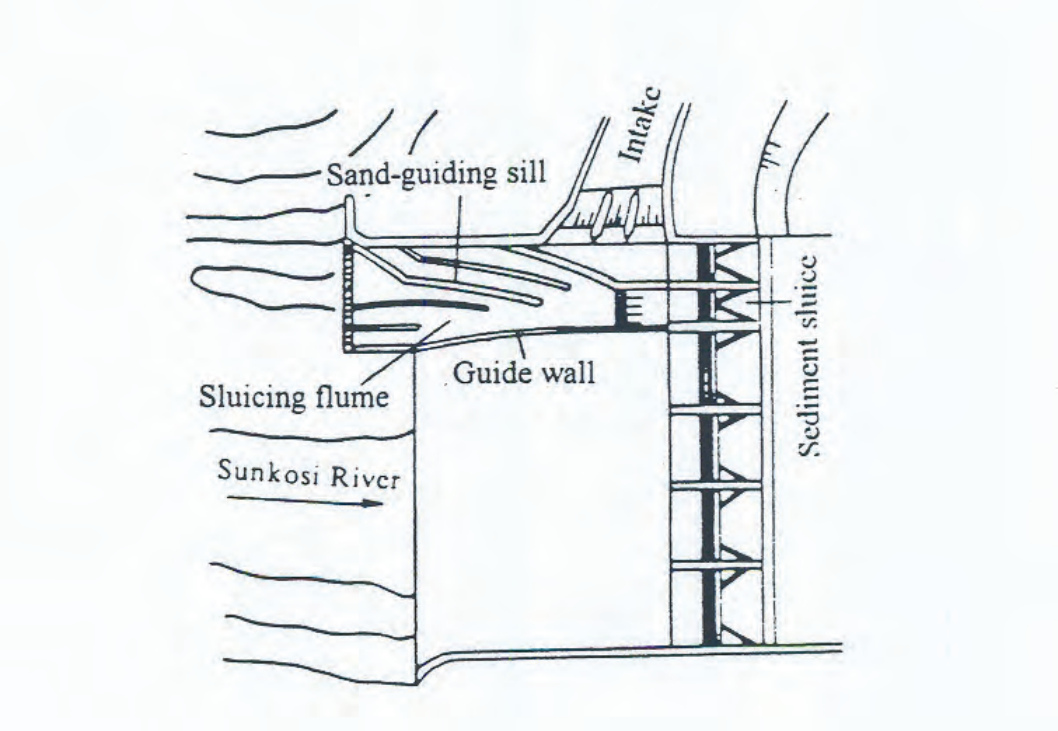

Figure 5-47 Sluicing flume of the Sunkosi hydropower station in Nepal (Tan, 1996)

Table 5-5 Main dimension of some completed sluicing flumes (Tan, 1996)

Name of headworks	Country	Intake		Sluicing flume			
		Discharge (m^3/s)	Width (m)	Discharge (m^3/s)	Width (m)	Length (m)	Slope (‰)
Yingxiuwan	China	240	54	270	20-12	50	0
Yuzixi-I	China	69	18	50	10-2.5	38	0
Shimian	China	19	15	120	20-12	20	60
Dazhai	China	39	20		16-5	30	0
Liujialang	China	64	33		27-24	45	10
Heihe							
Right bank	China	49	28	90	25-18	50	0
Left bank	China	74	42	192	39-23	50	10
Weihuiqu	China	30	32.8	114	30.6-19	46.4	0
Sunkosi	Nepal	40	23		17.5-12	55	46
Liar	Yemen	15	18		15-10	40	25
Sarda Barrage	India	328	116		68	113	
Harike	India	849	131		182	152	
Narora	India	241	62		125	69	
Dakpathar	India	245	61		122	88	
Ahsan	India	200	51		80	80	
Gandak	India	510	72		120	122	
Kosi Bihar							
Right bank	India	127	41		80	88	
Left bank	India	496	98		120	127	

5.4.6 SEDIMENT INTERCEPTING GALLERIES

A sediment-intercepting gallery is also called a tunnel type sediment excluder. It is usually used under the conditions of sufficient water head (higher than 2 m), small available discharge for releasing sediment, coarse sand and continuous diversion. There are generally three types of sediment intercepting galleries layouts: pressure tunnel-type, inverted siphon-type and cover slab-type.

The pressure tunnel type is more applicable in conditions of higher water head (> 3 m) with high velocities (> 4 m/s) and coarse bed load. A typical layout is shown in Figure 5-48.

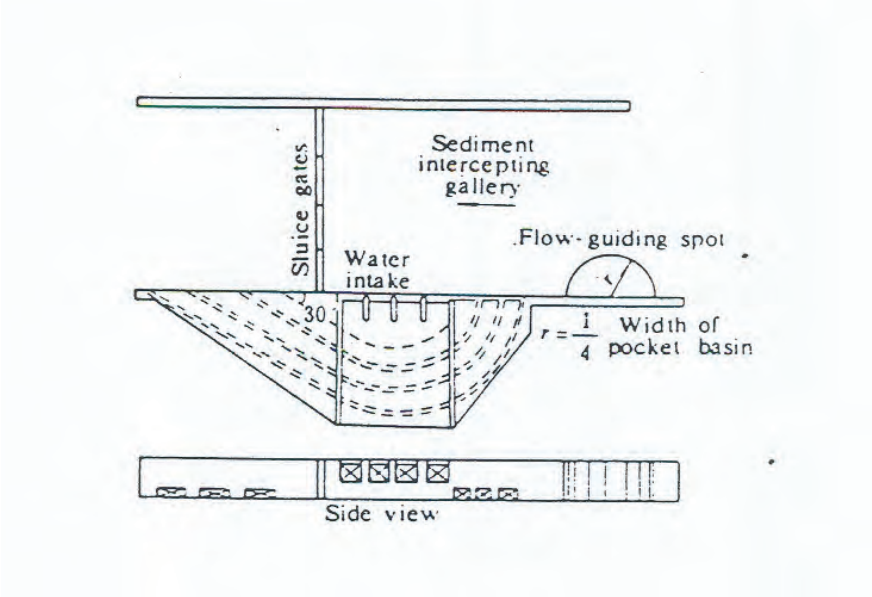

Figure 5-48 Pressure tunnel-type gallery (Tan, 1996)

The inverted siphon-type gallery is used in wide rivers with a low water head and fine sand (< 2 mm). A typical layout of the inverted siphon-type gallery is shown in Figure 5-49.

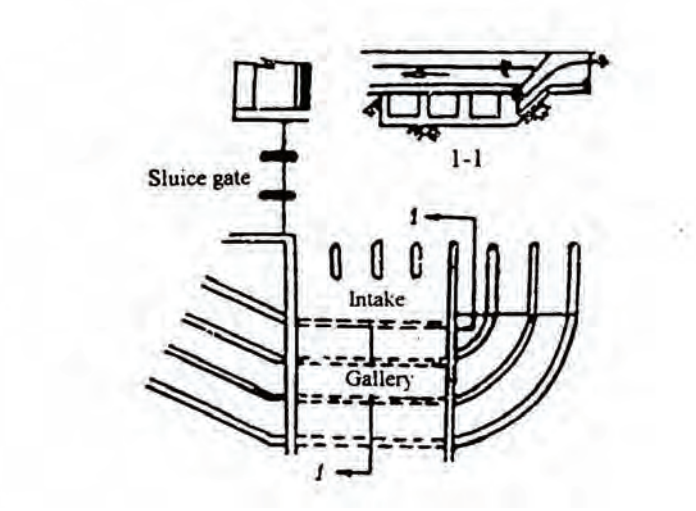

Figure 5-49 Inverted siphon-type gallery (Tan, 1996)

Both the pressure tunnel-type and the inverted siphon-type galleries are constructed on riverbanks. The inlet of the gallery should extend upstream of the intake to allow the approaching flow to enter the intake smoothly. In cases where the escaped flow from the gallery is submerged, a tailgate should be installed at its outlet to avoid the sediment from backing into it when the gallery stops operating. Generally the gallery has a rectangular cross-section of which the area depends on the available discharge and the allowable velocity (> 4 m/s). For the convenience of maintenance a minimum size of 2 m by 2 m is needed. The inner surface of the gallery should also be lined with an abrasion-resistant material to prevent it from abrasion damage by gravels or coarse sand moving at a high speed (Tan, 1996).

Figure 5-50 shows the cover slab-type galleries of the Khanki intake in India. The galleries are placed in a pocket basin before the sluice gates and is formed with cover slabs and partitioning walls.

The escape discharge of the galleries is usually fixed at 20-30 % of the canal discharge. The operating head should be higher than the head loss in the galleries and is usually varies from 0.6 m to 1.2 m. The gallery system should cover the width of the approaching flow that feeds the intake. The cover slab should be kept at an appropriate height to ensure minimum disturbance to the flow. In practice it is generally kept at a $\frac{1}{3}$ to a $\frac{1}{4}$ of the water depth with the top approximately flush with the crest of the sill of the intake. The size of the gallery should ensure that the head loss at the design discharge is smaller than the available operating

head and the convenience of maintenance should also be considered. The velocity in the galleries should be larger than the flushing velocity of the sediment.

Field observation in India indicated that one of the main factors governing the efficiency of excluders is the approaching conditions. The efficiency of the sediment releasing Chanki excluder in India is 70 % for sediment larger than 0.2 mm and 60 % for sediment larger than 0.075 mm and at the Narora excluder in India the efficiency is 50-87 % for bed load. The outflow from the galleries should be able to transport sediment freely downstream without forming shoals and obstacles at the outlet (Tan, 1996).

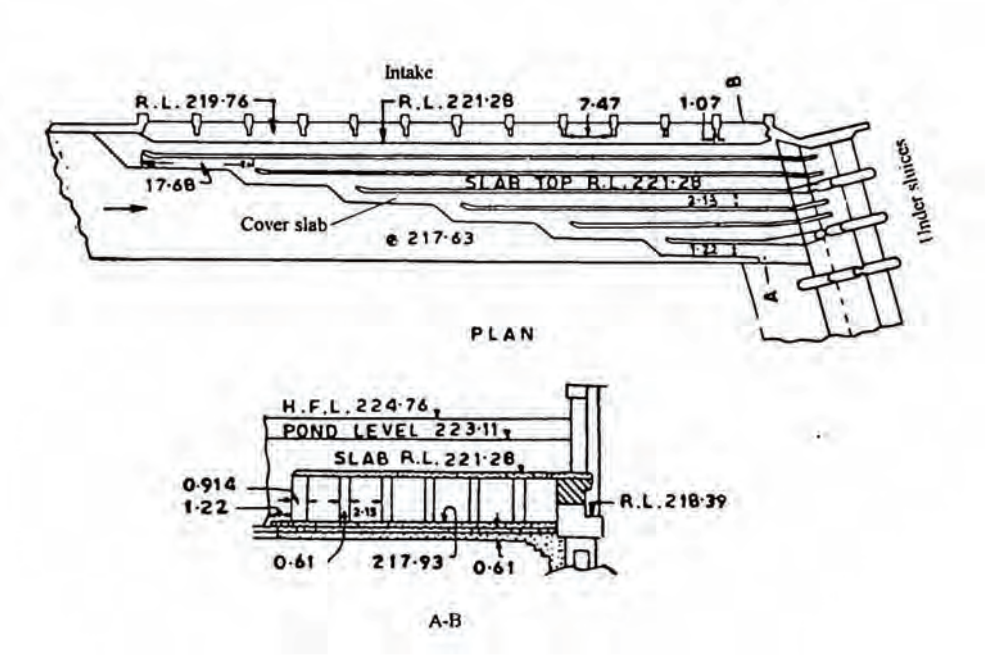

Figure 5-50 Cover slab-type excluder at the Khanki intake, India (Tan, 1996)

5.5 SAND ABSTRACTION SYSTEMS

5.5.1 DEFINITION

The term “sand abstraction system” refers to systems for the abstraction of water from sand. In the broadest sense the term is applied to any system designed to abstract water from an alluvial aquifer. This would include river sand beds, beach dunes and other primary alluvial aquifers.

Even in the context of abstracting water from river sand beds, are these perennial rivers or ephemeral sand rivers, the term sand abstraction system is broadly applied to a wide variety of applications and different types systems. Systems can be designed to abstract water flowing on the surface of a river through the river sand bed, or to abstract sub-surface river flow. Infiltration galleries, caisson type abstraction systems, vertical well points and horizontal screen abstraction systems can all be categorised as sand abstraction systems. Systems can differ vastly in scale and level of sophistication. In addition, the reasons for using such systems, as opposed to other abstraction methods, are numerous and varied.

A typical river sand abstraction system, of a caisson or infiltration gallery type, is shown in Figure 5-51.

A study of sand abstraction systems is currently being completed for the Water Research Commission "*Systems for the Abstraction of Water through River Sand Beds*" by Chunnett Fourie (a division of BKS), and should soon be published under the title "*A Critical evaluation of sand abstraction systems in Southern Africa"*, WRC Project No K5/829. This chapter is based on the findings of that specific study.

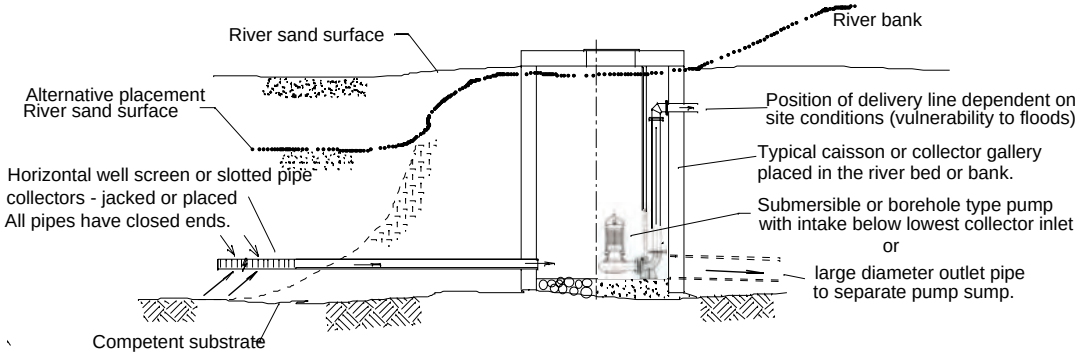

Figure 5-51 Typical River Sand Abstraction System

5.5.2 ADVANTAGES OF SAND ABSTRACTION SYSTEMS

Numerous advantages are associated with the use of sand abstraction systems. The reasons for using sand abstraction systems vary considerably, and different advantages are offered by these systems when used under different conditions.

5.5.2.1 ABSTRACTION OF WATERS WITH HIGH SEDIMENT LOAD

Numerous problems and high costs are associated with the storage, abstraction and treatment of highly turbid waters. These problems can be alleviated, and the associated costs be reduced, if surface water is abstracted utilising sand abstraction

systems as opposed to abstracting surface water directly ffrom the river using conventional abstraction methods. Some advantages offered by sand abstraction systems include:

- Diversion or impoundment structures are usually not required, with associated:
  a) reduction in capital costs;
  b) reduced environmental impacts, as it is usually not necessary to alter the natural river course at the point of abstraction.
- Sand abstraction systems can be installed in reservoirs where sedimentation has occurred and conventional abstraction methods can no longer readily be used.
- The storage in the sand bed can be utilised, although there will only be significant storage in the sand where the sand has a reasonably high permeability and depth.
- No conventional off take structures are required. The effective off take structures are buried in the sand, thus further sedimentation will have no impact on the functionality of the structure.
- By abstracting the surface water through the sand, the sand bed is used as a natural filter, reducing the turbidity and sediment load of the raw water during the process of abstraction. Raw water with reduced turbidity is therefore supplied to raw water pump stations and treatment plants.
- Minimal sedimentation problems in raw water pump sumps.
- Reduction in wear of raw water pumps and pipework, with an associated reduction in maintenance costs.
- Reduction in required capital outlay for water treatment plants, as water that must be treated will have a lower turbidity.
- Elements of the plant required for the treatment of turbidity and high sediment loads could be of considerably smaller capacity than would be required if conventional abstraction methods were used:
  primary settlers,
  coagulation & flocculation facilities,
  secondary settlers,
  filters,
  sludge removal, handling & disposal facilities.
- Reduction in the turbidity of raw water will result in a reduction in the time required for sedimentation, flocculation and filtration, with an associated increase in flow rates through the water treatment plant. The plant could therefore be sized smaller than if conventional abstraction methods were used.
- Reduced operation and maintenance costs for water treatment, arising from:

- Reduction in required cleaning of sedimentation tanks and backwashing of filters, resulting in:
  a) a reduction in the number of shut down periods;
  b) a reduction in the amount of water lost through use for cleaning and backwashing, with an associated reduction in the cost of pumping raw water to the plant.
- Reduction in the cost of chemicals required for coagulation and flocculation.

5.5.2.2 ABSTRACTION FROM SEASONAL AND SAND RIVERS

In Southern Africa, numerous rivers are seasonal, particularly in arid and semi-arid regions such as eastern Botswana and Namibia. Where rivers are seasonal, often the only source of water during the dry season is that stored and / or flowing in the sand of surface-dry rivers. Under such circumstances sand abstraction systems are commonly used for abstraction of water from the underlying water bearing sand. In these instances, the benefits arising from using sand abstraction systems include:

- access to continued, year-round water supply when rivers are surface-dry,
- utilisation of storage in river sand beds, particularly where sand storage dams are built specifically to trap sand and store water in the sand,
- reduced loss of water through evaporation, and
- effective pre-treatment of abstracted water as it is filtered through the river sand bed.

5.5.2.3 APPLICATION IN RURAL AND EMERGENCY SITUATIONS

In addition to the advantages mentioned above, there are numerous advantages associated with the use of small-scale sand abstraction systems.

Small-scale abstraction systems can be extremely simple in design and function. They can therefore be constructed using readily available and cheap materials, and using simple, labour-intensive construction methods, employing unskilled labour. Simplicity of function, coupled with the fact that the water is filtered through the sand river bed as it is abstracted, means that generally little operation or maintenance is required for these systems, and operators need not be highly skilled. In addition the method of treating the water once abstracted is simple and cheap, as normally only chlorination would be required.

These factors offer the following advantages, making them extremely suitable for use in rural and emergency situations:

- Local manpower can be employed for construction, thus providing employment for local people during the construction period.
- Systems can be installed at relatively short notice and relatively quickly.
- Although small-scale systems are usually not resistant to larger floods, they are cheap and relatively easy to repair. Local manpower can be employed to repair, rehabilitate, and / or upgrade such systems.
- Rural communities can easily operate and maintain their own systems, making the systems more sustainable.
- Minimal operation and maintenance requirements mean that operation costs are low. This is extremely important where rural communities are required to pay for the operation and maintenance of their own water supply schemes, as is now the case in South Africa.
- Minimal water treatment requirements after abstraction also reduce costs and do not demand high level of skill level for operation.

5.5.3 PROBLEMS EXPERIENCED WITH SAND ABSTRACTION SYSTEMS

Although sand abstraction systems offer many advantages, the behaviour of these systems has been found to be somewhat unpredictable. These include:

- low yield of sand abstraction systems i.e. where the yield of the system is considerably less than the design yield, with the design yield having been determined on what would be considered acceptable site investigations and investigations of the sand properties etc.,
- where yield is initially high, marked reduction of yield with time,
- flood damage,
- clogging of screens and pipes by what appears to be biologically induced fouling,
- changes in the physical properties of sand surrounding abstraction systems over time, including accumulation of fines in the sand, and reduction in the permeability of the sand,
- high iron and / or manganese content of abstracted water.

These problems have proved to be complex in nature and the reasons for their occurrence are not always evident.

5.5.4 TYPES OF SYSTEMS

The sand abstraction systems that one encounters in the field are as varied as the people who design them. Systems can, however be described under various general types of abstraction systems, which are discussed below.

5.5.4.1 CAISSON TYPE SYSTEMS

These systems generally incorporate a large diameter vertical caisson installed in the sand of the riverbed or the riverbank. The level of sophistication of caisson type systems varies from simple systems constructed using precast hollow blocks or even large perforated steel drums to structures constructed using precast manhole rings, reinforced concrete or no-fines concrete.

Provision must be made for infiltration of water into the caisson. This can be done in various ways, including:

- The use of no-fines concrete for the construction of the caisson. No-fines concrete is permeable, thus water can infiltrate into the system through the entire caisson surface.
- The inclusion of slots or openings in the caisson walls. Slots should be covered with a screen or mesh to prevent the ingress of sand into the caisson. A typical caisson with slot openings is shown in Figure 5-52.
- Use of selected aggregate or stone to construct the floor of the caisson. This will allow for infiltration of water through the floor of the caisson. Again, it is recommended that the surface of an aggregate floor be covered with screen mesh to prevent the ingress of fines into the system and retain the aggregate in place. Where caissons have both slot openings in the wall and an aggregate floor, it has been found that the majority of water infiltrates through the floor of the caisson. It is therefore recommended that caissons be constructed with a permeable floor, either packed aggregate or no-fines concrete.
- Horizontal well screens connected to the caisson can be installed in the sand bed surrounding the caisson. Water infiltrating the well screens will flow into the caisson. If multiple screens are installed these will be arranged radially from the caisson. A typical system of this type is shown in Figure 5-53.

Caissons lend themselves to the installation of submersible pumps. Water can then be pumped directly from the caisson to storage or treatment facilities. Alternately, an outlet pipe can be installed in the bottom of the caisson, connecting the caisson to the wet well of a pump station, or being connected to the suction of a centrifugal or mono-

type pump. Where more than one caisson is installed at a site, a common collector pipe can be used to deliver water from all caissons to the pump station.

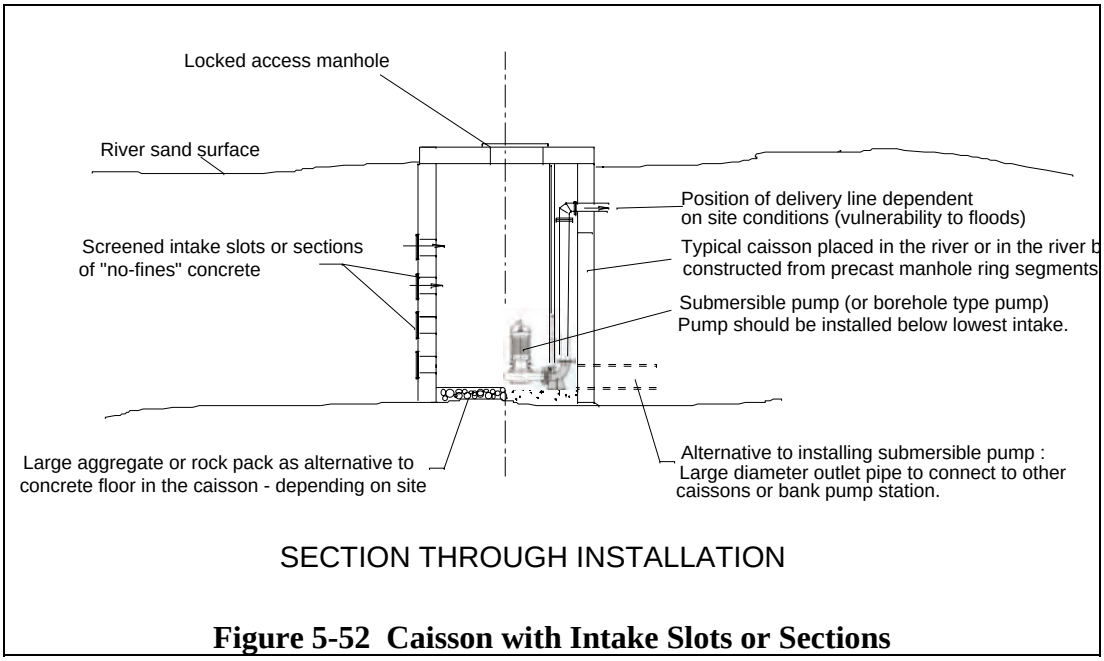

Figure 5-52 Caisson with Intake Slots or Sections

It is recommended that where possible caissons are founded on bed rock, being anchored to the rock by means of rock dowels or similar.

Although numerous successful applications of caissons exist, it has been found that caissons with slot openings are not ideally suited to conditions where there are a high percentage of fines in the river sand. Fines tend to enter the caisson and there is a build up of sludge in the bottom of the caisson under these conditions. Caissons with horizontal well screens with appropriate slot sizes would be more suited to these conditions.

Caissons are also not ideally suited to installation in rivers where extremely high flood flows occur, with associated bed fluidisation of the sand at depth. Caissons can then begin to "float" within the sand and can be overturned. Caissons installed in the riverbank are less susceptible to flood damage. The parameters of the alluvium in the riverbank must, however, be carefully investigated to ensure that sufficient infiltration can be achieved if the caisson is to be installed in the riverbank.

Caisson type systems are most suited to conditions where:

- The depth of the sand bed varies between 3 and 5 m. This gives sufficient depth for infiltration into the caisson, and allows for founding the caisson on the bedrock.

- The fines content of the river sand is not high, unless horizontal well screens are to be used.

A disadvantage of caisson type systems is that they do not lend themselves to backwashing or development of the sand around the caisson.

5.5.4.2 INFILTRATION GALLERIES WITH HORIZONTAL WELL-SCREENS

Infiltration galleries with horizontal well screens incorporate a horizontal gallery installed in the riverbed or riverbank. Horizontal well screens are connected to the gallery, near the invert of the gallery. These well screens project into the riverbed. The well screens are normally parallel to each other, although screens can be installed in the ends of the gallery, projecting perpendicularly to the screens installed in the sides of the gallery. A typical infiltration gallery with horizontal well screens is shown in Figure 5-53.

The length, diameter and slot size of the well screens will be determined by the parameters of the sand, and the required yield of the system. The screen diameter is also governed by the need to minimise head loss for flow through the screen pipe.

The collector gallery would normally be constructed from reinforced concrete, but other construction materials such as blockwork could also be used. It is recommended that the gallery be founded on bedrock, being anchored to the rock by means of rock dowels or similar.

Construction of these types of systems can be lengthy, and, when compared to other systems, costly. Systems with a collector gallery and horizontal well screens are therefore more suited to applications where demand is relatively high, and higher capital costs can be justified. For systems where demands are lower, other types of systems would be more suitable.

These systems are less susceptible to flood damage than are banks of vertical or horizontal well screens. This is generally because the well screens can be installed at greater depth than systems where the wells screens are connected to a manifold. The collector gallery also provides some anchorage under flood flow conditions.

Similar to caissons, these systems lend themselves to the installation of submersible pumps. Water can then be pumped directly from the collector gallery to storage or treatment facilities. Alternately, an outlet pipe can be installed in the bottom of the gallery, connecting the gallery to the wet well of a pump station, or being connected to the suction of a centrifugal or mono-type pump.

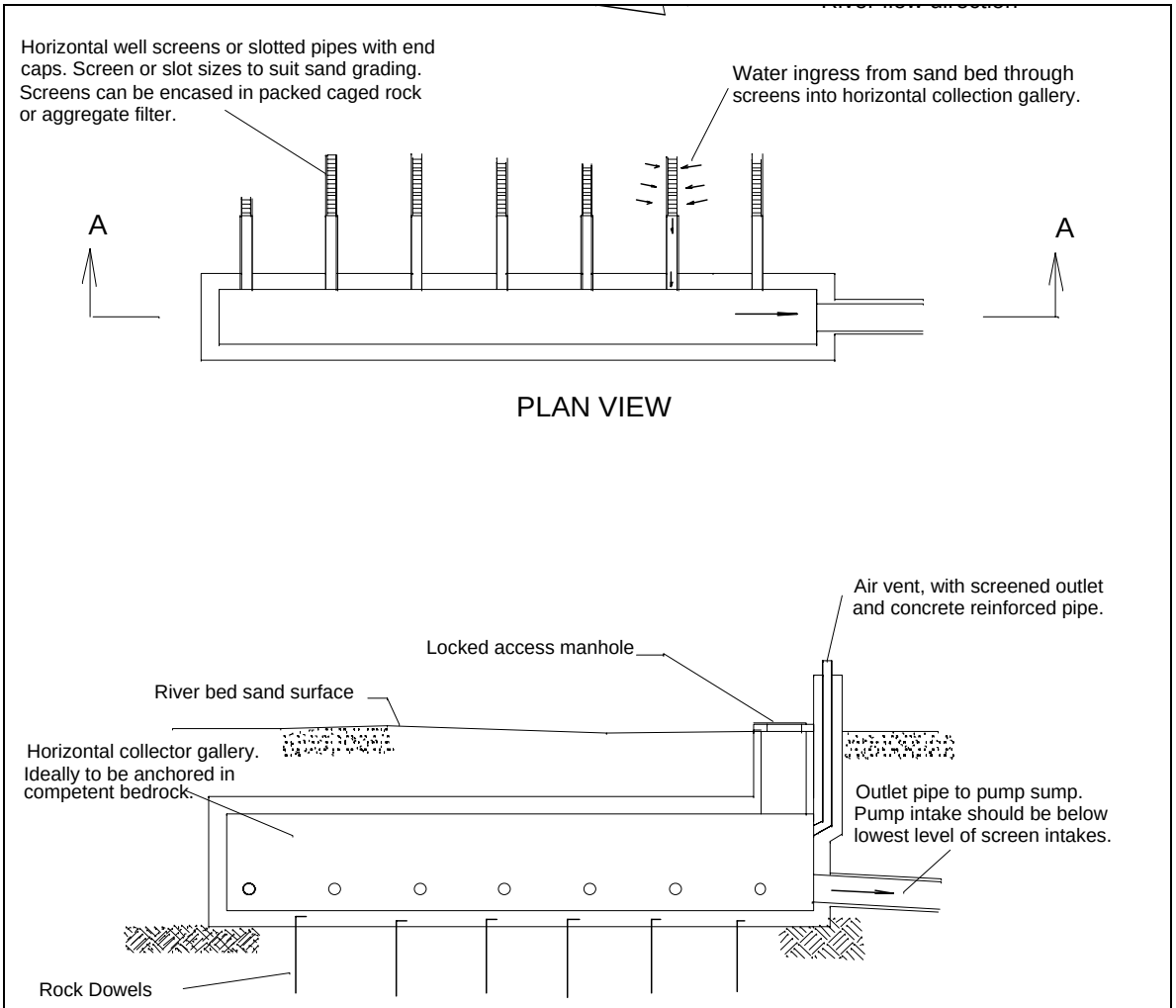

Figure 5-53 Collector Gallery with Horizontal Well Screens

A disadvantage of infiltration galleries with horizontal well screens is that they do not lend themselves to the incorporation of the facility for backwashing the screens, or to the development of the sand around the screens at the time of construction. The sand can be developed by isolating each screen independently, but it is far easier to develop the sand when installing banks of vertical or horizontal well screens connected to a manifold.

5.5.4.3 HORIZONTAL WELL SCREENS CONNECTED TO A MANIFOLD

Banks of horizontal well screens can be installed, connecting all the screens to a common manifold. The manifold can then be connected either directly to the intake of either centrifugal or mono-pumps, or water can flow under gravity to the wet well of a pump station. A typical horizontal well screen type system is shown in Figure 5-54.

The banks of screens can be installed in either the riverbed or riverbank. In general, although more susceptible to flood damage when installed in the riverbed, yields will be better than if the screens are installed in the riverbank.

When installing systems of this type, it is recommended that the manifold be installed on the riverbank. It is then possible to incorporate isolating valves at the head of each well screen, so that each screen can be isolated from the rest of the system. This is, however, not always possible, particularly when the riverbed is extremely wide and the main flow of the river (surface or subsurface) is not close to the riverbank.

The length, diameter and slot size of the well screens will be determined by the parameters of the sand, and the required yield of the system. The screen diameter is also governed by the need to minimise head loss for flow through the screen pipe.

It is recommended that the well screens be connected to the manifold by a length of flexible pipe (helical). This will allow for some movement of the well screens within the sand bed, without shearing the screens at the manifold.

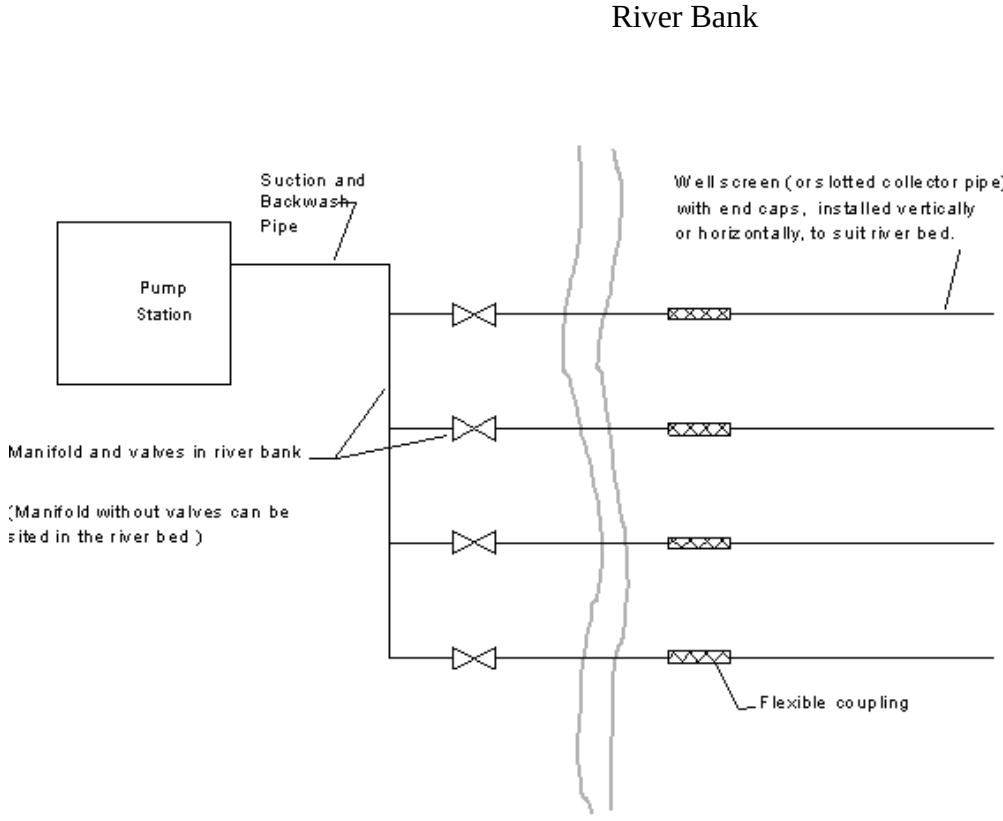

Figure 5-54 Horizontal / Vertical Well Screen System off Manifold

It has generally been found that the performance of systems that are backwashed regularly as part of normal operation procedures is better than that of systems that are not backwashed. Backwashing of the screens will remove any fines that have accumulated in the screens and will assist in breaking down and controlling the development and build up of scale and / or biofilm in the screens.

It is therefore recommended that where possible the system be designed such that it can be backwashed. This can either be done by incorporating a return flow from the storage tanks, with a bypass around the pumps, or by incorporating a circular return system, whereby water abstracted from one screen is pumped back into another screen to backwash it. The former system is however, preferred. In the case of the latter system, problems can arise if fines and biofilm etc. being washed out of the screen being backwashed is sucked into the screen that is being used to abstract the water for backwashing. This could lead to clogging of some of the screens.

It is also preferable that one screen can be backwashed at a time. If the entire bank is backwashed simultaneously, the backwash water will follow the path of least resistance, flowing out of the cleanest screens, and not effectively backwashing those screens that most require backwashing.

Well screens can be susceptible to flood damage, particularly when the screens are installed at relatively shallow depths in the sand. Measures should therefore be taken to protect the screens against flood damage. Alternatively, one can simply accept that the screens will occasionally be damaged or lost, replacing them if required. The latter approach has often been found to be more economical, particularly where the operating body has the skill to rapidly and easily replace the screens. This approach would not, however, be suited to schemes where the operating body do not have the skills to replace the screens, or are not likely to have the capital resources to pay for replacing lost screens e.g. large community water supply schemes. When a well screen is damaged by a flood it is not always possible to replace the screen due to the long duration of high flow conditions.

Methods and measures that have been implemented to protect horizontal well screens include:

- Installing the screens at the greatest possible depth, just above bedrock level.
- Tying the screens to anchor blocks buried in the sand.
- Encasing the screens in gabions or packed rock.
- Laying the screens on a mass concrete foundation and encasing them in aggregate enclosed in a mesh cage, which is bolted to the concrete foundation. The cage is

then covered with rock. (designed by Bradford, Conning and Partners, Newcastle) – see Figure 5-55. The system is relatively expensive to construct when compared to other horizontal screen systems, but it is believed that this system will remain successfully in operation for many years. The design has the added advantage of incorporating a graded filter around the screens. Problems of low yield are also therefore less likely to occur at this system.

- Attempts have also been made to anchor the well screens to the bank by means of a chain connected to rings on the end of the well points. This has, however, not been very successful.

1. SUBSOIL DRAINS UNDER CONSTRUCTION - MASS CONCRETE BASE WITH INVERTED STAINLESS STEEL U-BRACKETS BOLTED TO CONCRETE. 6 mm STONE CONTAINED BY 4,75 X 1,6 mm GALVANISED MESH. 3 X 200ϕ SLOTTED uPVC PIPES CONVEYS WATER TO MAIN PIPE AT BOTTOM OF WEIR (MAIN PIPE NOT SHOWN ON PHOTO).

2. 3 x SUBSOIL DRAINS BEING COVERED WITH BOULDERS FOR FURTHER PROTECTION AND IMPROVED FILTRATION. PRIMARY COLLECTION CHAMBER UNDER CONSTRUCTION.

Figure 5-55 Installation of sub-soil screens enclosed in graded filters and cages. Photographs and text courtesy of Bradford Conning and Partners, Newcastle

5.5.4.4 VERTICAL WELL POINTS

Vertical well points can either be installed independently, or in banks connected to a manifold.

Well points that are installed independently are similar to normal boreholes. They can be installed in the riverbed, or the alluvium of the riverbank. They incorporate a well screen installed vertically in the sand bed. The entire well point need not be screened. The upper section of the well point can be normal steel or uPVC casing, with the lower section that will be below the water table being screened.

Normally submersible borehole type pumps are installed in independent vertical well points. The depth to which the well point is installed will thus depend on the draw down level in the sand when water is being abstracted. The well point must be installed such that the pump intake is below the water table during operation.

Banks of vertical well points connected to a manifold can be installed in a manner similar to that in which banks of horizontal well points are installed. The well points can be installed at an offset from the manifold by incorporating straight lengths of pipe installed horizontally from the manifold to the well point.

It is normally not possible to install the manifold in the riverbank. Valves for isolating each well point are therefore also not normally incorporated in the system. The manifold is usually buried in the sand, at sufficient depth to give some protection during floods.

The manifold would normally be directly connected to the intake of pumps installed in a pumpstation on the riverbank. Either centrifugal or mono-type pumps can be used.

When using centrifugal pumps care must be taken in making provision for priming of the pumps. This is particularly important when the water level in the river drops below surface level. It is not, however, recommended that non-return valves be incorporated on the intake side of the pumps. This would prevent easy back washing of the pumps and it had been found that problems have been experienced with sealing of non-return valves through grit being trapped in the valve.

Provision for priming the pumps can be made by incorporating a vacuum tank on the intake side of the pump. The vacuum tank should have a volume equivalent to about 2½ times the volume of the pipework to the vertical well points. This tank should be connected to the delivery pipe of the pumps by a small diameter bypass with an isolating valve. Before starting the pumps, the vacuum tank can then be filled with

water from the delivery pipe of the pumps. This water will then be available for priming the pump. Alternatively, a small mono-type pump can be installed that can be used to pump water into a storage tank for priming the centrifugal pump.

Vertical well point installations are suited to conditions where the sand bed is very deep, and where the river is often surface dry. The largest system found in Southern Africa is that at Chisumbanje, Zimbabwe, incorporates three banks of vertical well points installed in the river sand of the Save River. The yield of this system is 1 020 ℓ/s.

5.5.4.5 GABION TYPE SYSTEMS

Gabion type systems incorporate a sump constructed out of gabions (rock packed in wire baskets). The sump is normally installed in the riverbed near the bank. The sump can either be founded on bedrock, on packed rock or on concrete. The sump is covered with a concrete slab with an access manhole, and a submersible pump is installed in the sump. Water flows through the gabion walls into the sump, from where it is directly pumped. A typical gabion type system, developed by Silk Kisch Peralta Engineers (SKP), Durban, is shown in Figure 5-56. The system can be augmented by the inclusion of horizontal well screens connected to the sump. These well screens can either be buried in the sand of the riverbed or be encased in gabions.

In many systems of this type the gabions are wrapped in geofabric. Kaytech geofabrics as opposed to bidum is recommended if geofabric is used. Generally problems will not arise through the inclusion of geofabric in these systems, **IF** the systems are installed where the turbidity of the river is low and there are a very low percentage of fines in the river. Even under these conditions though, the geofabric will however, show signs of reduced permeability. It is therefore **NOT** recommended that geofabric be used if a system of this type is to be installed at a site where there are a large percentage of fines in the sand. The geofabric will rapidly clog under such conditions, rapidly reducing the yield of the system.

Gabion type systems are ideally suited to applications where:

- The water demand is low.
- It is necessary to keep construction costs to a minimum.
- Operation and maintenance should be as simple as possible.

The systems are therefore ideal to use for rural water supply systems.

In addition, the system is suited to conditions where:

- The surface water is relatively clean.
- The alluvium of the riverbed is coarse.
- Flood levels are not very high.

These conditions normally occur at the head of a catchment.

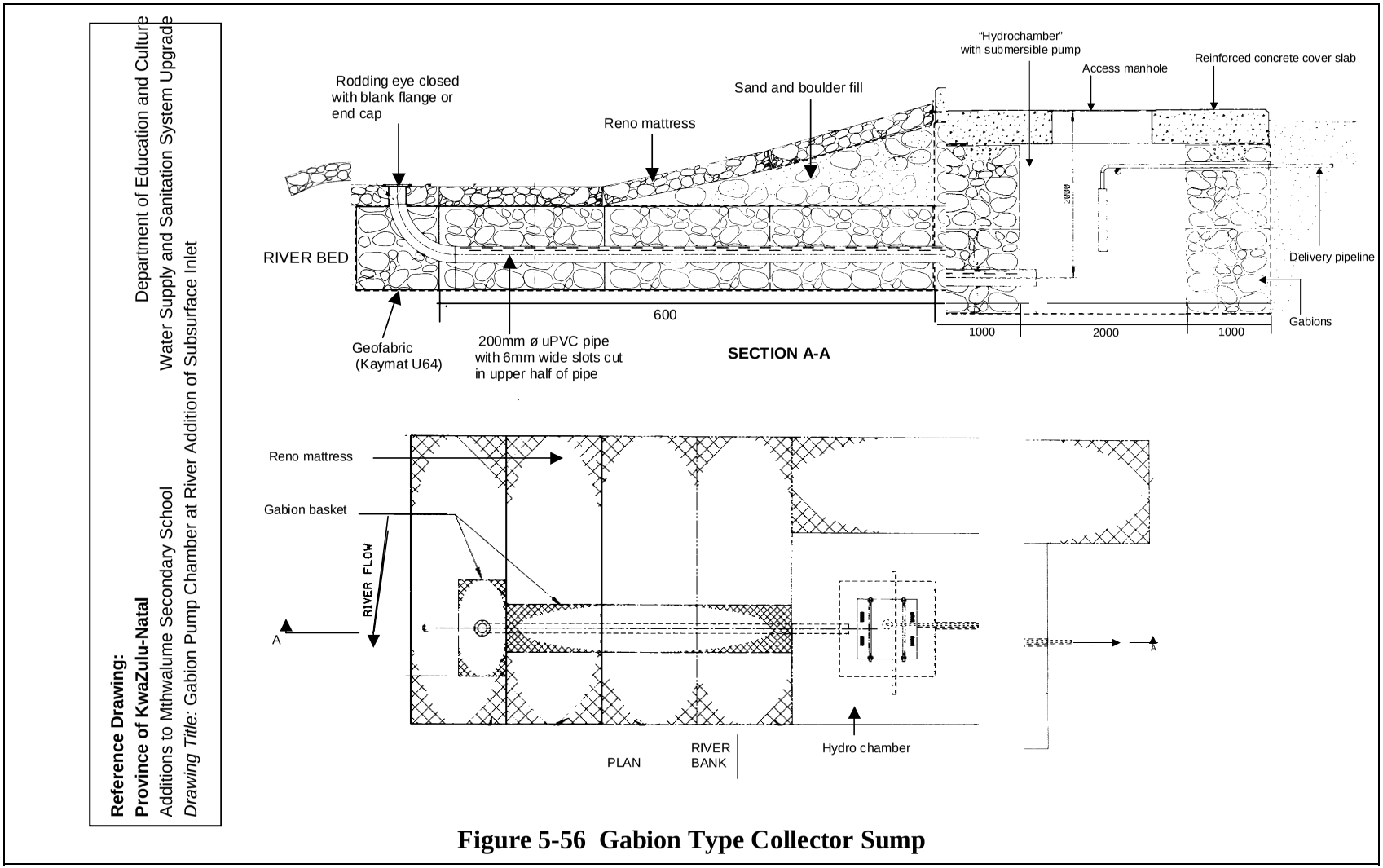

Figure 5-56 Gabion Type Collector Sump

5.5.4.6 ABSTRACTION CHAMBERS

As an alternative system to the caisson type abstraction chambers, horizontal abstraction chambers can be installed.

These are generally long, narrow sumps that are relatively shallow. The sump is installed in the riverbed. Provision is made for the flow of water into the sump either through the inclusion of screened openings in the sump walls, or through the use of no fines concrete. A pipe connects the sump to the wet well of a pump station installed in the riverbank. The invert level of the pump station wet well should be such that the water can gravitate from the sump to the wet well of the pumpstation. Submersible pumps or normal centrifugal pumps can be installed in the pumpstation.

It is recommended that the chamber be founded on bedrock, being anchored to the bedrock by means of rock dowels or similar.

A typical horizontal abstraction chamber is shown in Figure 5-57. This system was designed by Ernst Cloete and Associates, Vryheid, and has been successfully implemented at Makhosine and Opuzane, KwaZulu-Natal.

Horizontal collector chambers are ideally suited to applications where:

- The water demand is low.
- Operation and maintenance should be as simple as possible.
- A reasonable level of filtration is required.

The systems are therefore ideal to use for rural water supply systems, where the water is not treated (except for chlorination) prior to use.

In addition, the system is suited to conditions where:

- The surface water is relatively clean.
- The alluvium of the riverbed is relatively shallow.
- Flood levels are not very high.

These conditions normally occur at the head of a catchment.

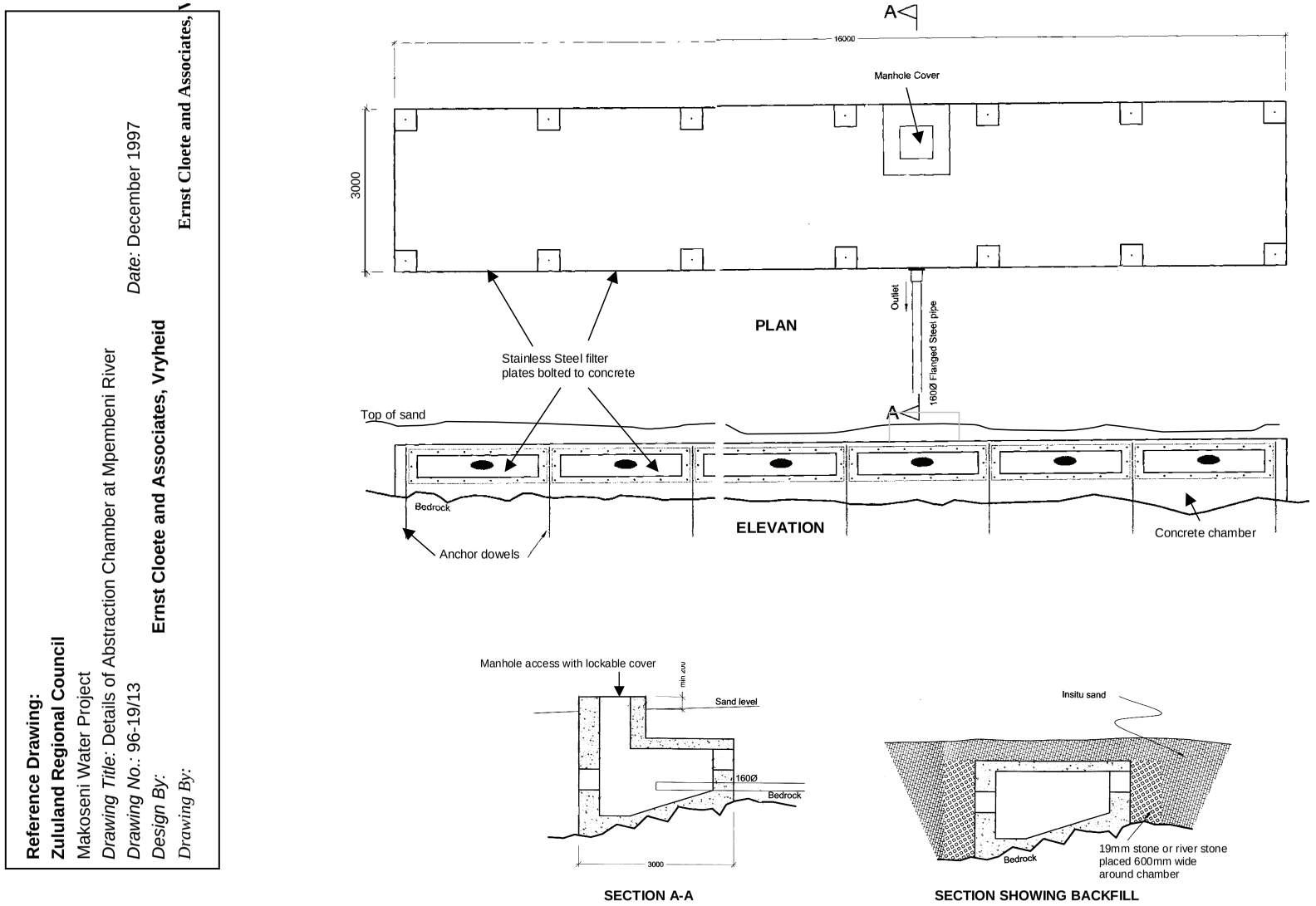

Figure 5-57 Horizontal Collector Chamber

5.5.4.7 SMALL-SCALE SYSTEMS

For many rural applications small-scale, low technology systems are often more suitable than larger more sophisticated systems. Simple hand-pumped sand abstraction systems have been developed by Dabane Trust, Zimbabwe, and successfully implemented for water supply for community market gardens.

Typically these systems incorporate a short well screen that is installed in the riverbed, at an angle to the surface. The well point is connected to a Rower-type hand pump installed on the riverbank just above the flood line. Water from the rower pump is discharged directly into a concrete or sealed blockwork sump installed in the riverbank.

If it is necessary to pump the abstracted water to a higher elevation, a second pump is installed. This pump, either a Joma or rower hand pump, is installed further up the embankment (Figure 5-58). It is used to draw water from the sump, which is filled using the first rower pump, and pump it further up the embankment to where it is discharged into a reservoir. The water can then either be used for domestic water supply or for irrigation. When used for irrigation canal systems can be installed to irrigate gardens from the reservoir. Details of a system of this type are shown in Figure 5-59.

With the simplicity of this system, women can easily operate and maintain it. As the major water users and collectors in rural communities, this is particularly important. It was noted by Dabane Trust that women quickly learned to undertake all basic maintenance and repair work to the pump. The women have cited the sustainability and low operation and maintenance costs, in addition to increased self-reliance, as reasons for their preference for using this system.

The design of these systems is simple, and the systems, including the pumps, can be built using commonly available materials. It is therefore possible to teach rural communities to construct and install systems of this type themselves.

These systems are ideally suited to applications where:

- The water demand is low.
- Simple appropriate technology is required.
- Operation and maintenance should be low cost and simple.
- Electricity or fuel supplies are not readily available.

In addition, the systems are suited to conditions where:

- The river is often surface dry.
- The alluvium of the riverbed is either shallow or deep.

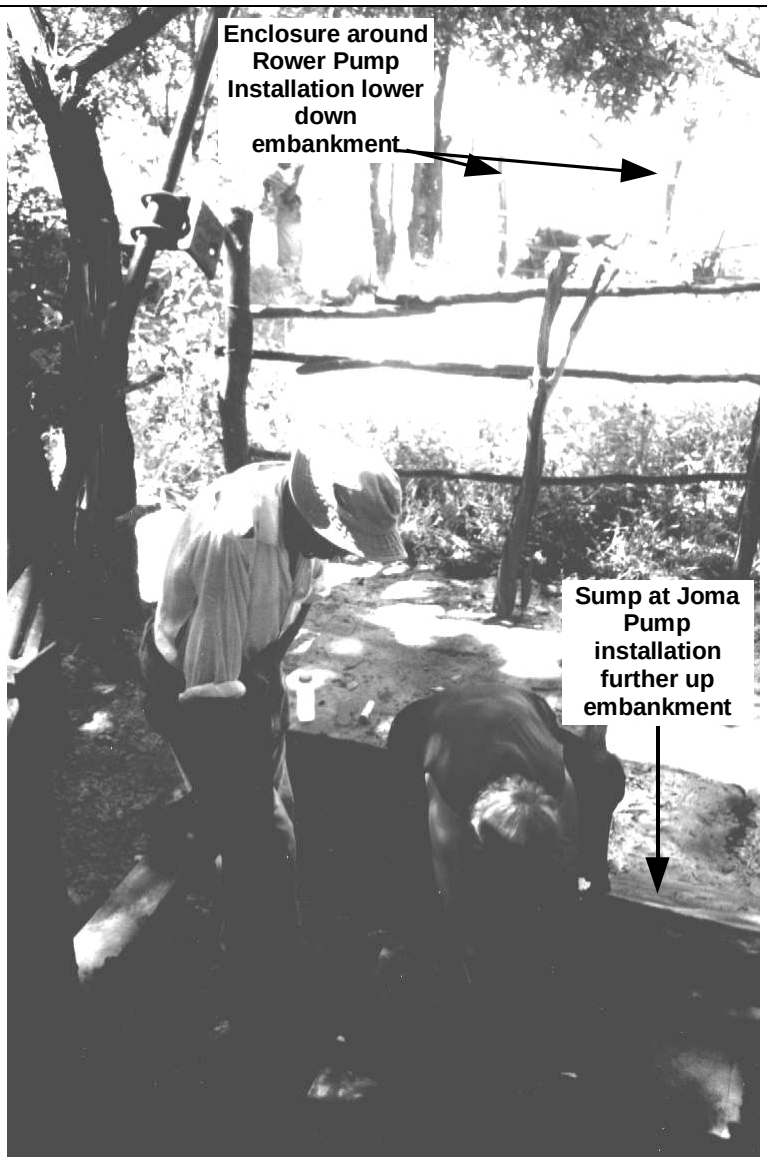

Figure 5-58 View of Joma Pump Installation at Small Scale Hand Pumped Abstraction System

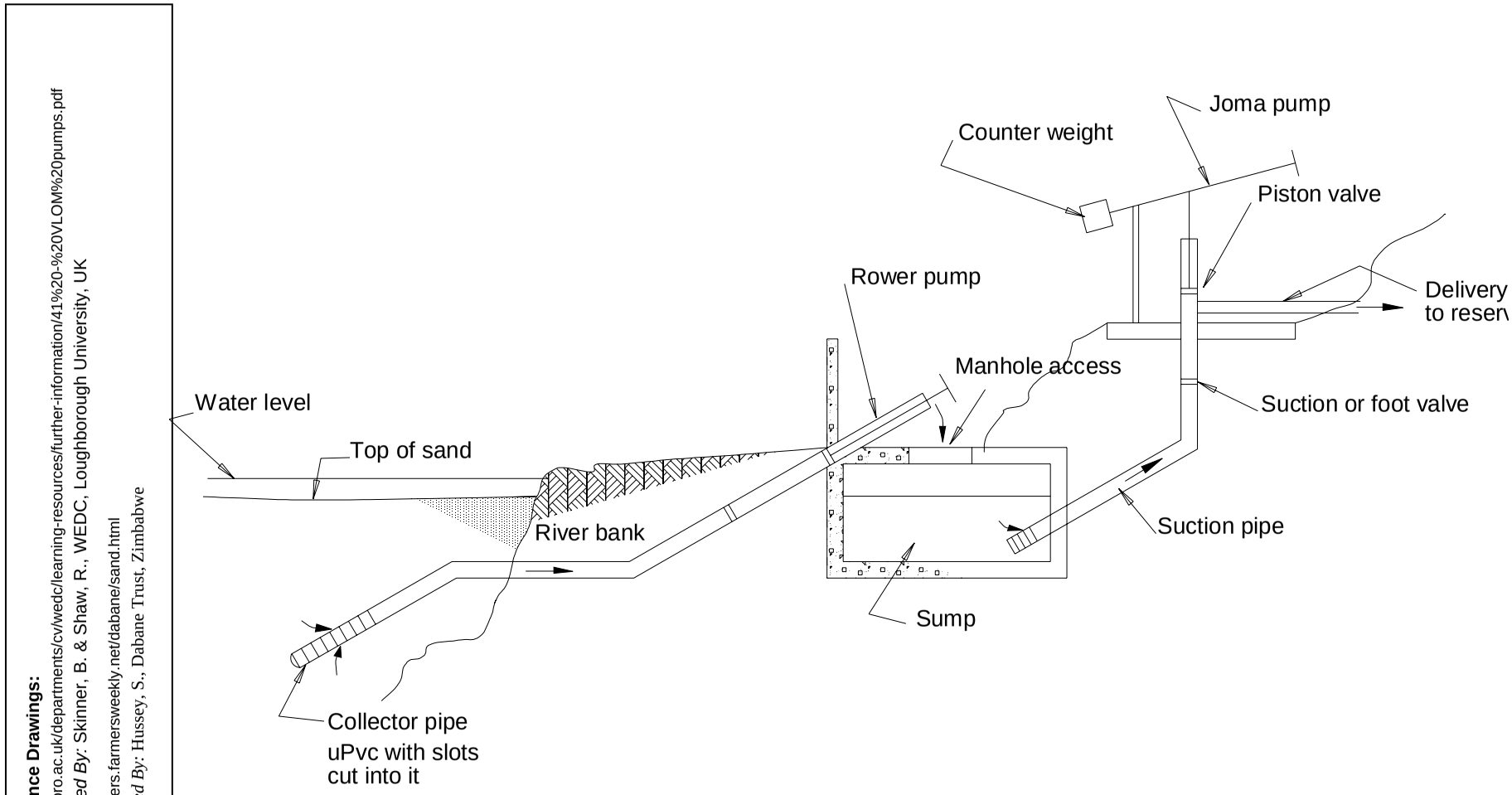

Figure 5-59 Small Scale Hand Pumped Abstraction System

5.5.5 PROBLEMS EXPERIENCED WITH SYSTEMS

Numerous and varied problems are experienced with sand abstraction systems. It must, however, be noted that although problems are experienced at a system, it does not mean that the system is not a successful application of sand abstraction methods. Many systems are well managed, operated and maintained, and measures are taken to prevent and remedy problems that occur in the systems. Thus, successful systems are not necessarily problem free systems, but systems where management and operation controls any problems in the system.

The main types of problems that occur with abstraction systems are:

- *Low Yield*
  The main causes of problems of low yield can be categorised as either one or a combination of the following factors:
  - Reduction in the permeability of the sand, through the accumulation of fines in the sand bed or on the surface of the sand.
  - Clogging of the well screens by iron or manganese precipitate.
  - Clogging of the screens by the development and accumulation of biofilm in the screens.

- *Flood Damage*
  All systems are at risk to flood damage, but in many instances have proven to be surprisingly resilient under flood flow conditions.

- *Operation Problems*
  Problems have been experienced in teaching, or persuading, operators to use sand abstraction systems, as there is an apparent difficulty for the operators to comprehend a system that they are unable to see as it is buried under the ground. Aspects such as this MUST be considered when designing a system. They are, however, difficult to predict.

- *Administrative Problems*
  Administrative problems have been experienced at some of the abstraction systems installed for community water supply in rural areas. These types of problems are not unique to sand abstraction systems. However, in one instance it is believed that the poor quality of the abstracted water has contributed to the administrative problem. The administrative problem has

resulted in the system not being used and standing idle, and this, in turn, has exacerbated the problems experienced with the sand abstraction system. *Other causes of problems of low yield include:*

- Degradation of materials
- Clogging of geofabrics
- Induced stress on the aquifer
- Drop in the level of the water table
- Movement of well screens within the riverbed
- Change of the course of flow of the river within the riverbed

Although systems are sometimes abandoned when problems are experienced with them, many different types of remedial actions have been implemented to improve the performance of systems. Remedial actions can either be preventative or curative.

Remedial actions can range from backwashing systems, dosing systems with peroxide to kill bacterial clogging, to driving herds of cattle into the river to break up a layer of fine sediment caked on the surface of the river bed. The level of success achieved by implementing remedial actions varies considerably, and in some instances it is still very much a case that practitioners are learning by trial and error.

5.5.6 SYSTEM PERFORMANCE

As noted previously, problems of low yield are experienced at many sand abstraction systems. Many of these systems are, however still being effectively utilised through good management and the implementation of remedial actions to improve the yield of the systems.

In general, the performance of small-scale systems is good, with the exception of problems occasionally being experienced with high iron concentrations in the abstracted water. This can be attributed to the fact that small-scale systems do not stress the alluvial aquifer in any way.

The performance of larger systems is varied, with no specific type of system appearing to give better performance than others. The extent of problems experienced tends to vary with geographic location, (associated with the types of sand which occur in specific areas). Fewer problems are experienced with systems in Zimbabwe (coarser quartzitic sands), whilst problems are experienced with virtually all medium to large-scale systems found on the

KwaZulu-Natal Coast, in Lesotho, and in the Northern Province (sands with high fines and clay content, and high iron and / or manganese content).

Problem systems are also associated with particular catchments, notably the Olifants River in the Northern Province, the White Mfolozi River in KwaZulu-Natal, and the Caledon River on the border of the Free State and Lesotho. Problems of a similar nature can also be linked with geographic regions.

Systems can be rated according to the extent of problems experienced at the system. This can be done for the different types of typical problems occurring in sand abstraction systems i.e.

- Low yield
- Biofouling
- Clogging of the sand
- Problems related to high iron and manganese concentrations in the system water.

This rating does not necessarily give an indication of the success or failure of a system, because, as previously mentioned, in many instances the problems are contained through good operational and management practices.

Plotting system parameters (e.g. sand grading) against the system performance ratings, it has been found that numerous system parameters, including water and geographical and geological parameters, exhibit some "correlation" with system performance. In general, where there is a correlation between sand parameters and system performance, these are "wedge-shaped" relationships. By this is meant that for either the minimum or maximum limit of the problem rating, the value of the parameters measured cover the full range of parameter measurements (minimum to maximum). For the other limit of the problem rating, only a small range of the parameter measurements are covered, usually near the minimum or maximum of the parameter measurements.

All can be used as indicators of potential problems, and when considered in combination, a fair assessment can be made of the possibility of problems developing at a system. It can actually not be expected that any single, or even a combination of a few, parameters, could be used to predict system performance. System performance is dependent on numerous interactive factors, each of which is defined by a number of parameters.

5.5.7 SUMMARY

Considering this brief discussion on sand abstraction systems, it can be seen that there are numerous applications for the use of these systems, particularly

where there are problems with high turbidity and sediment loads in waters that are to be abstracted.

These systems have however been shown to be somewhat pedantic and problematic in operation. The secrets of the design of these systems have not yet all been fathomed, despite what any "expert" may tell one. The benefits of using these systems must, however, be weighed up against the possibility of problems arising with the operation of the system. The beauty of using these systems under the correct circumstances and in the appropriate conditions should, however, also not is discarded out of hand.

If considering installing a sand abstraction system, the reader is therefore directed to the report of the study of sand abstraction systems which is currently being completed for the Water Research Commission "*Systems for the Abstraction of Water through River Sand Beds*" by Chunnett Fourie (a division of BKS), and should soon be published under the title "*A Critical evaluation of sand abstraction systems in Southern Africa"*, WRC Project No K5/829. This report will cover aspects from site investigations, through to design information, indications of problem sites etc.

6 EVALUATION OF RIVER ABSTRACTION DESIGNS USED IN SOUTH AFRICA

6.1 INTRODUCTION

Several designs are currently used in South Africa. For farms or small community abstractions it could be a simple layout with a single pump on the bank and suction pipe directly in the river, or more sophisticated with a gravel trap, sand trap and flushing capabilities.

In this chapter some of the typical river abstraction works used in South Africa are discussed. The site conditions at different diversions are unique and often warrants different designs.

The following cases are described in this chapter:

- Pumping from the Orange River from a canalised section
- River bank pumping with axial flow pumps, with no weir
- Design without a weir in a large river (Thukela River)
- Pumpstation with a weir, flushing canals, deep pit sand trap and jet pumps (Sabie River)
- Pumpstation with a weir, flushing of gravel trap and pump canals and sandtrap which can be flushed (Olifants River)
- Diversion with a weir, gravel trap and sand trap which can be flushed under gravity (Berg River)
- Pumpstation with river intake flushing and drywell pumpstation (Keiskamma River)
- Simple sand pumpstation system
- Large sand pump system with infiltration gallery (Komati River)
- Jet pump technology for sand dredging at pump intakes

6.2 UPINGTON WATER SUPPLY SCHEME PUMPSTATION (ORANGE RIVER)

Raw water for the potable water supply to Upington and surrounding areas is withdrawn from the Orange River. The water is drawn from the river via an inlet tower located near the northern bank of the river (Figure 6-1) from where it is pumped to a pre-sedimentation tank before it gravitates through the treatment works.

Orange River water is known to have a high silt load during high flow periods and it also transports large amounts of stone and gravel along the river bed. Catering for this type of material and its associated problems presents a unique challenge.

The existing inlet tower had a wet well equipped with turbine pumps. Apart from not having sufficient capacity, problems were experienced with silt and gravel settling in the wet sump, clogging the pumps and causing damage. Refurbishment of the inlet tower entailed converting the tower to a dry sump pumpstation, thus eliminating a still area where silt and gravel can settle out, and constructing an adjacent channel with downstream control to route low flows past the pumpstation. The new pumps draw water from this channel during low flow.

The pumpstation was equipped with 3 x 155kW immersible pumps which can pump 1.5 m^3/s against 25m of head to the pre-sedimentation tank. Provision was made for a fourth pump in future.

Figure 6-1 Upington pumpstation on the Orange River

6.3 RIVER BANK PUMPING WITH AXIAL FLOW PUMPS

Although promoted recently in SA to provide the solution to all low lift pump problems, they can only be used under very specific protected field conditions with limited sediment and debris. When the motor is stopped water flows back through the pump to flush away any obstructive materials in the turbine and intake

screen. Axial flow pumps can also be installed with an automatic reverse in the motor control panel (Figure 6-2).

Figure 6-2 Axial flow low lift pumps

When sediment and floating debris (even small) enters the suction pipe and clogs the turbine, especially at start-up, it could lead to breakage of the pump axis. This has occurred at several large pump stations in SA in the past. The benefits are large discharge capacity and installations that are relatively high above the water on the river bank.

6.4 DESIGN WITHOUT A WEIR: FAIRBREEZE DESIGN (THUKELA RIVER)

Ticor (SA) plans to extract various heavy minerals from old dune sand deposits at Fairbreeze, some 60 km South of Richards Bay and some 2 km inland from the coast.

The operation will require a continuous supply of up to 0.5 m^3/s of raw water (43 000 m^3/day). Mhlathuze Water has been requested to provide the bulk water supply to the mine. The Thukela River was identified as a possible source of water with the water to be pumped over a distance of 35 km to the mine. Figure 6-3 shows the site of the river pump station.

Particular features of the scheme's proposed design include an abstraction works which is self-scouring under all conditions, capable of abstracting water during very low river flows (but maintaining environmental reserve flows), capable of maintaining operations during major floods and under suspended solid loads of up to 50 000 mg/*l* and of minimal impact on the river bed (no weir or fish ladder required). Extensive hydraulic model testing was carried out to refine the design and verify predicted performance (Figure 6-4). The design uses variable speed drive pumps for maximum efficiency and flexibility of operation. Submersible pumps are used in the river which will pump to a sand trap on the bank, with high lift pumps pumping to a 7 day storage reservoir 150 m above the river from where the water will gravitate towards the mine.

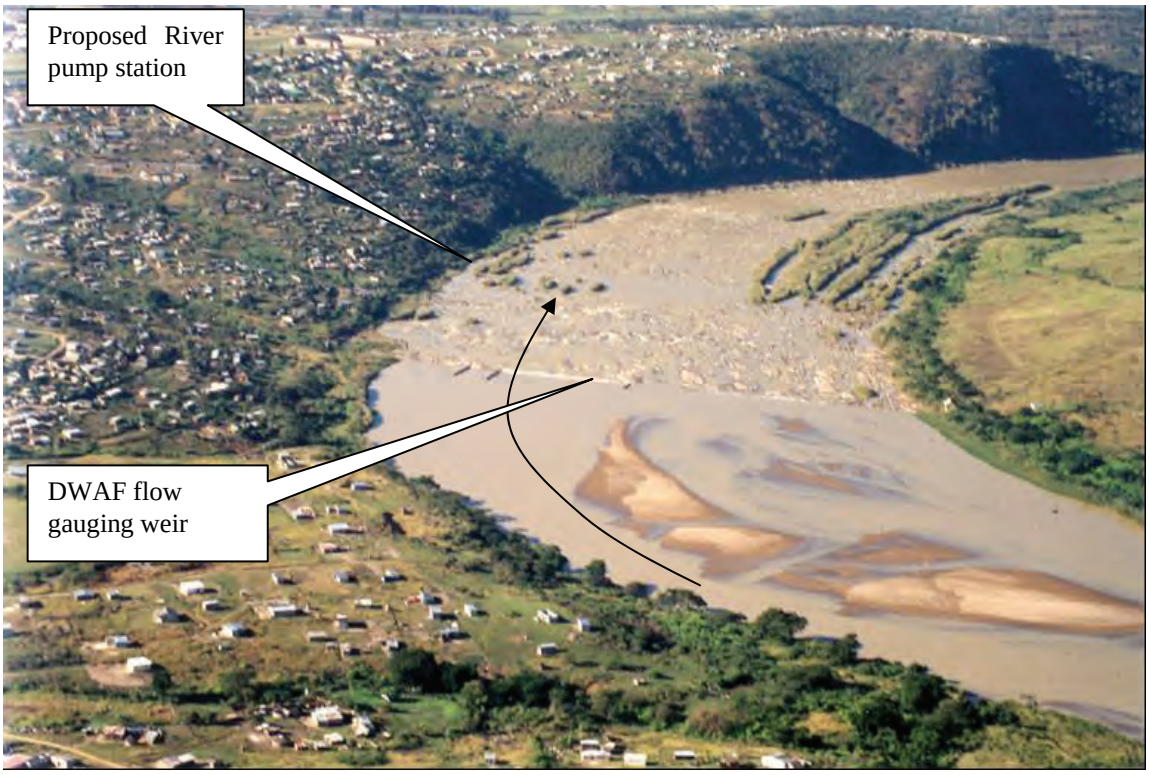

Figure 6-3 Thukela River pump station site

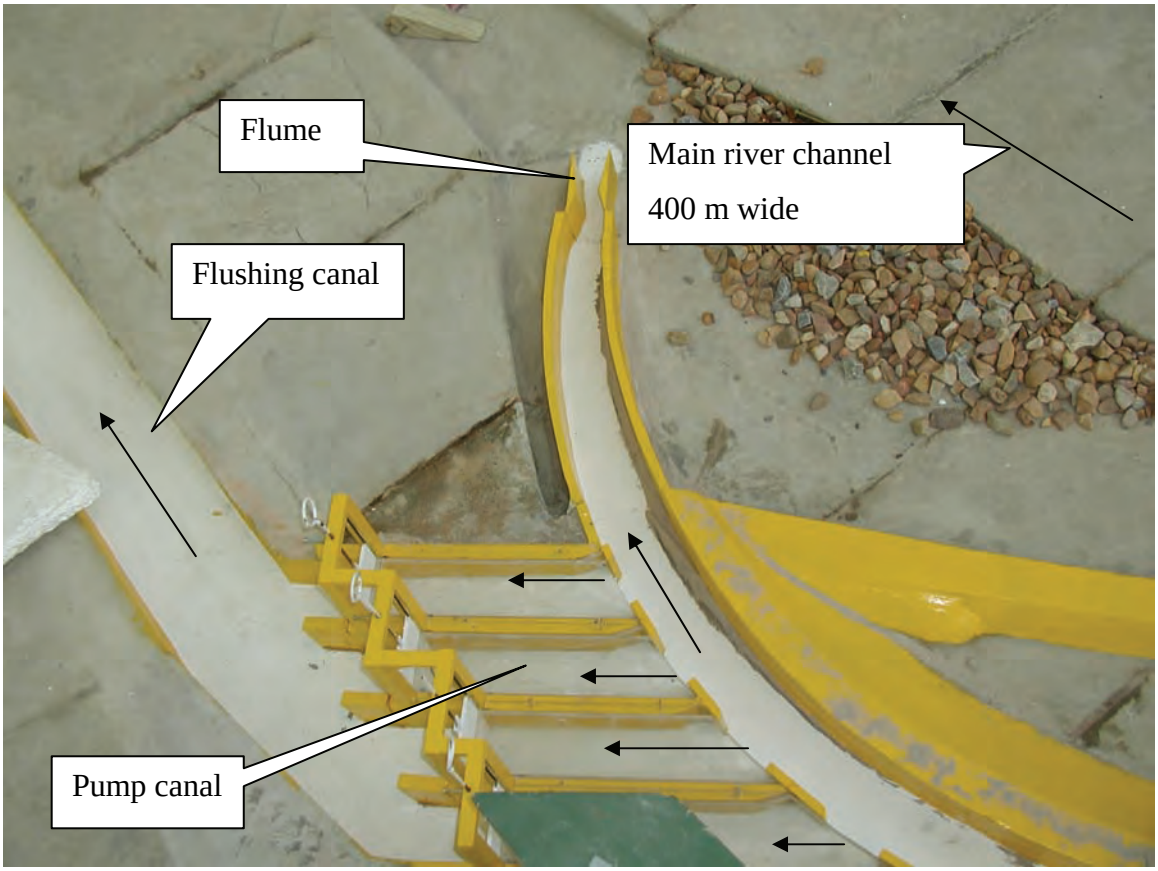

Figure 6-4 Layout of Fairbreeze abstraction works

The location is at the outside of a bend in the river. A curved concrete canal conveys the low flows and water level is controlled by a flume at the end of the canal. This canal is self cleaning at the Ifr flow. The pump canal takes water from this canal and these canals are relatively steep so that they can be flushed. At the end of each pump canal the pumps are located, originally designed to be located in the canal, but later moved to have a dry well with suction from the main pump canal (Figure 6-5). The pump canals are covered to prevent floating debris from entering. Gates at the end of the canals make it possible to flush sediment back to the river through a concrete lined flushing canal. The purpose of the pump canals is to obtain suitable flow conditions at the pumps and to deposit coarse sediment.

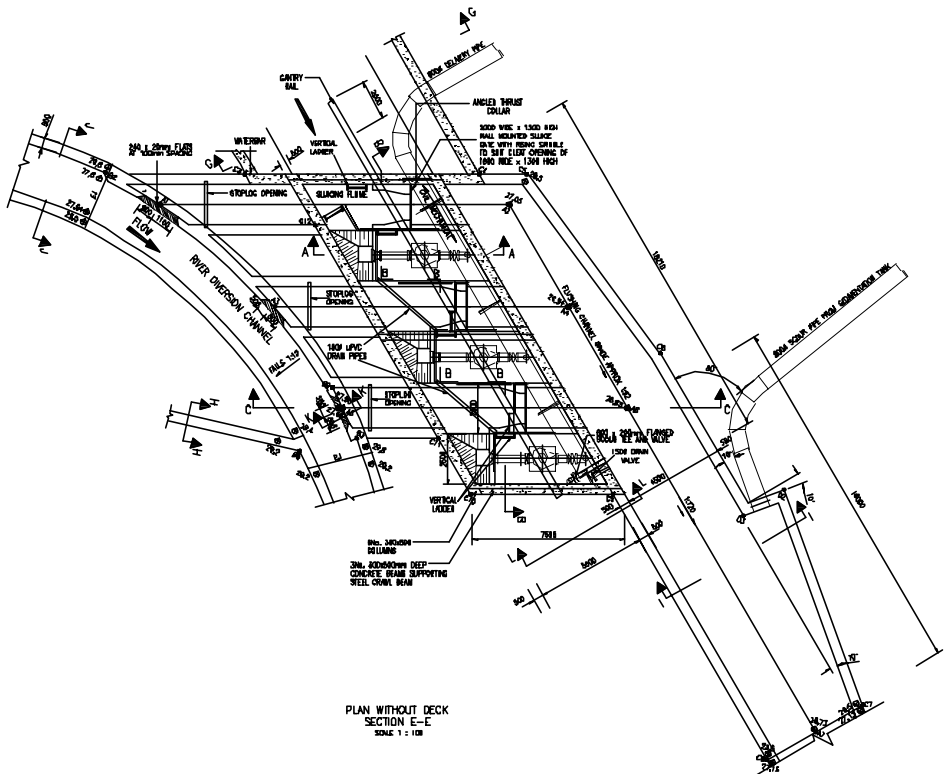

Figure 6-5 Pump flushing channels with dry well pump installation

During the model tests it was found that oscillation in the pump canals can be severe under certain flow conditions. This was solved by narrowing the entrances to the pump canals and by slightly lowering the roof of the pump canals into the water.

6.5 WEIR, FLUSHING CANALS, DEEP SAND TRAP (PIT) AND JET PUMP TECHNOLOGY (SABIE RIVER)

Recently, DWAF favours this design which uses a jet pump to clean the sand trap which forms an integral part of the abstraction works. In February 2003 the Hoxani pumpstation was commissioned on the Sabie River. Figure 6-6 shows the weir across the river with the abstraction works on the left bank. There is also another pumpstation on the right bank, not shown, which is actually on the outside of the bend in the river. Figure 6-7 shows the plan layout of the abstraction works. Water flows into the first canal which now also has a Crump weir at its upstream end, and is diverted to a second canal over a side weir. Both canals have radial

gates that are currently operated in closed position, but can be opened to flush out deposited sediment. The canals are about 23 m in length. From the second canal water is diverted into the sediment pit through a grid in the top of the canal and opening in the side wall. This grid which is submerged acts as trash rack since the specified jetpump can only pump sediment particles smaller than 40 mm. The jet pump uses water from the main pumps to operate.

The sediment pit (Figure 6-8) has a concrete roof slab to prevent sediment entering during floods. The pit has steep side slopes, is excavated in rock and is 7 m deep. The plan dimensions of the pit at the surface is about 9 m x 6 m (width x flow length). With such a short length only coarse sand would settle out. The full width of the pit is also not effective as has been observed in the field. Also typically due to high turbulence the entrance zone is also less effective in depositing fine sand. The effective flow depth at the pumps would be about 3 m, with the result that fine sand (0.03 mm) can reach the pumps when the approaching flow velocity through the pit is about 0.15 m/s.

The pump location perched at the end of the pit is not an ideal layout since the approaching flow pattern is not uniform.

The weir is about 2 to 2.5 m high above the bed level.

The key concerns with this layout are:

- Ineffective (short length and rapid transitions) and expensive sandtrap when about 70 % of the sediment transported during floods is silt and clay.
- Heavy reliance on power supply especially during floods
- Jet pump technology which is not well proven

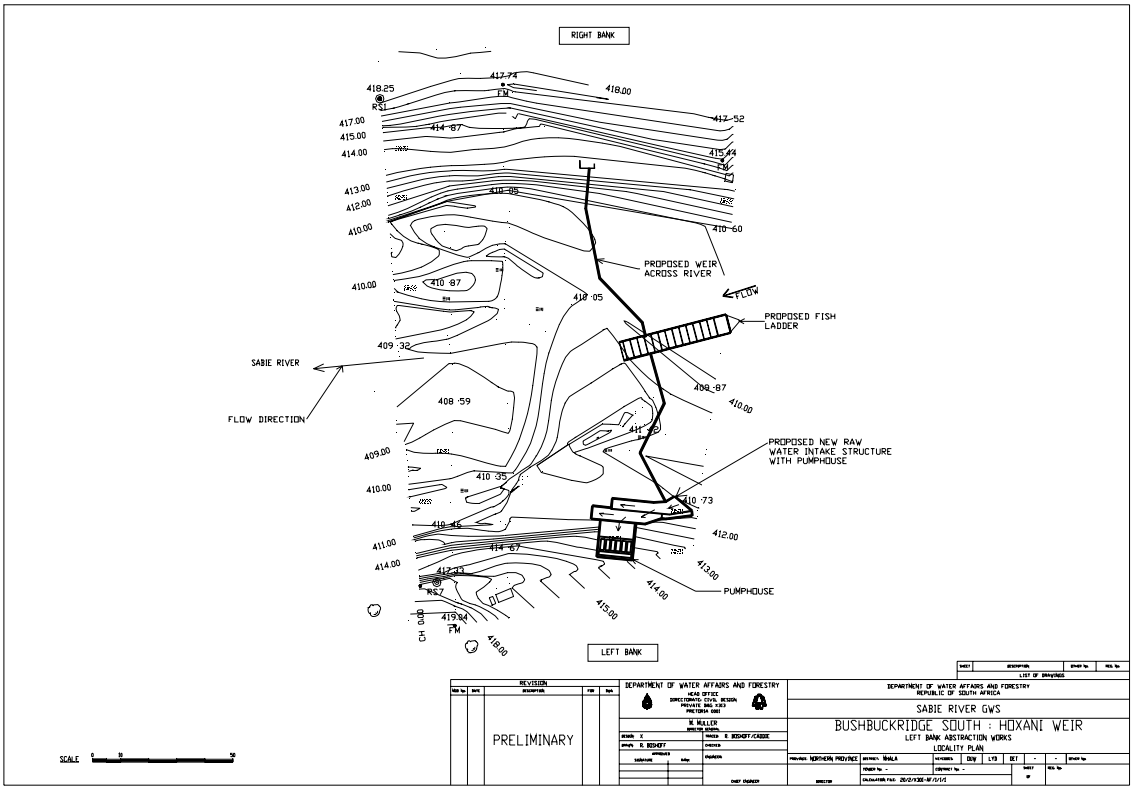

Figure 6-6 Hoxane abstraction works on the Sabie River

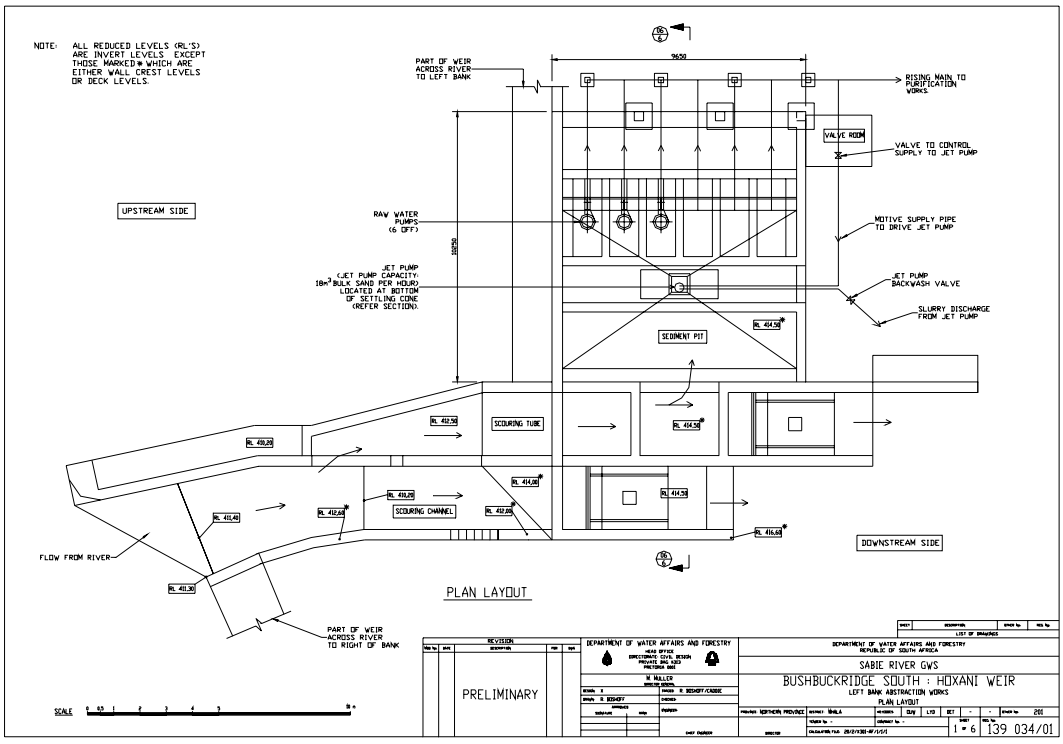

Figure 6-7 Hoxane abstraction works layout

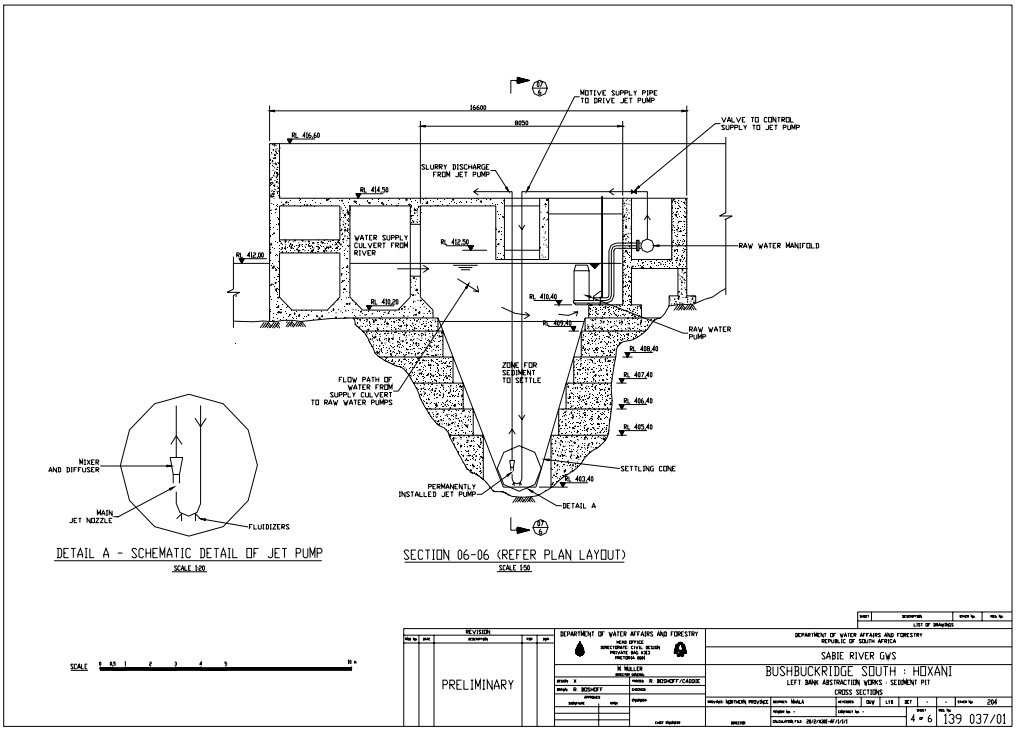

Figure 6-8 Hoxane Sand trap (pit) with jet pump

6.6 ABSTRACTION WORKS WITH TRASHRACK DOWNSTREAM OF GRAVEL TRAP: LEBALELO (OLIFANTS RIVER)

The Lebalelo Water User Association, comprising five mining houses and the Department of Water Affairs and Forestry which represents the communities in the area, require a reliable bulk supply of raw water of 84M*l*/d from the Olifants River near Penge to serve their mining developments along the eastern limb bushveld complex and the local communities. The mines produce platinum group metals, chrome and andalusite.

The pumpstation site is situated on the Olifants River, 400m downstream of the confluence with the Motse River. The catchment areas of the Olifants and Motse Rivers are 34 237km^2 and 820 km^2, while their Regional Maximum Floods (RMFs) are 8400m^3/s and 1800m^3/s respectively.

The pumpstation with submersible pumps, with pump canals which can be flushed, is located on the outside of a 90˚ bend in the river (Figure 6-9).

Figure 6-9 Lebalelo location on River Bend

The concrete weir is approximately 2m above river bed level with foundations approximately 6m below river bed level but with one local area reaching up to 13m. Special attention was also given to protecting the river fauna by making provision for a fish ladder. Water level recording instrumentation was also provided to facilitate the management of the release of water for the ecological reserve. The total cost of the river works was R12 million (2001).

The Lebalelo abstraction works on the Olifants River has a layout with the trashrack located downstream of the gravel trap as shown in Figure 6-10.

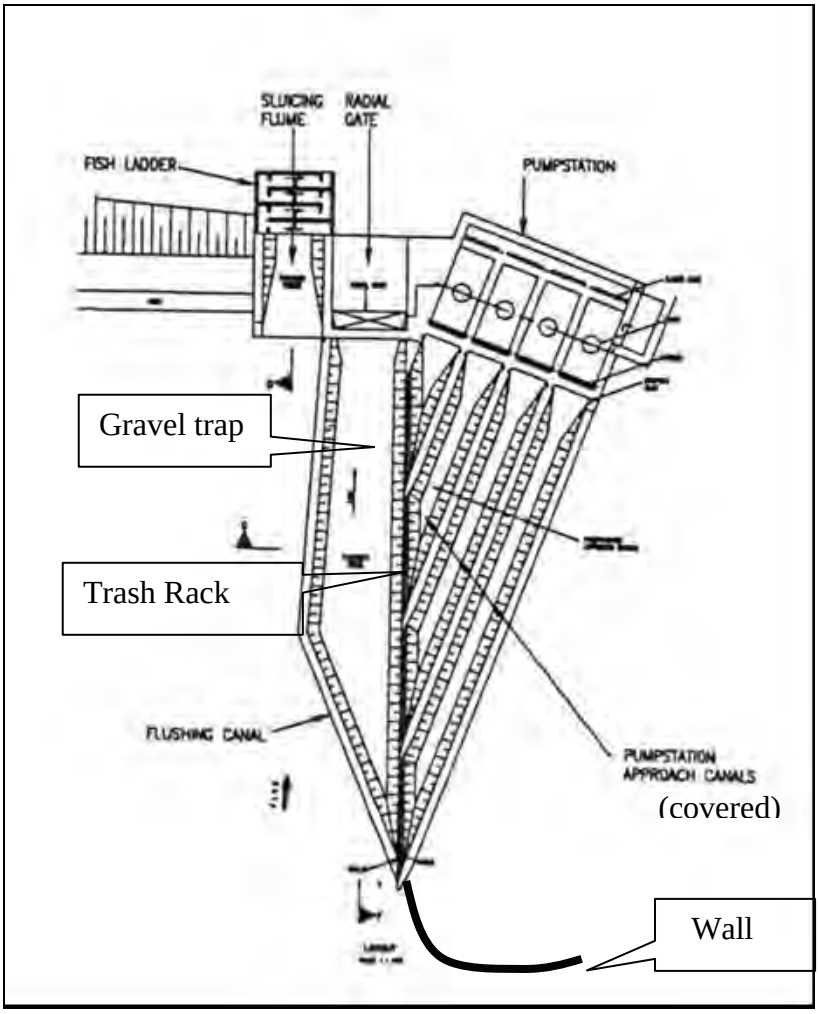

Figure 6-10 Lebalelo pumpstation layout

6.6.1 FIELD DATA OBTAINED AT LEBALELO PUMPSTATION ON THE OLIFANTS RIVER DURING FEBRUARY 2003

Flushing data were obtained during 2003 at the Lebalelo pumpstation. Sediment concentration peaks were high but the duration of flushing was short. The highest observed sediment concentration in the Olifants River was during the 1996 flood when it peaked at 96000 mg/l. Flushing of the gravel trap canal is shown in Figure 6-11 while Figure 6-12 shows flushing of one pump canal, with the observed sediment concentrations sampled immediately downstream of the canals shown in figure 6-13 and 6-14 respectively. The peak sediment concentrations are high during flushing, but the duration is very short and therefore the environmental impact should be limited.

Figure 6-11 Flushing of gravel trap looking downstream

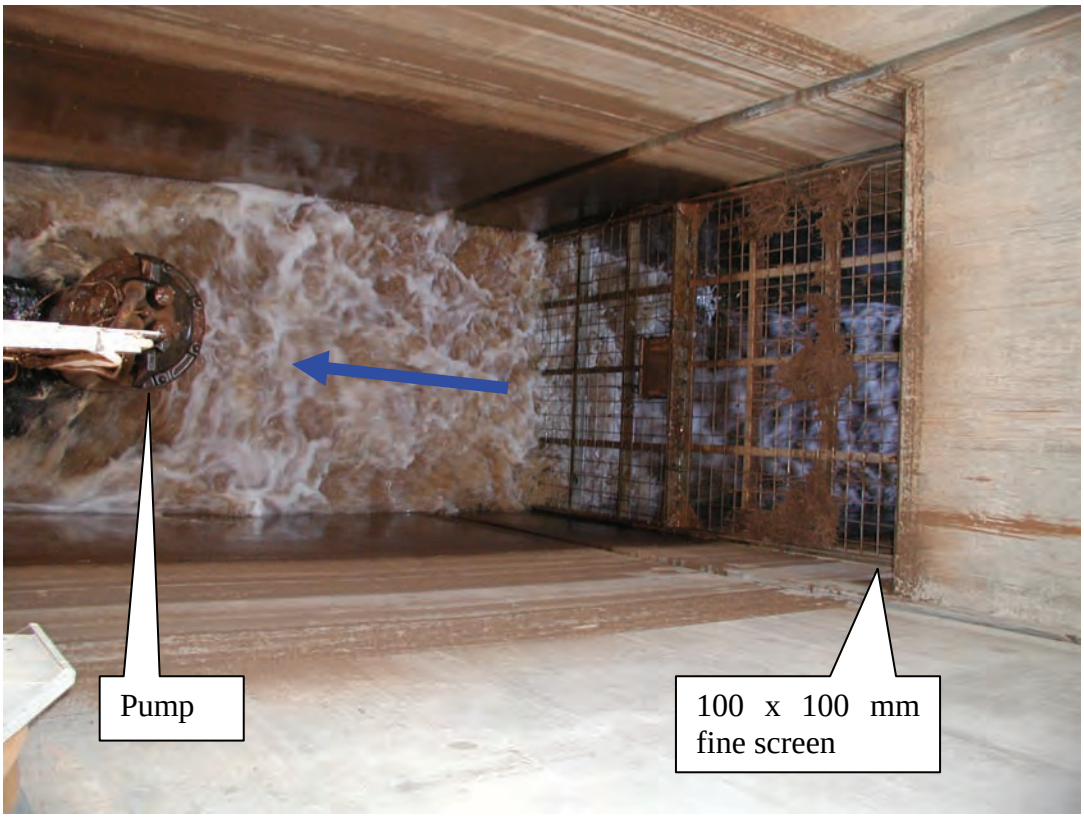

Figure 6-12 Flushing of pump canal viewed from top

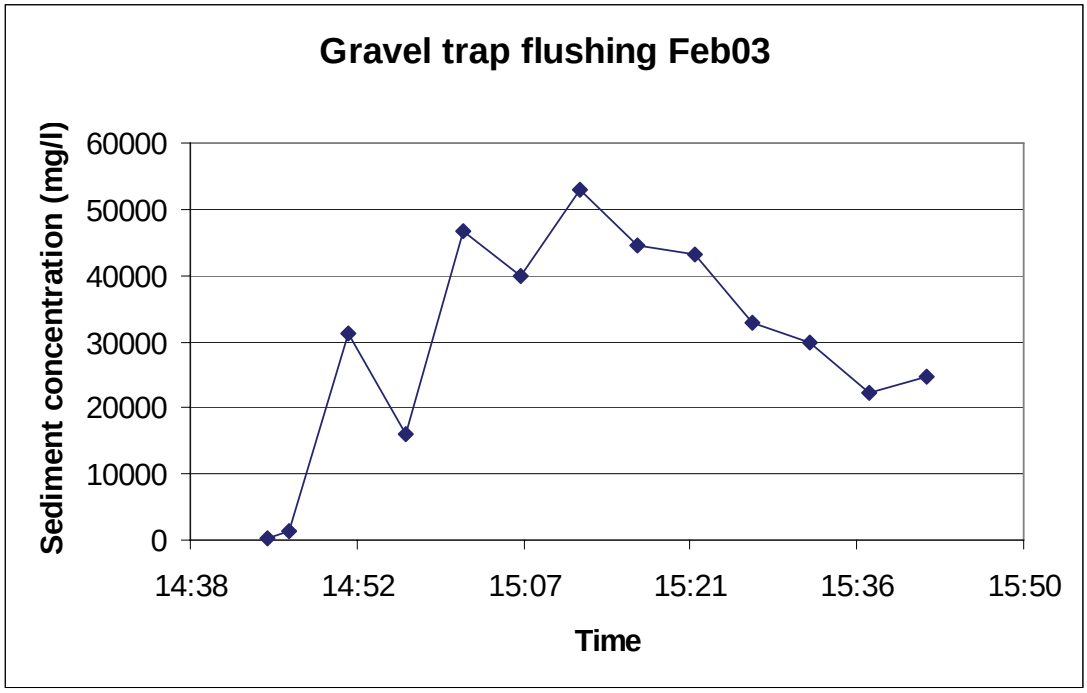

Figure 6-13 Lebalelo gravel trap flushing

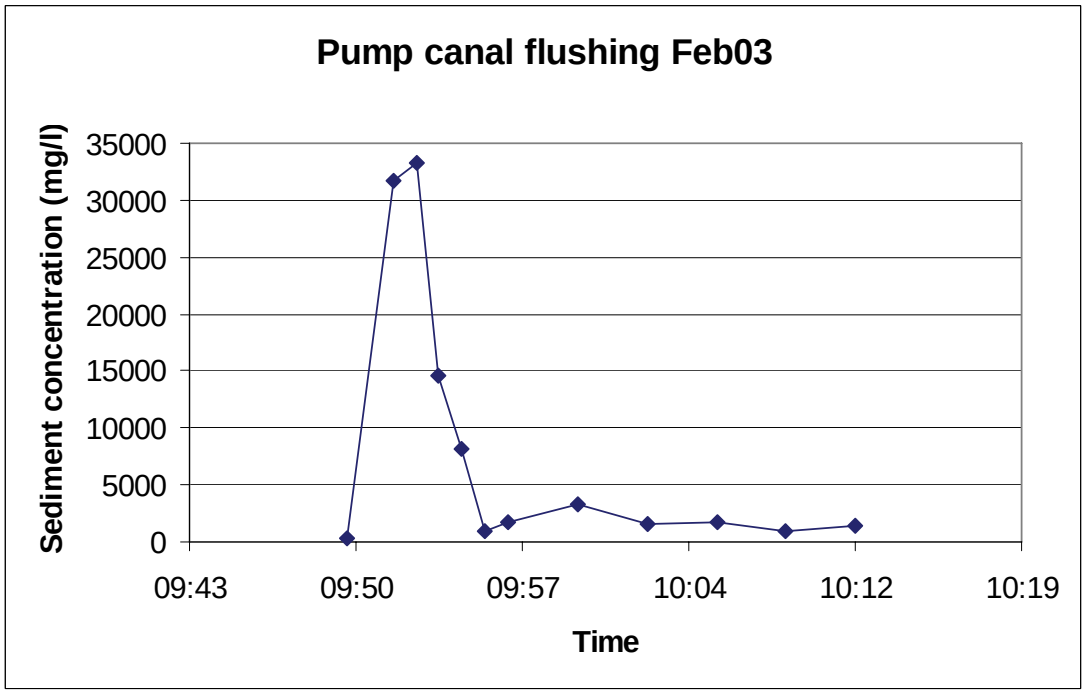

Figure 6-14 Lebalelo pump canal flushing

6.7 RIVER DIVERSION WITH WEIR, GRAVEL TRAP AND SAND TRAP FLUSHED UNDER GRAVITY (BERG RIVER)

The abstraction works proposed for the Berg River has to divert a maximum flow of 6 m^3/s when river flow exceeds the IFR. The works have the following characteristics: (Figure 6-15)

a. Ogee weir and roller bucket stilling basin, best suited for boulder bed river without rock
b. Abstraction works located on the right bank which is the outside of the bend; a stable position was found from aerial photos and model study
c. An Ifr sluice gate to the right of the 65 m long weir that can be controlled to release 0.5 to 10 m^3/s
d. A gravel trap 40 m in length, slightly skew to the flow to generate secondary flow patterns. Inflow to the gravel trap is through a trash rack with 30 mm openings. The gravel trap has a 2 % slope and can be flushed through a 4 m wide radial gate. This gate is usually closed.
e. The wall under the trash rack has a negative slope to allow more flow into the gravel trap at the upstream end during flushing. The gravel trap is also narrower at its upstream end to obtain higher velocities at this end during flushing.
f. The flow velocity through the trash rack < 0.5 m/s to allow fish to swim back to the river if they are diverted.
g. Six sand trap canals 3.76 m wide each and 50 m in length are provided. At the downstream end of each canal the water has to spill over a vertical gate and 3 m long openings in the side walls. This gives a hydraulic control length of about 40 m at the end of the sand trap which makes the diversion highly effective. Diverted water flows under gravity to the balancing dam 150 m from the abstraction works.
h. Gates are required at the upstream end of each sand trap to limit flow during floods when flushing the sand trap. The sand trap canals should be flushed one at a time during a high flow period in the river, at a minimum flushing flow of 2 m^3/s. Flushing is carried out by opening the flushing canal gate and the gates at the sand trap.

i. Proposed operation of the gates are as follows during diversion in winter (high flow period):

i. The IFR gate is adjusted to the required flow once per month

ii. Water is diverted under gravity to a maximum of 6 m^3/s which is limited by the diversion canal gate. This gate also closes when the balancing dam is full. When the diversion reaches 6 m^3/s and the river flow increases, the IFR gate drops (hinged at the bed) but comes up again when the flow decreases and the process is reversed. The IFR gate therefore also has a local flushing effect. Although several automatic gates are required, there is no risk of damage or loss of life when a gate fails to open or close; it will only lead to a decreased diversion efficiency.

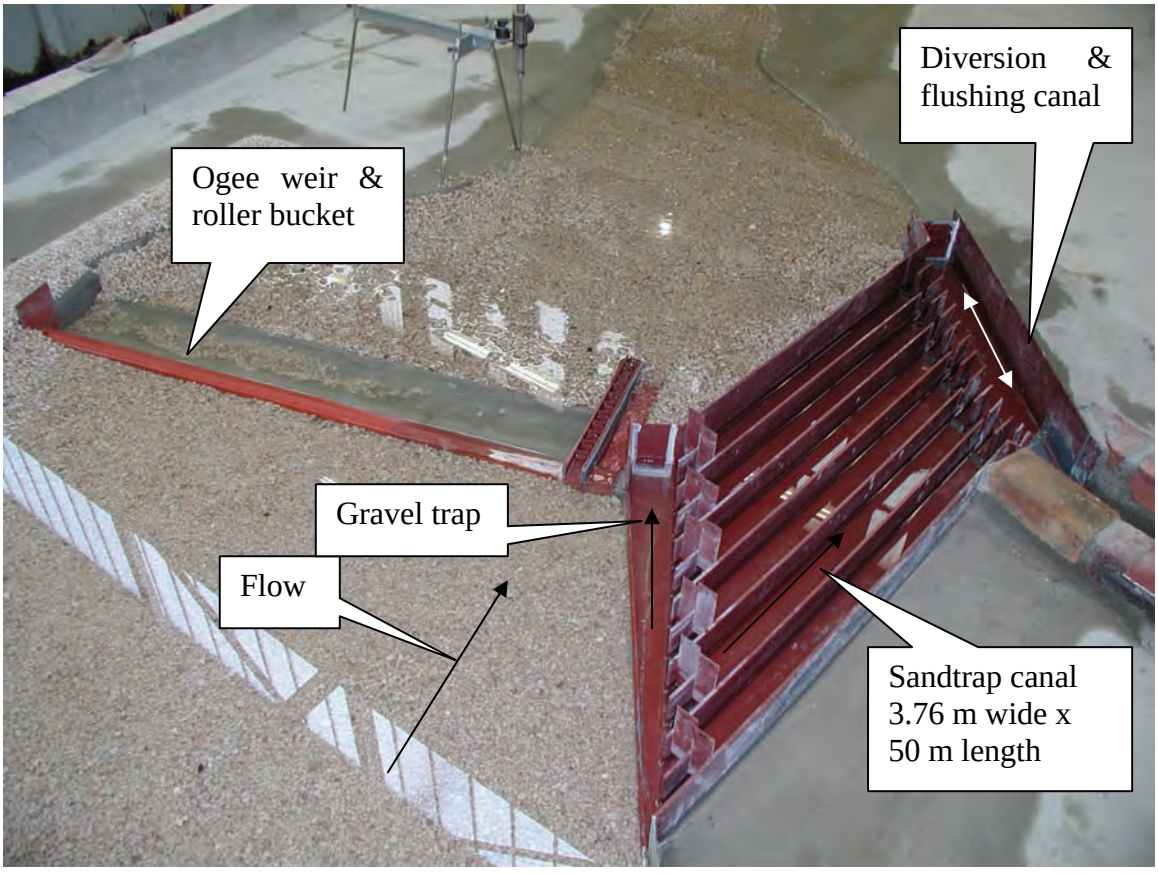

Figure 6-15 Proposed Drakenstein abstraction works on the Berg River

6.8 CRAIGHEAD PUMPSTATION ON THE KEISKAMMA RIVER

The existing river pumpstation was located on the right bank, upstream of a weir. Although the pumpstation was located on the outside of the bend, the curvature of the bend upstream of the pumpstation caused a dead zone near the intakes and sediment deposition. The intake was recently reconstructed by Amatola Water, as shown in Figures 6-16 and 6-17.

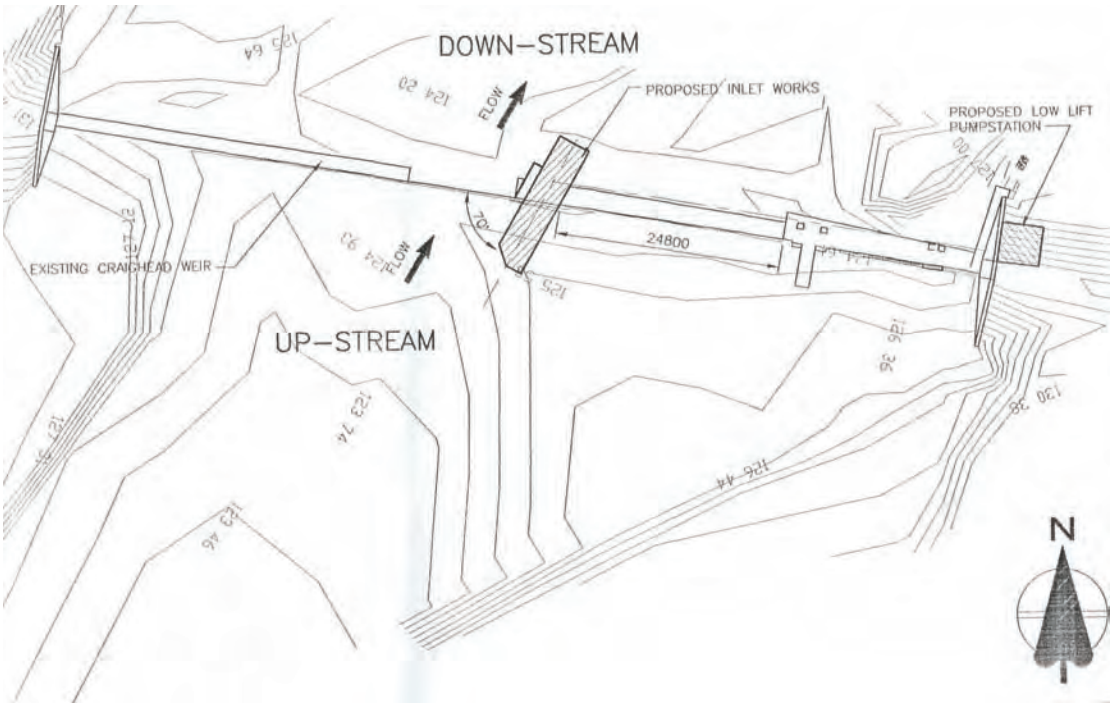

Figure 6-16 Layout of new river intake on the Keiskamma River

Figure 6-17 Craighead intake structure and weir

The raw water intake is positioned midstream on the weir with four sluices and an automatic Fulton type scour gate. A 350 mm diameter steel suction pipe of about 60 m length conveys the water to the right bank dry well pumpstation, where 3 Gorman-Rupp T8A3-B self-priming centrifugal pumps with 37kW Siemens motors pump the water to a settling tank at the high lift pump station at a design discharge capacity of 160 *l*/s. The impellers of these pumps can handle 76 mm diameter spherical solids. (Figure 6-18)

The reinforced concrete raw water intake structure is positioned over the existing weir about 45 m from the right bank. The intake structure consists of three chambers namely (Figure 6-19):

Figure 6-18 Craighead river pumpstation

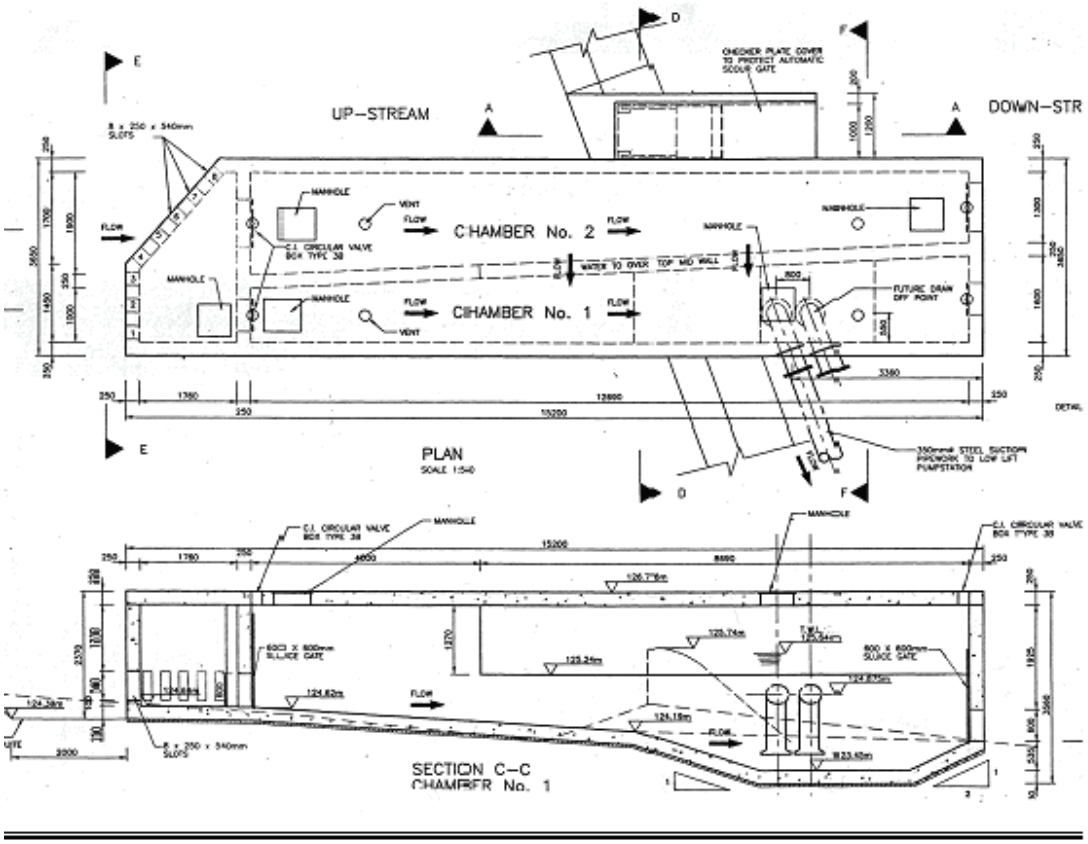

Figure 6-19 Design drawings of the river intake on the Keiskamma River

- The inlet chamber. This chamber forms the upstream end of the structure and has eight 250 mm x 540 mm inlet slots positioned 400 mm below the weir level. The outlet to this chamber is under normal operation via a 900 x 600 mm sluice into the primary chamber. The inlet chamber can also drain into the secondary chamber via a 600 mm x 600 mm sluice. This should only be done when the pumpstation is shut down and the downstream sluice of the secondary chamber is open for the purposes of scouring.
- The primary chamber. This chamber receives water from the inlet chamber via a 900 mm x 600 mm sluice. The water is transferred from this chamber to the secondary chamber via an internal weir. The primary weir also has a tapering width to facilitate an even flow distribution over the weir and thereby promoting settlement of suspended solids.
- The secondary chamber. Under normal operation the chamber receives water from the primary chamber via the internal weir. The chamber can also receive water from the inlet chamber via a 600 mm x 600 mm sluice. This should only be

opened when the pumpstation is shut down and the downstream sluice of the secondary chamber is open for the purpose of scouring.

The flushing of the primary and secondary chambers are carried out at least once a week and possibly more often after periods of heavy rainfall. During periods of low river flow the flushing is cautiously monitored to ensure that the weir pool is not drained.

An automatic gate is fitted next to the intake structure and is designed to open and close automatically. In its normal position, the gate remains closed under self-weight and seals off the scour tunnel (Figure 6-20).

Figure 6-20 Automatic gate viewed from downstream

The gate is normally closed. As the water level rises to the predetermined level, currently the top of the low-level weir notch, water flows into the inlet weir and

discharges into the float chamber through the inlet pipe. The rate of flow from the inlet pipe into the float chamber will exceed overflow from the permanently open discharge pipe and the water level will rise in the float chamber.

When the water depth in the float chamber is approximately 0.4 m, the gate will start to open automatically and will continue to open as more water flows into the float chamber, until the gate is fully open. As the water level recedes below the inlet weir level the inflow into the float chamber will decrease and finally cease to flow. The outlet from the float chamber will discharge the water from the float chamber and the gate will close automatically against the flow of water in the scour tunnel until it closes completely and seals off the scour tunnel. The automatic gate does not require regular manual intervention unless maintenance is to be carried out.

Evaluation of this design:

Benefits:

- Intake well protected during large floods and submerged
- Pumps well protected on the bank and can deal with coarse sediment
- The intake slots are placed below weir crest level to reduce clogging of the intake slots by small floating debris.
- Intake structure orientated to minimize impact on flood flows and sediment deposition upstream of the weir.

Possible disadvantages:

- Can only flush intake after floods, not during.
- Upstream and downstream gates required for flushing
- Long suction pipe with risk of blockage with fine sediment
- Intake slots located 10 m upstream of automatic gate and it is doubtful whether scour will occur this far upstream due to this gate, and it will probably only be effective when the weir level is drawn down, in which case scour along the left flank of primary chamber is expected, with limited scour at the slots.
- The intake slots are located on the upstream end of the intake structure to improve flushing conditions and for improved sediment deposition in the primary chamber,

and also in a good position for local scour during a flood, but debris such as trees could wrap around the upstream end of the intake and cause blockage.

- Pipe inlet in secondary chamber is 0.54 m deeper than the outlet gate invert which could make it impossible to flush out coarse sediment that reaches the hole at the inlet during flushing.

6.9 SIMPLE SAND PUMP SYSTEM: GABION STRUCTURE WITH CONCRETE SLAB

Such structures have apparently been used for many years in the Eastern Cape in sand bedded rivers. (Figure 6-21)

Figure 6-21 Small pumpstation consisting of gabion boxes and concrete slab

If the bidim wrapped around the gabions is used as filter to keep fine sediment out of the gabions, then it will quickly clog which will limit the flow of water. Access to the pumps in the water is difficult. During low flow conditions the low flow channel could be far away from the intake. This layout will only be suitable for very small pumpstations where the required assurance of supply is low.

6.10 MAGUDU SAND PUMP SYSTEM WITH INFILTRATION GALLERY ON THE KOMATI RIVER

6.10.1 BACKGROUND

This irrigation pump station constructed recently on the Komati River in Mpumalanga, supplies 373 ha irrigation to the Mawewe tribal authority. It consists of 2 parallel pumps on the river bank, with each having a set of 4 suction pipes located in

the river bed (Figure 6-22 and 6-23). Two KSB Omega 250 – 600 A's were installed with a duty point of 777m³/h @ 115m each. The total pump capacity is 432 *l*/s.

The 300 mm diameter suction pipes located in the alluvial river bed are each 42 m long and about 3 m apart.

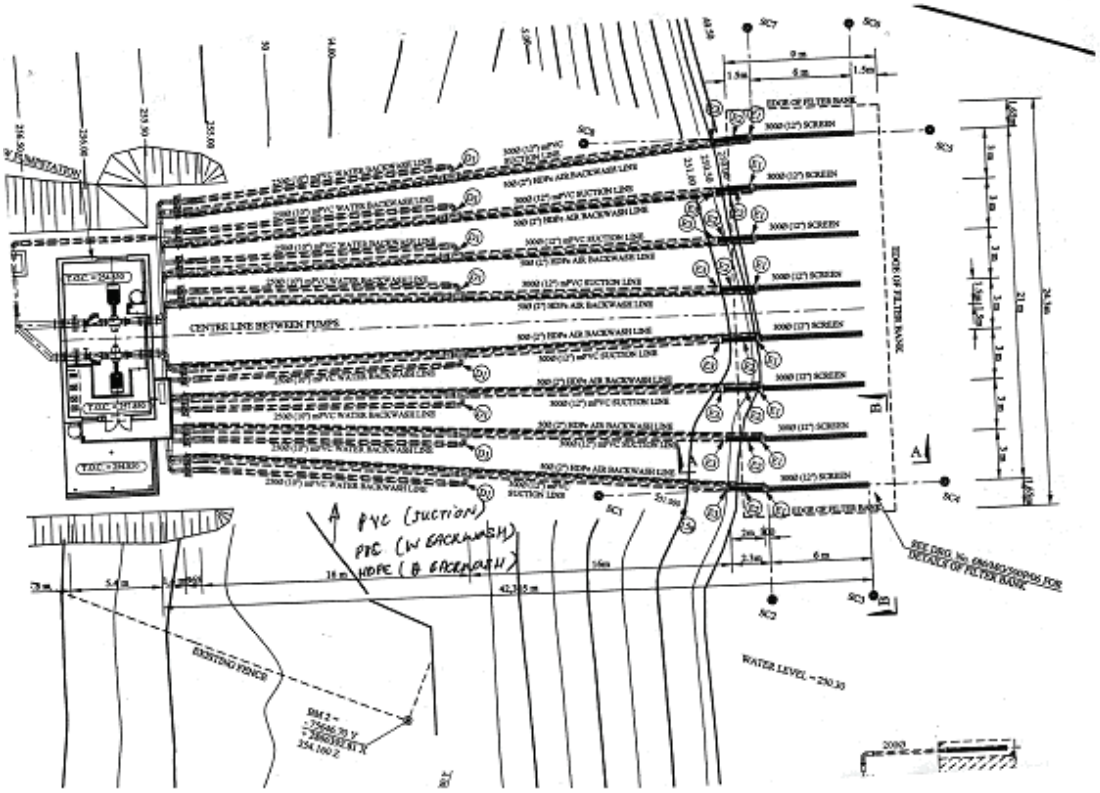

Figure 6-22 Layout of sand pump system at Magudu, Komati River

Figure 6-23 Magudu suction pipe system under construction (Burger du Plessis)

In the river bed, the river sand is replaced to a depth of 1.7 m by a filter (Figure 6-24) layer consisting of:

- 0.9 m layer of coarse 6.7 mm gravel around the suction pipes
- 0.7 m layer of 2.4 to 4.8 mm sand filter on top of gravel layer
- 0.1 m layer of in situ river sand

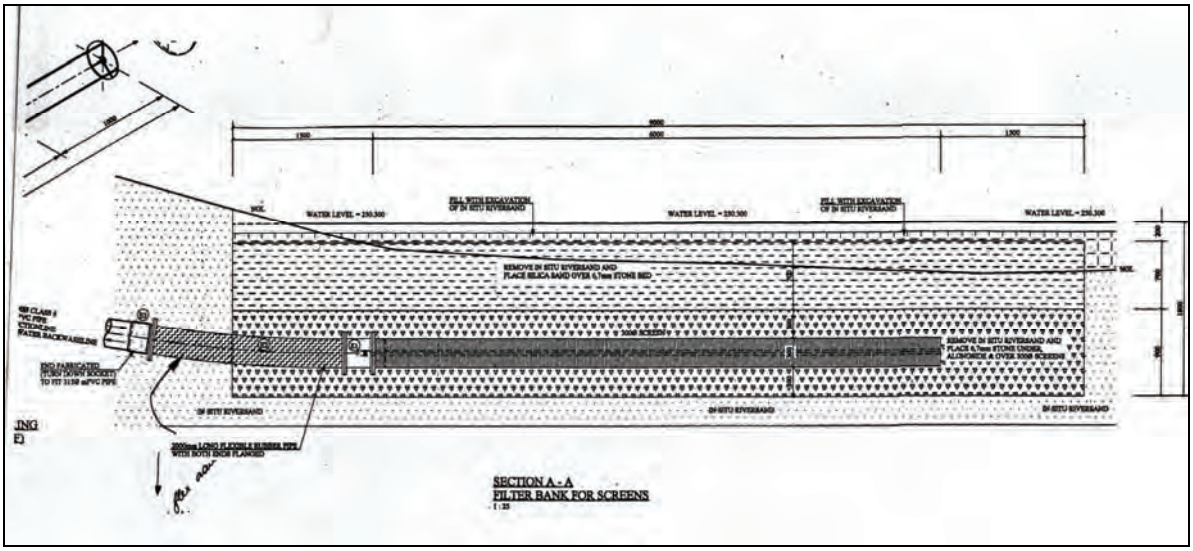

Figure 6-24 Magudu infiltration gallery design

Fine silt and clay have deposited through the filter layer and blocked the openings of the suction pipes. But this has been catered for in a backwash system. The system is backwashed every day for one hour with a 50% water and 50% air mixture at a rate double the pump delivery. The mixture is pumped through a 50 mm diameter pipe which is located centrally in each of the suction pipes, to further clean the graded filter around the pipe.

The benefits of such a design are:

- the pumps can be placed relatively far away from the river on the river bank, well protected from floods, with limited risk of blockage of the intake pipes
- no weir is required or hydraulic structure in the river

Concerns are related to floods:
No large floods have been experienced since operation of the pumpstation started, and this is probably the biggest concern with the design. On the Komati River in 2000 the water depth was recorded as 15 m deep by DWAF during a major flood. The maximum dune height that formed in the river would have been in the order of 15/6 = 2.5 m which is deeper than the 1.7 m depth of the filter layers. Also general scour of the river would occur during a flood and the gravel filter layer would be resistant to re-entrainment like a broad crested weir, but immediately downstream of the gravel, river sand could be scoured forming a deep hole and retrogressive erosion will cut back upstream into the filter material. Damage to the suction pipe system is therefore quite possible during a future flood event.

6.10.2 IMPORTANT DESIGN CRITERIA FOR INFILTRATION GALLERIES

A major design principle for infiltration galleries involves the orientation of the screen relative to the surface water or groundwater flow directions. For bed-mounted galleries, the screen is oriented perpendicular to the stream flow. For bank-mounted galleries, the screen is placed perpendicular to the groundwater flow to minimize the head loss; that is, the screen is placed parallel to the stream or river.

Important design criteria of infiltration galleries include:

a) Entrance velocity through the screen slot openings should be 0.03 m/s or less.

b) Axial velocity inside the screen should be 0.9 m/s or less, so that the head loss, h, will be 0.3 m or less. The following equation is used to determine flow velocity:

$$V = \frac{1.16x10^{-3}Q}{\pi r^2} \qquad (6\text{-}1)$$

Where

V = velocity, in m/s

Q = yield, in m^3/day

R = radius, in m

c) Screen slot size is based on the grain-size distribution of the filter pack; always retain 100 percent of the filter pack.

d) Use 304 stainless steel for fresh water, and 316 stainless steel or monel for salt water. Do not use monel if the Ryznar stability index is 9.5 or greater.

e) Filter pack recommendations:

- The surface area of the filter pack material is determined on the basis of water entering the pack at a rate of 117 to 293 m^3/day per m^2 of surface area. The actual hydraulic conductivity of the pack is usually much higher.
- Filter pack design is similar to that for a vertical well, but with a slightly more liberal multiplier of 6 to 7 times the 70-percent-retained size.
- Filter pack material should be clean, siliceous, rounded and uniform.

6.10.3 BED-MOUNTED INFILTRATION GALLERIES

Typical screen configurations for bed-mounted in infiltration galleries are shown in Figure 6-25. Design criteria applying specifically to bed-mounted galleries include the following:

a) The screen burial depth should be 0.9 to 1.5 m below the stream bed. There should be 0.3 m of filter pack beneath the screen.
b) To minimize excessive sedimentation on the gallery surface, the stream selected should have a velocity of at least 0.3 m/s.
c) Space the screens approximately 3 m apart. Refer to Figure 6-26 for a typical design configuration and suggested dimensions for positioning screens in the infiltration gallery.
d) If the stream has a large bed load transport, a single screen should be oriented parallel to the bank, but not in the main channel if possible.
e) Screens should always be placed in the straight reaches of the river or stream, not near the meander bends to limit scour

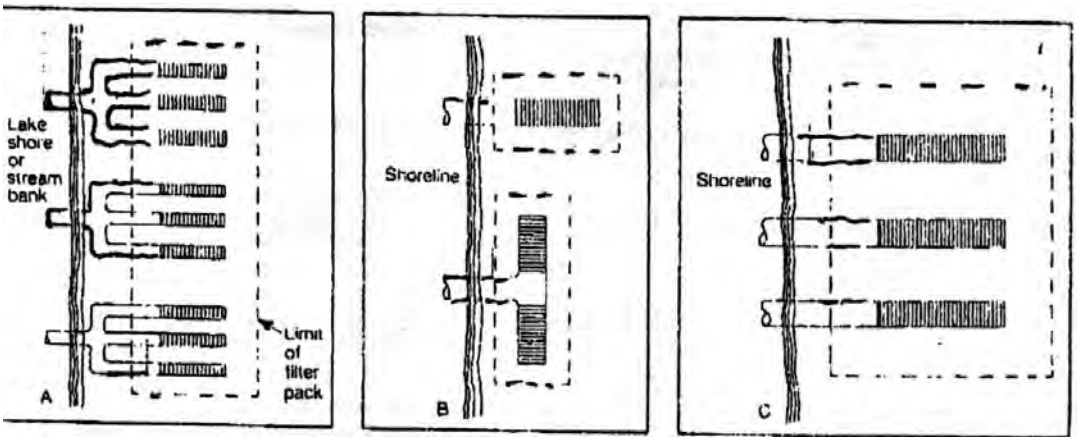

Figure 6-25 Screen arrangements for bed-mounted infiltration galleries

Field experience indicates that actual infiltration rates from streams and lakes range from 0.5 to 3.1 m^3/day per m^2 per m of head loss (Walton, 1963; Bennet, 1970). In general, the infiltration rate will be high when the stream gradient is steep and the bed load is coarse. Infiltration rates from lake beds will ordinarily decrease more with time when compared with streams, unless wave activity is particularly vigorous and the bottom is continually disturbed so that fine sediment cannot settle. Wave energy can be transmitted to the bottom if the water depth over the gallery is less than one-half the typical wave length (distance from wave crest to wave crest).

The screens and filter pack material used for infiltration galleries may become partially plugged with sediment over time. Thus, it is good engineering practice to

estimate the plugging potential and allow for excess entrance area to maintain the required flow. To maintain yield over time, the actual open area of the screens should be twice the required open area, that is the screen length should be doubled. Backwashing capabilities may be specified for some infiltration galleries. The flushing rate is usually twice the pumping rate for the screen configuration. For example, if a series of three infiltration gallery screens were producing 16 400 m^3/day each screen should be backwashed at a rate of 10 900 m^3/day. Backwashing techniques include (1) gravity backwashing, (2) piping and valve systems to pump from several screens while backwashing others, and (3) air back flushing.

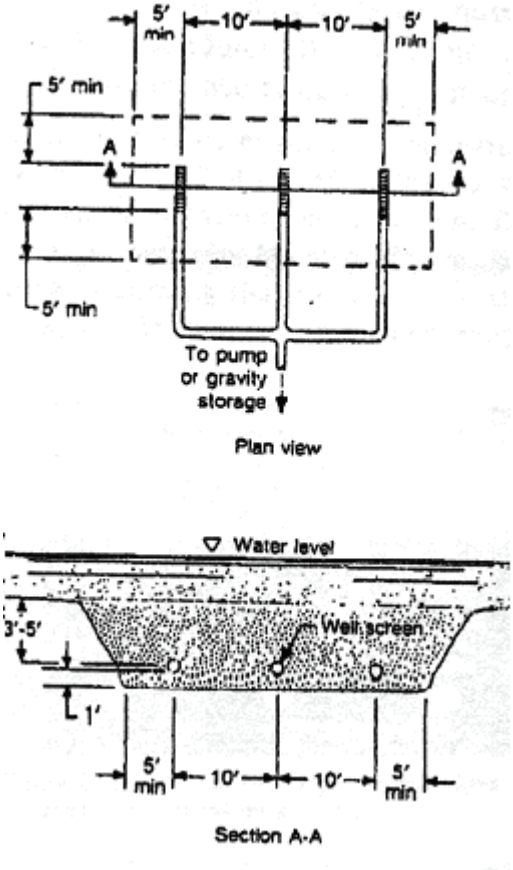

Figure 6-26 Standard spacing and depth setting for infiltration gallery

6.11 JET PUMP TECHNOLOGY FOR SAND DREDGING AT PUMP INTAKES

Jet pumps have been used for maintenance dredging at ports in South Africa over many years. The benefit of these pumps are that no moving parts come in contact with the sediment. Clear water is pumped through a nozzle into a mixing chamber where

water and sediment mixes for transport through a pipeline (Figure 6-27). Water jets can also be used to loosen sand. A jet pump is generally not as efficient as a centrifugal pump.

In a recent research project sponsored by the WRC, jet pump technology for the removal of sand at DWAF pumpstations in Mpumalanga was investigated (Bosman et al, 2003).

Where pumpstations are not located and designed properly, the pool where water is abstracted from could fill with sand. Jet pump technology could help to remove the sediment, as shown in Figures 6-28 to 6-30, with fixed or movable installations. The jet pumps are driven by water from the main pumps in the pumpstation.

The field tests by DWAF showed that dredging with a jet pump is expensive and should be seen as a last resort. Added to this is also the problem of disposal of dredged material (Figure 6-31).

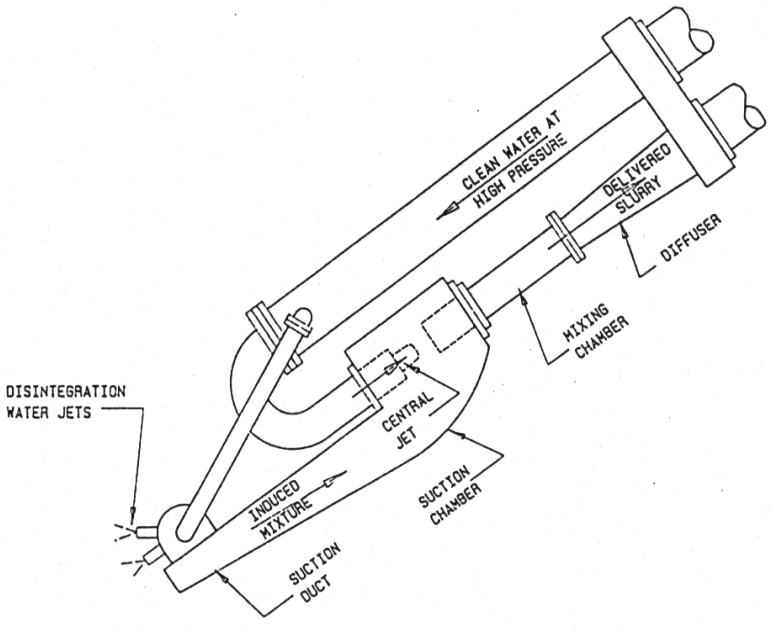

Figure 6-27 Jet pump technology (Bosman et al. 2003)

(a) Jet pump motive supply tap off from raw water discharge pipe in foreground and installed fixed jetpump in background.

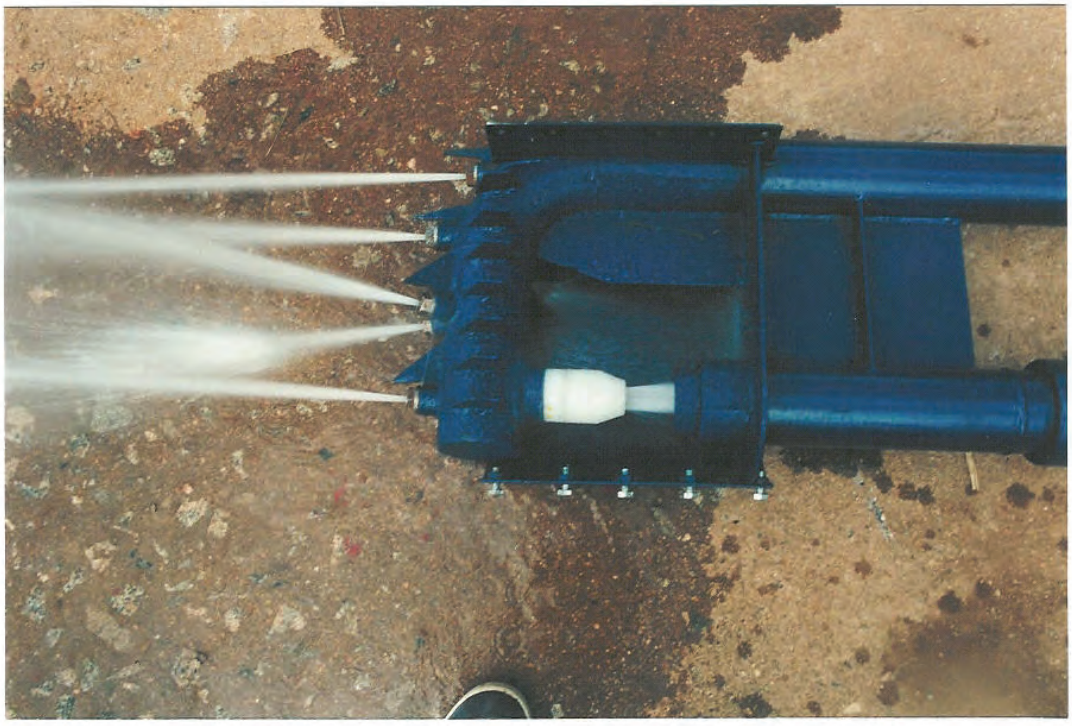

(b) Close up of activated GENFLO SANDBUG ® activated showing main and fluidizer/disintegrater nozzles. (half of cowl removed).

Figure 6-28 Movable jet pump operating to create pool (top) and jet pump with nozzles (bottom) (Bosman et al, 2003)

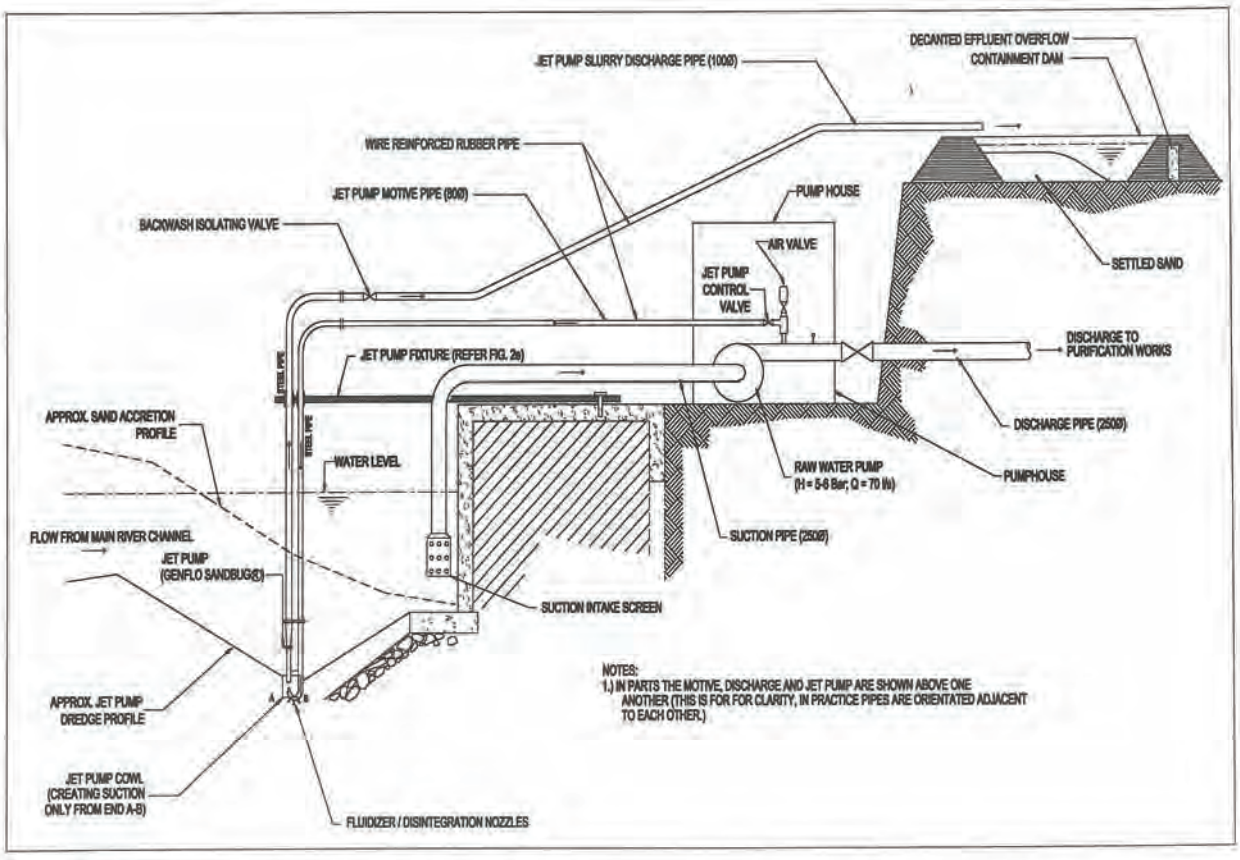

Figure 6-29 Typical design of a fixed jet pump test system at a river pump station (Bosman et al., 2003)

Figure 6-30 Mobile jet pump system mounted on trailer in operation (Bosman et al, 2003)

Figure 6-31 Dredged material disposal creates ecological problems and is expensive.

7 SEDIMENT DYNAMICS AND WATER INTAKE DESIGN

7.1 SEDIMENT CHARACTERISTICS IN SOUTH AFRICA

Sediments transported in South African alluvial rivers during floods are relatively fine with say 40% clay, 40% silt and 20% sand transported in suspension. Due to this grading the vertical and horizontal sediment distribution at a cross-section in the river is quite uniform. Mountainous reaches and the Western Cape however differ from this with more bed load transport.

The typical sediments found in river beds after floods are fine sand, with medium diameters of 0.2 mm to 0.5 mm. Silt and clay is however added to the river system from the catchment during storm events.

Where sediment loads consist mainly of fine sediments (silt and clay), the loads are generally found to have limited availability from the catchment. This means that there is a poor correlation between the discharge and the corresponding sediment transport capacity, and actual sediment transport. The fine sediment loads are highly variable from year to year and long term annual loads. Average annual data from historical daily grab sampling in many large South African rivers are available prior to the 1970's. This data can be used to determine how quickly a diversion weir will silt up, but more detailed data such as peak sediment concentrations are required to determine for example the sand trap dimensions. Where local data on suspended sediments are not available, estimates can be made based on regional sediment yields (Rooseboom et al, 1992) at smaller abstraction works. Annual flood sediment concentrations are typically less than 20 000 mg/ℓ, while on rivers with high sediment yields the concentrations could go up to say 40 000 mg/ℓ during a 1:10 year flood, and to say 60 000 mg/ℓ during an extreme event such as the 1:50 year flood. The concentration peak duration is however usually short. Typical observed peak concentrations on our rivers are:

Olifants, Limpopo Province (1996):		96000 mg/ℓ @ 1000 m^3/s
Thukela at Mandini	:	60000 mg/ℓ
Caledon	:	65000 mg/ℓ @ 80 m^3/s

South Africa is one of a few countries without a sediment sampling programme in the world. It is important that a network of sampling stations are re-instated in our main rivers to obtain data that can be used for water resources development such as river diversion, but also to assess the environmental impacts and the Reserve.

7.2 SEDIMENT YIELDS AND AVAILABILITY

Sediment yields in South Africa typically vary between about 100 to 400 ton/km^2.a, with higher values on the Eastern Cape and free state of 1000 t/km^2.a. While the sediment yields are not the highest in the world, their impacts can be dramatic due to the large catchment areas and the high temporal variability in sediment yield in the semi-arid climate. Added to this is the problem of land degradation due to deforestation and overgrazing.

Several methods are available to determine the catchment sediment yield, such as:

- Sediment yield map based on a statistical regional approach (Rooseboom et al., 1992)
- Surveys of sediment deposits in a reservoir
- Sediment load-discharge rating curves obtained from observed suspended sediment concentrations in conjunction with long-term flow records. Seasonal trends and variability can be obtained from this data, but the data are however very limited in South Africa.

In the evaluation of a sediment yield it is important to use local river data if available. If reservoir sedimentation basin survey data is used, the record should be longer than 10 years between surveys to cancel out the effect of consolidation and the reservoir should be relatively large to obtain a reliable sediment trap efficiency.

In the case of observed suspended sediment data on a river with fine sediment transport during a flood, the general rule is to add 25 % to allow for bed load and non uniformity in sediment transport across the river. It is also necessary to have at least 5 years of continuous daily samples, with more sampling during floods. As many of the

larger floods should be sampled as possible. The sampling methodology should be investigated to assess the reliability of the data.

Sediment transport during large floods (1:50 year) has been observed on the Pongola and Thukela Rivers to be 8 to 13 times the mean annual sediment yield. Smaller more frequent floods combined however also transport a large portion of the total sediment load and are as important as the large resetting floods.

In order to describe sediment transport in a river it is necessary firstly to determine whether critical conditions for re-entrainment from the bed is exceeded. The vertical distribution of sediment concentrations is also important when designing the abstraction works, and will be discussed in the next sections.

7.3 CRITICAL CONDITIONS FOR RE-ENTRAINMENT OF NON-COHESIVE SEDIMENT

The forces acting on a grain on the bottom in steady uni-directional flow are (see Figure 7-1):

The drag force

$$F_D = \frac{1}{2}\rho \cdot C_D \frac{\pi d^2}{4}(\alpha \cdot u_*)^2 \qquad (7\text{-}1)$$

The lift force

$$F_L = \frac{1}{2}\rho \cdot C_L \frac{\pi d^2}{4}(\alpha \cdot u_*)^2 \qquad (7\text{-}2)$$

The self weight

$$W = (\rho_s - \rho)g\frac{\pi d^3}{6} \qquad (7\text{-}3)$$

The friction force

$$F = f(W - F_L) \qquad (7\text{-}4)$$

Where C_D = drag coefficient

C_L = lift coefficient

D = sediment grain diameter (m)

A = coefficient

u_* = friction velocity (m/s)

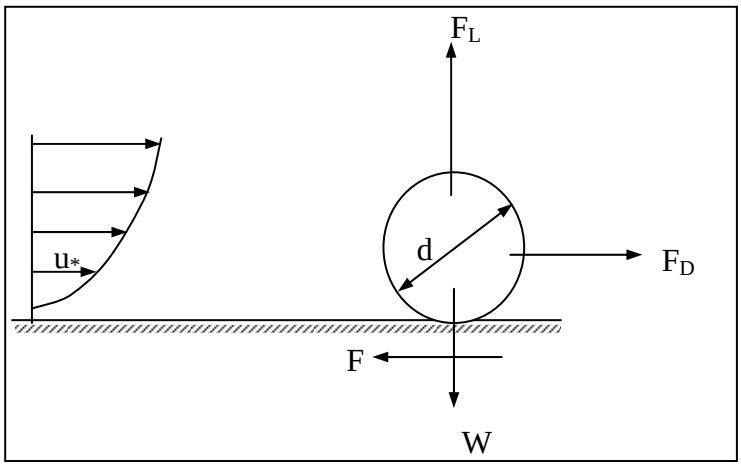

Figure 7-1 Forces acting on a sediment particle resting on the bed

At the start of movement $F_D = F$. from this the Shields parameter θ can be derived:

$$\theta = \frac{u_*^2}{(s-1)gd} = \frac{\tau}{\rho(s-1)gd} \quad \text{.....(7-5)}$$

where = specific gravity of sediment

τ = bottom shear stress (N/m^2)

Now it is possible to define different conditions when sediment particles will start to move:

$$\theta > \theta_c \quad or \quad \tau > \tau_c \quad \text{.....(7-6)}$$

where θ_c = critical Shields parameter $= \dfrac{\tau_c}{\rho(s-1)gd}$

τ_c = critical bottom shear stress

The critical Shields parameter can be determined from the Shields diagram in Figure 7-2, as a function of the grain Reynolds number *Re*.

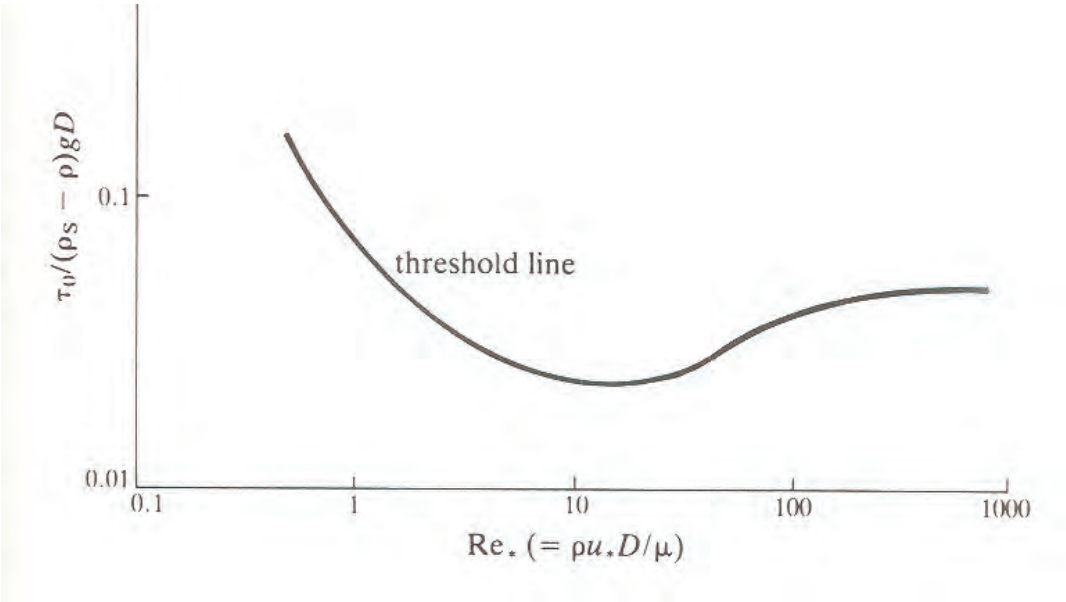

Figure 7-2 Shields' diagram (Chadwick and Morfett, 1998)

Although the Shields criterion is still widely used, Rooseboom and Mülke (1982) have shown that incipient motion can be described more comprehensively in terms of stream power.

The unit stream power (per unit volume) required to suspend a particle with mass density ρ_s and settling velocity w is equal to

$(\rho_s - \rho)g\,w$ ……..…(7-7)

In rough turbulent flow, the unit stream power applied in maintaining motion along a plane bed, is proportional to

$$\frac{\rho g S D \sqrt{gDS}}{d} \quad \text{……..……(7-8)}$$

where S = energy slope

D = flow depth

Particles will be entrained when the power required to suspend particles becomes less than the power required to maintain motion.

$$(\rho_s - \rho) g w \propto \frac{\rho g S D \sqrt{gDS}}{d} \quad \text{……..…....……(7-9)}$$

By manipulating the above equation, the condition of incipient motion under rough turbulent flow conditions is given by

$$\sqrt{gDS} \Big/ w = constant = 0{,}12 \quad \text{……..……(7-10)}$$

Similarly, in smooth turbulent and laminar flow, the applied unit stream power equals

$$\frac{(\rho g D S)^2}{\rho \nu} \quad \text{……(7-11)}$$

where ν = kinematic viscosity

And for values of $\frac{\sqrt{gDS}\cdot d}{\nu} < 13$, the incipient motion criteria has been calibrated as follows

$$\frac{\sqrt{gDS}}{w} = \frac{1.6}{\frac{\sqrt{gDS}\cdot d}{\nu}} \quad \text{.....(7-12)}$$

This criteria is illustrated in Figure 7-3.

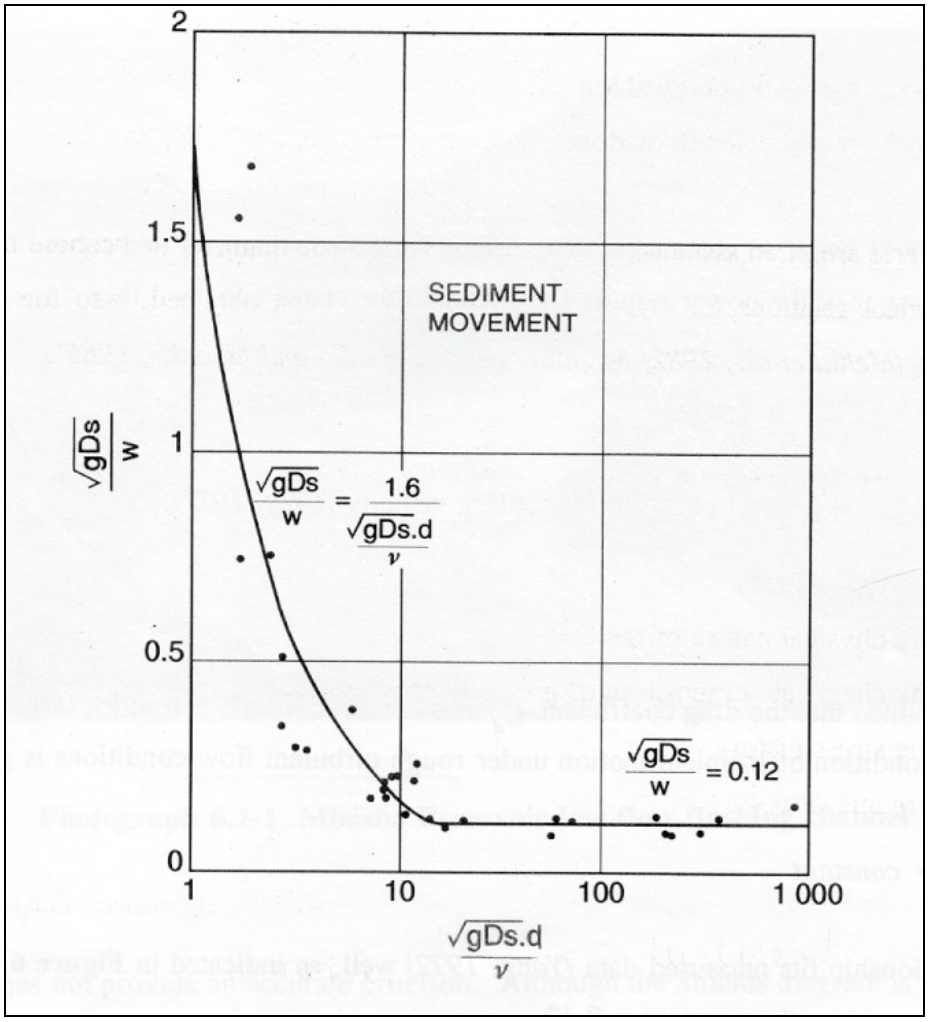

Figure 7-3 Incipient motion conditions for cohesionless sediment particles (Rooseboom and Mülke, 1982)

7.4 VERTICAL SUSPENDED SEDIMENT DISTRIBUTION

Vertical variation in sediment concentrations within a stream can be described by the formula of Rouse (1937).

$$\frac{C}{C_a} = \left(\frac{D-y}{y} \cdot \frac{a}{D-a} \right)^z \qquad (7\text{-}13)$$

with z $= \dfrac{w}{\kappa \sqrt{gDs}}$

and w = settling velocity of particles

κ = von Karman coefficient

g = gravitational acceleration

D = depth of flow

S = energy gradient

C = sediment concentration at distance y above bed

C_a = sediment concentration at reference distance "a" above the bed

When the particles are relatively small relative to the flowing stream, sediment concentrations will vary little across the flow cross-section and suspensions will be near-homogeneous. As the value of z increases the near bed concentrations increase relative to those above and eventually a stage is reached where suspended transport ceases with only bed load transport (near bed) occurring. As z increases further, bed load transport also ceases when the threshold for re-entrainment of sediment is reached.

The flow patterns around a riverbend induces secondary currents that creates a deep scour hole at the outside of the bend and limits coarse sediment extraction if an abstraction works is placed at the outside of the bend. The hydraulics and fluvial morphology of riverbends are described in more detail in the following sections.

7.5 RIVER BEND HYDRAULICS

7.5.1 GENERAL LITERATURE

During the extensive literature survey that was performed a number of references to curvilinear flow were found. Presenting all of this information is beyond the scope of the current research and only the relevant information that is applicable to the topic of the current research will be presented. The aspects that will be addressed in this section include a description of curvilinear flow, the position of the maximum velocity, the development of secondary flow and the strength of spiral flow.

However, the other related information that will not be addressed in this document is listed below. With regard to the various topics the reader is referred to:

Two-dimensional velocity distribution

Avery (1989), Chen and Shen (1983), Chow (1959), De *Vriend and Struiksma (1983), Henderson (1967), Hussein and Smith (1986), Kalkwijk and De Vriend (1980), Lee and Yu (1990), Leliavsky (1965), Liu et al (1982), Raudkivi (1993), Rozovskii (1957), Shen (1971 and Shukry (1950).*

Three-dimensional velocity distribution

Rozovskii (1957), Rozovskii (1962) and *Yalin (1992).*

Energy losses

Chang (1983), *Müller (1943), Shukry (1950)* and *Yalin (1992).*

Shear stress

Avery (1989), Bathurst (1979), Bridge and Jarvis (1982), Chen and Shen (1983), Choudhary and Narasimhan (1977), Francis and Asfari (1971), Khalid (1964), Mandouh and Townsend (1979), Okoye (1989), Shukry (1950) and *Varshney and Garde (1975).*

Scour depth relationships

Avery (1989), Apmann (1972), Blench (1969), Bridge and Jarvis (1982), Chatley (1931), Lacey (1929), Lacey (1930), Leliavsky (1965), Liu et al (1982), Nelson and Smith (1989), Nwachukwu (1973), Ripley (1927), Rzhanitsyn (1960), Sharma (1973),Tyagi (1967) and *Yen and Lee (1995).*

Bed configuration

Bridge (1983), Rzhanitsyn (1960) and *Shen (1971).*

7.5.2 CURVILINEAR FLOW CHARACTERISTICS

The characteristics of flow around a river bend are described by numerous researchers, among other *Avery (1989), Bathurst (1979), Bouvard (1992), Bridge (1977), Bridge (1983), Bridge and Jarvis (1982), Chow (1959), Christian (1988),* De *Vriend and Struiksma (1983), Henderson (1967), Hussein and Smith (1986), Jackson (1975), Lee, Yu and Hsieh (1990), Leliavsky (1965), Minikin (1920), Odgaard (1986), Okoye (1989), Raudkivi (1993), Rzhanitsyn (1960), Shen (1971), Shukry (1950), Snell (1994), Thompson (1876), Thorn and Hey (1979), Varshney (1977)* and *Yalin (1992)*.

The following section gives a summary of the characteristics of flow in river bends.

Consider open channel flow through a bend with outside radius (*R2*) and inside radius (*R1*) (see Figure 7-4). Centrifugal acceleration is generated by streamline curvature in the region of the flow where the velocity is approximately constant. The combination of the local accelerations at all the points across the stream leads to super-elevation of the water surface. The super-elevation is the increase in the elevation of the water surface on the outer (concave) bank of the bend and the decrease of the water surface on the inner (convex) bank of the bend. The order of magnitude being (*Bouvard, 1992*):

$$\Delta h = \int_{R1}^{R2} \frac{v^2}{gR} dR \quad \text{..... (7-14)}$$

where Δh = change in water level [m]

$R1$ = inner radius [m]

$R2$ = outer radius [m]

v = local velocity

R = radius of curvature of the local streamline

g = gravitational acceleration

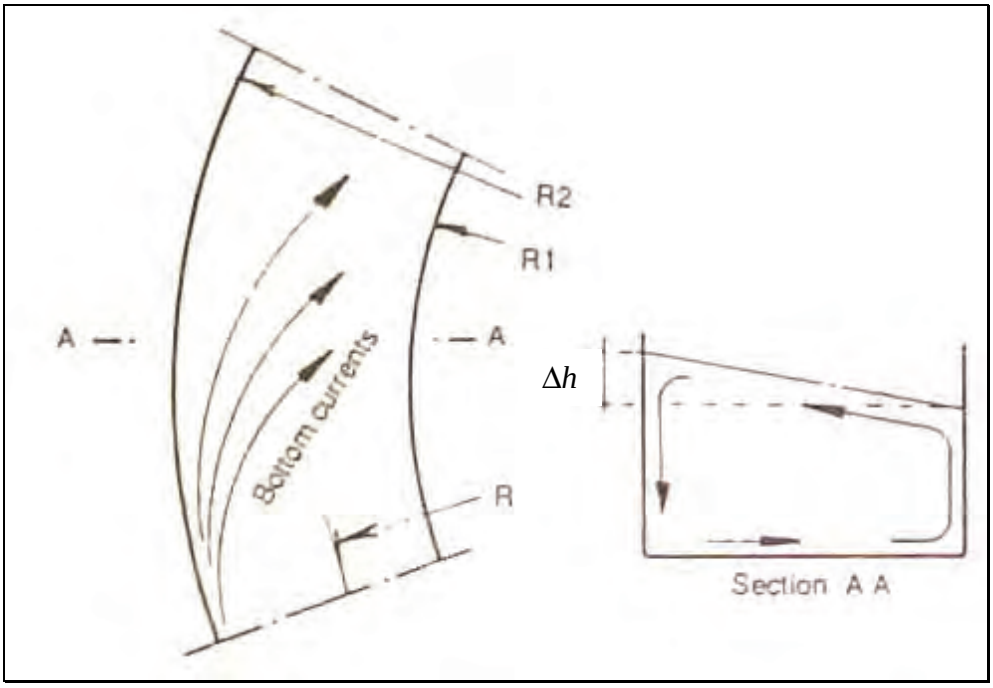

Figure 7-4 Curvilinear flow in an open channel bend *(Bouvard, 1992)*

The velocity (viewed in cross-section) near the walls is extremely low and vanishes at the wall itself. This has the effect that the centrifugal acceleration also virtually vanishes. The imbalance due to the greater hydrostatic pressure head on the outside wall will then force the heavily sediment laden bottom layers to move inwards towards the centre of the curvature of the channel. The rise in level (Δh) is thus countered by the wall friction associated with the centrifugal bottom flow. The result is that the top layers, where the sediment concentration is the least, will move towards the outside of the bend.

A spiral motion is created with the direction being anti-clockwise for a bend to the right (see Figure 7-4) and clockwise for a bend to the left looking in the downstream direction. The bed load will then mainly be transported towards the inside of the bends, the very reason for diverting water from the outside of river bends.

The spiral motion (secondary flow) changes the velocity distribution and is responsible for the development of higher local velocities and higher boundary shear stress on the channel bed. By forcing the streamlines of high velocities towards the outer bank, the centrifugal force creates a reduction in the effective flow area. This decrease in effective flow area as well as the increase in the form resistance due to the direction change of flow causes a backwater effect. The redistribution of shear stress in a channel bend with a mobile boundary introduces bed deformation.

The point of maximum velocity moves close to the outer bank and also downward. Thus, the maximum velocity streamline is meandering not only in plan but also in elevation. The result of this phenomenon is that the increased velocity gradients, i.e. boundary shear stress at the outer boundary of the bend lead to increased erosion along the outer bank. The eroded material from the outer bank is carried by the bottom current towards the downstream side of the inner bank of the bend.

In natural rivers this flow pattern has a very important effect on the sedimentation processes. Natural rivers have the tendency to scour from the outside of the curve and to deposit on the inside. The consequence of this scouring mechanism is that if a branch channel is taken from the outside of the curve, the sediment concentration will be much less in the branch than in the main channel. This fact being the explanation for diverting water from the outside of river bends. The remains of such diversion schemes date back to ancient Mediterranean civilizations *(Henderson, 1967).*

The resultant velocity due to the spiral motion is at an angle (ϕ), the flow deviation angle, to the velocity normal to the cross section. The flow deviation angle is defined as:

$$\tan\phi = \frac{Ky_o}{r} \quad \text{..... (7-15)}$$

where ϕ = flow deviation angle

y_o = flow depth [m]

r = radius of curvature [m]

K = constant

The *K*-values are dependant on the roughness of the bed with *C* being the Chezy coefficient. For smooth beds ($C/\sqrt{g} \approx 19$) the values are in the range of $-10.25 \le K \le -12.90$ with $\overline{K} = -11.58$ and rough beds ($C/\sqrt{g} \approx 10$) the values are within the range of $-4.6 \le K \le -12$ with $\overline{K} = -5.30$.

7.5.3 POSITION OF MAXIMUM VELOCITY

The position of the maximum velocity in river bends is described by a number of researchers among other *Bridge (1977)*, *Bridge (1983)*, *Bridge and Jarvis (1982)*, *Christian (1988)*, *Hussein and Smith (1986)*, *Lee, Yu and Hsieh (1990)* and *Minikin (1920)* to shift from the inner (convex) bank upstream of the bend to near the outside of the bend downstream of the apex of the bend (Figure 7-5).

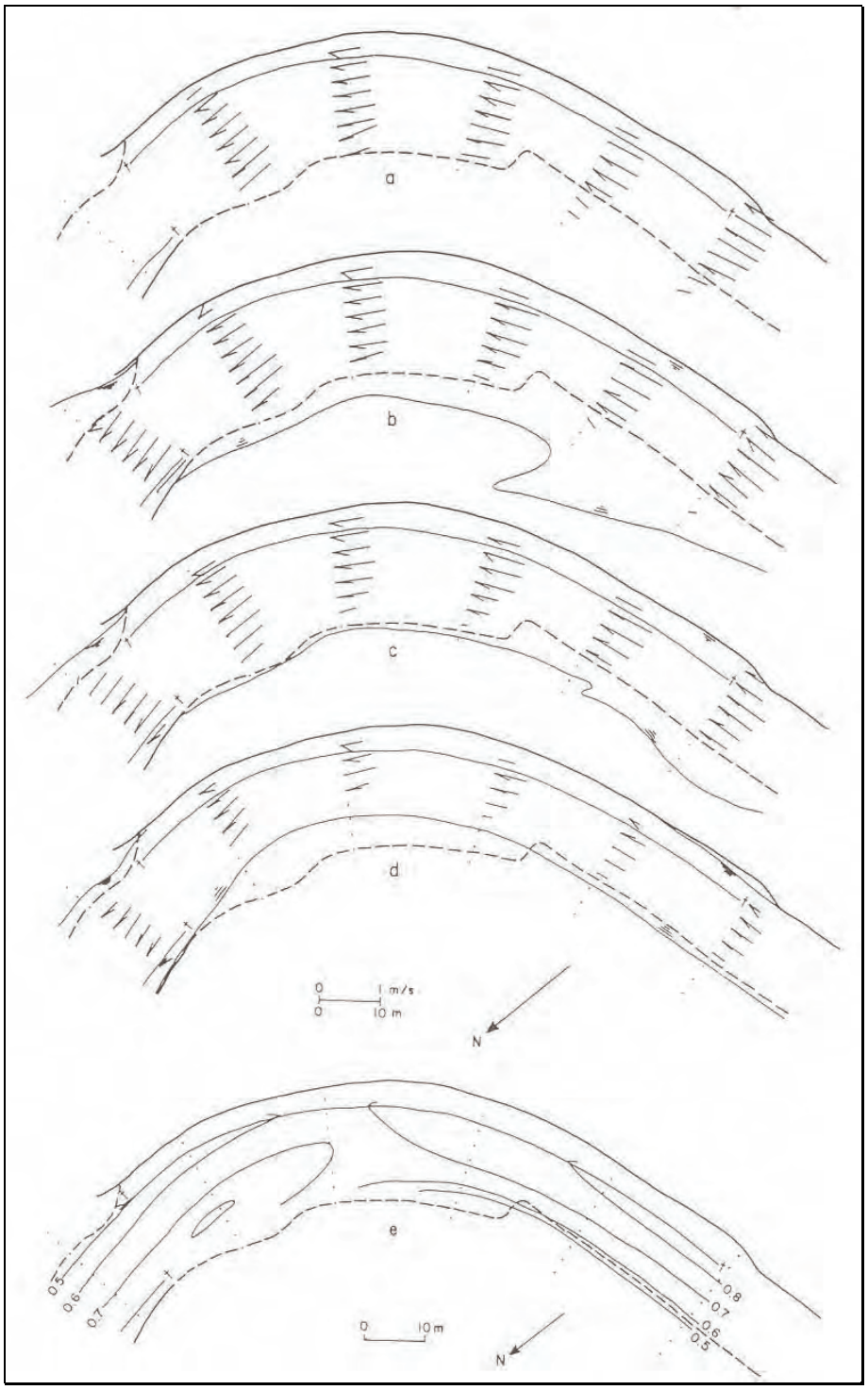

Figure 7-5 Aerial distribution of mean velocity vectors for a range of discharges (a)–(d) and contour map of mean velocity magnitudes for near bank full discharge (e) (*Bridge and Jarvis, 1982)*

The non-uniform flow features that change in time with discharge can explain the path of the maximum velocity (thalweg). In the flow direction there are convective accelerations associated with the changing cross-sectional shapes, curvature and secondary flow. In the transverse direction a net convective momentum flux occurs due to stream-wise variations in secondary flow (*Bridge ,1983).*

Christian (1988) found that during extreme floods, the highest velocity could be closer to the inner (convex) bank (Figure 7-6).

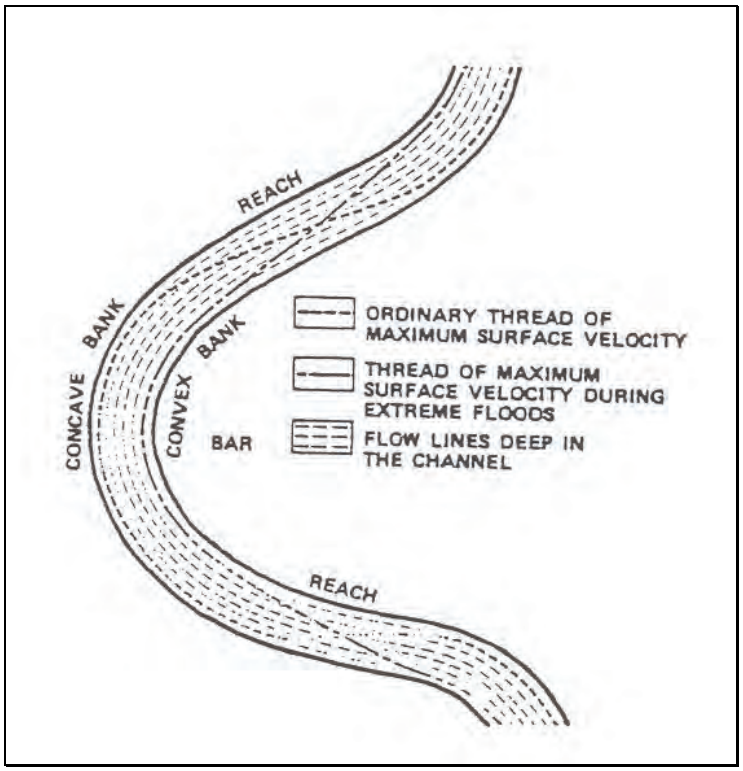

Figure 7-6 Location of maximum surface velocity during normal and flood flows *(Christian, 1988)*

Minikin (1920) found that the maximum velocity is located on the outer (concave) bank of the bend at a distance of one third of the width to the inner bank as is shown in Figure 7-8.

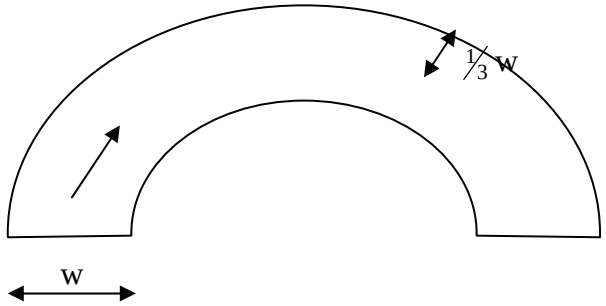

Figure 7-7 Maximum velocity location (*Minikin, 1920)*

The positions of the maximum velocity in river bends are related to the following:

- Curvature of the bend *(Minikin, 1920).*
- The width to depth ratio *(Lee, Yu and Hsieh, 1990).*
- The strength of the centrifugal force *(Lee, Yu and Hsieh, 1990).*
- Position moves downstream with an increase in discharge *(Bridge, 1977).*
- Location shifts downward from the water surface *(Lee, Yu and Hsieh, 1990).*

The magnitude of the secondary currents is up to 15% of the average channel velocity. *(Simons, 1971)*

7.5.4 DEVELOPMENT OF SECONDARY FLOW

The following guidelines were found in the literature survey to determine the status of the developed secondary (spiral) flow:

Raudkivi (1993) showed that the development of secondary flow (with reference to Figure 7-8) is essentially complete after

$$\theta = 1.5\frac{C}{\sqrt{g}}\frac{y_o}{r} \quad \text{..... (7-16)}$$

where θ_{sec} = angle after which secondary flow is completed [radians]

C = Chezy coefficient

y_o = depth of flow [m]

r = radius of curvature [m]

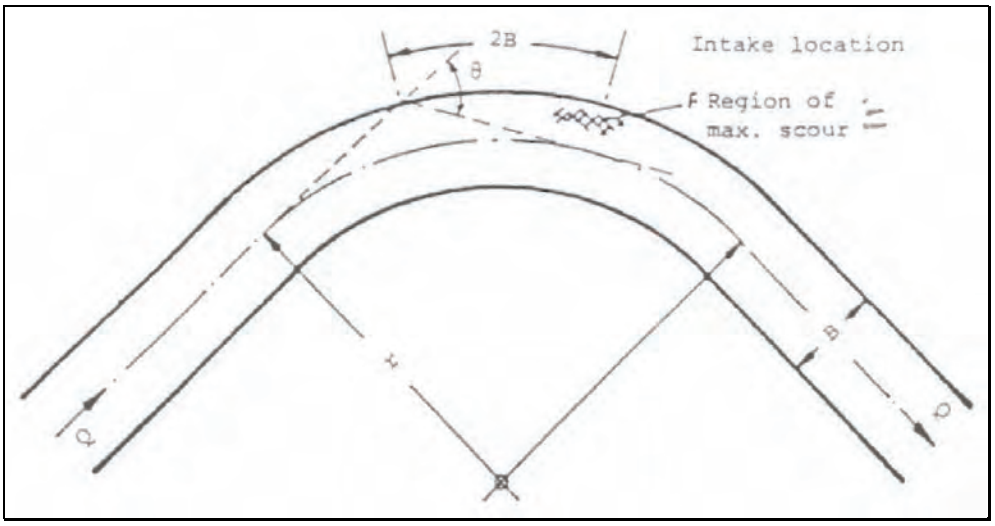

Figure 7-8 Location of maximum scour hole in a river bend (Raudkivi, 1993)

Raudkivi (1993) found that the secondary current in a river bend is not fully developed if the angle $\theta < 30°$ (Figure 7-9). Thus a longer bend with $\theta > 30°$ is required to ensure that the secondary currents are fully developed.

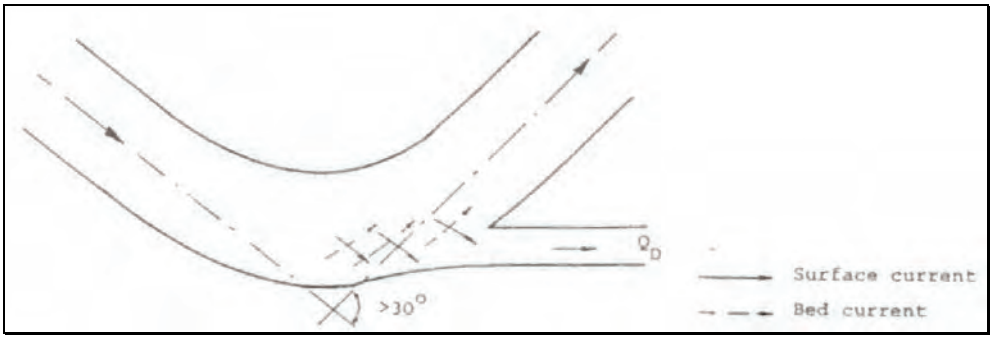

Figure 7-9 Secondary current development in a river bend *(Raudkivi, 1993)*

Mandouh and Townsend (1979) found that in a system that consists of a single bend followed by a straight section, the total length affected by secondary flow (T) can be calculated by means of the following equation where the second term represents the effective decay region that extends downstream of the bend.

$$T = \frac{\pi R \theta_{bend}}{180} + \frac{1.77Ch}{\sqrt{g}} \quad \text{..... (7-17)}$$

where T = total length
R = mean radius of curvature
θ_{bend} = central angle of bend in degrees
C = Chezy coefficient
h = flow depth

Rozovskii (1961) concluded that the flow is fully developed after it has progressed a certain distance downstream from the entrance of the bend. The angle for flow development can be given by:

$$\theta = \frac{2.3CD}{\sqrt{g}r_c} \quad \text{..... (7-18)}$$

where θ = angle of flow development
C = Chezy coefficient
D = flow depth
r_c = mean channel radius

7.5.5 STRENGTH OF THE SPIRAL FLOW

Choudhary and Narasimhan (1977) studied the strength of the spiral flow and found that it originates in the early reaches of the bend, develops to its full strength in the central region and then decays towards the exit reach of the bend. The bend can therefore be separated into the early developing, central developed and final decaying zones.

In the early developing zone, the spiral motion is very weak and its presence is confined to a region close to the surface of the flow. The origin appears to be at the free surface near the outer wall. The spiral motion develops earlier with an increase in Froude number and its intensity is higher for narrow than for wide channels.

In the central zone, the maximum intensity of the strength of the spiral is reached along the inner wall and changes slightly with the value of angle of the bend (θ) and r/r_c (where r is the distance from the centre of the bend and r_c the centreline radius of the bend). A typical result of fully developed spiral flow is shown in Figure 7-10.

In the decaying zone, the strength of the spiral decays from the inner to the outer wall and the decay spreads outward as the flow traverses downstream. The decaying rate is faster for wider than for narrow channels.

From the above, *Choudhary and Narasimhan (1977)* concluded that the boundary resistance has a predominant effect in the growth and decay of spiral motion. The Froude number plays a lesser part in the distribution of the spiral flow.

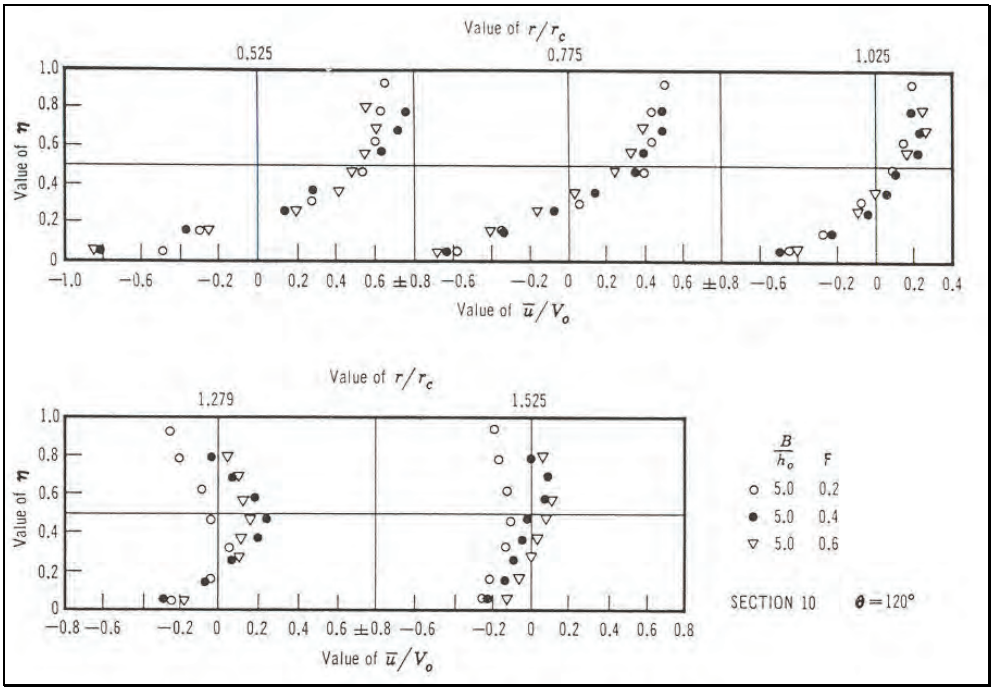

Figure 7-10 Distribution of Radial Mean Velocity $\bar{u}$ for *B/h$_o$=5.0 (Choudhary and Narasimhan, 1977)*

The strength of a spiral flow is defined as the percentage ratio of the mean kinetic energy of the lateral motion to the total kinetic energy of flow at a given cross-section.

When the streamlines are all parallel to the axis of the channel, $S_{xy} = 0$. With reference to Figure 7-11 the strength of the spiral flow is given by *(Chow, 1959)*:

$$S_{xy} = \frac{\bar{u}}{V_o} * 100 \quad \text{..... (7-19)}$$

where S_{xy} = strength of the spiral

$\bar{u}$ = radial velocity (xy plane)

V_o = Q/A (mean velocity)

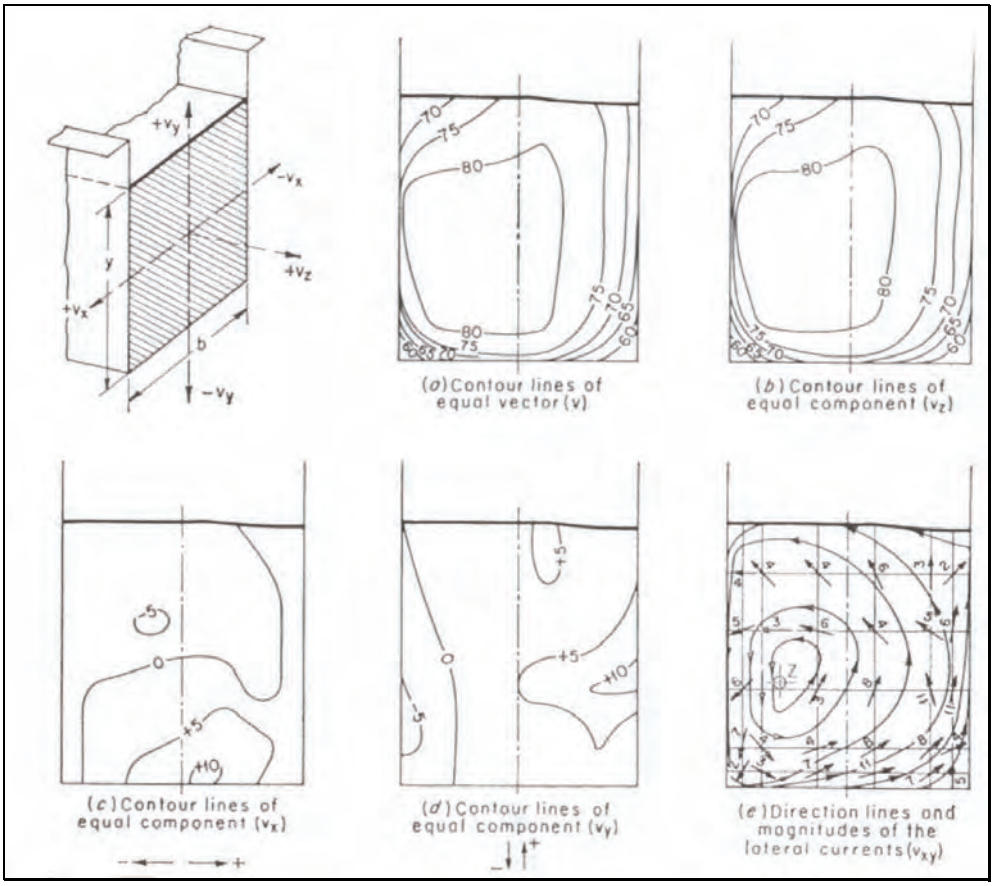

Figure 7-11 Distribution of velocity components *(Chow, 1959)*

In summary, the strength of the spiral flow (S_{xy}) after *Choudhary and Narasimhan (1977), Chow (1959), Shukry (1950)* and *Rozovskii (1963)* is characterised by the following:

- S_{xy} is relative high at a low Reynolds number of the approach flow, but decreases with increasing Reynolds number.
- S_{xy} decreases with an increase of the radius-width ratio. The curve effect approaches its minimum at $r_c / w = 3.0$.
- S_{xy} decreases as the depth to width ratio increases.
- S_{xy} increases as the diversion angle of the bend (θ) becomes large (see Figure 8-1 for definition of θ). For the range ($\theta/180 = 0 - 0.5$) the increase in S_{xy} is nearly twice that of for the range ($\theta/180 = 0.5 - 1.0$).
- The relative strength of the spiral increases with an increase in r/r_c.
- With an increase in Froude number the maximum spiral decreases and the rate of lateral spread of the spiral increases.
- The kinetic energy of the lateral currents in the bend is relatively small compared with the energy in the longitudinal currents. Thus, the lateral currents play a minor role in the energy loss due to bend resistance.
- The secondary circulation is the weakest at low and high discharges and is the strongest at medium discharges.

7.5.6 SUMMARY

Curvilinear flow is characterised by the development of secondary (spiral) flow. The centrifugal acceleration in bends leads to the super-elevation of the water surface and the formation of spiral flows.

The path of the maximum velocity (thalweg) shifts from the inside of the bend towards the outside in the downstream direction with the maximum velocity being near the outside of the bend, downstream of the apex.

The effect on the strength of the spiral flow can be summarised as follows:

i) The strength of the spiral flow increases in the downstream direction in the central developed zone *(Choudhary and Narasimhan, 1977)* and it increases with an increase in the diversion angle *(Shukry, 1950).*

ii) The strength of the spiral flow decreases with an increase in the Reynolds number, with an increase in the depth to width ratio and with an increase in the radius of curvature ratio (r_c/w) *(Shukry, 1950)*.

iii) Secondary currents are the weakest at high and low discharges and the strongest at medium discharges *(Rozovskii, 1963)*.

The central bend angle that is necessary for the secondary flow to develop fully can be determined by one of the following relationships:

i) Equation 7-16 (*Raudkivi, 1993*)

ii) Equation 7-17 (*Mandouh and Townsend, 1979*)

iii) Equation 7-18 (*Rozovskii, 1963*)

7.6 THE FLUVIAL MORPHOLOGY OF RIVER BENDS

7.6.1 THE FORMATION OF BENDS

Shen (1971) described the formation of bends in alluvial channels to be usually part of a meander or deformed meander system. Bends are normally formed as a result of the natural tendency for sinuous flow in channels when the slope of the river (S) is less than $S = 0.0017Q^{1/4}$ (Q is in cubic feet per second and S in ft/1000). The tendency for bends to develop in alluvial channels that eventually flatten the slope has been demonstrated by *Lane (1955).*

The shape of the bend in natural alluvial channels varies from symmetrical patterns to deformed bends that are most frequently encountered in nature *(Shen, 1971)*.

A sharp bend subtends a deep, narrow section along the concave bank with a resultant intense attack on that bank. A long flat bend is associated with a wide, shallow unstable channel with a tendency toward the movement of bars along the concave bank. A bend of optimum radius will subtend a section that approaches a rectangle. Figure 7-12 illustrates a typical cross-section of a sharp, optimum and flat bends *(Vanoni, 1977)*.

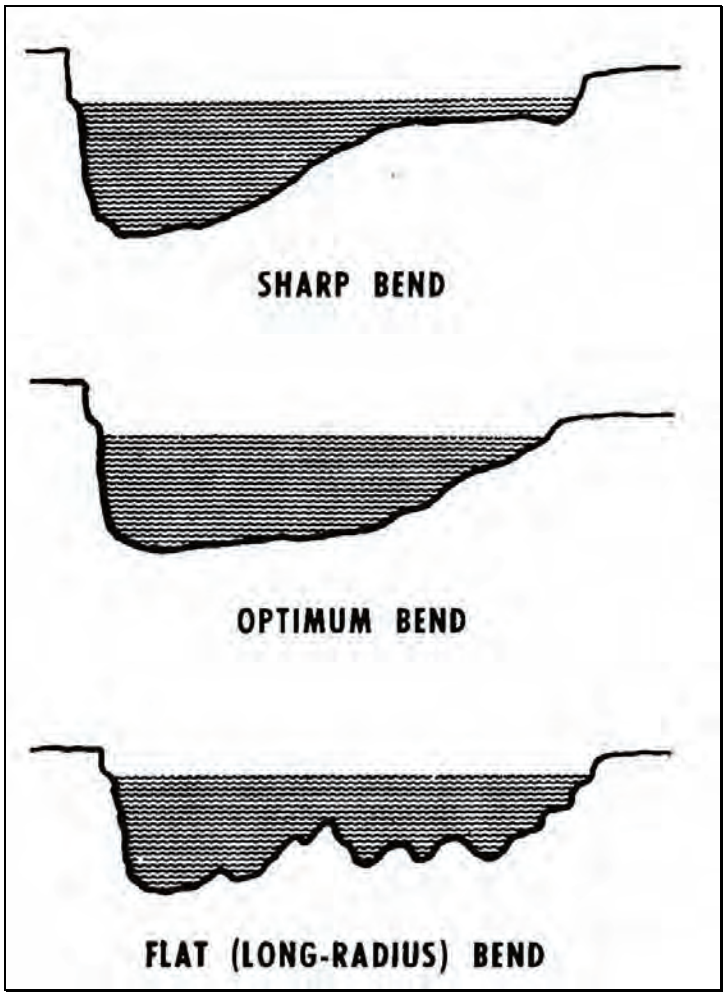

Figure 7-12 Cross-section of sharp, optimum and flat bends *(Vanoni, 1977)*

Shen (1971) classified the types of bends that form in alluvial channels to be of three types, i.e. entrenched bends, meandering surface bends and forced bends.

The entrenched or deepened bends include those that follow the curves of the valley so that each river bend includes a promontory of the parent plateau.

Meandering surface bends include those that are formed only by the river on a flat, alluvium covered valley floor where the slopes of the valley are not involved in the formation of the bend.

Forced bends are often encountered under natural conditions in an alluvial river. This bend is formed when the stream impinges on a non-eroding parent bank that forms a

forced curve that is gradually transformed into a river bend of a more constricted shape.

In all types of bends the density of the material composing the banks is important and determines the radius of curvature to a certain degree. In a free bend the radius of curvature increases with the density of the material. The radius of curvature is the smallest in a forced bend *(Shen, 1971)*.

From the standpoint of the action of the stream and the interaction between the stream and the channel as well as from the general laws of their formation, one can distinguish between the following three types of bends, i.e. free, limited and forced bends.

Free bends are where both banks are composed of alluvial flood plain material that is usually quite mobile. This type of bend corresponds to the common concept of surface bends.

In the case of limited bends the banks of the stream are composed of consolidated parent material that limits the intensive development of lateral erosion by the stream. This corresponds to entrenched or deepened bends.

The formation of forced bends is due to the stream that impinges onto an almost straight parent bank at a large angle in the range of 60° to 100° *(Shen, 1971)*.

There are two characteristic features of all the different types of bends. Firstly, there is a close relationship between the type of bend and the radius of curvature. The forced bend has the smallest radius of curvature, followed by the free bends. The limited bends have the greatest radii. Secondly, there is a relation of the type of bend to the distribution of depths along the length of the bends. In the case of free and limited bends the depth gradually increases in a downstream direction and the maximum depth is found some distance downstream of the apex. As for forced bends, the depth sharply increases at the beginning of the bend and then gradually

diminishes. The greatest depth is located in the middle third of the bend where concentrated scour takes place *(Shen, 1971)*.

7.6.2 THE MECHANICS OF SCOUR AT BENDS

The channel in a bend is deep along the outer (concave) bank and shallower at the inner (convex) bank. The reason being that there is a concentration of stream power, turbulence, flow and sediment transport ability at the outer (concave) bank. The dimensions of the bend channel are dynamic. The length, width, depth, shape and position of deepest scour hole vary with sediment and water discharge, radius of curvature, angle of the bend, slope of the energy gradient, characteristics of the bed and bank material and other less significant variables *(Shen, 1971)*.

Yen and Lee (1995) described the mechanics of sediment transport in river bends to have a twofold complexity. One the one hand, the non-uniform sediment is subjected to the longitudinal and transverse transport induced by the secondary flow associated with river bends. The other factor is the effect of the unsteadiness of flow in natural rivers that can affect the motion of the sediment particles.

It is stated that a wide variation of the standard deviation of the bed material (σ_g) will affect the maximum scour depth and the rate of scour. *Rouse (1950)* observed that a larger value of σ_g would cause the coarser particles to remain in the scour hole and thus pave it with the coarser material. This reduces the rate of scour due the armouring action. It was found that the value of σ_g lies between 1.2 and 1.7 for alluvial material up to a size of 0.6 mm.

The mechanics of scour in river bends have been widely studied by among others, *Kalkwijk and De Vriend (1980)*, *Mandouh and Townsend (1979)*, *Minikin (1920)* and *Raudkivi (1993)*. It is concluded that the path of maximum scour in river bends will gradually shift from the middle of the cross-section to the outside of the bend in the downstream direction, reaching a maximum just downstream of the apex (see Figure 7-13). Typical bed topography of a river bend is shown in Figure 7-14 where it can be seen how the maximum scour shifts towards the outside of the bend in the downstream direction.

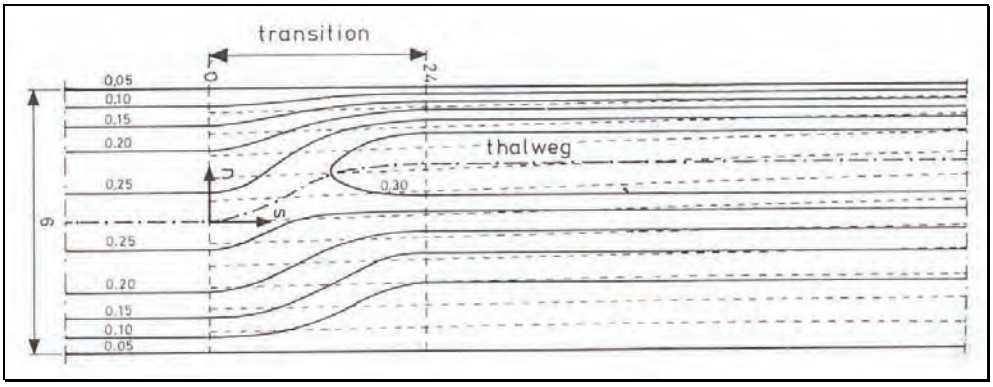

Figure 7-13 Typical depth contours obtained in experiments
(Kalkwijk and De Vriend, 1980)

The effect on scour in river bends due to the change in the following parameters were found in the literature by among other, *Kalkwijk and De Vriend (1980), Minikin (1920), Mandouh and Townsend (1979), Nwachukwu (1973), Thompson (1876)* and *Yalin (1992)* as:

- The position of maximum scour moved downstream with an increase in bend angle.
- The position of maximum scour is at the outside of the bend downstream of the apex.
- Scour depth increases with increase in Froude number.
- Scour depth decreases with increase in the depth to width ratio.
- Scour depth increases as the relative curvature increases.

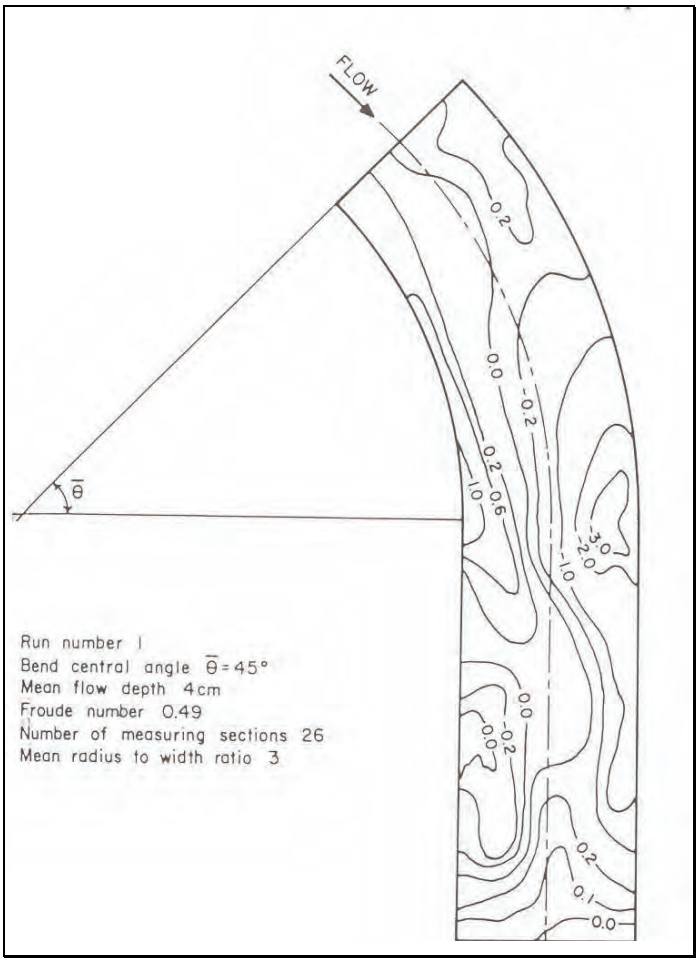

Figure 7-14 Bed topography [cm] for r_c / w =3.0 with $\bar{\theta}$ = 45° and w = 0.3 m

(Mandouh and Townsend, 1979)

8 SECONDARY FLOW PATTERNS AT RIVER BENDS TO LIMIT SEDIMENT EXTRACTION

8.1 INTRODUCTION

Several methods have been devised to draw as little sediment into a river abstraction as possible. However, in order for these to work effectively and efficiently the river hydrodynamics and geomorphology must be examined so as to determine their effect on sedimentation.

It would make sense to place an abstraction at a spot in a river where little sedimentation or deposition of sediment takes place. One of the more reliable places where such scour takes place is in river bends. The secondary, spiral flows that establish themselves here ensure that the water at the outer, or concave, bank is relatively free of sediment. A consequence of this is that erosion is prominent here.

8.2 RIVER BEND ABSTRACTION WORKS

8.2.1 BEND DIVERSION REQUIREMENTS

The general objective of diversion works for irrigation is to divert water that does not carry coarse sediment, but water that is laden with fine sediment (silt) that plays a significant role as fertilizer for agricultural land use. Coarse particles are mainly concentrated near the bed, while the fine sediment is more evenly distributed at all levels. Therefore it is fairly obvious that the abstraction of water should be from the top layers in order to prevent the coarse sediment from entering the diversion works (Leliavsky, 1965).

Avery (1982) made the following recommendations for designing the diversion works:

i) The location of the diversion works should be on the outside (concave) bank of the bend where the flow velocities are higher and where the sediment is unlikely to settle out.

ii) The diversion angle should be as small as possible: between 90° and 180° (see Figure 8-1), i.e. between the direction of main flow and the direction of abstracted flow.

iii) Stagnation areas should be avoided since it will encourage accumulation of sediment.

iv) When the pumps can convey sediment in suspension, the approach flow should be uniform at a constant velocity high enough to keep the sediment from settling out.

v) The sediment settling technique that is used, should be adequately designed to avoid possible problems such as too small settling basins or insufficient spare water for flushing or sluicing.

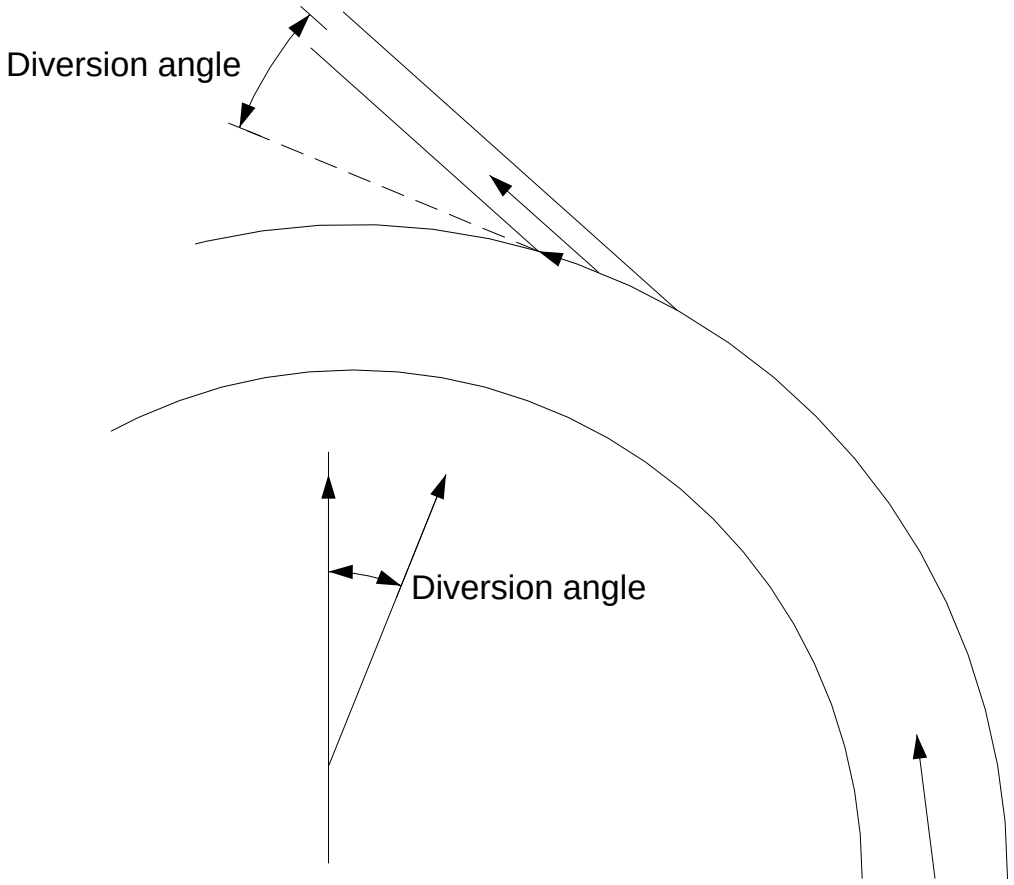

Figure 8-1 Diversion angle

Another factor that needs to be considered is the river flow with the frequency of the project's demand ($Q_{\%}$). The ratio Q_d / $Q_{\%}$ is used to indicate whether a diversion weir

is necessary or not. Q_d is the diverted discharge and $Q_{\%}$ the frequency of the project's water demand. A weir is necessary if $Q_d / Q_{\%} > 0.25$. If the result is smaller, the diversion can be achieved without a weir, provided that the flow depth in the river, at demand, is large enough. The flow depth should preferably not be less than 1.5 m. (Raudkivi, 1993). If a weir is not provided with large gates for flushing of sediment, it would silt up quickly and thus its initial balancing storage cannot be relied upon.

The intake velocity should also be less than the river velocity for $\overline{Q} > Q_c$ where $\overline{Q}$ is the long-term average river flow. Bottom currents should be prevented from entering the intake since it is most heavily laden with sediment. Surface currents should also be prevented from entering the intake since it could carry large quantities of floating debris. One of the most important requirements of diversion works is that the diverted flow should carry as little sediment as possible. Methods to achieve this can be classified into passive and active control. Passive control consists of locating the diversion structure at the optimum location and therefore taking preventive measures to ensure the optimum operation of the structure. Active control conditions refer to the optimum operation of the diversion structure (Raudkivi, 1993).

When a river is in a state of equilibrium, diverting water, thus reducing the river flow, could lead to aggradation downstream. Morphological changes will be the result of the localised stream flow. Aggradation can be prevented if the downstream river channel is narrowed or deepened to increase the transport capacity of the remaining flow (Raudkivi, 1993). In South Africa this is usually not a major problem since the abstractions are relatively small compared to the river flow, and the river morphology is dominated by floods.

8.2.2 BEND DIVERSION LOCATION

Factors such as the stability of the riverbanks and additional stabilisation measures to stabilise the intake should all be taken into account when selecting the diversion location. Special attention should be given to bends of meandering rivers since they generally erode rapidly, cut-offs could occur that may lead to the river bypassing the intake altogether. Braided gravel-rivers can create essentially the same problems as

meandering rivers. The individual stream channels could change their locations and therefore the channel pattern would be different from what existed before. Therefore, ideal locations for diversion structures include stable bends, cliff faces and gorges (Raudkivi, 1993).

Bouvard (1992) and Avery (1989) found that the diversion location should always be located on the concave bank. Secondary- current phenomena in bends will concentrate bed load material on the inside (convex) of the bend. Off-takes should almost never be placed on the convex side of the bend. The off-take on the concave bank would therefore always divert water containing a minimum of bed load.

The intake should be located on a stable reach to ensure that the intake is directed to the main current and that the flow path does not wander often. The optimal location of an intake is usually just below the apex of a concave bank (Tan, 1996).

The relation between the central angle of a bend and the optimal location based on experimental data (SC and Ches, 1992) is given in Table 8-1 and the angles are defined in Figure 8-2.

Table 8-1 Relation between central angle of a bend and optimal location of intake (SC and Ches, 1992)

Central angle of bend (˚)	<45	60	90	120	150	180
Optimal location of intake (˚)	0 (end)	45	60	80	95	110

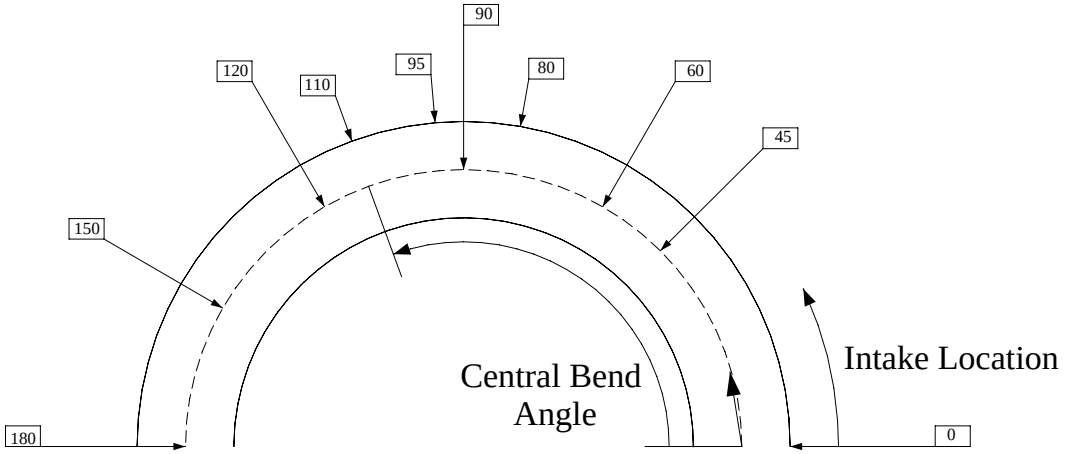

Figure 8-2 Definition sketch in relation to Table 8-1

SC and Ches (1992) found that the optimal location of an intake can also be related to the width and radius of curvature of a bend by the following empirical equation:

$$L = \xi B\sqrt{\frac{4R_c}{B}+1} \quad \text{..... (8-1)}$$

where L = distance

ξ = 0.8 (coefficient)

R_c = average radius of curvature

Considering the above there are a number of suitable natural diversion locations on rivers. These include bends, gorges, rapids and cliffs to mention but a few. Figure 8-3 show the natural locations for diversion structures. The points marked (1) indicate the locations making use of the bend effect and point (2) indicates a gorge, where there are fixed deep-water cross-sections with deep and relative tranquil flow. Cliff faces with flow curvature and down flow are marked (3) and rapids where the suspended sediment is low are marked as (4), Raudkivi (1993).

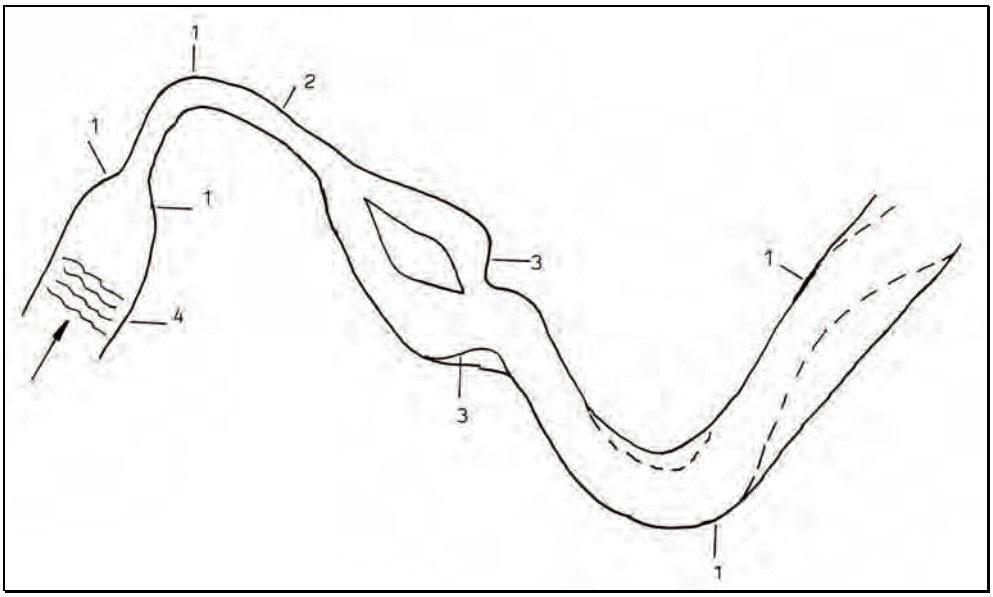

Figure 8-3 Ideal locations for diversion structures on a natural river (Raudkivi, 1993)

A natural scour hole forms at the outer (concave) bank with its deepest point approximately twice the river width downstream of the intersection of the upstream axis with the bank. The location of the deepest scour hole is shown in Figure 8-4 Raudkivi (1993).

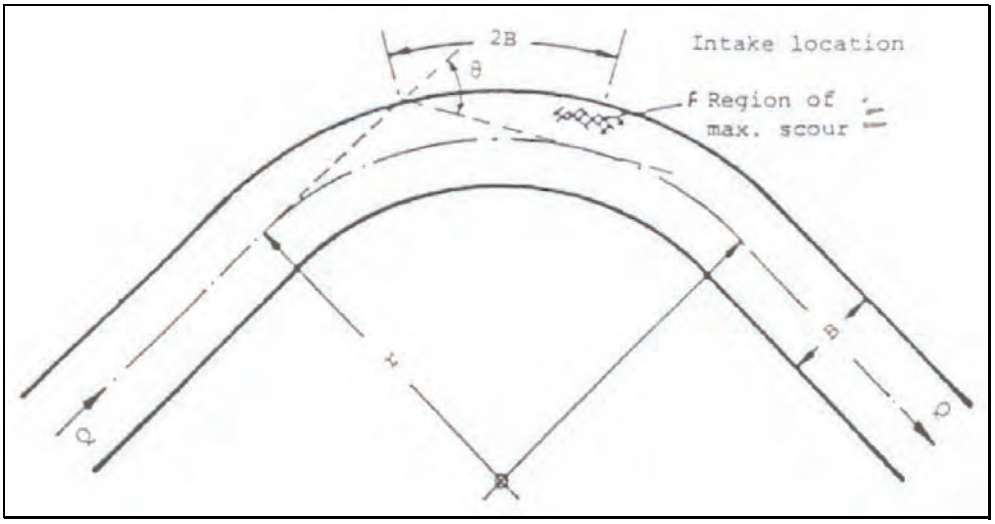

Figure 8-4 Location of maximum scour hole in a river bend (Raudkivi, 1993)

The deepest part of the pool and the shallowest part of the crossing are downstream of the points of greatest and least curvature. For free and limited type of bends the distance is approximately one fourth of the length of the pool plus the length of the crossing. In the case of forced bends the greatest depth of the pool lies at the point of maximum constriction. (Rzhanitsyn, 1960)

Apart from the hydraulic aspects that determine the diversion location, the economical aspects should also be taken into account.

The selected diversion location will have an important bearing on the amount of sediment that enters the diversion structure. Generally rivers have a much higher transporting capacity per unit of flow than the diversion channel. Therefore, specific measures for sediment exclusion must usually be made. The characteristic of river behaviour that makes the selection of the point of diversion very important is the control of the sediment that will enter the diversion structure. The flow phenomena in river bends (particularly the presence of secondary flow) can be used to minimise the sediment entering the diversion structure.

The selection of the diversion location is an important factor in minimising the amount of sediment that will enter the diversion structure. Generally, the outer (concave) bank of the bend is the best location. The reason being that the heavy bed load is swept towards the inside of the curve and the sediment concentration at that point is lower than at other points in the river. This phenomenon is due to spiral flow that was first explained by Thompson (1876). The spiral flow is shown in Figure 8-5. The helicoidal flow sweeps the bed load to the inside of the curve and forms point bars. Thus, it is this action that makes the outside of a bend most suitable for the diversion location (Vanoni, 1977).

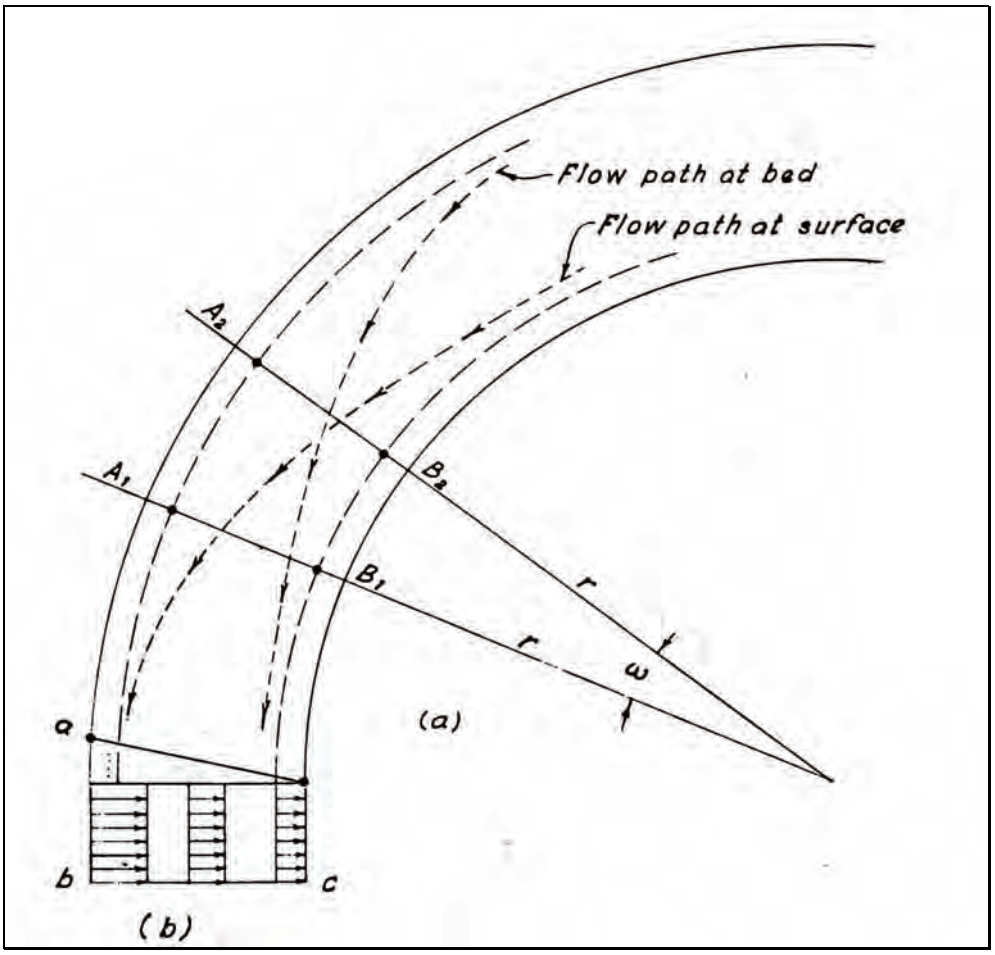

Figure 8-5 Schematic diagram of flow in a curved channel (Vanoni, 1977)

Experiments carried out by Bulle (1926) indicated that the secondary currents established in the bends of rivers carry the sediment particles toward the inner (convex) side of the bend. Intakes must therefore always be placed on the outer (concave) bank of bends. The results of these experiments are shown in Figure 8-6.

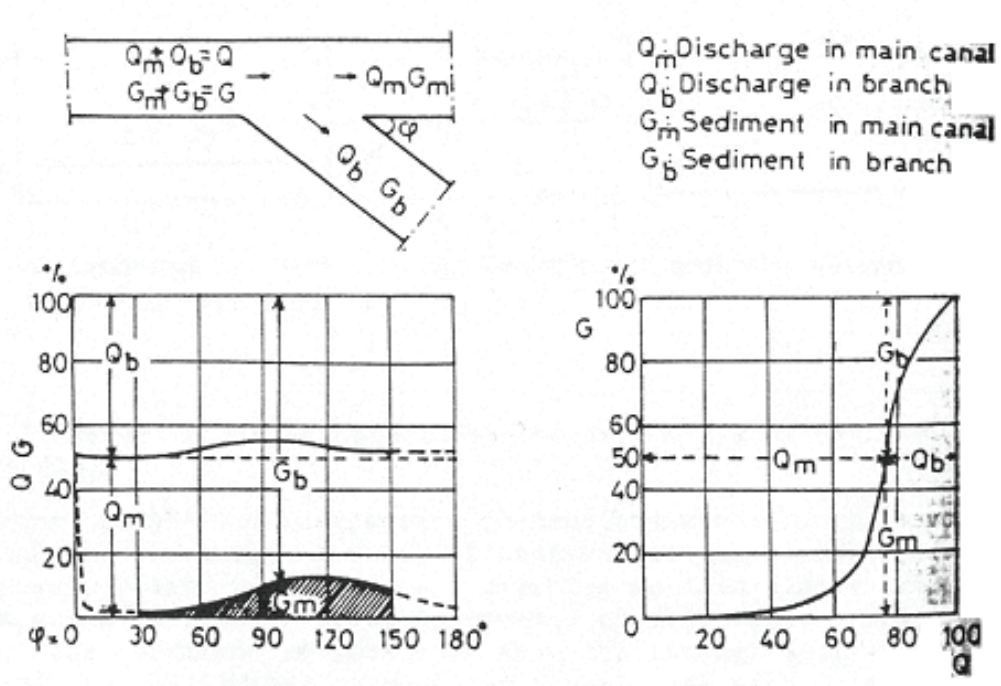

Figure 8-6 Sediment entry into the diversion channel (Bulle, 1926)

The water intake structures must always be located on the outer (concave) bank of the bend in the second half of the bend (Figure 8-7) (Cecen, 1988).

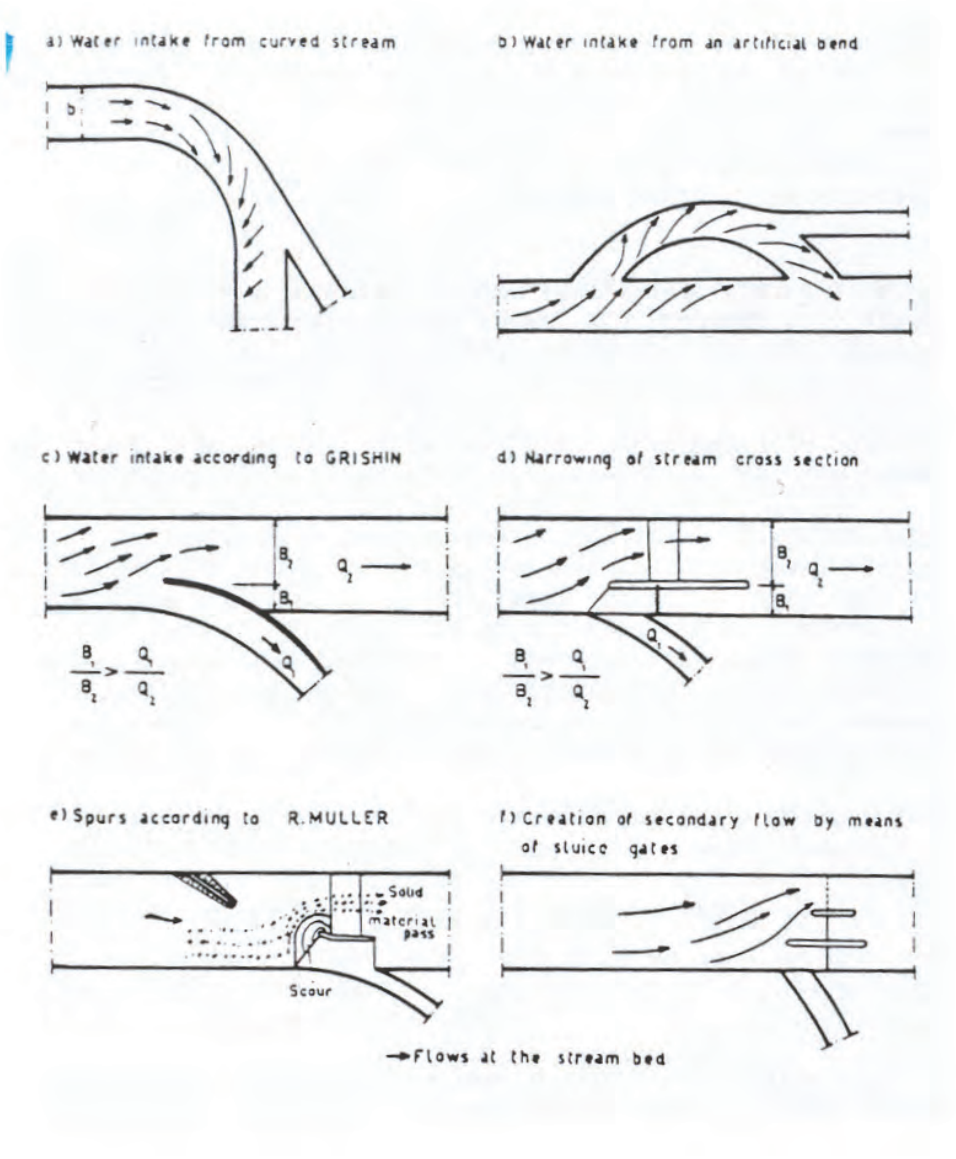

Figure 8-7 Lateral diversion types (Cecen, 1988)

Snell (1994) found that the most suitable location for a bend-type intake is on the outer (concave) bank towards the downstream end of the bend. The correct intake location is essential as an incorrect location can draw up to 80% of bed load through the intake even thought the DDR is only 25%.

8.2.3 DIVERSION ANGLE

As was mentioned in the previous sections the location of the intake should be on the concave bank of the bend. The diversion angle is defined in Figure 8-8. The optimal

angle between the intake and the tangent of the radius of curvature should be 35˚ - 40˚ (Liu et al, 1982).

The intake location should be aligned to produce a suitable curvature of flow into the intake. Thus, changing the flow direction as little as possible. When the flow is diverted through a large angle, the flow patterns will be disturbed and bed load will be attracted to the intake. Avery (1989) recommends diversion angles between 10º and 45º. The optimal angle of diversion was found to be dependent on, among other, the diverted discharge ratio (DDR) and the width of the river and intake.

Leliavsky (1965) described the movement of a particle of water through a diversion (Figure 8-8). It can be seen that the change in direction of a moving particle of water that is diverted from its natural path ab to bc cannot take place abruptly at the apex b, but must occur gradually as are indicated by the dotted lines. The range of tests performed is shown in Figure 8-9. From the tests it was found that the average radius of the curved trajectory depends on the diversion angle. If the radius of curvature is correlated with the diversion angle, it is shown that the centrifugal force is also correlated with the diversion angle. This point is illustrated in Figure 8-10. Although the above tests were conducted for straight channels with diversions, they are also applicable for bends of an alluvial river. Leliavsky (1965) suggested that the relationship between the radius of curvature, width of the diversion and the diversion angle could be given by:

$$r = \frac{b}{2}\tan\left(\frac{\pi - K}{2}\right) \quad \text{..... (8-2)}$$

where r = average radius of curvature [m]
b = bed width of the diversion [m]
K = diversion angle [radians]

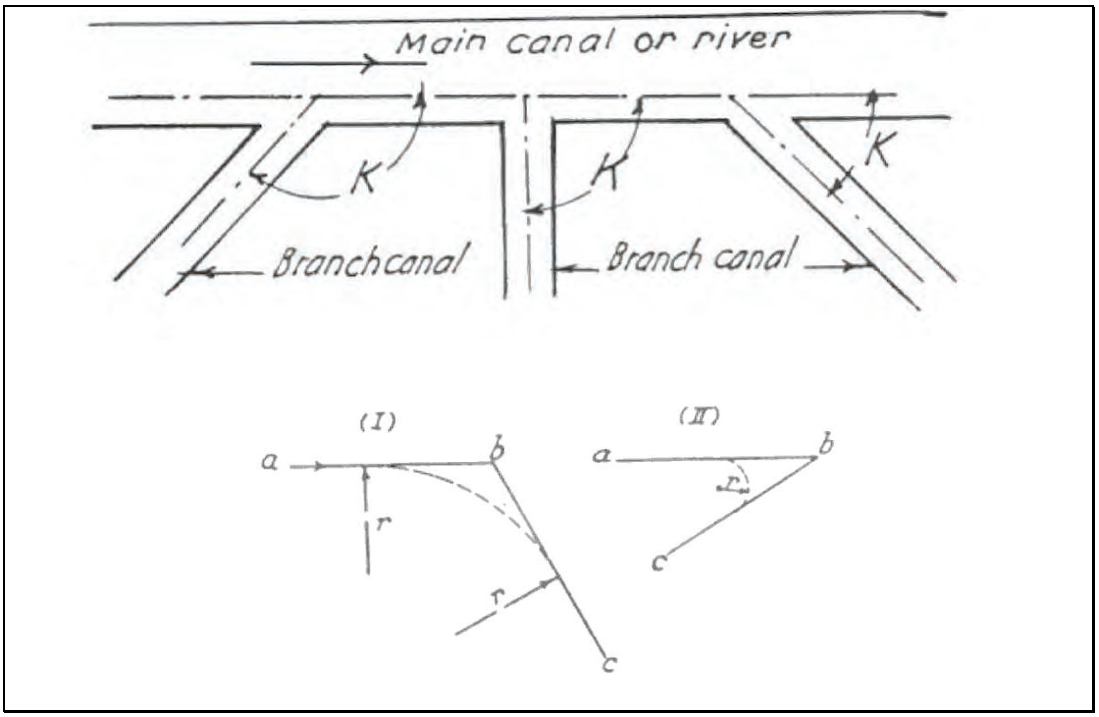

Figure 8-8 Diversion angle (Leliavsky, 1965)

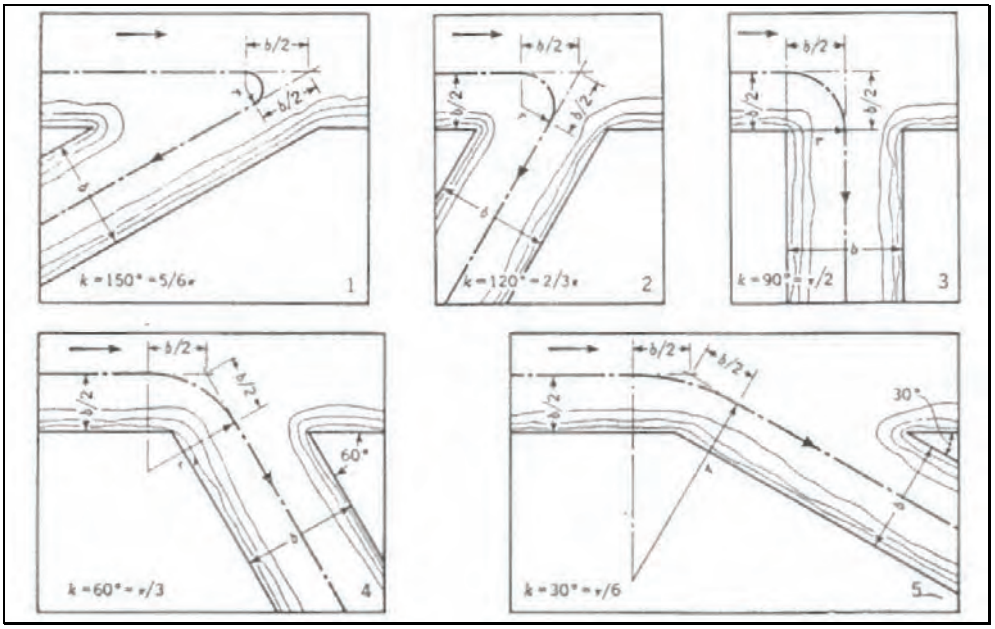

Figure 8-9 Plan layout of tests on the diversion angle (Leliavsky, 1965)

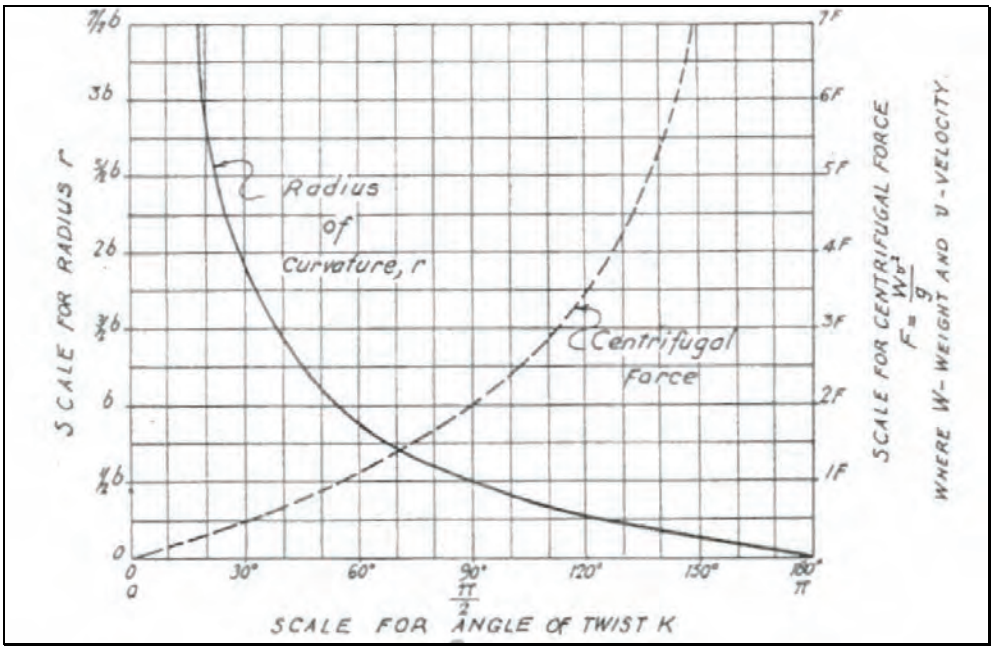

Figure 8-10 Test results on the diversion angle (Leliavsky, 1965)

The characteristic empirical parameter of this complex phenomenon is the average transverse slope of the eroded bed (S). Since it is stated that the erosive power is correlated with the radius of curvature (r), and that r is correlated with the deviation angle (K). Adbed, Azim, Ismail (1949) found the relationship of the transverse slope (S) and the deviation angle (K) to be:

$$S = \frac{K}{50\pi} \quad \text{..... (8-3)}$$

where S = transverse slope
K = deviation angle

Bulle (1926) found that there is no such thing as an optimum diversion angle since the angle varies with the diversion ratio (DDR) and the location of the intake. It was also found that the optimum diversion angle increases as the diversion ratio decreases.

The following diversion angles are recommended:

- *Avery (1989)* recommends a diversion angle between 10º and 45º.

- *Liu et al (1982)* recommends a diversion angle between 5˚ and 40˚.
- *Hufferd* and *Watkins (1972a)* recommends a diversion angle between 30° and 45° if a model study is not carried out.

8.2.4 DIVERSION RELATED PARAMETERS

8.2.4.1 GENERAL

By simultaneously solving the flow continuity equation, resistance equation, sediment carrying capacity equation and the hydraulic geometry equation, the width, slope, water depth and the velocity in a diversion bend can be obtained.

Data on dimensions of some diversion bends are given in Table 8-2 (Tan, 1996).

Table 8-2 Diversion structure parameters (Tan, 1996)

Name of intake	River				Canal		Artificial bend			
	Ave. runoff	Slope	Size of bed material (mm)		Design discharge	Irriga-tion area	Length L	Ave. radius R	L/R	Slope
	($10^6m^3/yr$)		d_{50}	d_{max}	(m^3/s)	(10^3ha)	(m)	(m)		(‰)
Qingnian	215	1/60		800	25	13.3	186	176.2	1.05	1/67
Santunhe	235	1/80	20	300	65	43.3	180	150	1.2	1/150
Bayingouhe	328	1/80	20	400	60	32.0	450	430	1.04	1/80
Awati	1990	1/167		150	40	28.0	154	161	0.96	1/167
Manasihe	1317	1/132	60	600	140	166.7	218	295.5	0.74	1/132
Jingouhe	321	1/100		300	52.5	35.3	148.5	190	0.78	1/100
Kashihe	4012	1/150	45	650	100	80.0	200	162.5	1.36	1/150

Here follows a list of diversion related parameters as well as formulae to estimate them. In the equations below, A is a coefficient of stable width in the Altunin formula that depends on the size of the bed material. The larger the size of the bed material, the larger the value of A (Liu et al., 1982).

8.2.4.2 WIDTH OF THE DIVERSION BEND

Liu et al. (1982) calculated the width of the diversion bend with the equation below:

$$B = \frac{0.52A^{1.05}Q^{0.71}d_{cp}^{0.085}}{n^{0.41}G_b^{0.11}} \quad \text{.....(8-4)}$$

where B = width of diversion bend [m]
Q = design discharge of the bend [m^3/s]
d_{cp} = average diameter of bed load [m]
n = Manning roughness of bed
G_b = bed load discharge [kg/s]
A = 0.7-1.0

Avery (1989) stated that according to the regime method that relates to channels with mobile boundaries, the width of the diversion bend (B) should be the following:

$$B = 5\sqrt{Q_o} \quad \text{..... (8-5)}$$

where Q_o = incoming discharge from river bend [m^3/s]

8.2.4.3 AVERAGE DEPTH OF THE DIVERSION BEND

The average depth of the diversion bend can be calculated with the equation below (Liu et al., 1982):

$$h = \frac{0.55n^{0.23}Q^{0.48}d_{cp}^{0.076}}{A^{0.57}G_b^{0.10}} \quad \text{..... (8-6)}$$

where h = average depth of the bend [m]
Q = design discharge of the bend [m^3/s]
d_{cp} = average diameter of bed load [m]
n = Manning roughness of bed
G_b = bed load discharge [kg/s]
A = 0.7-1.0

The configuration of an alluvial river bend can be represented by the following empirical equation (in feet) developed by Ripley (1927).

$$y = 6.35D\left(\sqrt{0.437 - \frac{x^2}{T^2}} - 0.433\right)\left(1 + \frac{xK}{r_o}\right) \quad \text{..... (8-7)}$$

where y = ordinate of depth [ft]
D = hydraulic depth [ft]
x = abscissa [ft]
T = top width [ft]
K = 17.52
r_o = outside radius of bend [ft]

The following remarks should be noted when using the equation above:

i) For $r_o > 100\sqrt{A}$ the equation is not valid.

ii) If $r_o < 40\sqrt{A}$ the value of r_o in the above equation should be replaced with $40\sqrt{A}$. This is due to the fact that no further deepening seems to result from the increased curvature. Bends are constructive and stable when $r_o > 40\sqrt{A}$, where sharper bends are destructive and tend to shift the channel.

iii) The equation can be applied to curved channels not occupying the whole river. The value of y that is computed should be increased by 14% and K = 26.28.

iv) On a crossover bar where the channel is neither on a curve nor in a straight reach, the maximum depth is about 14.5% less than the computed value.

v) Generally, the equation gives the width of the channel as 20% more at the hydraulic depth than the actual width.

Lacey (1929) estimated the stable channel depth of an unregulated channel to be of the relationship as is shown below. According to the empirical rules of the regime method that apply to bank full flow and not to low flow, equations 8-8 and 8-9 must be multiplied by a bend factor (K) to accommodate the bend phenomenon.

$$R = 0.4726K\left(\frac{Q}{f}\right)^{\frac{1}{3}} \quad \text{..... (8-8)}$$

or

$$R = 1.34K\left(\frac{q^2}{f}\right)^{\frac{1}{3}} \quad \text{..... (8-9)}$$

where R = hydraulic mean radius [m]
Q = discharge [m^3/s]
q = unit discharge
f = silt factor
$= 1.76\sqrt{d_{(mm)}}$
and $d_{(mm)}$ = particle size [mm]
K = bend factor
= 1.5 for moderate bends
= 1.75 for severe bends
= 2.0 abrupt right angel bends
= 2.25 – 2.50 alongside cliffs or walls

Blench (1969) suggests the following equations for the fixed banks and bends in rivers:

$$y_o = \left(\frac{q^2}{F_b}\right)^{\frac{1}{3}} \quad \text{..... (8-10)}$$

where y_o = depth [m]
q = unit discharge
F_b = bed factor
$= 0.58\sqrt{d_{(mm)}}(1 + 0.12c)$
and c = volumetric concentration

8.2.4.4 AVERAGE VELOCITY IN THE DIVERSION BEND

The average velocity in the diversion bend can be calculated width the equation below. (Liu et al, 1982)

$$U = \frac{n^{0.18} G_b^{0.21}}{0.29 A^{0.48} Q^{0.19} d_{cp}^{0.16}} \quad \text{..... (8-11)}$$

where
U = average velocity in the bend [m/s]
Q = design discharge of the bend [m^3/s]
d_{cp} = average diameter of bed load [m]
n = Manning roughness of bed
G_b = bed load discharge [kg/s]
A = 0.7-1.0

8.2.4.5 SLOPE OF THE DIVERSION BEND

The average slope of the diversion bend can be calculated with the equation below. The slope should be approximately the same as that of the river or smaller than the river slope (Liu et al., 1982):

$$J = \frac{n^{2.05} G_b^{0.55}}{0.037 A^{0.25} Q^{1.05} d_{cp}^{0.145}} \quad \text{..... (8-12)}$$

where J = slope of the bend
Q = design discharge of the bend [m^3/s]
d_{cp} = average diameter of bed load [m]
n = Manning roughness of bed
G_b = bed load discharge [kg/s]
A = 0.7-1.0

8.2.4.6 CROSS-SECTION OF THE DIVERSION BEND

The cross-section of the diversion bend can be built in a trapezoidal shape to promote the formation of the spiral flow and secondary currents that will ensure that deposition

occurs on the convex bank. Typical side slopes within the range of 1:1 - 1:1.5 are usually constructed (Liu et al., 1982).

8.2.4.7 RATIO OF RADIUS OF CURVATURE AND WIDTH FOR THE DIVERSION BEND

Liu et al (1982) recommends that the radius of curvature for a diversion bend be in the order of 4-8 times the average width of the bend ($r_{avg} / b = 4 - 8$). Chow (1959) recommends the ratio to be equal to three ($r_{avg} / b = 3$), since it will give the smallest radius at which the effect due to spiral flow is minimized. Avery (1989) suggested that the ratio be in the range of 3 to 5 ($r_{avg} / b = 3 - 5$). Shen (1971) found a relation between the type of bend and the ratio of curvature to width for a bend. For free bends the ratio is $r_{avg} / b = 4.5 - 5.0$, for limited bends $r_{avg} / b = 7 - 8$ and for forced bends the ratio is $r_{avg} / b = 2.5 - 3.0$. Bagnold (1960) made a theoretical evaluation indicating that an optimum channel curvature should exist with a ratio of bend radius (r) to channel width (b) between 2 to 3 ($r_{avg} / b = 2.0 - 3.0$).

On the Missouri River bend radii varying between 10 and 20 times the controlled width (r_{avg} /b= 10 – 20) have been associated with minimum maintenance, whilest ratios of up to six (r_{avg} /b = 6) have been extremely difficult to hold. Rzhanitsyn (1960) did an analysis on a number of European streams and showed that the ratio decreases to become relatively constant at 10 to 14 (r_{avg} /b = 10 - 14).

Varshney (1977) analysed some of the North Indian rivers and concluded that their bends have an average of 2.45 (r_{avg} /b = 2.45). A similar study of American rivers by Yen (1965) showed that their rivers have an average ratio of 2.3 (r_{avg} /b = 2.3).

8.2.4.8 LENGTH OF THE DIVERSION BEND

The length of the diversion bend is usually adopted to be 1.1 – 1.4 times the radius of curvature ($L_{tot} / r_{avg} = 1.1 - 1.4$). (Tan, 1996)

8.2.4.9 DIVERSION RATIOS

The most unfavourable condition for preventing sediment from entering the intake is for the scenario of high Diverted Discharge Ratio (DDR) with large incoming sediment load (G_o). The aim of the diversion structure should be to minimise the Diverted Sediment Ratio (DSR) for all the incoming flows from the river (Q_o) (Tan, 1996).

8.2.4.9.1 Diverted Discharge Ratio (DDR)

The diverted discharge ratio (DDR) is calculated using the following equation:

$$DDR = \frac{Q_d}{Q_o} \quad \text{..... (8-13)}$$

Where Q_d = diverted discharge

Q_0 = incoming discharge from river

The discharge for sediment releasing is equal to 1-1.2 times the diversion discharge (Q_d). A DDR = 2.0 - 2.2 can therefore be recommended. The bend should also be able to convey the common flood of the river that, for example, occurs at least for 2-5 days of each year (Tan, 1996).

Avery (1989) studied some curved channel sediment excluders (Figure 8-11) and recommended a DDR = 1.3 - 1.5.

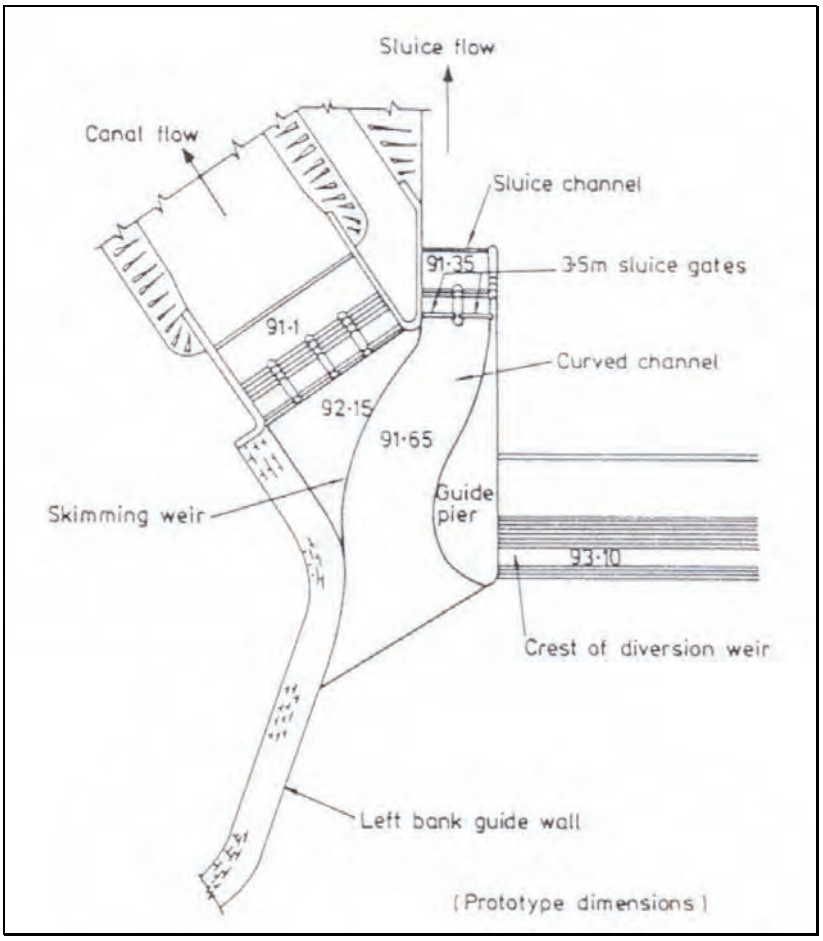

Figure 8-11 Diversion structure (Avery, 1989)

The diversion flow rate (Q_d) should be less than the long-term average river flow ($\overline{Q}$) and less than the critical discharge required (Q_c) that initiates bed load transport. The discharge necessary to transport coarse sediment from upstream of the intake to downstream, and still continuing transport further downstream is the difference ($Q_c - Q_d$) (Raudkivi, 1993).

8.2.4.9.2 Diverted Sediment Ratio (DSR)

The diverted sediment ratio (DSR) is calculated with the following equation:

$$DSR = \frac{G_d}{G_o} \quad \text{..... (8-14)}$$

Where G_d = diverted sediment load

G_0 = incoming sediment load from river

Avery (1989) stated that it is often the case that the proportion of sediment abstracted with relation to the total river sediment load is greater than the proportion of water abstracted. Tan (1996) noted that the DSR is directly proportional to the DDR.

Habermaas (1935) did a serious of model experiments to measure the diverted sediment ratio (DSR). The DDR of these tests were constant at 50%. These results are summarised by Mosoyi (1965) and is shown in Figure 8-12. The result of model 1 is noteworthy since all the sediment was diverted. The reason being that the curvature of flow into the offtake swept essentially the entire bed load against the convex face and into the branch channel.

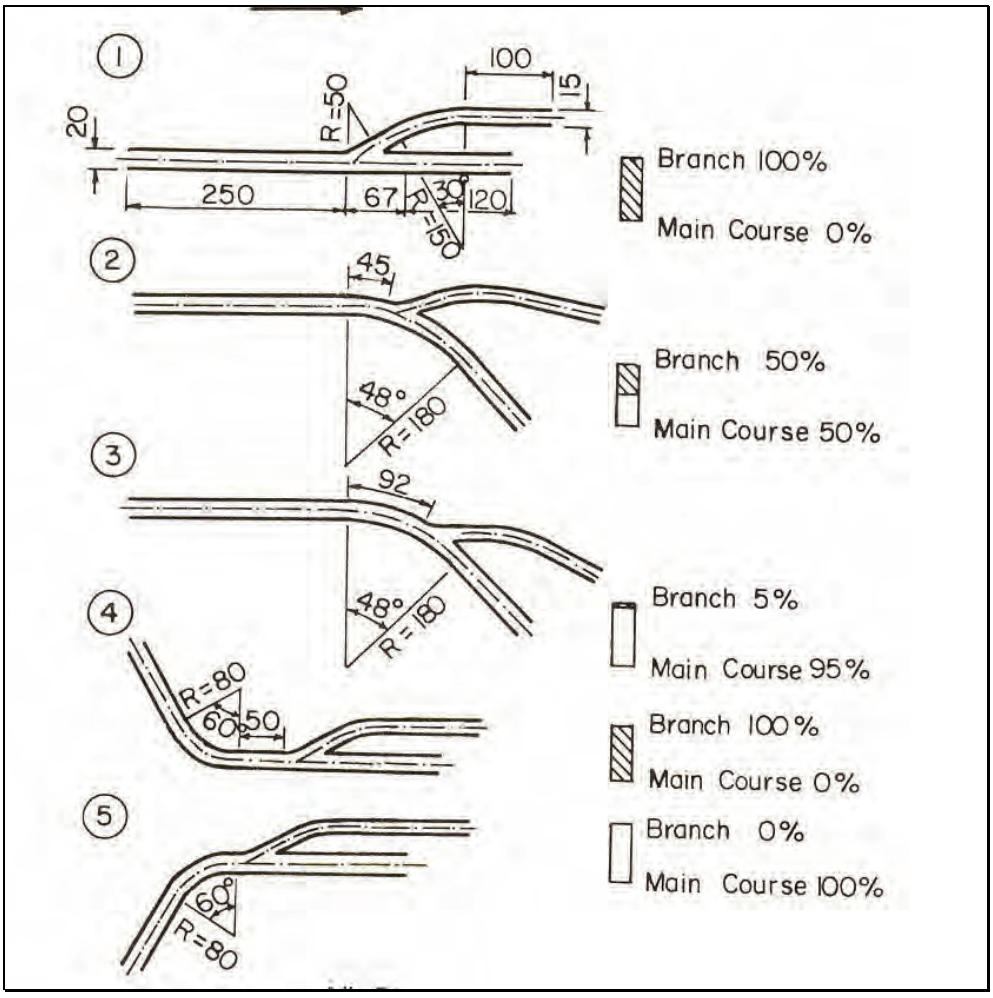

Figure 8-12 Model experiments of diversion structures (Mosoyi, 1965)

9 LABORATORY TESTS ON CURVILINEAR FLOW

9.1 INTRODUCTION

This chapter describes tests carried out at the Hydraulic Laboratory of the University of Stellenbosch in order to:

- Better understand the location of maximum velocity in a bend
- Investigate movable bed conditions at a bend
- Investigate larger radii of curvature to width, more typical of South African conditions
- Obtain data on bend hydraulics to calibrate a 3D hydrodynamic model
- Obtain data on bend hydraulics to calibrate and validate a 2DH hydrodynamic model with sediment transport
- Assess effect of diversion on bend flow patterns

9.2 EXPERIMENTAL SET-UP

A series of laboratory experiments were carried out in the Hydraulic Laboratory of the University of Stellenbosch. A model was constructed to simulate the flow behaviour in a river bend that is preceded by a straight section. The plan layout of the model is shown in Figure 9-1. .....

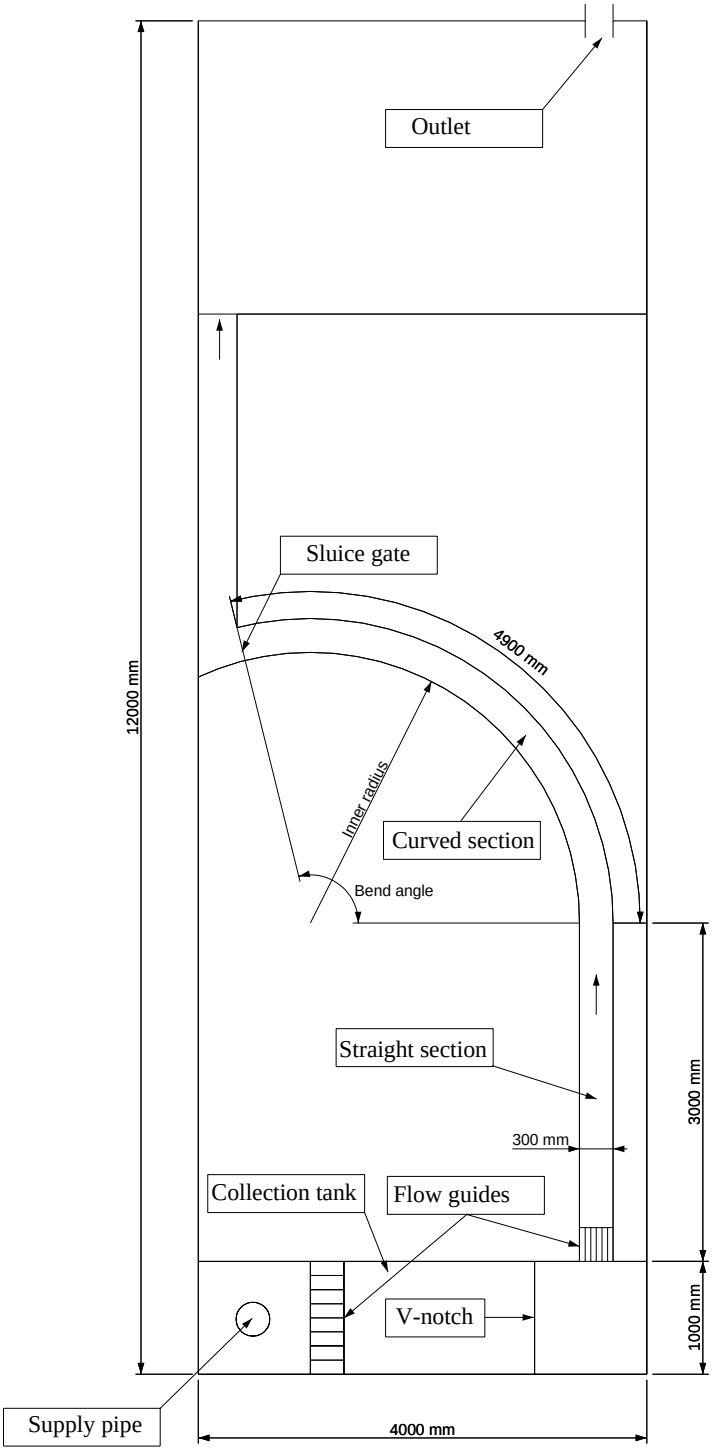

Figure 9-1 Plan layout of model

The choice of the range of r_c/w ratios that were to be tested was done in relation to the recommended ratios that were found in the literature (Section Figure 9-2). With the

available space where the model was to be constructed and with the range of recommended length to radius ratios (L/r_c) of 1.0 to 1.4 *(Tan, 1996)* it was decided to construct a bend with r_c/w of 8.5, 11.8 and 15.2 with the total length of the bend being 4.9 m. This resulted in an acceptable L/r_c of 1.1 to 1.9. Larger r_c/w ratios are more representative of South African rivers. A summary of the recommended r_c/w ratios that was found in the literature together with the r_c/w ratios that was used in the current research is shown in Figure 9-2. Tests were carried out on 300 mm and 600 mm wide canals.

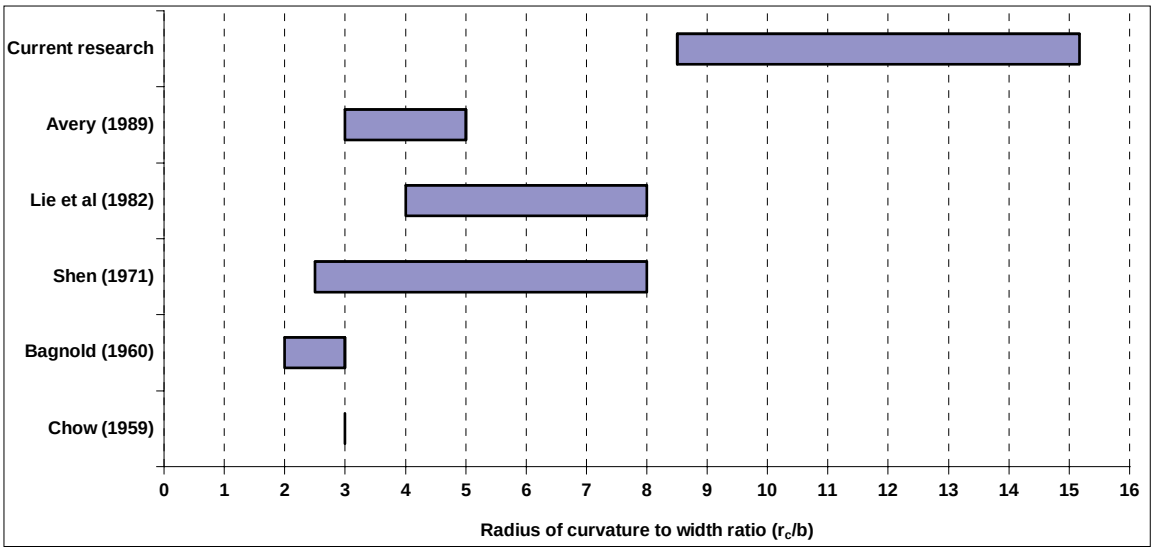

Figure 9-2 Summary of radius of curvature to width ratio (r_c/w)

The model consisted of a straight channel, followed by a curved section. The dimensions of the channel were as follows: 6.9m in length and 0.3m in depth. The outer diameter was kept at a constant 2.7m. The inner diameter however was first held at 2.4m making the channel 0.3m wide. For the second series of tests the inner diameter was decreased to 2.1m making the channel 0.6m in wide.

The discharge into the channel was measured using a rectangular v-notch weir that was located upstream of the straight section in the collection tank. At the downstream end of the curved section a sluice gate was inserted to control the water level in the channel. By ensuring a control point at the downstream end of the channel, the

possibility of a control point developing in the bend was cancelled. Flow directors were placed at the entrance to the straight channel to dampen turbulence and to ensure uniform flow conditions. Figure 9-3 and Figure 9-4 show photographs of the laboratory model.

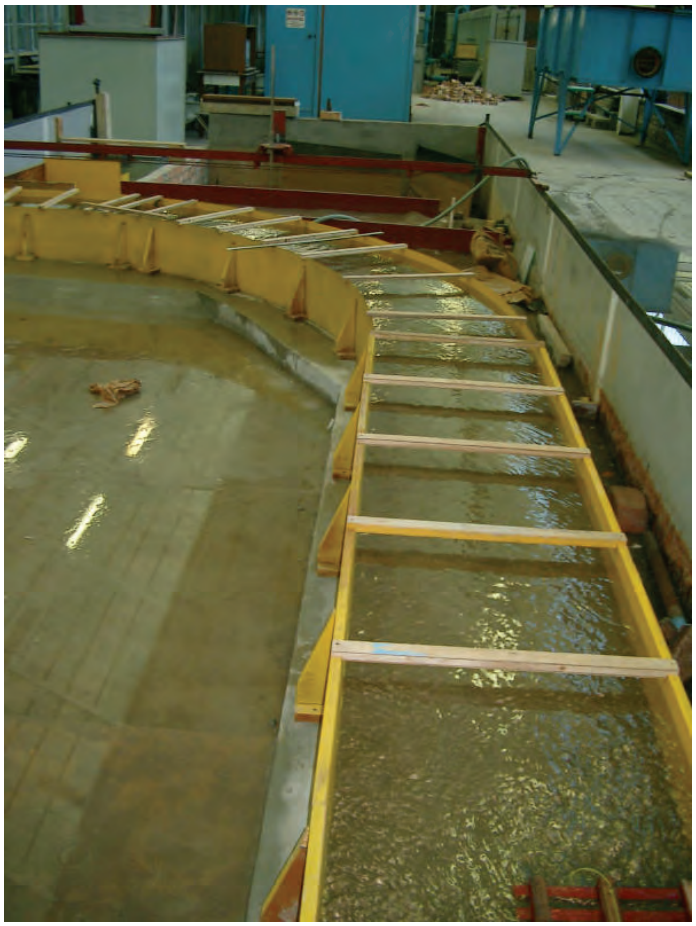

Figure 9-3 Straight section of channel (600 mm width)

Figure 9-4 Curved section of channel

The channel was filled with a level layer of sand 0.15m thick. Water was then allowed to dam up behind the closed sluice until the water level above the sand reached a depth of 0.1m above the sand. At this stage the sluice was opened and constantly adjusted so that the water level would remain the same despite the large discharge into the channel.

The experiment was run for as long as possible or until it appeared that an equilibrium condition had been reached. Throughout the duration of the experiment measurements of water levels were taken every meter along the length of the channel and near the left, the middle and right side of the channel. No sediment was fed into the canal upstream.

When the test was declared complete the sluice was closed and the water was allowed to drain very slowly so as not to disturb the bed forms that had been created. The bed profile was then recorded by measuring the sand height in a grid of 100 mm along the length and 50 mm across the width of the channel.

9.3 TEST PROCEDURE

9.3.1 VELOCITY RELATED TESTS

It was decided to test three different centreline radii, i.e. r_c = 2.55, 3.55 and 4.55 m. For each radius, conditions were set-up to represent a range of Froude numbers (Fr). Tests were carried out for Fr = 0.1, 0.3, 0.5 and 0.7 with no sediment in the channel and one sediment related test with a Fr = 0.3. The water level in the channel was controlled by the downstream sluice gate. The targeted water depth for all tests was 100 mm. With the Froude numbers known the corresponding discharges and water levels above the v-notch were calculated with the following equations

$$F_r = \frac{V}{\sqrt{gy}} \quad \text{..... (9-1)}$$

From continuity,

$$V = \frac{Q}{by} \quad \text{..... (9-2)}$$

Substituting equation 9-2 in equation 9-1 yields,

$$F_r = \frac{Q}{by\sqrt{gy}} \quad \text{..... (9-3)}$$

The v-notch equation that was used goes as follows:

$$Q = {}^{8}\!/_{15} C_d \sqrt{2g}\, \tan\left({}^{\theta}\!/_{2}\right) H^{5/2} \quad \text{..... (9-4)}$$

Substituting equation 9-3 into equation 9-4 and rearranging to get H,

$$H = \left[\frac{15 F_r by\sqrt{gy}}{8 C_d \sqrt{2g}\, \tan\left({}^{\theta}\!/_{2}\right)} \right]^{2/5} \quad \text{..... (9-5)}$$

where H = water level above v-notch
Fr = Froude number
y = depth of water in channel

$$C_d = 0.61$$

$$\theta = 90°$$

From equation 9-5, H is solved to get the desired water level above the v-notch.

Velocities were measured in 50 mm intervals across the channel at 14 cross sections that were perpendicular to the flow direction and at three depths, i.e. 30, 50 and 70 mm from the channel bed. The cross-sections were at 500 mm intervals except at the change over from the straight to the curved channel where the spacing was 190 mm between the last cross-section of the straight section and the first cross-section on the bend. Thus, a total number of 210-point velocities were measured for each test run. Water levels were also measured at the same grid as previously explained by means of a needle gauge that was fitted to the measuring unit. The grid layout where measurements were taken is shown in Figure 9-5.

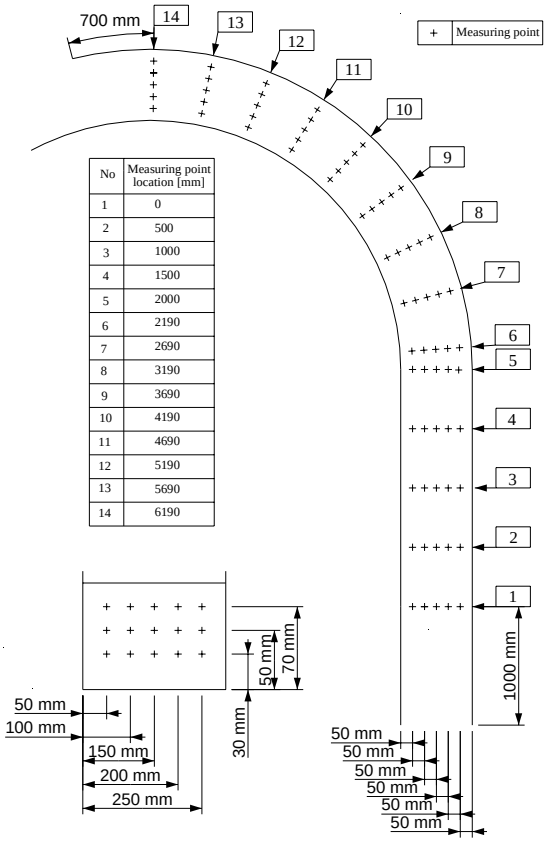

No	Measuring point location [mm]
1	0
2	500
3	1000
4	1500
5	2000
6	2190
7	2690
8	3190
9	3690
10	4190
11	4690
12	5190
13	5690
14	6190

Figure 9-5 Velocity measurement positions for diversion location related tests

An A.Ott-meter (Figure 9-6) was used to measure the velocities. The A.Ott-meter consisted of a propeller and a counting device that counted the number of rotations. At every measuring point the number of revolutions in a 30 second interval where obtained. At each measuring point, the revolutions in three 30-second intervals were taken in order to obtain a reliable average revolution. The average duration of a test was approximately 12 hours. The unit was mounted on a cart that could move across the model and also move in the longitudinal direction. The measuring unit could also change direction to accommodate measuring in the curved section, since measurements were made perpendicular to the direction of flow. A protractor was fitted to this unit to ensure that the propeller was perpendicular to the flow direction.

Figure 9-6 Velocity measurements with an A.Ott-meter

Two types of propellers were used. A larger propeller was used for the tests where Fr = 0.1 and 0.3 and a smaller propeller was used for fr = 0.5 and 0.7. The number of revolutions where converted to point velocities by the following equations for the smaller and bigger propeller respectively.

$V = 0.0923\ n + 0.035$ for $n < 1.13$…….. (9-6)

$V = 0.1020\ n + 0.024$ for $n > 1.13$…… (9-7)

$V = 0.0583n + 0.030$ for $n < 7.11$…….. (9-8)

$V = 0.0545\ n + 0.057$ for $n > 7.11$…….. (9-9)

A typical test procedure was as follows:

- The valve in the 150 mm diameter pipe was adjusted to obtain the required water level above the v-notch.
- Once the required water level was reached, the valve was left in that position to let the water level stabilise. Continuous adjustments were made at the valve until the water at the v-notch stabilised at the required level.
- The measuring unit was placed at section 6 and the needle gauge was adjusted to represent a water level of 100 mm above the model bed.
- The sluice gate at the downstream end of the curved section was then adjusted to obtain the required water level in the model. Time was given for the water level to stabilise before measurements commenced.
- At every measuring point the water level was first measured.
- The measuring unit was then rotated until the propeller was perpendicular to the direction of flow and the counter was activated to obtain the number of revolutions. This was repeated three times to obtain a reliable average.
- Before moving the unit the water level at that particular point was measured again to ensure that a constant supply of water was obtained.
- The unit was then moved to the next measuring point where the above-mentioned steps were carried out.
- After all the measurements were completed, the water level at the v-notch was once again verified.

On the completion of each test a continuity check was done. The measured velocities were integrated over area to determine the measured discharge ($Q_{avg,\ measured}$) and compared with the input discharge (Q_{in}) at the V-notch. The comparison is shown in

Figure 9-7 from where it can be seen that the measured discharges were over estimated by approximately 9%, when considering the average for the whole series of experiments that were done. The figure of 9% was deemed as being reasonable when considering the accuracy of the measured water levels which is within the range of 1 mm.

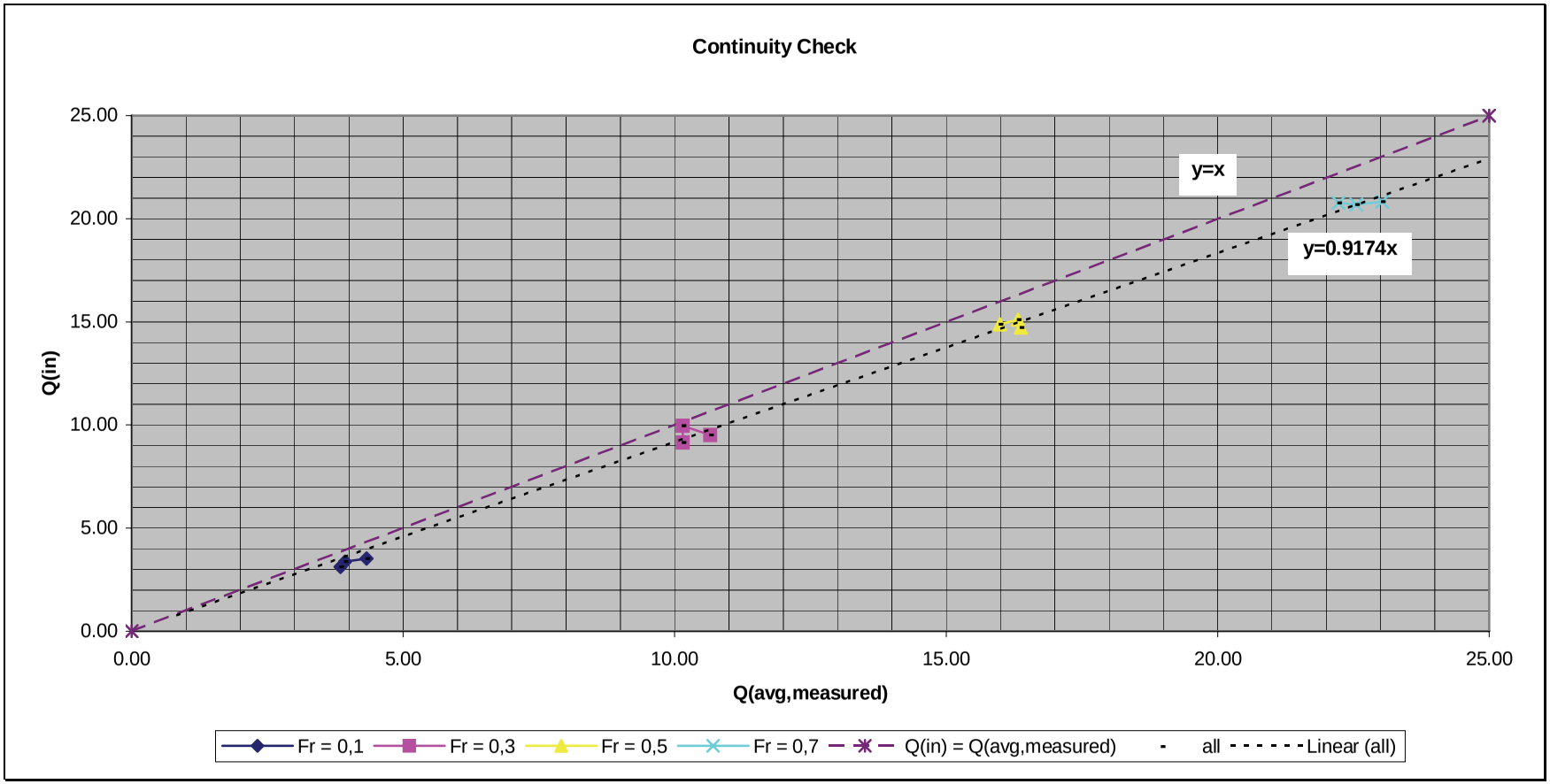

Figure 9-7 Evaluation of measured flow

9.3.1.1 CONDUCTED EXPERIMENTS

A) TEST A1 (FROUDE = 0.1)

The test was carried out with an average water level of 106.4 mm above the model bed and a discharge of 3.38 l/s. The velocities that were measured at 70 mm, 50 mm and 30 mm from the bed are shown in Figures 9-8 to 9-10 respectively. From these figures it is clear that the velocity distribution develops in such a manner that the velocity on the outer (concave) bank is greater than on the inner (convex) bank. The highest velocities were measured on the outer bank near the downstream end of the bend. A maximum velocity of 0.137 m/s was measured between 5.19 m and 5.69 m on the outer bank of the bend.

Figure 9-11 indicates the velocity distribution in the vertical plane measured at 50 mm, 100 mm, 150 mm, 200 mm and 250 mm from the inside of the bend. From this figure the presence of a secondary current that creates a clockwise spiral flow is noted when studying the path of maximum velocity. It is once again clear that the maximum velocity is located on the outside of the bend near the bend exit.

Figure 9-12 is a cross-sectional plot of the velocity distribution that was measured at the 14 sections. The cross-sections are plotted in a downstream direction from top left to bottom right. From this figure it is also evident that the maximum velocity is situated on the outside of the bend near the bend exit and that it shifts downwards in the downstream direction.

From Figure 9-11 and Figure 9-12 a three dimensional view of the velocity distribution in a curved section can be formed. It is clear that higher velocities develop in the downstream direction of the bend; the velocity is higher on the outside of the bend than on the inside and that it shifts downwards in the downstream direction. Thus confirming the presence of a clockwise spiral flow in the bend.

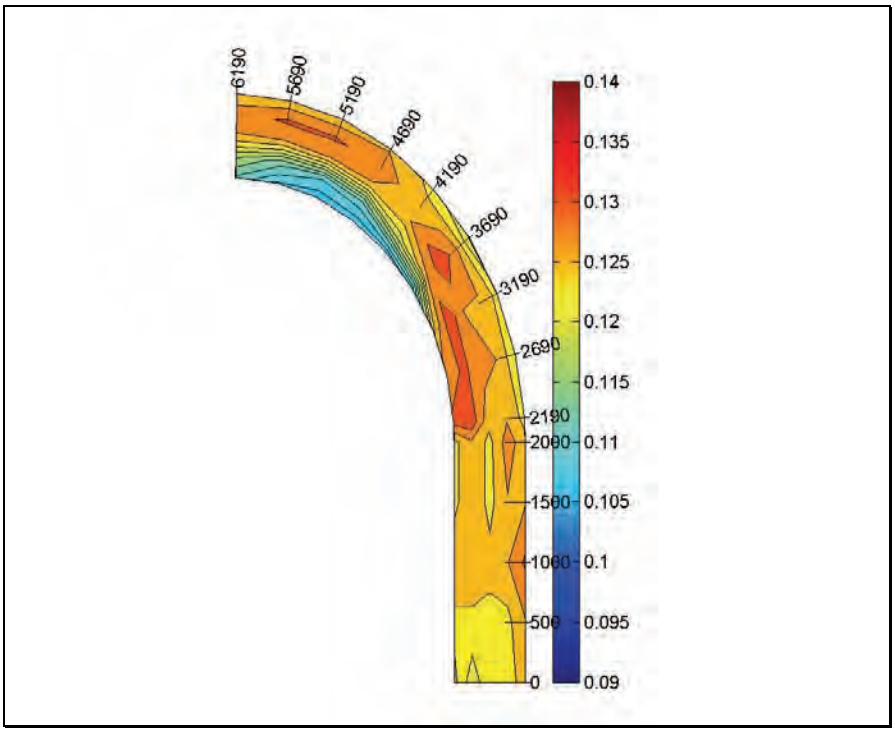

Figure 9-8 Test A1-Velocity distribution in a horizontal plane measured at 70 mm above the bed

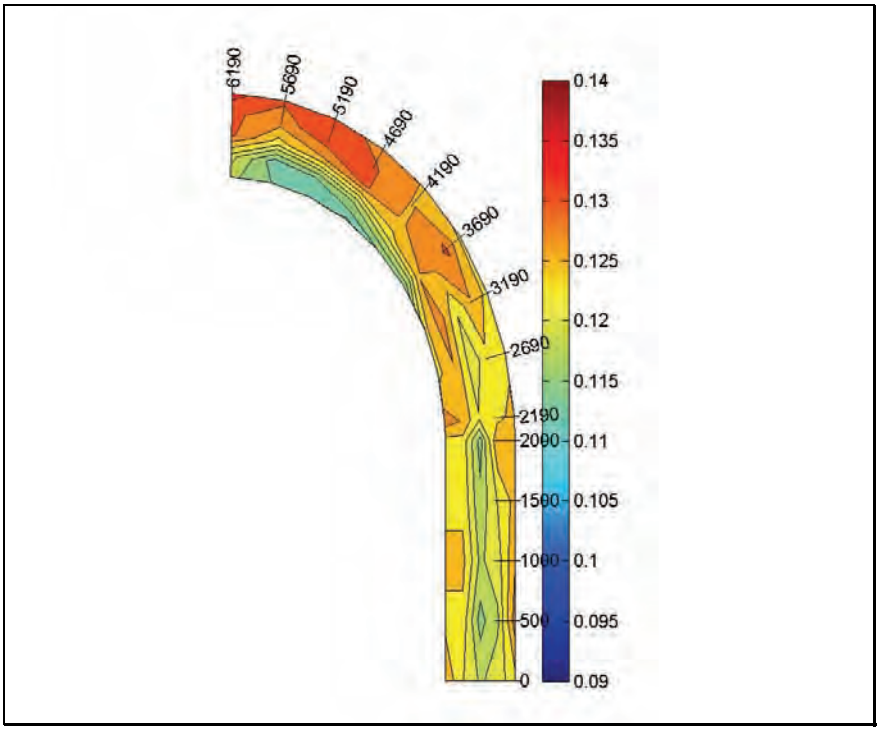

Figure 9-9 Test A1-Velocity distribution in a horizontal plane measured at 50 mm above the bed

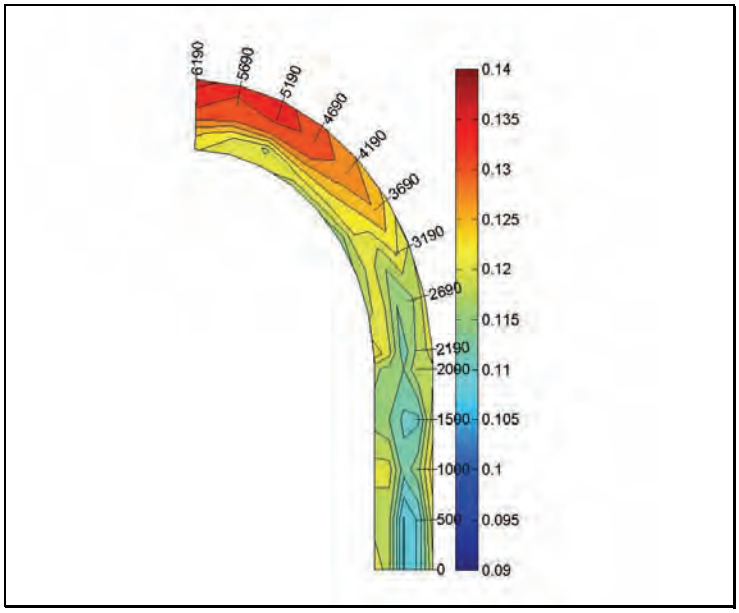

Figure 9-10 Test A1-Velocity distribution in a horizontal plane measured at 30 mm above the bed

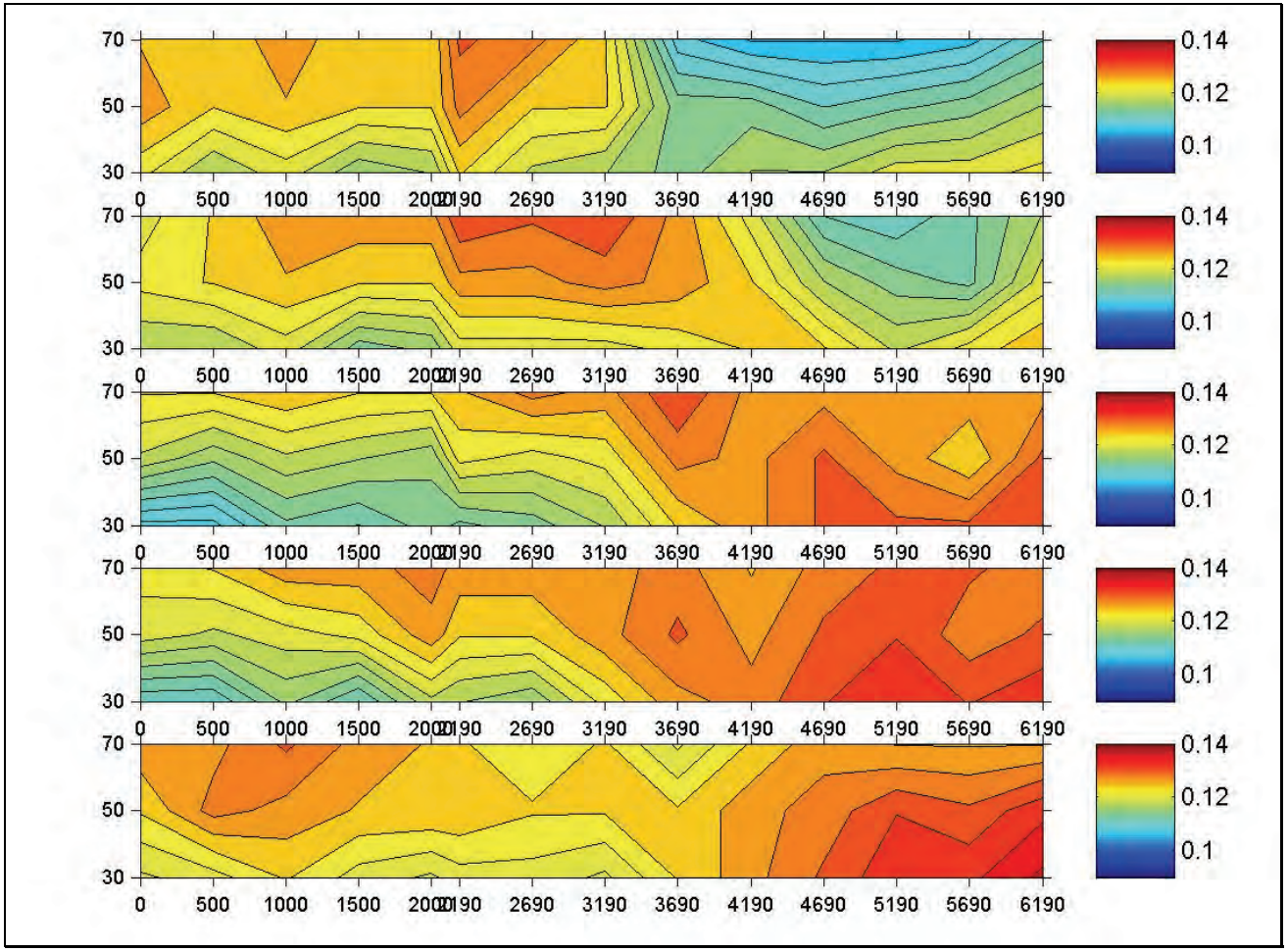

Figure 9-11 Test A1-Velocity distribution in the vertical plane

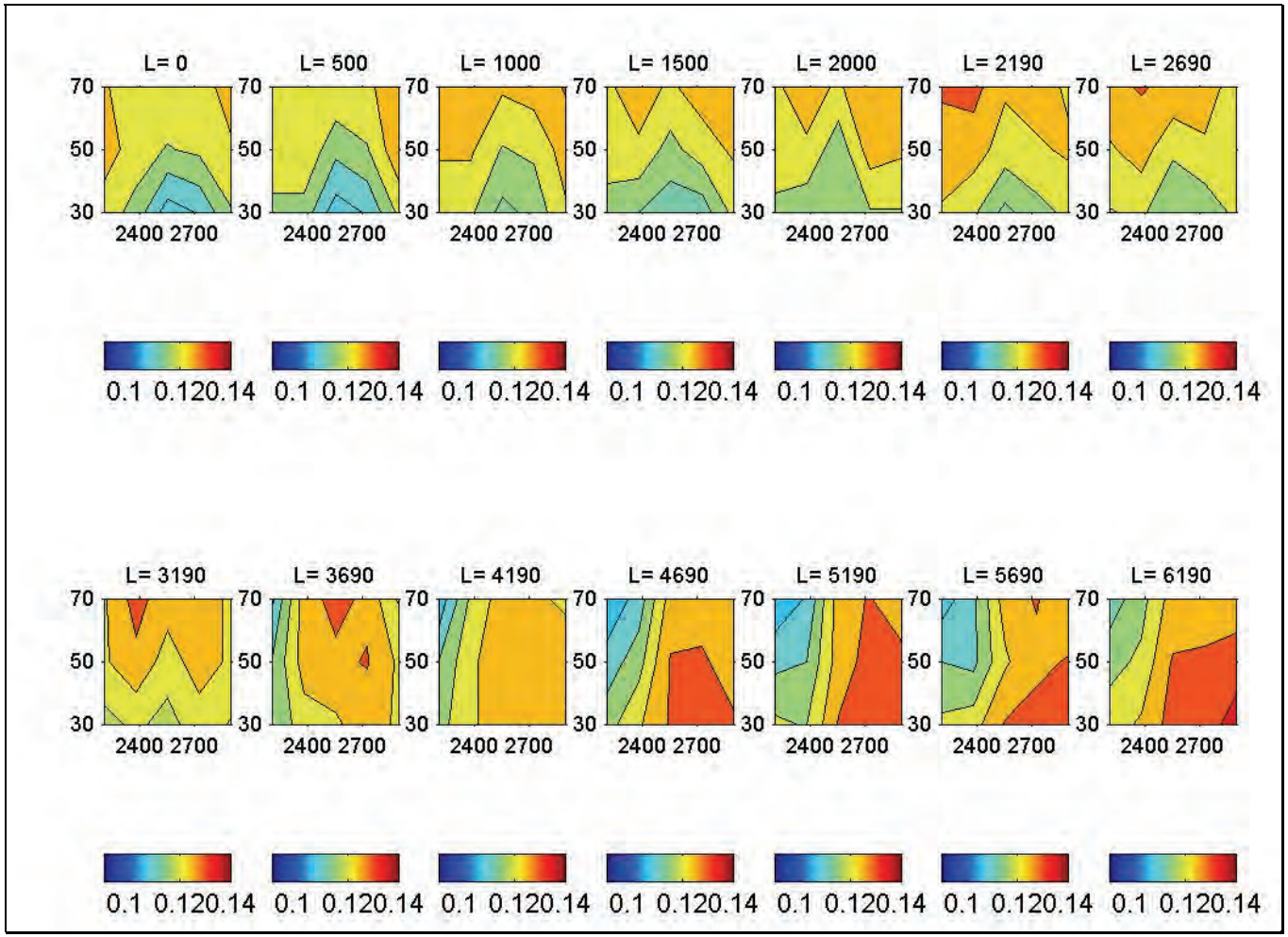

Figure 9-12 Test A1-Cross-sectional velocity distribution

B) TEST A2 (FROUDE = 0.3)

The discharge during this test was 10.15 l/s and the average water depth was 108.9 mm. The following figures 9-13 to 9-17 indicate the velocity distribution obtained for the scenario where the Froude number is equal to 0.3. A maximum velocity of 0.34 m/s was measured at the location 5.69 m on the outside of the bend.

The path of maximum velocity follows the centre of the channel up to 2.0 m where it gradually shifts towards the outside of the bend in the horizontal plane. In the vertical it dives downward from approximately 2.19 m towards the bottom in the downstream direction.

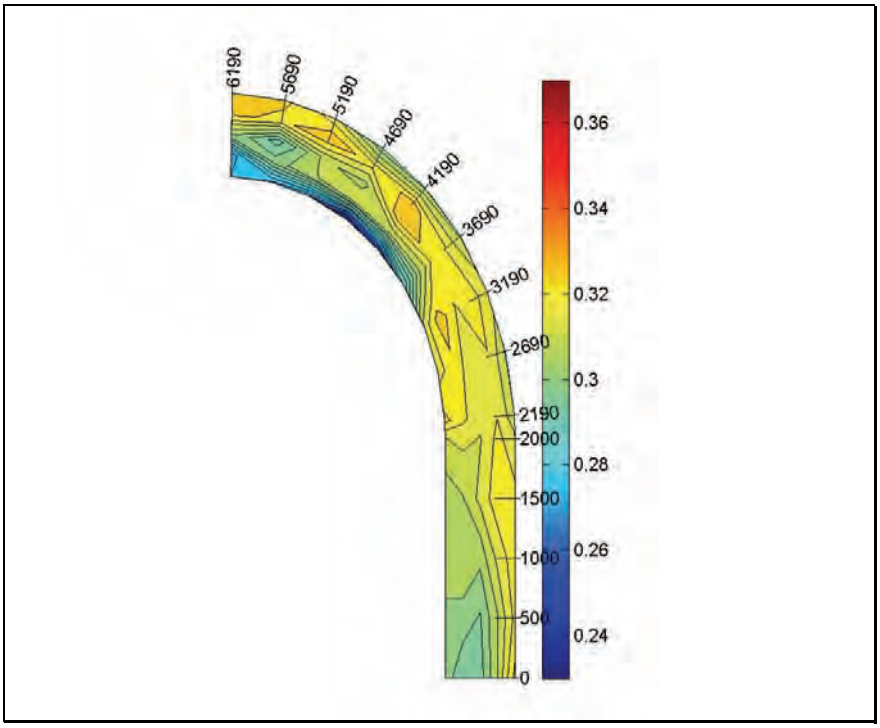

Figure 9-13 Test A2-Velocity distribution in a horizontal plane measured at 70 mm

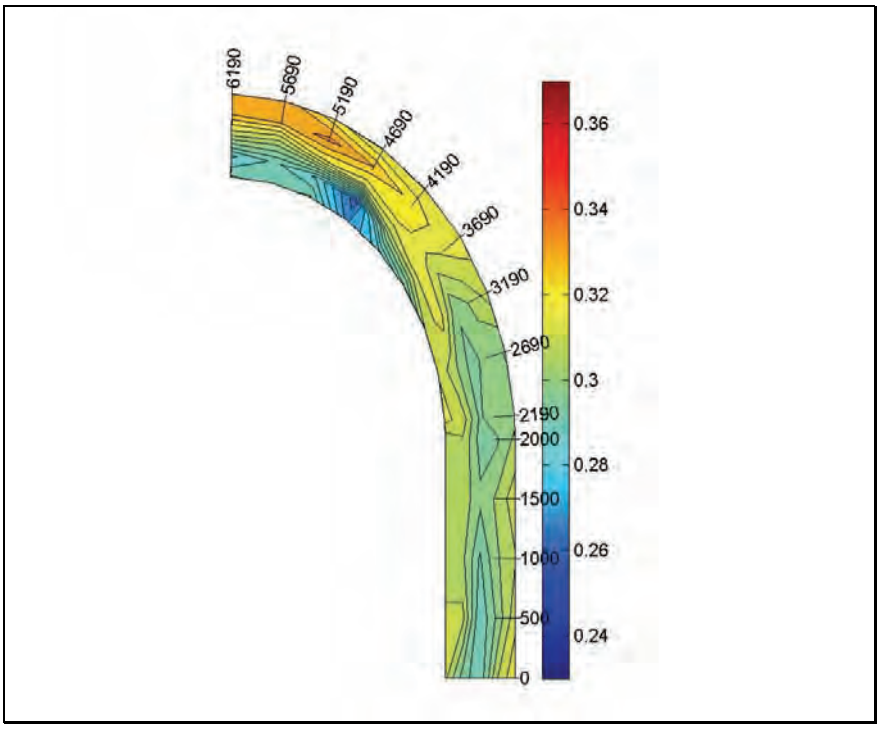

Figure 9-14 Test A2-Velocity distribution in a horizontal plane measured at 50 mm

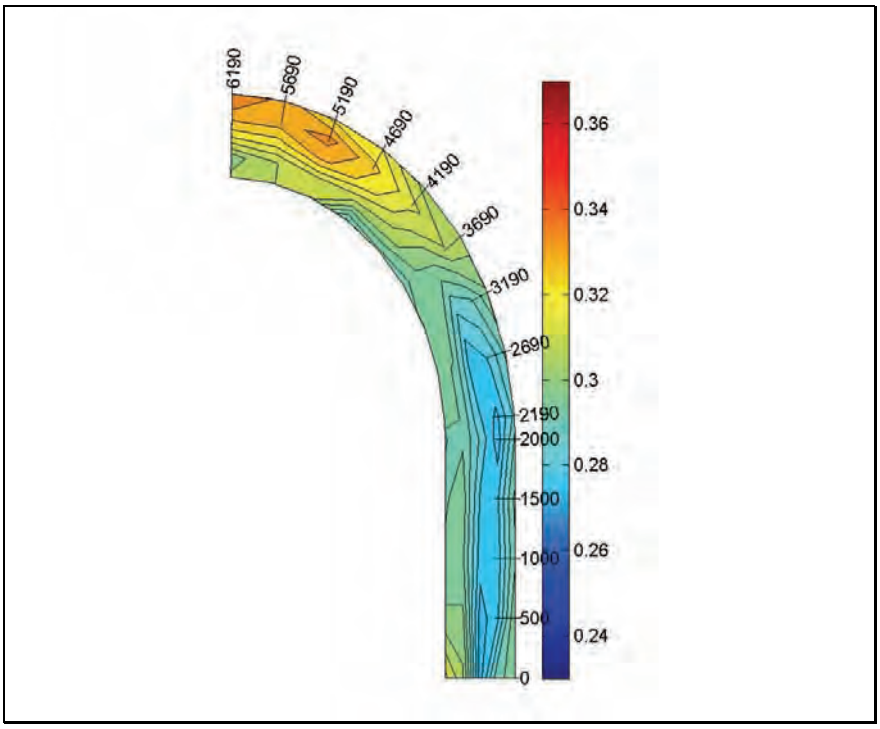

Figure 9-15 Test A2-Velocity distribution in a horizontal plane measured at 30 mm

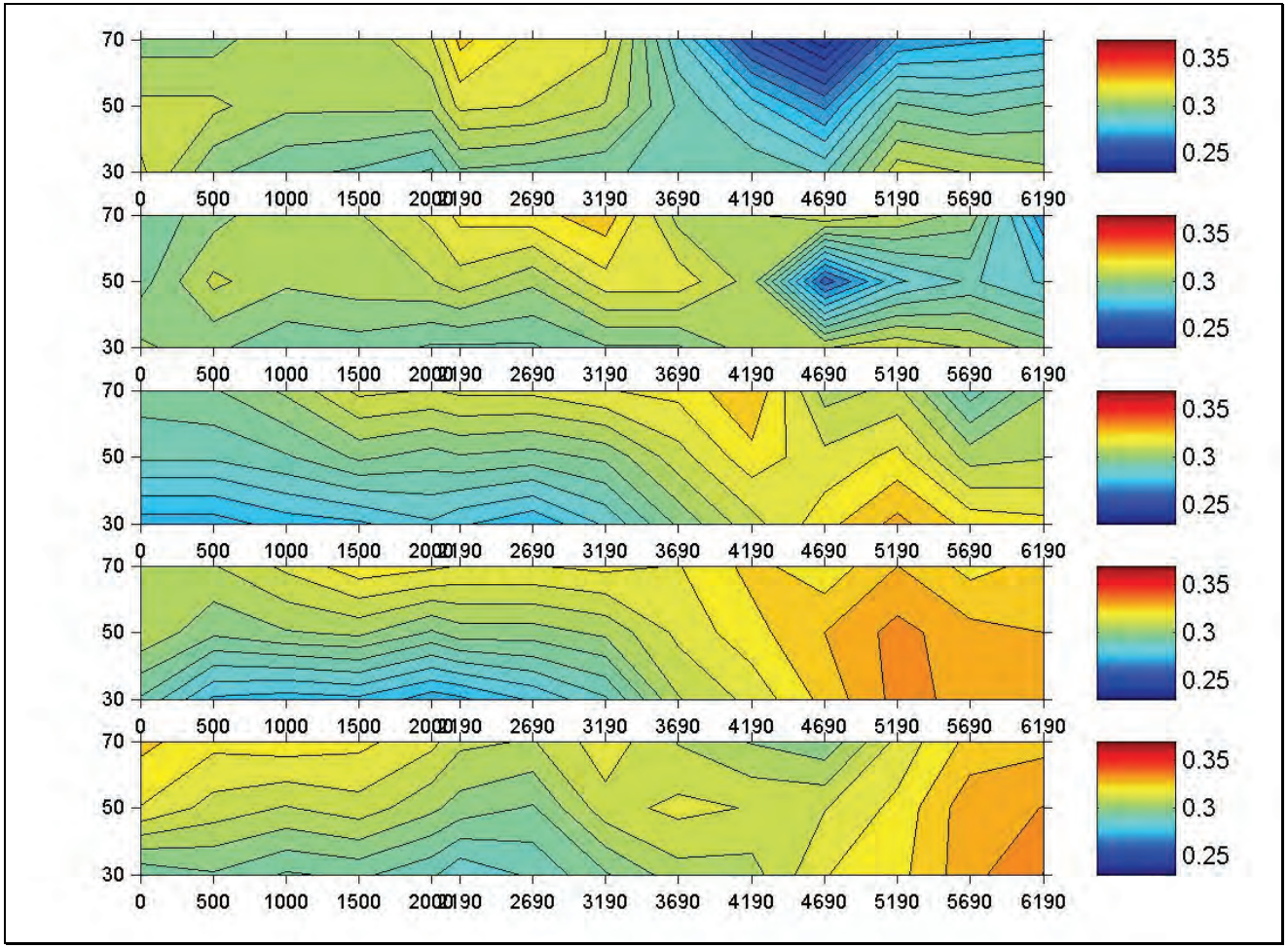

Figure 9-16 Test A2-Velocity distribution in the vertical plane

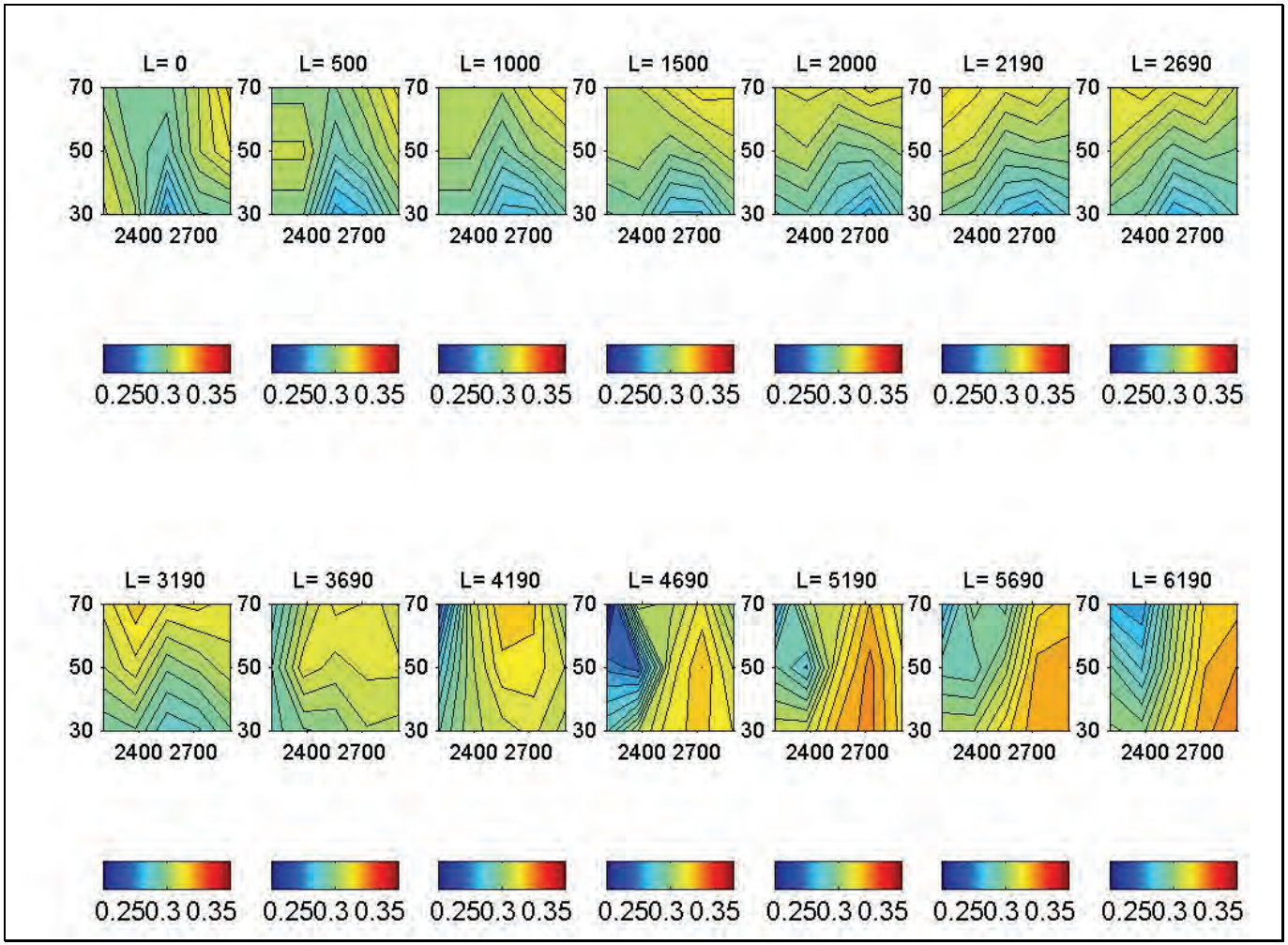

Figure 9-17 Test A2-Cross-sectional velocity distribution

C) TEST A3 (FROUDE = 0.5)

The measured discharge was 14.88 l/s and a maximum velocity of 0.477 m/s was measured on the outside of the bend between 5.19 m and 5.69 m with an average water depth of 125.6 mm. The path of maximum velocity follows the centre of the channel towards the region of 2.19 m where it shifts towards the outside of the bend in the horizontal plane. It remains near the outside of the bend throughout the curved section. In the vertical plane it moves downward in the downstream direction. The relevant figures are presented in Appendix A.

D) TEST A4 (FROUDE = 0.7)

In the horizontal plane the path of maximum velocity is near the centre of the channel up to 1.5 m where it shifts towards the inside of the channel. In the region of 2.69 m it gradually shifts towards the outside of the bend until the end of the curved section is reached and in the vertical plane it shifts downwards in the downstream direction. The maximum velocity measured was 0.52 m/s between 5.19 m and 5.69 m with a discharge of 20.77 l/s and an average water depth of 156.9 mm. The relevant figures are presented in Appendix A.

E) TEST B1 (FROUDE = 0.1)

The discharge during the test was 3.12 l/s with a maximum velocity of 0.14 m/s at the outside of the bend between 5.69 m and 6.19 m. The average water depth in the canal was 99.9 mm. The path of maximum velocity in the horizontal plane can be described as being in the centre of the canal for the first 1.5 m. Then upon entering the bend at 2.19 m it shifted towards the inside of the bend up to 3.19 m where it changed direction and moved towards the outside of the bend. In the vertical plane it can also be seen that it dives from 2.19 m towards the end of the measurements at 6.19 m. Thus, the maximum velocity shifts towards the outside of the bend and dives towards the lower measuring points as it moves in a downstream direction towards the end of the bend. The relevant figures are presented in Appendix A.

F) TEST B2 (FROUDE = 0.3)

The maximum velocity that was measured was 0.37 m/s at the outside of the bend between 5.19 m and 5.69 m. The average water level was 108.8 mm with a discharge of 9.51 l/s. The path of the maximum velocity follows essentially the same pattern as described above. In the horizontal plane it moves from the centre of the channel towards the inside at 2.19 m and then

shifts rapidly towards the outside of the bend at 3.69 m where it follows the outside of the bend until the end of the bend. From the vertical velocity distribution it is seen how it moves downwards from 2.69 m to the end of the measurements at 6.19 m. The relevant figures are presented in Appendix A.

G) TEST B3 (FROUDE = 0.5)

The average water level during the test was 107.1 mm with a discharge of 14.72 l/s. Between 5.19 m and 5.69 m a maximum velocity of 0.58 m/s was measured at the outside of the bend. In the horizontal plane the path of maximum velocity was once again in the middle of the channel up to 2.19 m where it moved towards the inside of the bend as is shown in Figure 9-18. At 3.19 m it gradually moved towards the outside of the bend where it followed the outside of the bend until the end. From Figure 9-19 and Figure 9-20 it is shown that the maximum velocity moves downwards from 2.690 m towards the end of the curved section in the vertical plane.

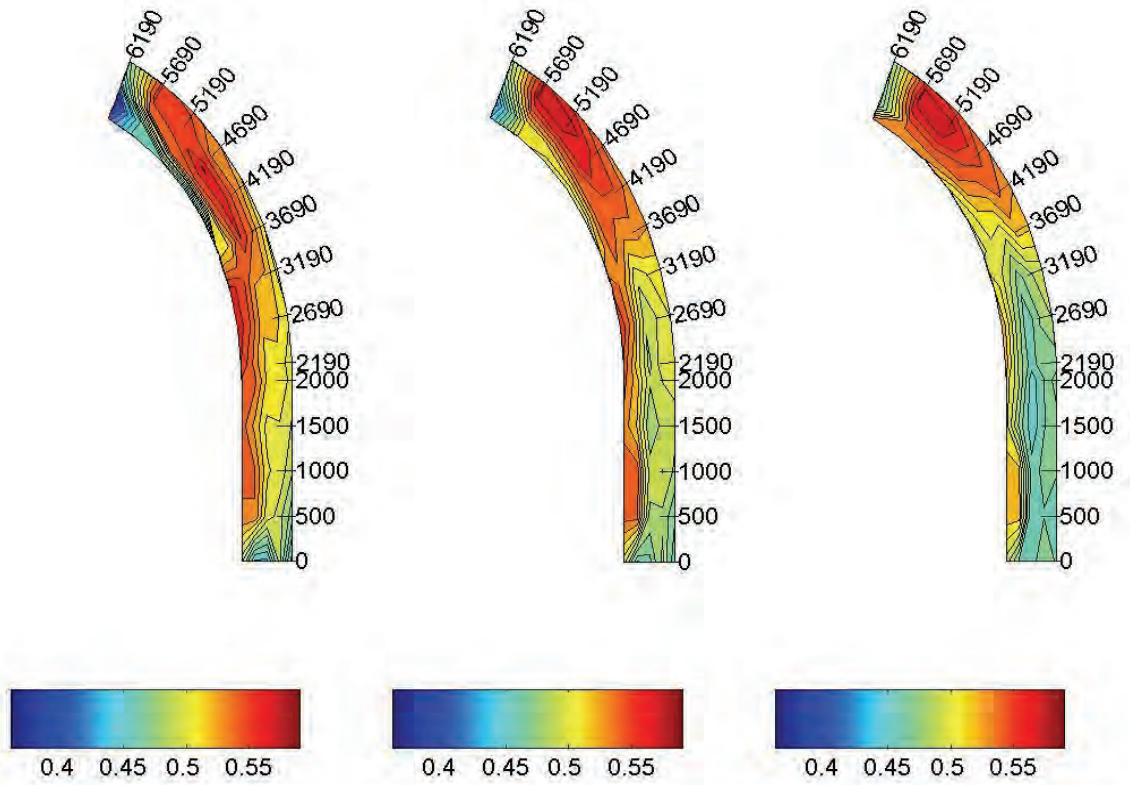

Figure 9-18 Test B3- Velocity distribution in the horizontal plane measured at 70, 50 and 30 mm

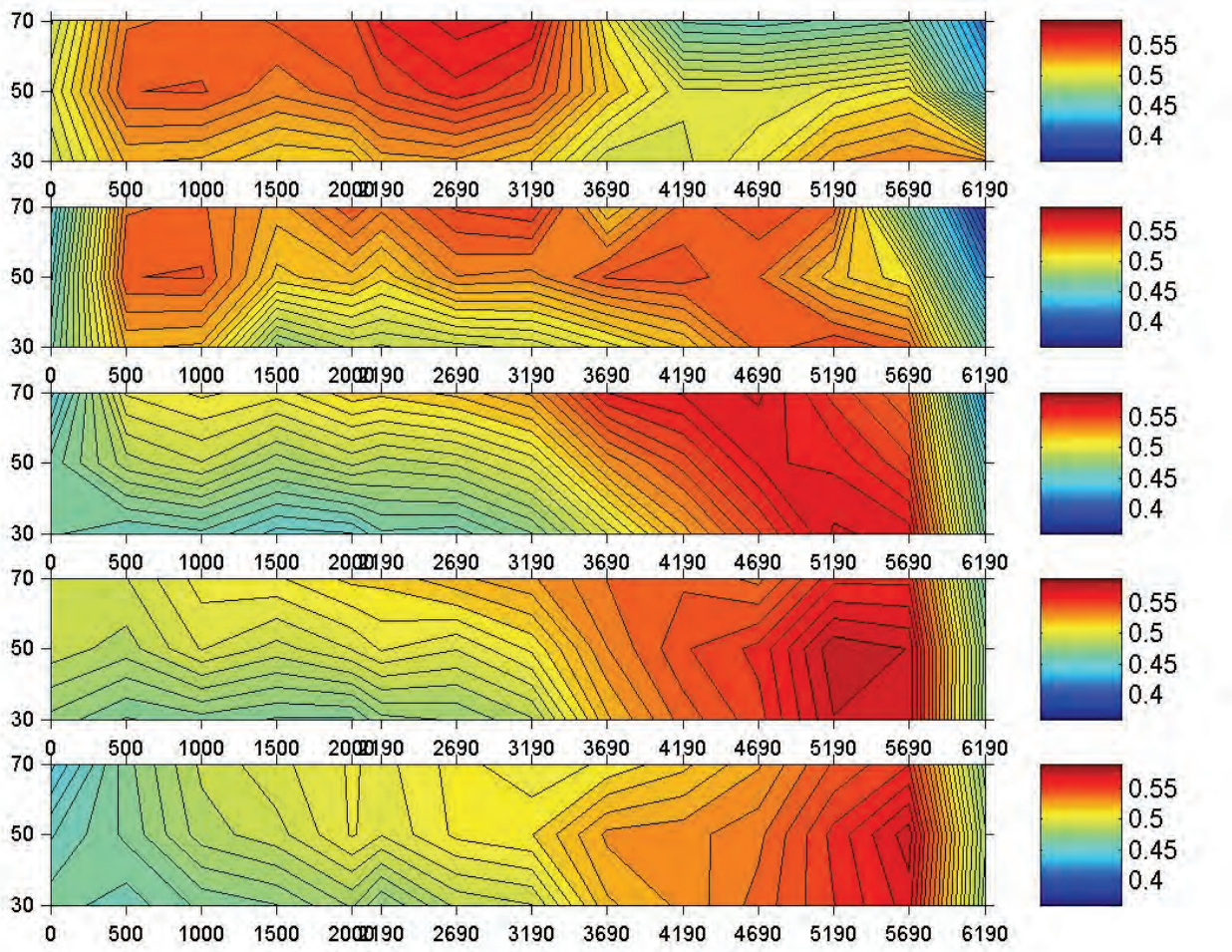

Figure 9-19 Test B3- Velocity distribution in the vertical plane

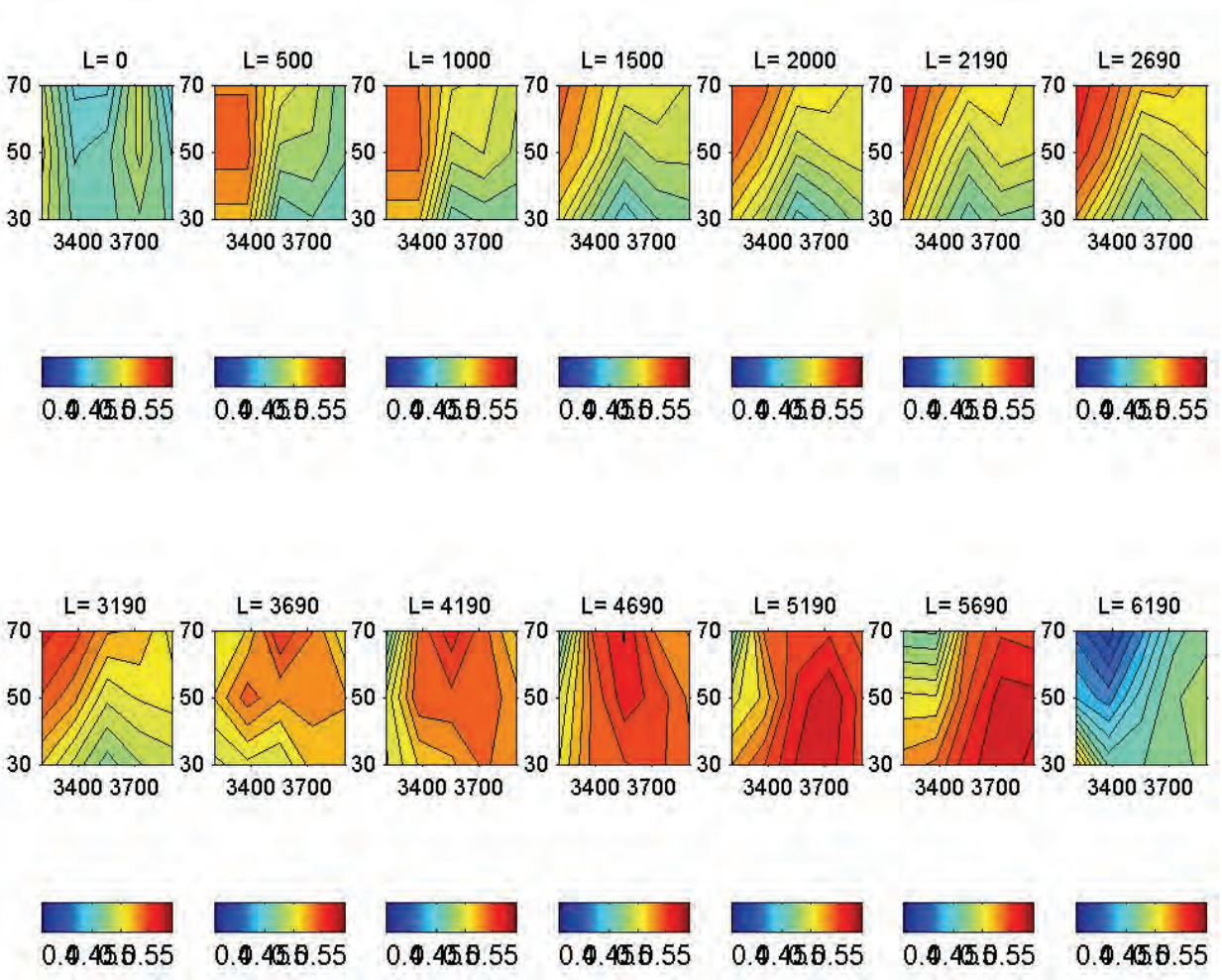

Figure 9-20 Test B3-Cross-sectional velocity distribution

H) TEST B4 (FROUDE = 0.7)

A maximum velocity of 0.63 m/s was measured around 5.69 m at the outside of the bend. The discharge was 20.69 l/s with an average water depth of 135.4 mm. The maximum velocity followed the route of being fairly in the centre of the channel in the horizontal plane up to 1.5 m where it suddenly shifted towards the inside of the bend and then at 3.19 m it shifted towards the outside of the bend until the end of the bend. In the vertical plane it also moved downwards from about 2.69 m in the downstream direction. The relative figures are presented in Appendix A.

I) TEST C1 (FROUDE = 0.1)

In the horizontal plane the maximum velocity moved from being in the centre of the channel towards the inside at about 2.69 m and shifted swiftly towards the outside of the bend at 4.19 m where it followed the outside of the bend up to the point where measurements were taken. It shifted downwards from around 2.69 m towards the bottom in the downstream direction in the vertical plane. The average water depth during the test was 128.3 mm with a discharge of 3.53 l/s. A maximum velocity of 0.127 m/s was recorded in the region of 6.19 m near the outside of the bend. The resultant figures are presented in Appendix A.

J) TEST C2 (FROUDE = 0.3)

A maximum velocity of 0.31 m/s was measured at the outside band at 6.19 m while the average water depth was 122.6 mm with a discharge of 9.14 l/s. The path of the maximum velocity in the horizontal plane was in the middle of the channel up to 3.19 m where it slightly shifted towards the inside of the bend before moving towards the outside of the bend in the vicinity of 4.19 m. It remained on the outside of the bend towards the end of the curved section. In the vertical plane it moved downward in the downstream direction. The related figures are presented in Appendix A.

K) TEST C3 (FROUDE = 0.5)

The maximum velocity followed the centre of the channel until 3.19 m where it shifted towards the outside of the bend in the horizontal plane. It followed the outside of the bend up to 6.19 m where the maximum velocity of 0.591 m/s was recorded. In the vertical plane the position of the maximum velocity also shifted from being in the upper region to the lower region in the

downstream direction. The discharge during the test was 15.11 l/s with an average water depth of 103.8 mm. Figures describing this test are attached in Appendix A.

L) TEST C4 (FROUDE = 0.7)

The discharge during the test was 20.82 l/s with an average water level of 168.7 mm. At 6.19 m the maximum velocity was measured on the outside of the bend. In the horizontal plane the maximum velocity shifted from being essentially in the centre of the channel up to 2.69 m towards to outside of the bend at 3.19 m where it remained until the end of the bend and in the vertical plane it moved downwards from 2.19 m, towards the bottom in the downstream direction. The exceptionally low velocity indicated on the velocity distribution figures at 3.19 m near the inside of the bend are due to a measuring mistake and does not reflect the actual velocity. The relevant figures are presented in Appendix A.

9.3.1.2 ANALYSIS OF TESTS ON DIVERSION LOCATION

A summary of the position of the maximum velocity as were measured is given in Table 9-1. The location of the maximum velocity (L_{vmax}) for r_c = 2.55 m was found to be in the region of 3.19 m from the beginning of the bend. When this length is converted into an angle, with zero being at the beginning of the bend, the angle where the maximum velocity is located (θ_{vmax}) is at 68°. The ratio of the position of the maximum velocity to the total bend angle ($\theta_{v\max}/\theta_{bend}$) was calculated at 0.65.

Similarly, the location of the maximum velocity for r_c = 3.55 m was at 3.69 m with θ_{vmax} = 57° and $\theta_{v\max}/\theta_{bend} = 0.75$. For r_c = 4.55 m the maximum velocity was measured at 4.19 m with θ_{vmax} = 51° and $\theta_{v\max}/\theta_{bend} = 0.85$. A summary of the relation between the radius of curvature and the maximum axial flow velocity position is given in Table 9-2.

Table 9-1 Summary of maximum velocity location in curved section

Test No	r_c [m]	fr	L_{vmax} [m]
A1	2.55	0.1	3.19-3.69
A2	2.55	0.3	3.69
A3	2.55	0.5	3.19-3.69
A4	2.55	0.7	3.19-3.69
B1	3.55	0.1	3.69-4.19
B2	3.55	0.3	3.19-3.69
B3	3.55	0.5	3.19-3.69
B4	3.55	0.7	3.69
C1	4.55	0.1	4.19
C2	4.55	0.3	4.19
C3	4.55	0.5	4.19
C4	4.55	0.7	4.19

Table 9-2 Relation of radius of curvature to maximum velocity position

r_c	θ_{bend} [°]	$\theta_{v\max}$ [°]	$\theta_{v\max}/\theta_{bend}$
2.55	104	68	0.65
3.55	76	57	0.75
4.55	60	51	0.85

In summary, the maximum velocity is found near the bend exit on the outside of the bend; the velocities are higher on the outside of the bend than on the inside and the maximum velocity shifts downwards while moving towards the outside of the bend in the downstream direction.

This confirms the presence of a clockwise spiral that develops in the bend as was found in the literature.

The vertical velocity distributions obtained from the laboratory experiments were plotted as a line graph to further analyse the diving phenomenon that was observed from the vertical velocity distributions. The velocity measured at 70 mm from the bottom is represented as V70 while the velocity measured at 50 mm is represented as V50 and the velocity measured at 30 mm as V30. The line graphs for Test B2 are shown Figure 9-21, Figure 9-22 and Figure 9-23 while the relevant figures for the other tests are presented in Appendix A.

The following characteristics in the downstream direction is noted from the abovementioned figures:

i) The measured velocity at 70 mm from the bottom (V70) has a decreasing tendency near the inside of the bend. (Figure 9-21)

ii) In the centre of the bend all the measured velocities have an increasing tendency. (Figuer 9-22)

iii) Near the outside of the bend the measured velocity at 30 mm from the bottom (V30) shows an increasing tendency. (Figure 9-23)

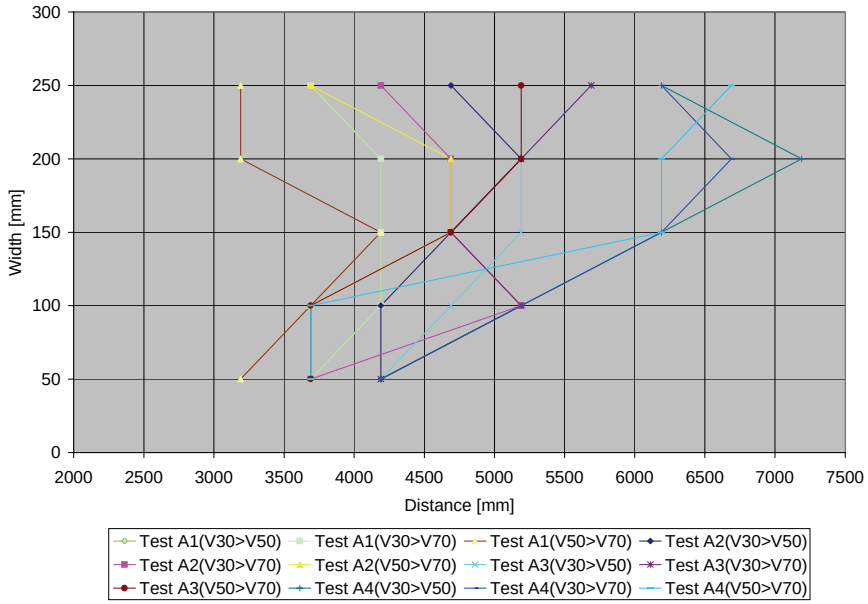

Figure 9-21 Location of turning points where V30>V50, V30>V70 and V50>V70 for Test A1, A2, A3 and A4

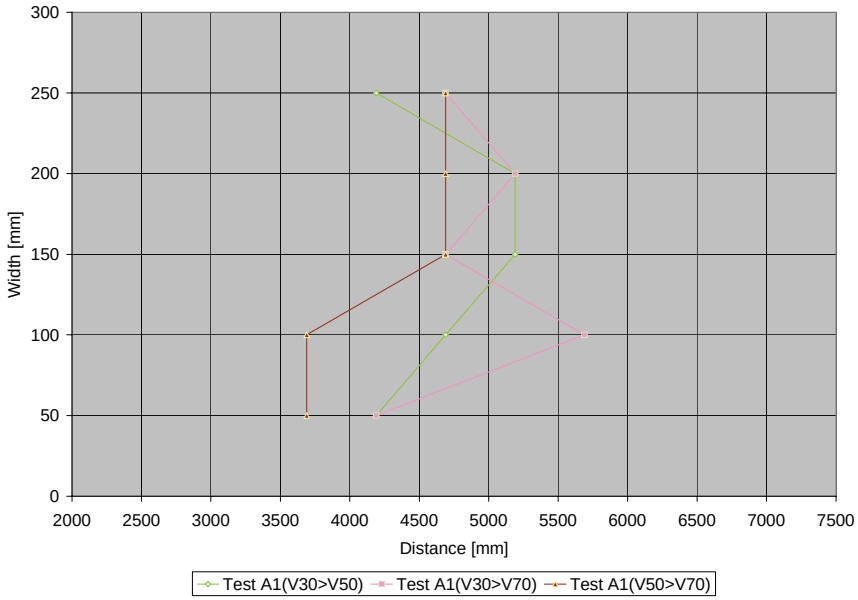

Figure 9-22 Location of turning points where V30>V50, V30>V70 and V50>V70 for $r_c/w = 8.5$ and Fr = 0.1

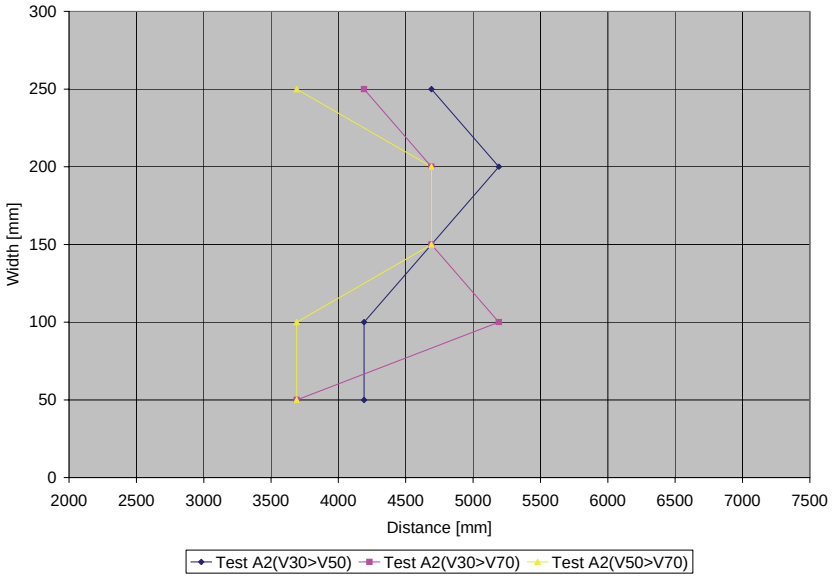

Figure 9-23 Location of turning points where V30>V50, V30>V70 and V50>V70 for $r_c/w = 8.5$ and Fr = 0.3

Figure 9-24 to 9-28 indicate the location of the turning points for Test A with the range of Froude numbers that were tested. The relevant figures for Test B and Test C are presented in Appendix D.

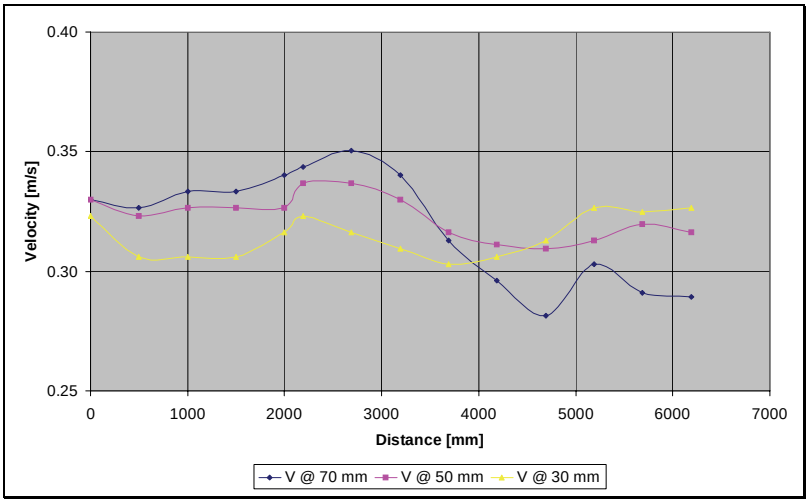

Figure 9-24 Decreasing tendency of V70 near the inside of the bend with $r_c/w = 11.8$ and $F_r = 0.3$

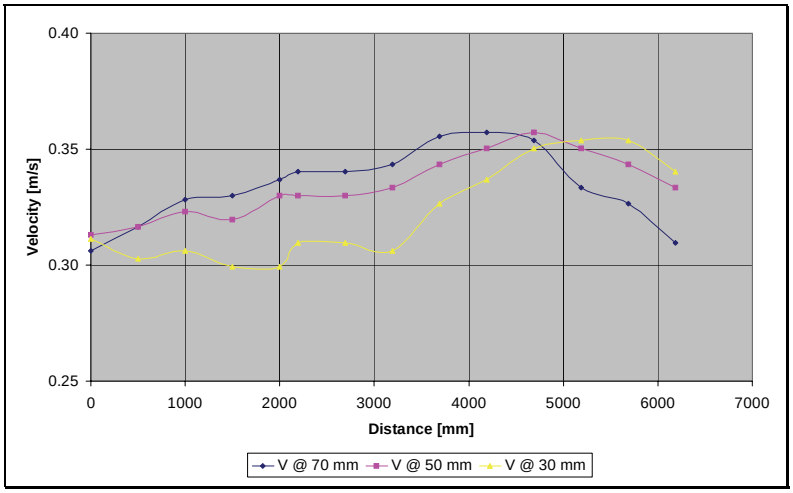

Figure 9-25 Increasing tendency of V70, V50 and V30 at the centre of the bend with $r_c/w = 11.8$ and Fr = 0.3

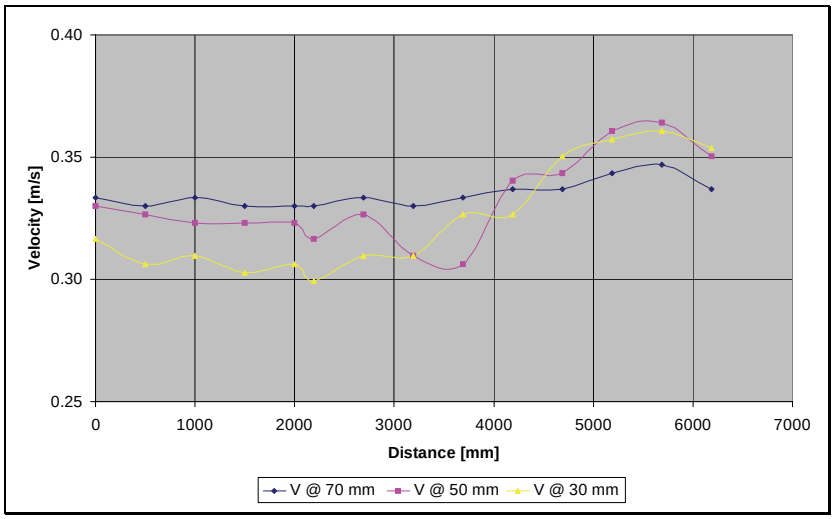

Figure 9-26 Increasing tendency of V30 near the outside of the bend with $r_c/w = 11.8$ and Fr = 0.3

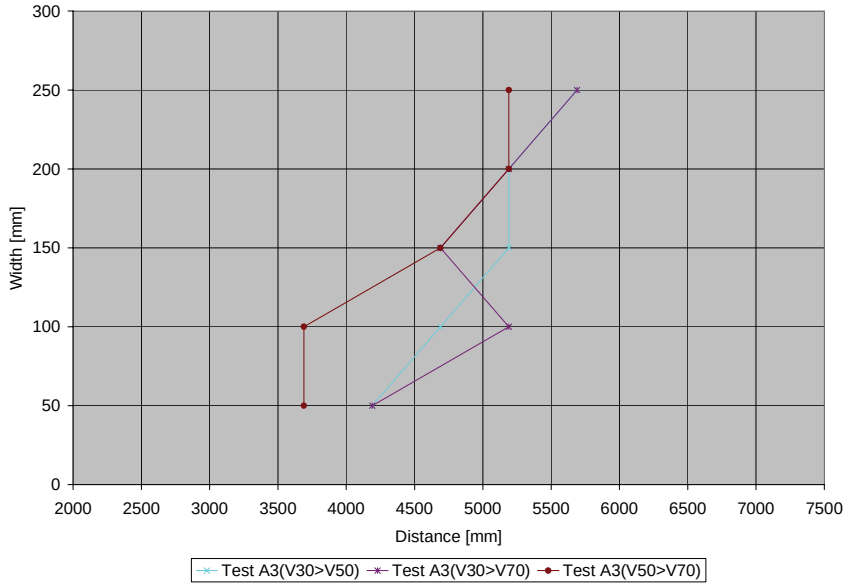

Figure 9-27 Location of turning points where V30>V50, V30>V70 and V50>V70 for $r_c/w = 8.5$ and Fr = 0.5

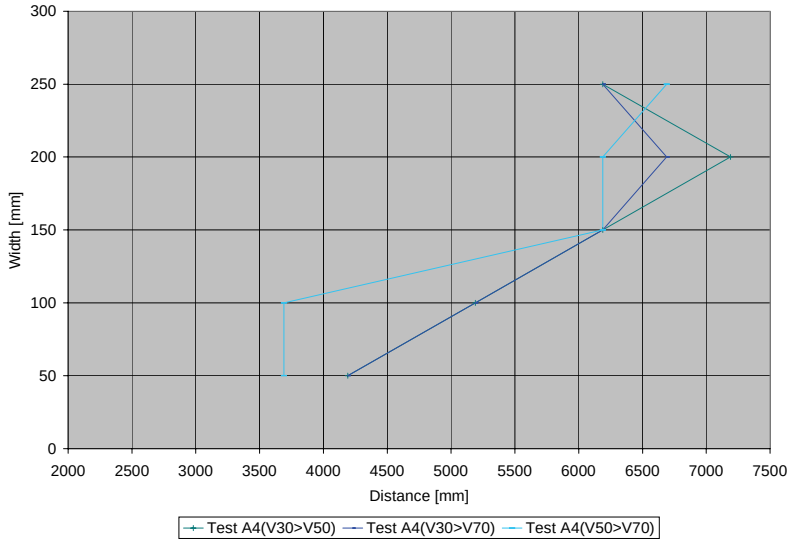

Figure 9-28 Location of turning points where V30>V50, V30>V70 and V50>V70 for $r_c/w = 8.5$ and Fr = 0.7

From these figures it is noted that the turning points where V30>V50, V30>V70 and V50>V70 stay relatively constant near the inside of the bend but at the outside of the bend it moves in the downstream direction with an increase in Froude number. When comparing the location of these

turning points of Test A, Test B and Test C, it is noted that the turning points also move in the downstream direction with an increase of the radius of curvature. The range of locations of the turning points increase on the inside and outside of the bend for an increase in the radius of curvature. This turning phenomenon of V30, V50 and V70 can only occur due to the presence of the secondary (spiral) flow.

The recommendation by *Raudkivi (1993)* that the angle has to be greater than 30° for secondary flow to develop fully was applied to the data of the laboratory experiment carried out in the current research. With reference to Figure 9-29 the calculations were done as follows:

$$180^\circ = \theta + \beta + \gamma$$

$$\gamma = 90° - \alpha$$

$$\alpha = \cos^{-1}\left(r_c / r_o\right)$$

$$\beta = \sin^{-1}\left(r_c / r_o\right)$$

where θ = angle for fully developed secondary flow [°]

r_c = centerline radius [m]

r_o = outside radius [m]

therefore $180^\circ = \theta + \beta + (90° - \alpha)$

and $90^\circ = \theta + \beta - \alpha$

$$\theta = 90^\circ - \beta + \alpha$$

thus,

$$\theta = 90^\circ - \sin^{-1}\left(r_c / r_o\right) + \cos^{-1}\left(r_c / r_o\right) \quad \text{..... (9-10)}$$

The results are shown in Table 9-3 and it can be seen that the secondary flow was fully developed, according to *Raudkivi (1993)*, for the tests with a r_c/w of 8.5 and 15.2 and that the secondary flow was not fully developed for Test C with r_c/w = 15.2.

Evaluating equation 9-10 and solving r_c and r_o for $\theta = 30°$ resulted in the relationship of $r_c/r_o < 0.9659$ for the secondary flow to develop fully (ie $\theta > 30°$). Expressing this in terms of the centerline radius (r_c) and the width of the channel (w) yields, $r_c/w < 14.16$ to ensure that $\theta > 30°$.

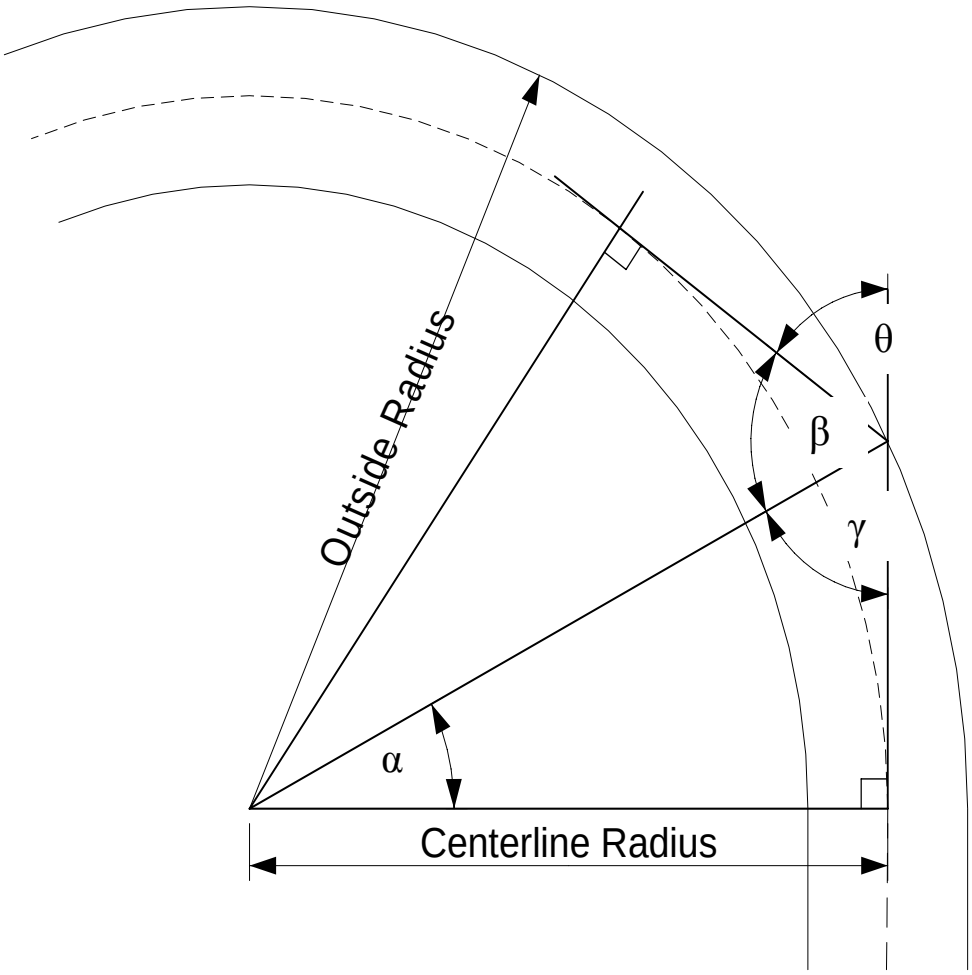

Figure 9-29 Calculations for fully developed secondary flow

Table 9-3 Angle for fully developed secondary flow (See Figure 9-29)

Test	r_c	W	r_c / w	θ [°]
A	2.55	0.3	8.5	38.4
B	3.55	0.3	11.8	32.7
C	4.55	0.3	15.2	29

Equations 7-17 and 7-18 were applied to the data obtained from the current research and is shown in Figure 9-30. The Chezy coefficient (*C*) was calculated with $C = R^{\frac{1}{6}} / n$ *(Featherstone and Nalluri, 1995)*, where *R* is the wetted perimeter and *n* is the Manning value of 0.013 (concrete with bends). The result obtained from the current research was also plotted on Figure 9-30 under the assumption that the secondary flow was fully developed at the location of the maximum measured velocity.

From Figure 9-30 it is noted that equation 7-17 resulted in the angle where the secondary flow is fully developed being bigger than the central bend angle. The data of the current research takes the shape of equation 7-18, except for Test C with a central bend angle of 104° and r_c/w = 15.2.

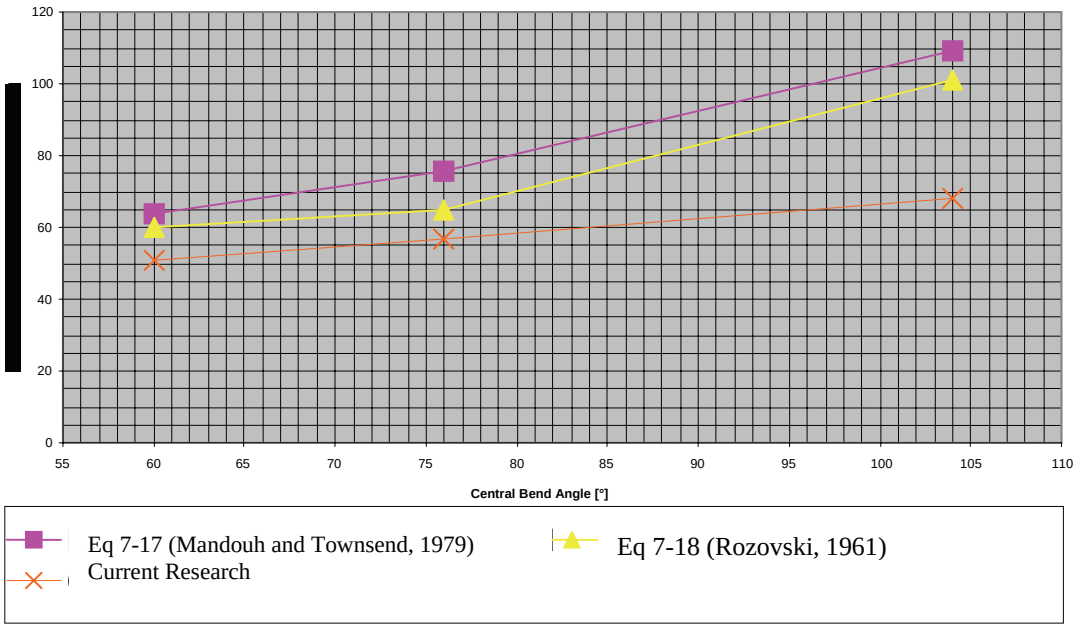

Figure 9-30 Central bend angle (θ) needed for secondary flow to develop fully

In analysing the optimum diversion location, the diversion location as recommended by *SC and Ches (1992)* (Table 8-1), *SC and Ches (1992)* (equation 8-1) and *Raudkivi (1993)* (equation 7-16) were applied to the data of the current research. The diversion location as were recommended by *SC and Ches (1992)* (Table 8-1) were found to be in very good agreement with the diversion location of the current research, while the diversion location from equation 8-1 and equation 7-16 were not in good agreement. This is shown in Figure 9-31.

Raudkivi (1993) found that the diversion location is approximately twice the river width downstream of the intersection of the upstream axis with the outer bank (Figure 7-8). For the present research it was found that the diversion location could be reasonable well predicted with the distance being 8.8 times the width of the channel downstream of the intersection of the upstream axis with the outer bank, which does not agree with the findings of Raudkivi. Simple empirical relationships should therefore be used with caution, especially outside their calibration ranges.

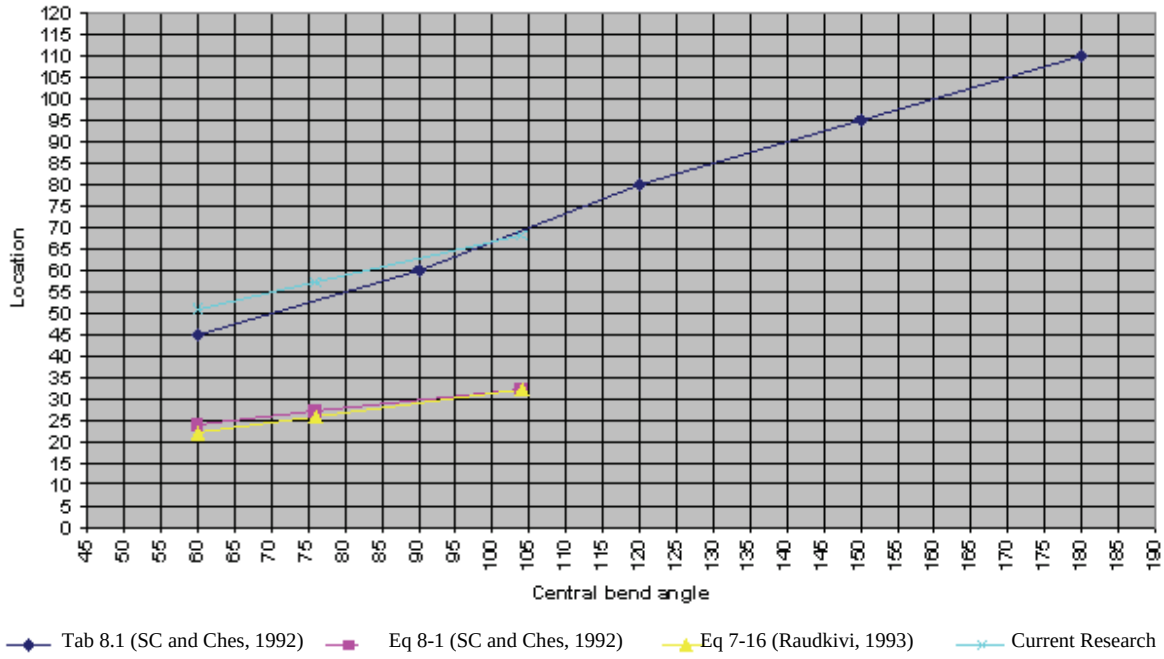

Figure 9-31 Diversion location in terms of the central bend angle

The analysis of the tests on the diversion location can be summarised as follows:

The position of the maximum velocity moves in the downstream direction with an increase in the radius of curvature (r_c) while the position is not much affected by varying froude numbers for a specific radius (Table 9-1 and Table 9-2).
The observed scour patterns have the same tendency with varying radii of curvature to width ratios (r_c/w). Three main scour holes were identified with the location of the third scour hole being in good agreement with the location of the maximum velocity.

The maximum velocities were found near the outside of the bend near the exit with higher velocities on the outside of the bend than on the inside. The maximum velocity shifts downwards

while moving towards the outside of the bend in the downstream direction. This confirms the presence of a clockwise spiral motion (for a bend to the left).

Evaluating the development of secondary flow according to *Raudkivi (1993)*) leads to the relationship that r_c/w <14.6 in order for secondary flow to develop fully in the bend.

From Figure 9-31 it can be seen that the recommended diversion location (Table 8-1) by *SC and Ches (1992)* is in very good agreement with the diversion location found in the current research.

9.3.2 SEDIMENT RELATED TESTS

9.3.2.1 300MM CHANNEL

Three laboratory tests were conducted on the same 300mm channel to determine the effect secondary flow has on sediment scour. All three were carried out under similar hydraulic conditions. The discharge into the channel for each test run was 0.01m^3/s whilst the water depth was started at 0.1m above a layer of sand 0.15m thick. No sediment was fed into the canal during the test. The duration of each test was roughly between two to two and a half hours.

The surveyed bed level changes after the tests were completed are shown in Figure 9-32, Figure 9-33 and Figure 9-34. They indicate the change in bed level due to the helical flow in the curved channel. The red colours denote positive values meaning that deposition occurred. The opposite is true for the blue colours.

As expected, due to the secondary flows that were established the deepest scour that took place was found at the outer bank of the curving channel. The sizes of the scour holes were also roughly identical: around 0.08m below the original bed level. Another more surprising similarity between the tests is that the deepest scour holes formed in the same position along the length of the channel.

It has been suggested that a natural scour hole forms at the outer (concave) bank with its deepest point approximately twice the river width downstream of the intersection of the upstream axis with the bank. Figure 7-8 (Raudkivi, 1993). Though this seems to be the case for these tests it can be seen from the next section that this statement is not universally true.

9.3.2.2 600MM CHANNEL

A few more tests were also conducted on a wider 0.6m channel. The purpose of the wider channel was to investigate shallower, wider conditions, more typical of natural rivers. The inner wall of the channel was adjusted so as to make the channel width 0.6m while the discharge was increased to $0.02m^3/s$. The original movable bed thickness was once again 0.15m.

A first experiment run was conducted for a period of two hours. At this stage the bed profile was measured and is presented in Figure 9-35. A maximum scour depth of 0.1m was recorded. Of note is the fact that although a scour hole did form at twice the width from the upstream axis intercept, it is not the deepest. The deeper scour hole formed further downstream, almost four times the breadth from the intercept point.

After the previous test the channel was slowly filled with water once more and the experiment was continued from where it was halted. The test was then allowed to run until the deepest scour holes began exposing the concrete floor beneath the layer of sand.

The measured bed profile is shown in Figure 9-36. It is clear that the longer run test is merely an extension of the shorter test, as one would expect. The deepest scour hole was measured at 0.148m below the original bed level. A photograph of this bed profile can be seen in Figure 9-37.

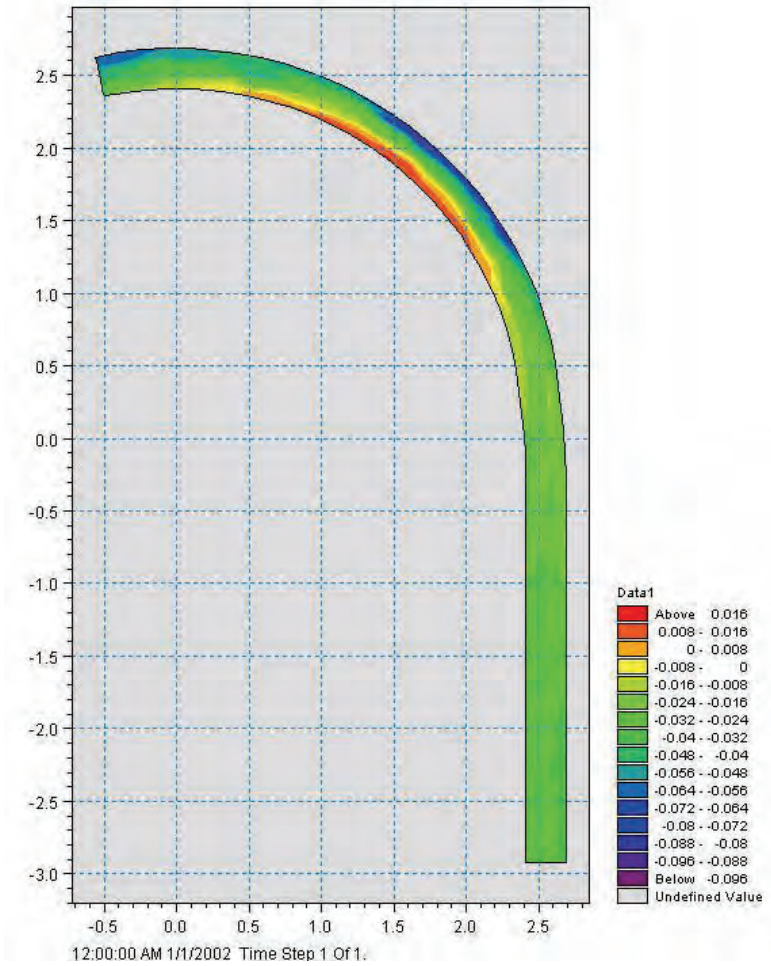

Figure 9-32 Test run 1 for 0.3m wide channel

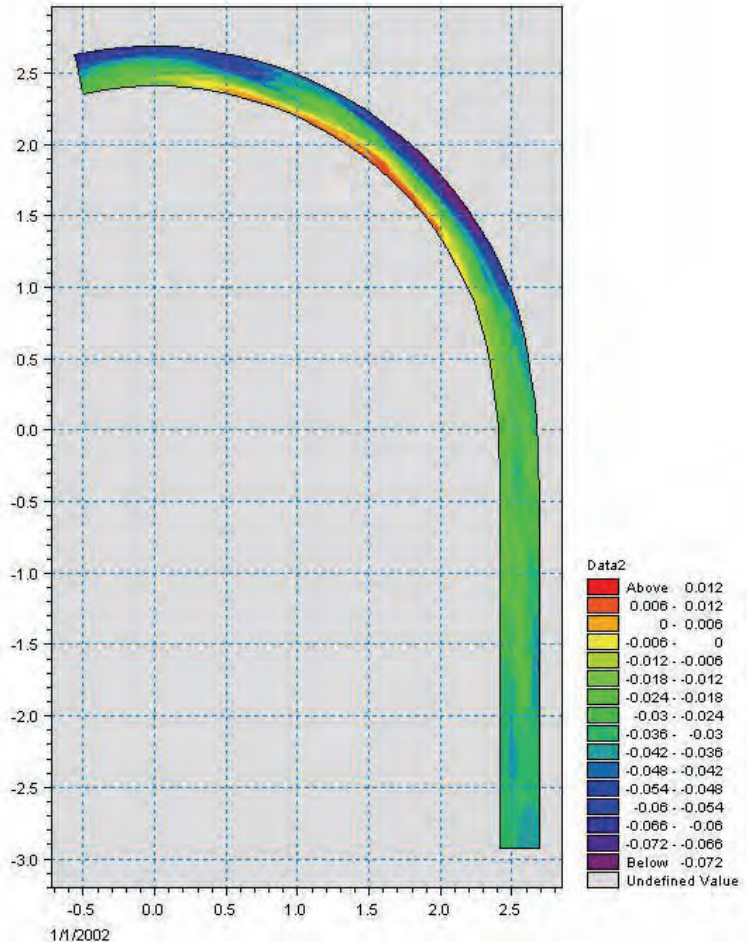

Figure 9-33 Test run 2 for 0.3m wide channel

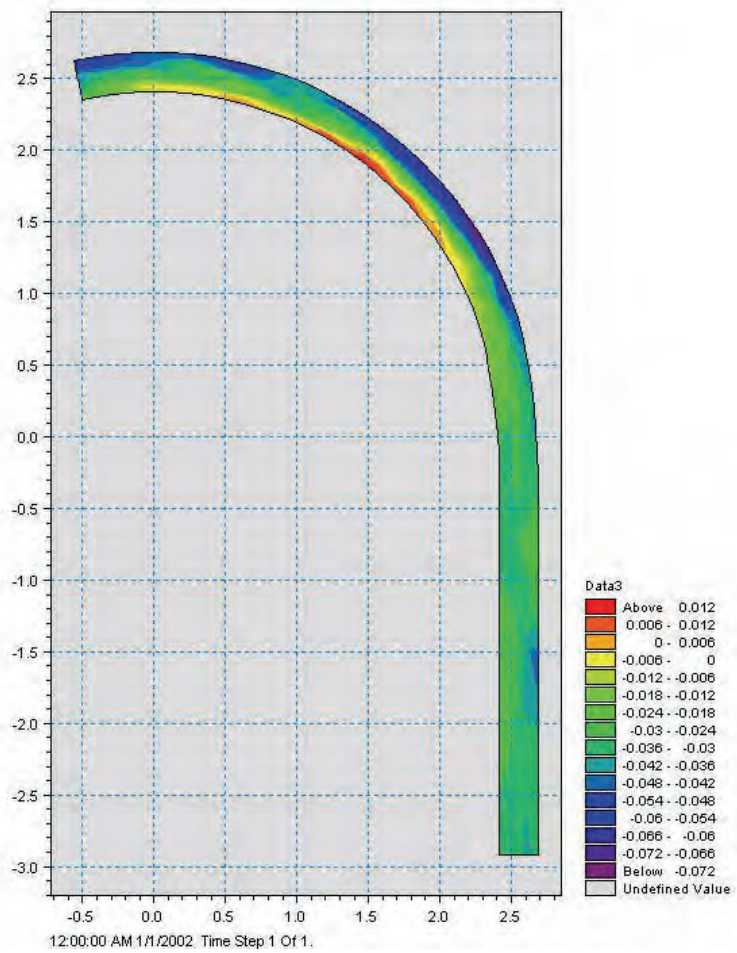

Figure 9-34 Test run 3 for 0.3m wide channel

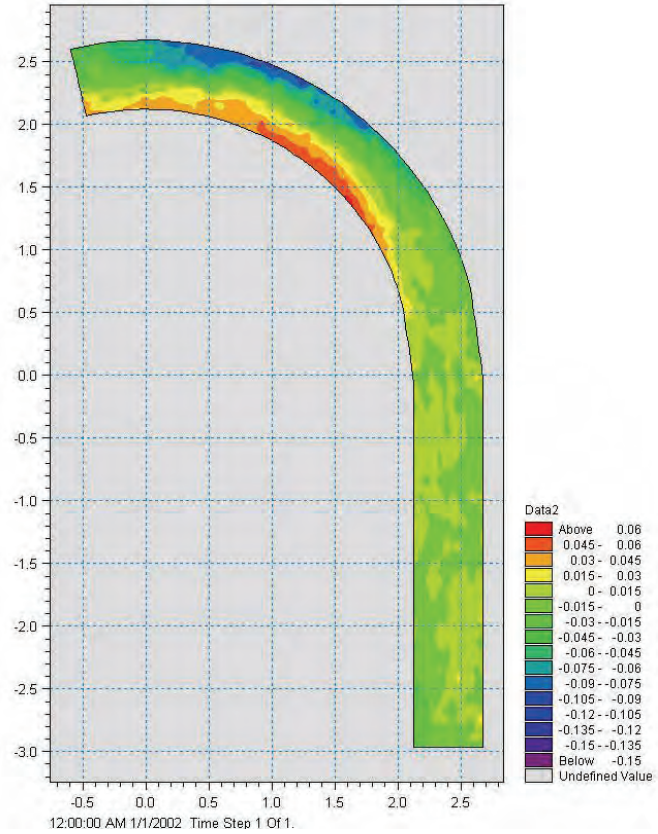

Figure 9-35 Observed bed profile changes after 2 hour run in 0.6m wide bed.

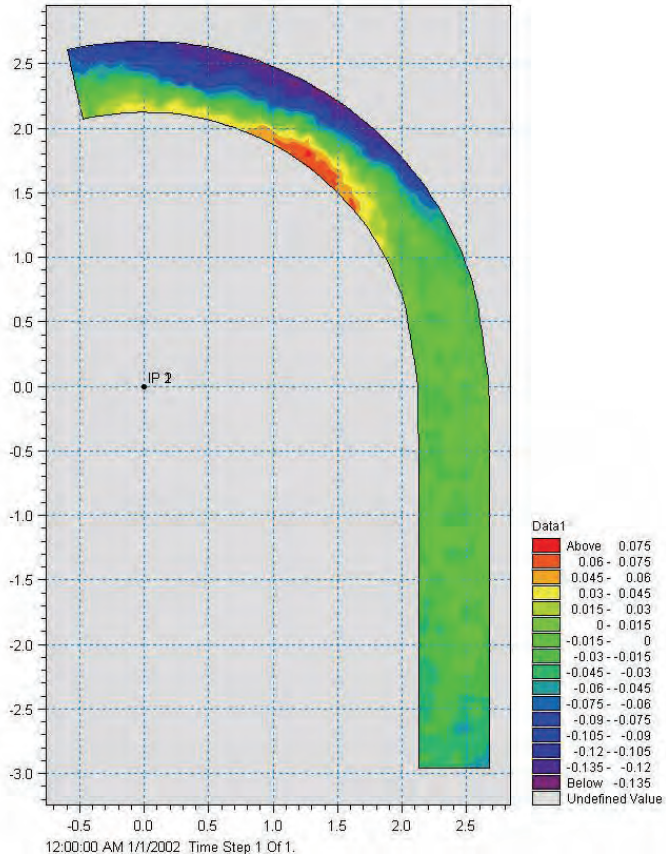

Figure 9-36 Observed bed profile changes after 8 hour run in 0.6m wide bed.

Figure 9-37 Picture of bed profile of 0.6m channel taken from upstream of channel

10 LABORATORY TESTS AND ANALYSIS ON DIVERSION ANGLE

10.1 EXPERIMENTAL SETUP

Three diversion angles were studied, i.e. diversion angles (θ) of 20°, 35° and 50° which are in good agreement with the recommended range of diversion angles found in the literature (Figure 10-1) The diversion angle (θ) is zero on the centreline in the channel direction, looking downstream, as shown in Figure 10-2.

The basic experimental set-up of Test A with r_c = 2.55 *m* was used for all the tests on the optimum diversion angle. The diversion channel was installed at 3.69 m from the beginning of the bend on the outside of the bend that coincides with the location of the maximum velocity zone. The diversion channel was 1.5 m in length and the width varied according to the diversion angle. The width at the entrance of the diversion channel was 150 mm measured on the tangent.

A second V-notch was erected at the downstream end of the main channel in order to be able to calculate the discharge through the diversion channel. The plan layout of the model is presented in Figure 10-2 and a photograph of the diversion channel is shown in Figure 10-3.

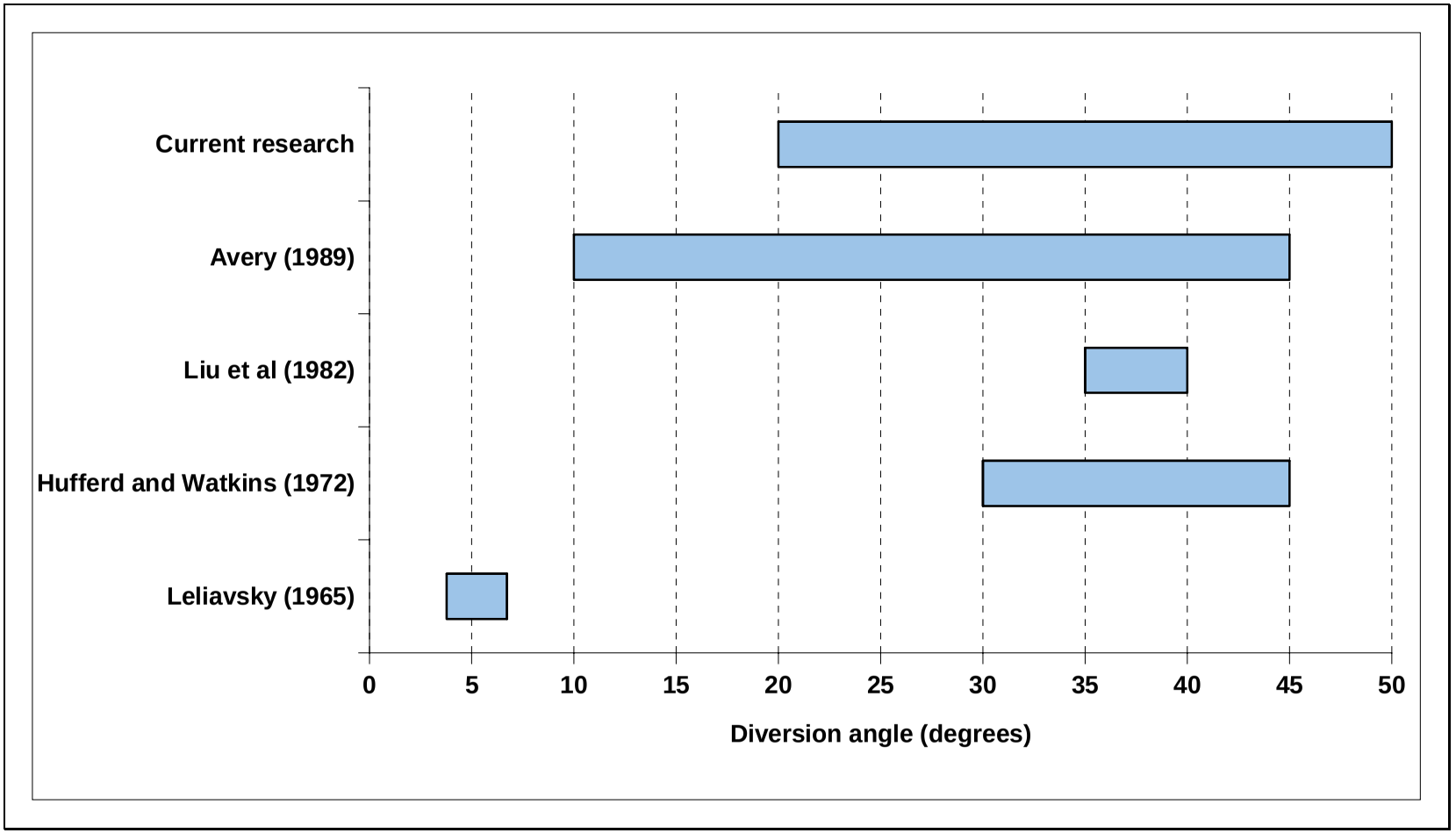

Figure 10-1 Summary of diversion angles in literature

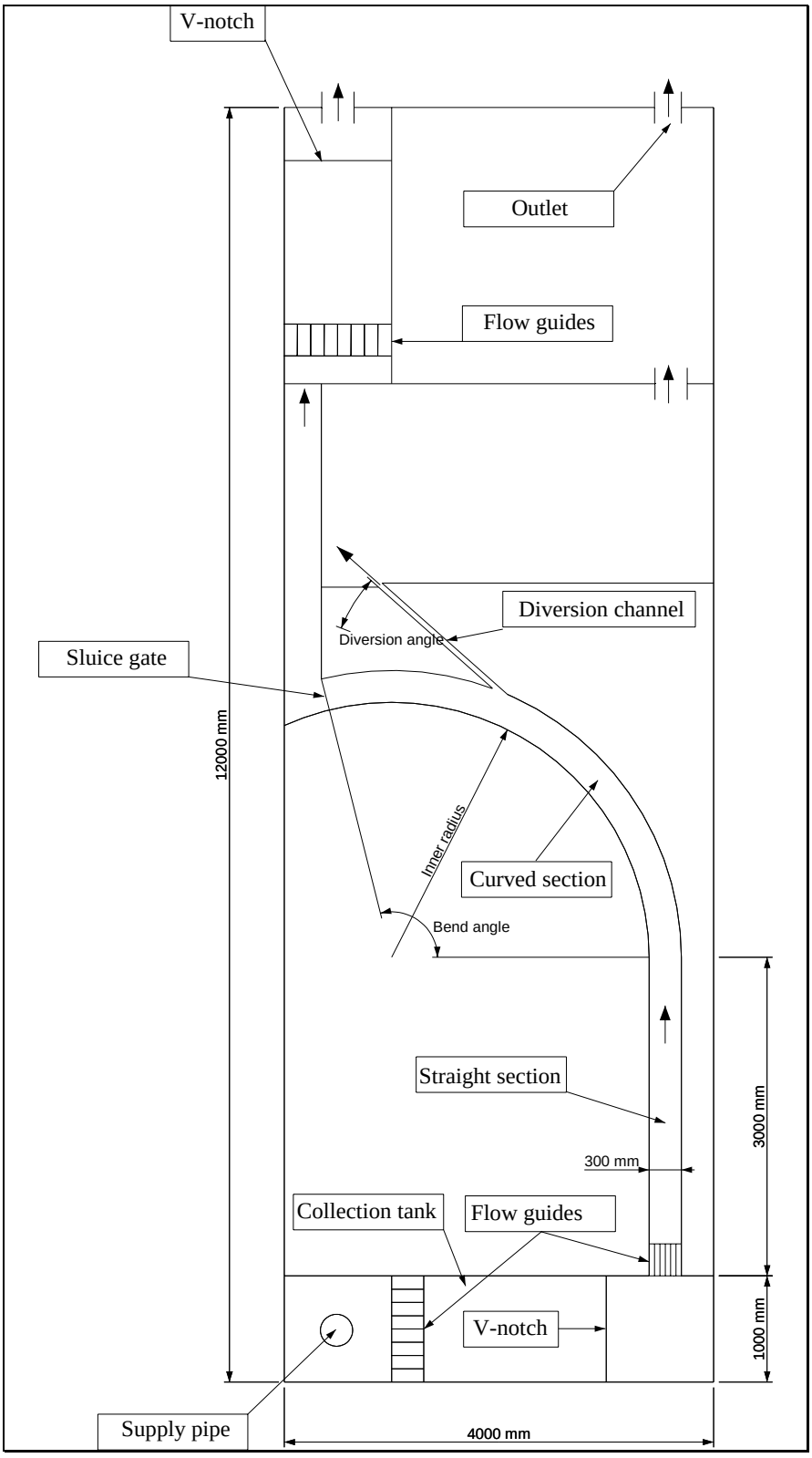

Figure 10-2 Plan layout of model for determining the optimum diversion angle (not to scale)

Figure 10-3 Photograph of the diversion channel

10.2 TEST PROCEDURE

Point velocities were measured in the curved section at 13 cross-sections perpendicular to the direction of flow. The cross-sections were located at 500 mm intervals from 2.19 m to 4.19 m and then at 250 mm intervals from 4.44 m to 6.19 m. Across the width of the channel, velocities were measured at 50 mm, 100 mm, 150 mm, 200 mm and 250 mm from the inside of the bend and in the vertical plane velocities were measured at 30 mm, 50 mm and 70 mm from the bed of the model. Thus, a total of 195 point-velocities were measured during each test. Figure 10-4 shows the plan layout where measurements were taken.

For each diversion angle four scenarios were studied. For the first three scenarios the sluice gate at the downstream end of the diversion channel was completely opened to allow the maximum diversion of water. For the fourth scenario the sluice gate was closed to ensure that no water was diverted. This was done to simulate a scenario where for example the pumps in a diversion channel were shut down and no water was abstracted from the main channel. The four scenarios tested were for Froude

numbers *(fr)* of 0.3, 0.5 and 0.7, in the main channel upstream of the diversion, with maximum diversion and fr = 0.3 with no abstraction from the main channel.

The test description is the same as in the previous section with the addition of measuring the discharge at the second V-notch to determine the diverted discharge.

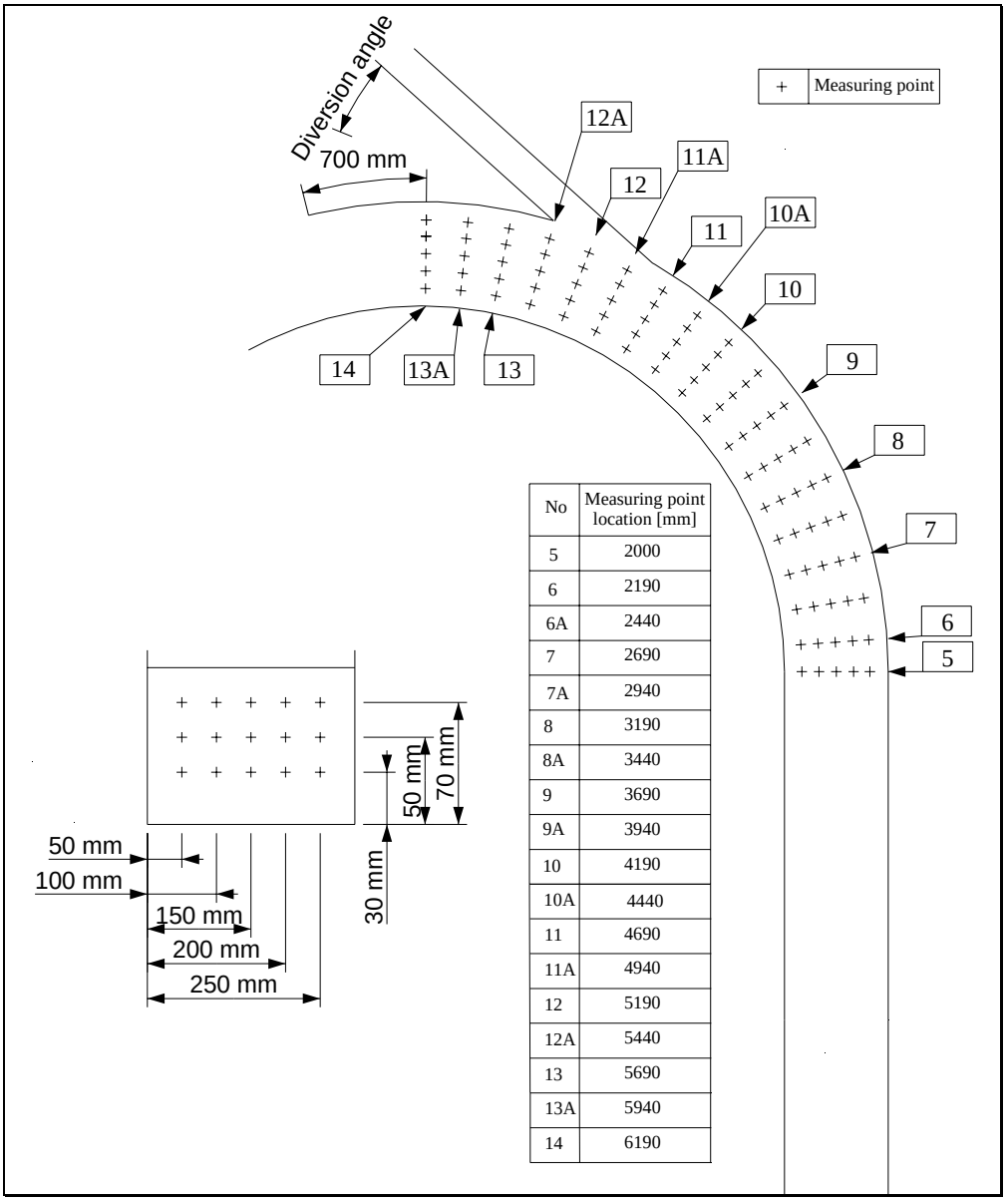

No	Measuring point location [mm]
5	2000
6	2190
6A	2440
7	2690
7A	2940
8	3190
8A	3440
9	3690
9A	3940
10	4190
10A	4440
11	4690
11A	4940
12	5190
12A	5440
13	5690
13A	5940
14	6190

Figure 10-4 Velocity measurement positions for diversion angle related tests (not to scale)

10.2.1 TEST D (Θ = 20˚)

The diversion location was installed at 3.69 m from the beginning of the bend. The diversion angle is 20 º .

A) TEST D1 (FR = 0.3)

The total discharge during the test was 10.35 l/s with an average water level of 110.3 mm. A maximum velocity of 0.39 m/s was measured at 5.69 m on the outside of the bend. The diverted discharge was 3.97 l/s with a diverted discharge ratio (DDR) of 38.4 %.

The velocity distribution in the horizontal plane measured at 70 mm, 50 mm and 30 mm is presented in Appendix B: Figure B-1. It is interesting to note that the path of maximum velocity shifts from being near the inside of the bend between 2.19 m and 3.69 m to the outside of the bend downstream of 3.69 m up to 5.69 m where the maximum velocity is obtained.

When studying the velocity distribution in the vertical plane (see Appendix B: Figure B-2) it is clear that the path dives towards the bottom of the model bed while it moves towards the outside of the bend (see Appendix B: Figure B-3) where the diversion channel is situated.

The velocity distribution is presented as a line graph in Figures B-4 to B-8 (see Appendix B) with the location of the turning points in Figure E-2 (see Appendix E).

B) TEST D2 (FR = 0.5)

The test was carried out with an average water level of 125 mm and a total discharge of 15.53 l/s. A DDR of 31.2 % was obtained with the diverted discharge being 4.85 l/s.

The path of maximum velocity shifts from near the inside of the bend up to 3.19 m to the outside of the bend in the horizontal plane where it remains up to 5.69 m where the maximum velocity of 0.53 m/s was measured. In the vertical plane it moves

downwards in the downstream direction (see Appendix B: Figures B-9 to B-16). The location of the turning points is presented in Figure E-3 (see Appendix E).

C) TEST D3 (FR = 0.7)

A DDR of 32.1 % was obtained with the diverted discharge calculated at 6.86 l/s. The average water level during the test was 170.9 mm while the total discharge was 21.36 l/s.

The velocity distribution is presented as a line graph in Figures B-20 to B-24 (see Appendix B) with the location of the turning points in Figure E-4 (see Appendix E).

Once again the maximum velocity followed the same path as for the scenarios of fr = 0.3 and 0.5, i.e shifting from near the inside of the bend towards the outside while diving towards the bottom in the downstream direction (see Appendix B: Figures B-17 to B-19).

10.2.2 TEST E ($\Theta = 35^{\circ}$)

The diversion location was installed at 3.69 m from the beginning of the bend. The diversion angle is 35 º .

A) TEST E1 (FR = 0.3)

The diverted discharge of 4.7 l/s was measured with a DDR of 46.8 %. The total discharge during the test was 10.04 l/s with an average water level of 108.5 mm and a maximum velocity of 0.42 m/s.

The path of maximum velocity moved on the inside of the bend up to 3.69 m where it shifted towards the outside of the bend at 4.19 m. It remained on the outside of the bend up to 5.69 m where the maximum velocity was measured. In the vertical plane the maximum velocity moved gradually towards the bottom of the bed in the downstream direction (see Appendix B: Figures B-25 to B-27).

The velocity distribution is presented as a line graph in Figures B-28 to B-32 (see Appendix B) with the location of the turning points in Figure E-6 (see Appendix E).

B) TEST E2 (FR = 0.5)

The total discharge during the test was 14.9 l/s with a diverted discharge of 5.3 l/s, thus resulting in a DDR of 35.6 %. The average water level was 123.1 mm. The velocity distribution in the horizontal and vertical plane as well as the cross-sectional velocity distribution are presented in Appendix B: Figures B-33 to B-35. In this case a more uniform distribution across the width of the channel was obtained up to 3.19 m where the maximum velocity shifted towards the outside of the bend at 3.69 m. The maximum velocity moved downward in the downstream direction until the diversion channel is reached where the maximum velocity of 0.45 m/s was measured.

The velocity distribution is presented as a line graph in Figures B-36 to B-40 (see Appendix B) with the location of the turning points in Figure E-7 (see Appendix E).

C) TEST E3 (FR = 0.7)

A DDR of 33.9 % was calculated with the diverted discharge of 7.49 l/s that was obtained while the total discharge was 22.08 l/s. The average water level during the test was 134.5 mm.

Between 2.19 m and 2.69 m higher velocities were measured on the inside of the bend than on the outside. The maximum velocity then shifted towards the outside of the bend at 3.69 m where it remained until the location of the diversion channel was reached at 5.69 m. The maximum velocity of 0.7 m/s was measured at this point. from the vertical velocity distribution it is noted that the maximum velocity shifted downward to the outside of the bend in the downstream direction (see Appendix B: Figures B-41 to B-48). The location of the turning points is presented in Figure E-8 (see Appendix E).

D) TEST E4 (FR = 0.3, DDR = 0)

The average water level during the test was 113.5 mm while the discharge was 9.6 l/s. The velocity distribution is presented as a line graph in Figures B-52 to B-56 (see Appendix B).

The path of the maximum velocity in the horizontal plane can be described with reference to Figure B-49 (see Appendix B). The maximum velocity moves from being near the inside of the bend up to 3.69 m towards the outside of the bend at 4.94 m. The maximum velocity of 0.34 m/s was measured at 5.94 m near the outside of the bend. Figures B-50 and B-51 (see Appendix B) represent the velocity distribution in the vertical plane. From these figures it is noted that the maximum velocity moves down towards the outside of the bend in the downstream direction.

10.2.3 TEST F (Θ = 50˚)

The diversion location was installed at 3.69 m from the beginning of the bend. The diversion angle is 50 º .

A) TEST F1 (FR = 0.3)

With reference to Figures B-57 to B-59 (see Appendix B), the path of the maximum velocity can be described as follows:

In the horizontal plane the maximum velocity is near the inside of the bend between 2.19 m and 3.96 m where it then shifts towards the outside of the bend up to 4.96 m. Further downstream it remains on the outside of the bend until 5.69 m where the diversion channel is positioned. The maximum velocity of 0.45 m/s was measured at this location.

In the vertical plane the maximum velocity moves downward and to the outside of the bend in the downstream direction.

The average water level during the test was 111.2 mm with a total discharge of 11.04 l/s. The diverted flow was 5.25 l/s, representing a DDR of 47.6 %. The

velocity distribution is presented as a line graph in Figures B-60 to B-64 (see Appendix B) with the location of the turning points in Figure E-10 (see Appendix E).

B) TEST F2 (FR = 0.5)

A DDR of 40.6 % was obtained with the total discharge of 15.7 l/s and the diverted discharge of 6.37 l/s. The average water level during the test was 123.4 mm.

The maximum velocity follows the outside of the bend throughout the bend although there is a zone of high velocities near the inside of the bend between 2.19 m and 2.69 m. The maximum velocity of 0.56 m/s was measured at the diversion location of 5.69 m (see Appendix B: Figures B-65 to B-67).

The velocity distribution is presented as a line graph in Figures B-68 to B-72 (see Appendix B) with the location of the turning points in Figure E-11 (see Appendix E).

C) TEST F3 (FR = 0.7)

The average water level during the test was 124.5 mm with a total discharge of 21.6 l/s. A DDR of 34.4 % was obtained with the diverted discharge being 7.44 l/s. The velocity distribution is presented as a line graph in Figures B-76 to B-80 (see Appendix B) with the location of the turning points in Figure E-12 (see Appendix E).

The path of the maximum velocity in the horizontal plane can be described with reference to Figure B-73 (see Appendix B). The maximum velocity is on the inside of the bend up to 3.19 m where it shifts outwards to the outside of the bend at 4.19 m. The maximum velocity remains on the outside until the diversion point is reached at 5.69 m where the maximum velocity of 0.74 m/s was measured.

In the vertical plane the maximum velocity gradually moves downward in the downstream direction up to the diversion location (see Appendix B: Figures B-74 and B-75).

D) TEST F4 (FR = 0.3; DDR = 0)

The total discharge during the test was 9.6 l/s with an average water level of 115.8 mm.

In the horizontal plane the maximum velocity moves along the inside of the bend until 3.19 m where it steadily shifts towards the outside of the bend. From 4.94 m it remains on the outside of the bend up to the diversion location at 5.69 m. The maximum velocity of 0.32 m/s was measured at 6.19 m.

In the vertical plane the maximum velocity dives to the bottom while shifting towards the outside of the bend in the downstream direction (see Appendix B: Figures B-81 to B-88).

10.3 ANALYSIS OF TESTS ON DIVERSION ANGLE

In general the velocity distributions obtained from the laboratory experiments shows the same tendency. The maximum measured velocity during the series of test was located at the point of diversion. In the horizontal plane the maximum velocity is near the inside of the bend up to 3.19 m. It then shifts towards the outside of the bend and at approximately 3.69 m it reaches the outside of the bend where it remains up to the point of diversion at 5.69 m (3.69 m from the beginning of the bend). A typical observed velocity distribution is presented in Figure 10-5.

From the vertical velocity distribution it is noted that the path of the maximum velocity dives towards the bottom in the downstream direction while moving towards the outside of the bend. A typical velocity distribution in the vertical is presented in Figure 10-6 and the cross-sectional distribution in Figure 10-7.

Presenting the vertical velocity distribution as a line graph, the following tendencies are observed in the downstream direction (see Figure 10-8 to Figure 10-10):

- The velocity measured at 70 mm from the bottom (*V70*) decreases near the inside of the bend.
- All the measured velocities (*V70*, *V50* and *V30*) increase at the centre of the bend.
- All the measured velocities (*V70*, *V50* and *V30*) increase near the outside of the bend with a sharp increase at the diversion location followed by a sharp decrease immediately downstream of the diversion.

The typical tendency of the location of the turning points, i.e where *V30>V50*, *V30>V70* and *V50>V70,* is reflected in Figure 10-11.

In analysing the location of the turning points where *V30>V50, V30>V70* and *V50>V70* the following conclusions can be made (see Appendix E: Figures E-1, E-5 and E-9):

- The location of the turning points where *V30>V50*, *V30>V70* and *V50>V70* stays relatively constant near the inside of the bend but at the outside of the bend it moves in the downstream direction with an increase in Froude number.
- The range of the locations of the turning points near the inside of the bend increases with an increase in the diversion angle.
- The range of the locations of the turning points near the outside of the bend decreases with an increase in the diversion angle.
- The location of the turning points for *V30>V50*, *V30>V70* and *V50>V70* was always upstream of the diversion location of 5.69 m.

The velocity distributions of Test E4 and Test F4 (DDR=0) and those with a DDR>0 is essentially the same. The only difference is that there exists a small area with lower velocities around the point of diversion for the tests with DDR=0 than for the tests with DDR>0.

Based on the above-mentioned results no real conclusion can be made regarding the optimum diversion angle. This is due to the fact that the results obtained from the three diversion angles that were analysed are essentially the same. It is well-evident that the diverted discharge ratio (DDR) increases with an increase in the diversion angle while it decreases with an increase in Froude number. The velocity distribution obtained with a Froude number of 0.3 and 0.5 is also more favourable than those obtained with a Froude number of 0.1 since the bend effect is more prominent. An important conclusion from the tests is that the diversion does not influence the secondary flow patterns (for the range of DDR's tested) and that the maximum velocity zone stayed in the same location as in the tests without a diversion.

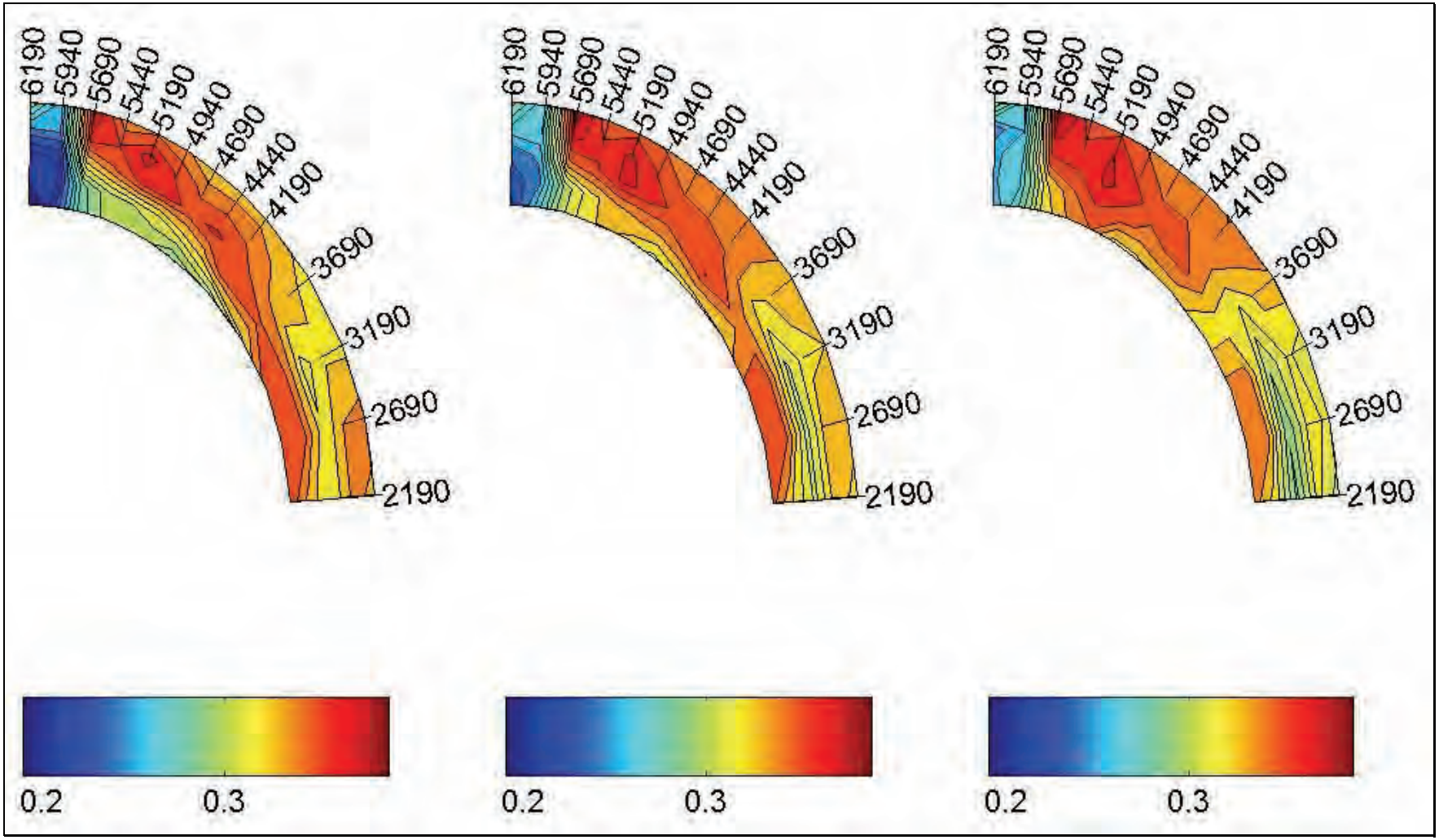

Figure 10-5 Typical velocity distribution in the horizontal plane measured at 70, 50 and 30 mm above the bed [m/s]

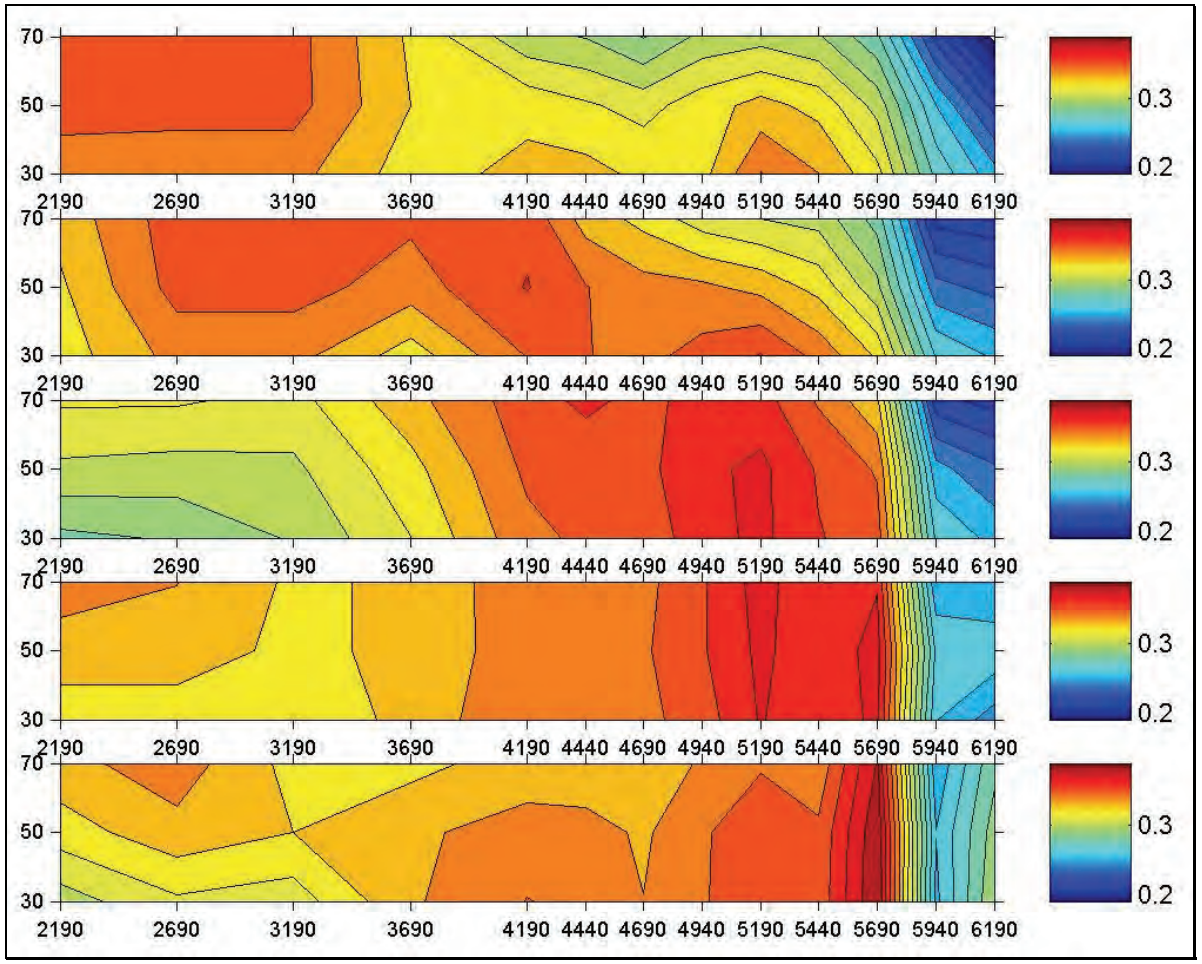

Figure 10-6 Typical velocity distribution in the vertical plane [m/s]

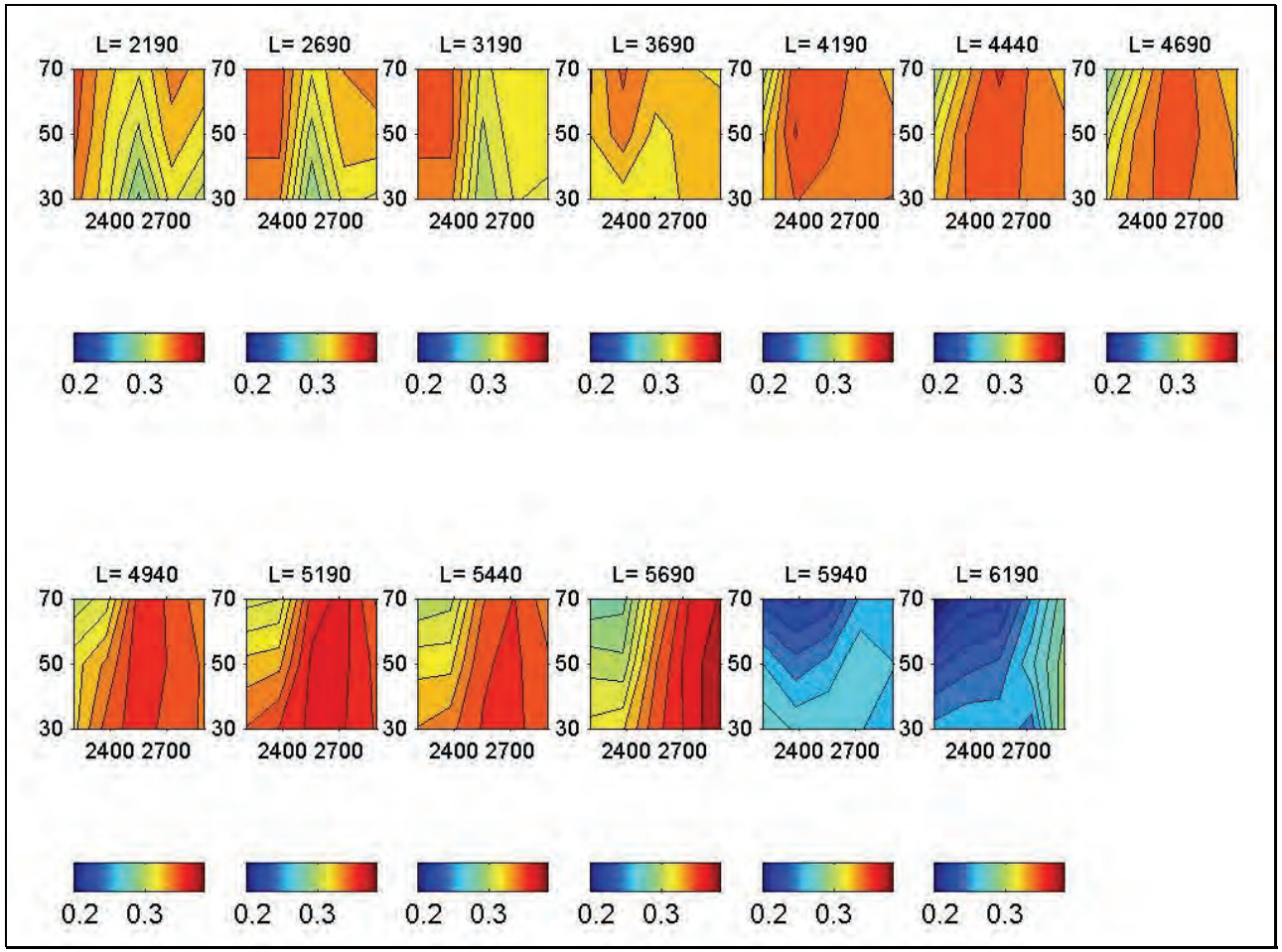

Figure 10-7 Typical cross-sectional velocity distribution [m/s]

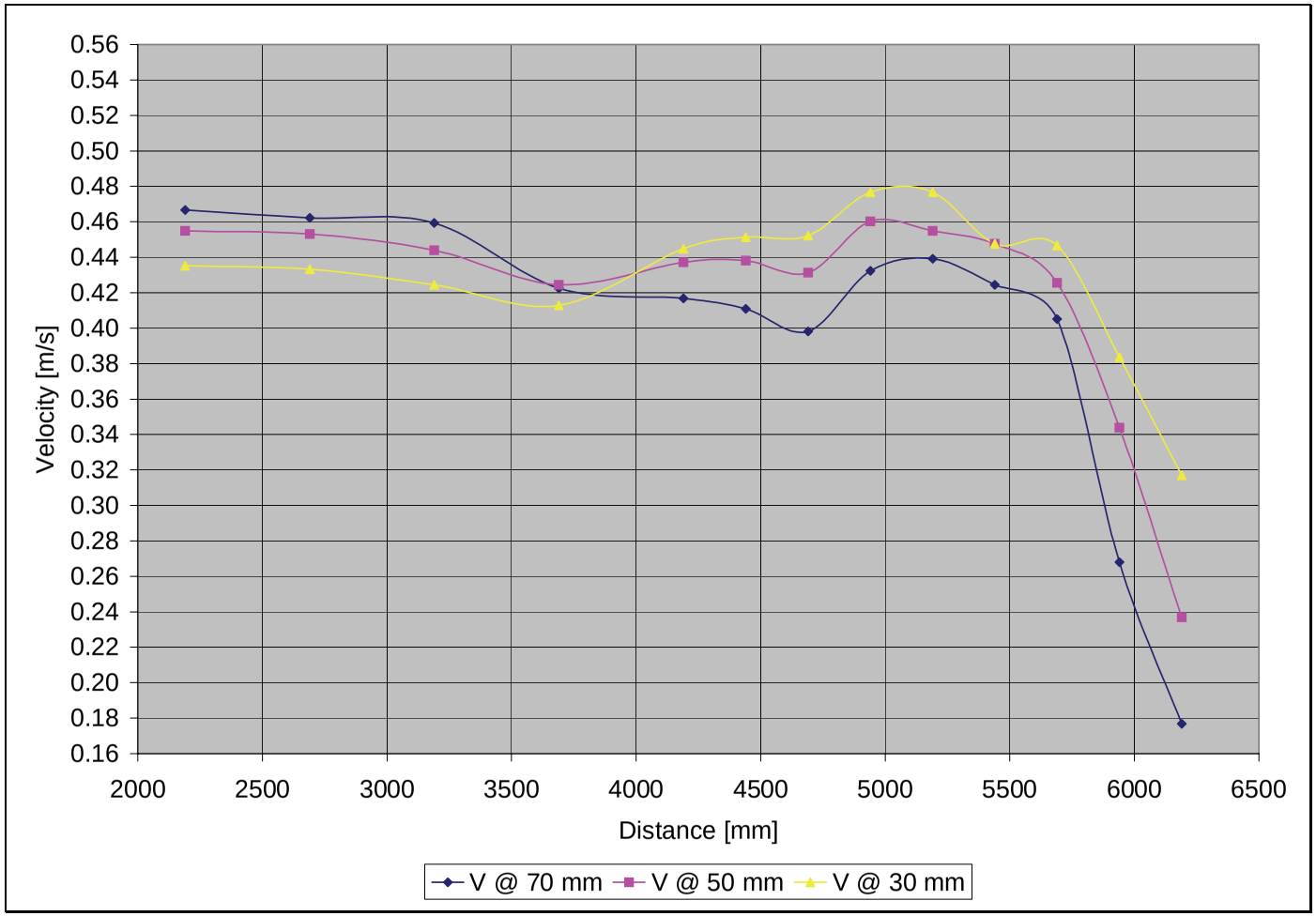

Figure 10-8 Decreasing tendency of *V70* near the inside of the bend with $r_c/w = 8.5$, $fr = 0.3$ and $\theta = 50°$

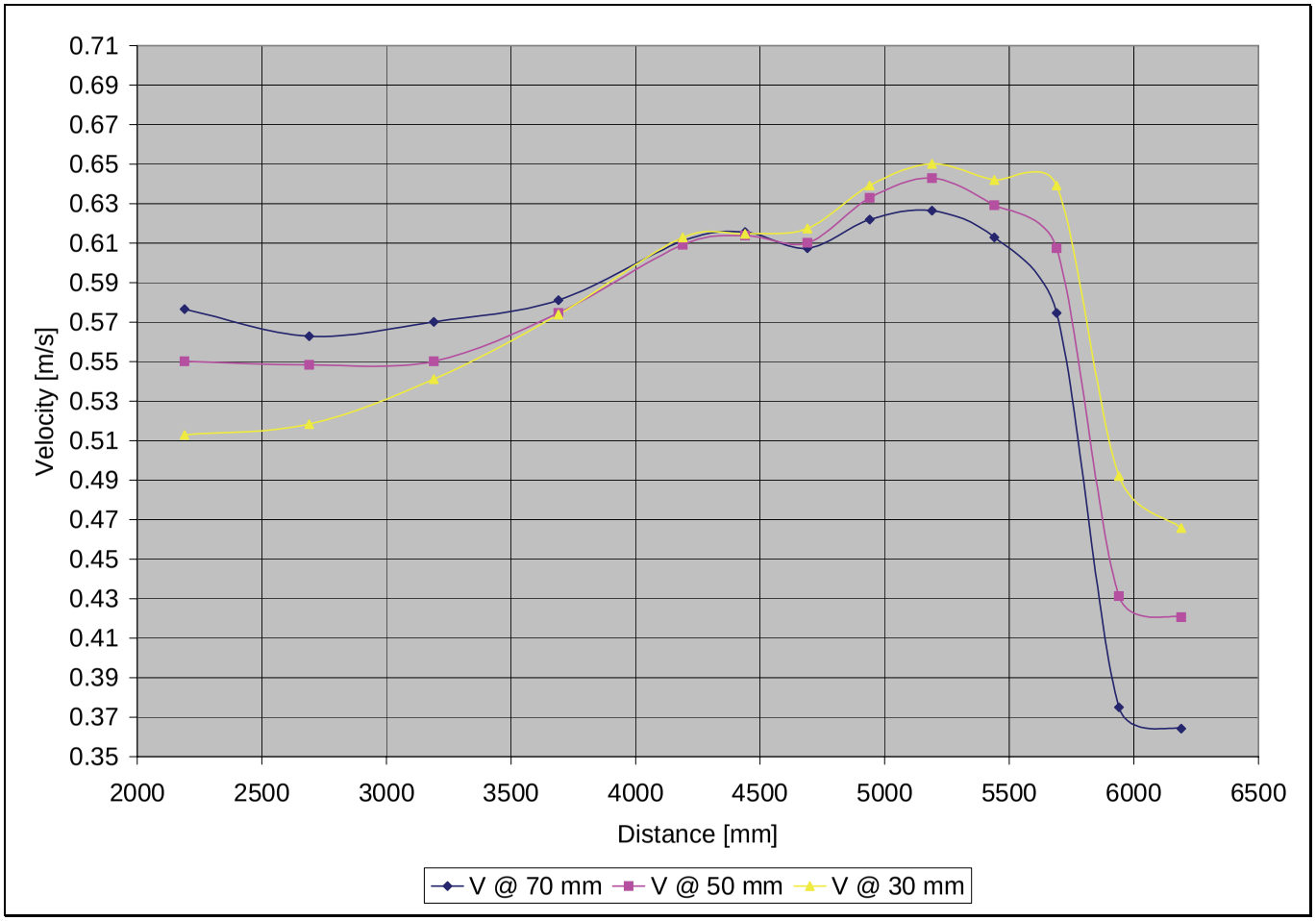

Figure 10-9 Increasing tendency of *V30, V50 and V70* at the centre of the bend with $r_c/w = 8.5$, $fr = 0.5$ and $\theta = 35°$

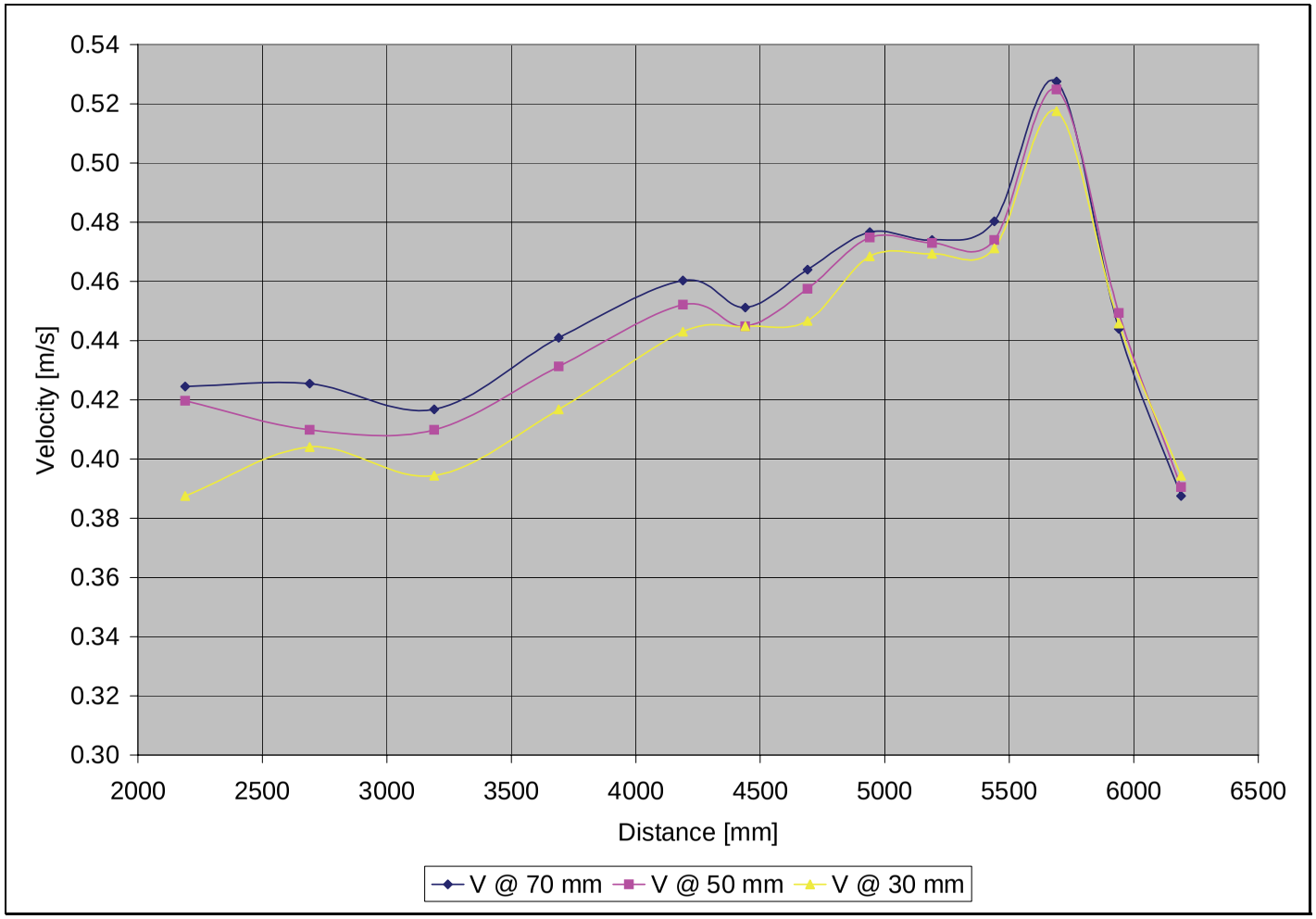

Figure 10-10 Increasing tendency of *V30, V50 and V70* near the outside of the bend with $r_c/w = 8.5$, $fr = 0.7$ and $\theta = 20°$

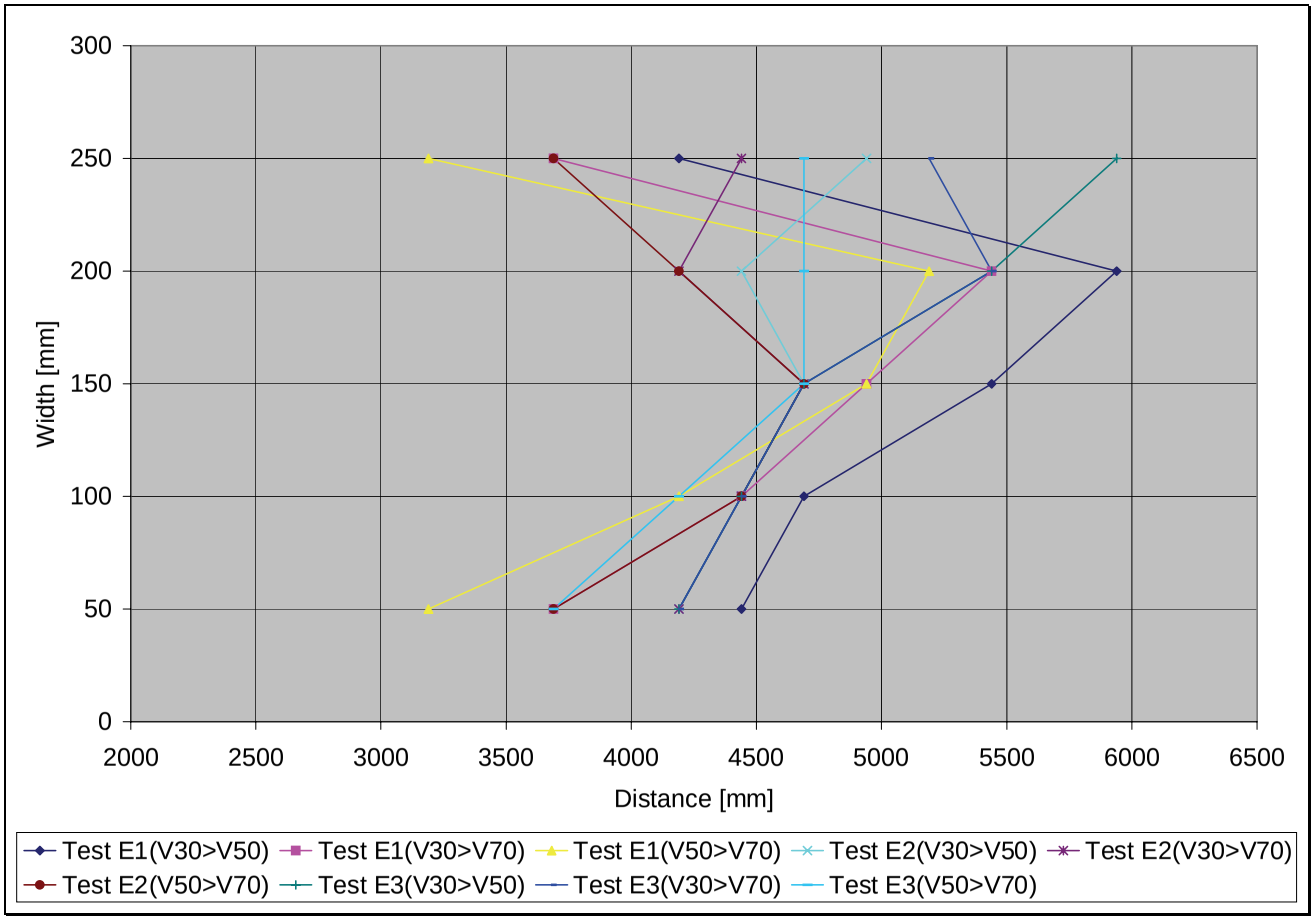

Figure 10-11 Location of turning points for *V30>V50, V30>V70* and *V50>V70*

11 MATHEMATICAL MODELLING

11.1 INTRODUCTION

Mathematical modelling was carried out based on the laboratory experiments both in 3D and 2D, as well as on river bends typically found in the field, to establish whether such models can predict bend flow patterns with accuracy.

The hydrodynamic programme DELFT 3D was used to simulate the hydrodynamics of the laboratory experiments for the case where $r_c = 2.55\ m$ (Test A). The aim of the simulation was to establish whether the programme could be used to simulate the hydrodynamics of the laboratory experiments and secondary flow patterns with reliability in 3D.

The software Mike 21C was used to simulate the hydrodynamics and sediment dynamics of Test A5. Mike 21C is a two-dimensional vertically integrated programme (2DH) with sediment transport by using a curvilinear grid, secondary flow relationships for the bend sediment transport, where bank stability and bed slope are considered.

11.2 DELFT 3D (HYDRODYNAMICS)

11.2.1 DESCRIPTION OF HYDRODYNAMIC COMPONENT OF MODEL

The hydrodynamic model (DELFT3D-FLOW), capable of solving the time-dependent shallow water equations in three dimensions, is designed to simulate tidally and wind-driven flows in shallow seas, coastal areas, estuaries, rivers and lakes. The model includes formulations and equations that consider:

- tidal forcing
- wind shear stress on the water surface
- wave-driven flows
- the effect of the earth's rotation (Coriolis force)

- free surface gradients (barotropic effects)
- secondary currents
- bed shear stresses on the seabed
- drying and flooding on tidal flats
- turbulence induced mass and momentum fluxes (*k*-ε turbulence closure model).

The system of equations in Delft3D-FLOW comprises the horizontal momentum equations and the continuity equation, the equation of state and the advection-diffusion equation for heat, salt and other conservative tracers which are solved using the Alternating Direct Implicit scheme. The computation grid is an irregularly-spaced, orthogonal, curvilinear grid in the horizontal and a sigma coordinate grid in the vertical.

The equations and their numerical implementation are described in detail in the DELFT3D-FLOW user manual (WL|Delft Hydraulics, 2003) of which simplified versions are provided below:

Conservation of momentum in x-direction:

$$\frac{\partial u}{\partial t} + u\frac{\partial u}{\partial x} + v\frac{\partial u}{\partial y} + g\frac{\partial \eta}{\partial x} - f.v + \frac{g.u\,|U|}{C^2(d+\eta)} - \frac{F_x}{\rho(d+\eta)} - \upsilon\left(\frac{\partial^2 u}{\partial^2 x} + \frac{\partial^2 u}{\partial^2 y}\right) = 0 \qquad (11\text{-}1)$$

Conservation of momentum in y-direction:

$$\frac{\partial v}{\partial t} + u\frac{\partial v}{\partial x} + v\frac{\partial v}{\partial y} + g\frac{\partial \eta}{\partial y} + f.u + \frac{g.v\,|U|}{C^2(d+\eta)} - \frac{F_y}{\rho(d+\eta)} - \upsilon\left(\frac{\partial^2 v}{\partial^2 x} + \frac{\partial^2 v}{\partial^2 y}\right) = 0 \qquad (11\text{-}2)$$

Conservation of mass, continuity equation:

$$\frac{\partial \eta}{\partial t} + \frac{\partial[(d+\eta)u]}{\partial x} + \frac{\partial[(d+\eta)v]}{\partial y} = 0 \qquad (11\text{-}3)$$

11.2.2 HYDRODYNAMIC MODELLING

The numerical model was set up to simulate only the hydrodynamics of the laboratory experiments for Test A. Initial problems were encountered regarding the choice of some of the variables for the model. Special attention was given to the horizontal viscosity that determine the interaction of the different 'layers' of water with each other in order to simulate the spiral flow in the curved section. Once these initial constraints were overcome, the Chezy coefficient was adjusted until the simulated and measured water levels were in good agreement. Some of the important parameters used in the simulation are given in Table 11-1.

Table 11-1 Hydrodynamic model parameters

Parameter	**Value**
Time step	0.25 minutes
Chezy coefficient (C)	55 $m^{1/2}/s$
Uniform flow depth	Average measured water level from laboratory experiments
Horizontal viscosity	0.01 m^2/s

The simulated results compared well with those obtained from the laboratory experiments and the programme was then applied with a great degree of confidence.

Three-dimensional simulations were carried out first, followed by two-dimensional (in plan) simulations. Two-dimensional vertically integrated models are often used in sediment transport in river systems that are relatively shallow to save computational time. With a two-dimensional approach, empirical coefficients are incorporated in the software, calibrated against three-dimensional simulations during model development.

11.2.3 SIMULATION RESULTS

11.2.3.1 3D-SIMULATION

a) Test H1 (Fr = 0.1)

The simulated velocity distribution shows that higher velocities on the outside of the bend develop from halfway through the curved section up to the end of the curved section. The maximum velocities are found on the outside of the bend near the end. When the simulated and laboratory velocity distributions are compared they are in good agreement. The simulated water levels show the super elevation of the water level on the outside of the bend and were found to be as expected (see Appendix C: Figures C-7 to C-11).

b) Test H2 (Fr = 0.3)

The simulated velocity distributions are in good agreement with the measured laboratory velocity distributions. The maximum velocity is found on the outside of the bend near the end of the curved section with higher velocities on the outside of the bend from approximately the middle of the bend up to the end. The water levels generated were as expected with higher water levels on the outside of the bend indicating the super elevation of the water (see Appendix C: Figures C-12 to C-16).

c) Test H3 (Fr = 0.5)

The simulated velocity distributions at the surface (see Appendix C: Figure C-17) and at a distance of 70 mm, 50 mm and 30 mm from the bed are shown in Figures 11-1 to 11-3 respectively. From these figures it is clear that higher velocities on the outside of the bend start to develop from about halfway through the bend and remain higher on the outside until the end of the curved section is reached. The zone of highest velocities is found on the outside of the bend near the bend exit.

Figure C-21 (see Appendix C) indicates that the simulated water levels and the higher water levels on the outside of the bend are once again prominent indicating the super elevation of the water levels on the outside of the bend.

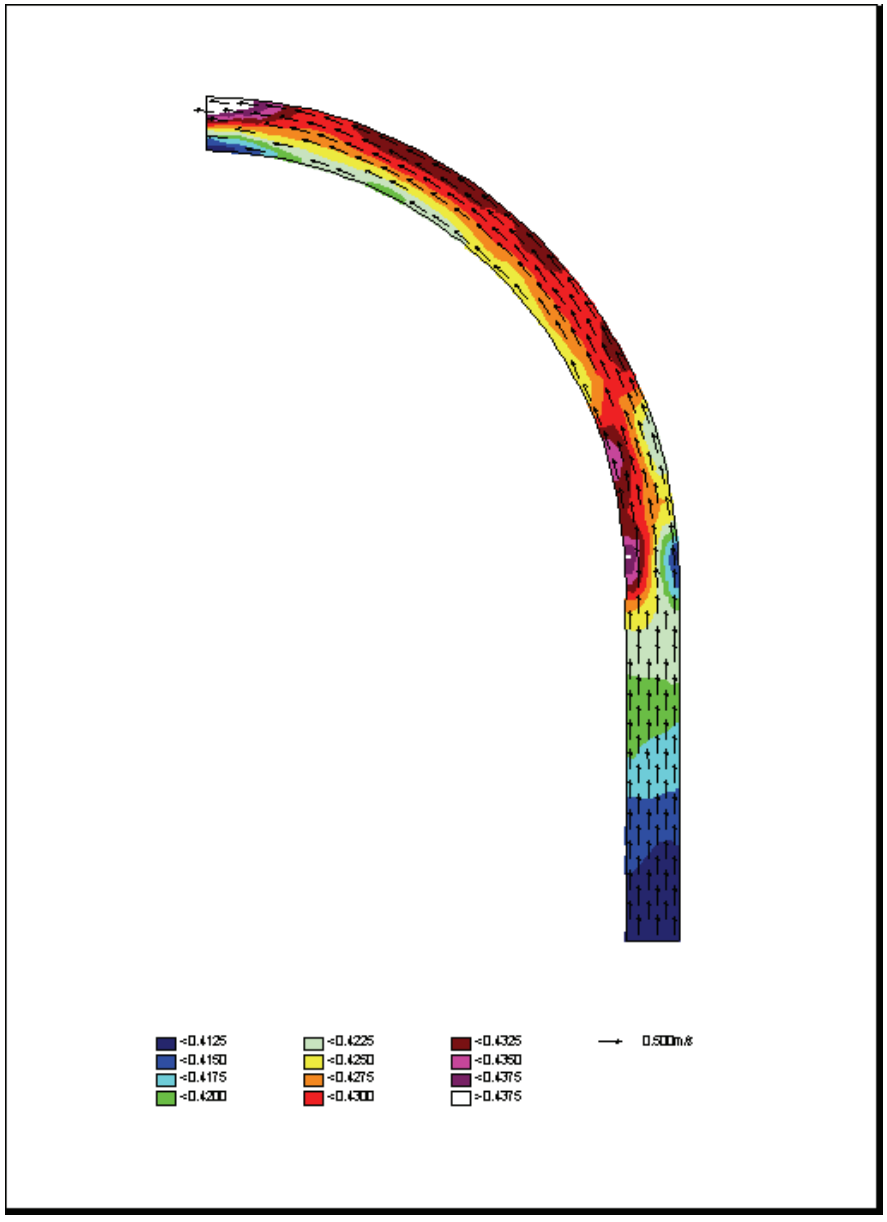

Figure 11-1 Test H3-Simulated velocity distribution in the horizontal plane at 70 mm above the bed

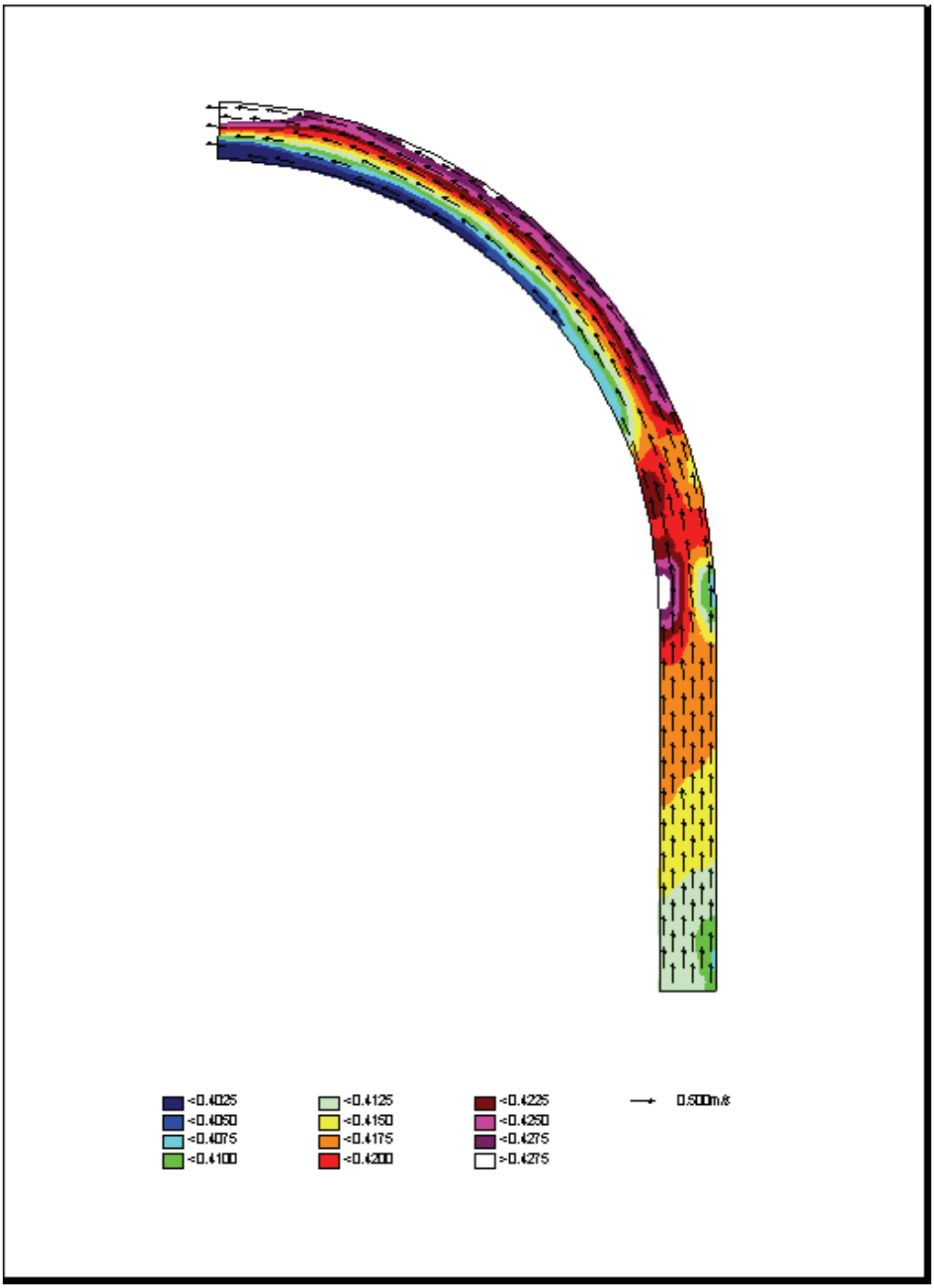

Figure 11-2 Test H3-Simulated velocity distribution in the horizontal plane at 50 mm above the bed

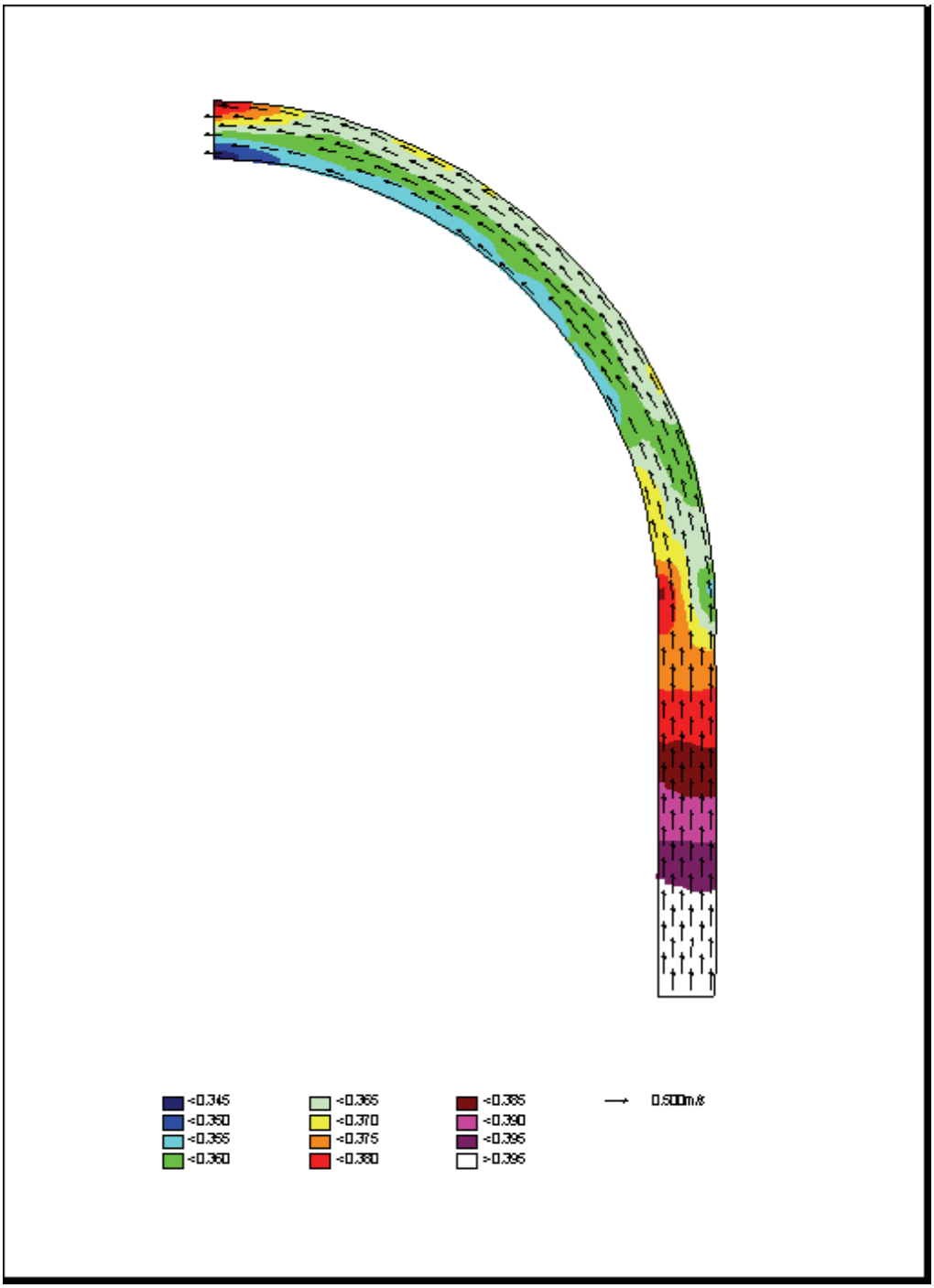

Figure 11-3 Test H3-Simulated velocity distribution in the horizontal plane at 30 mm above the bed

11.2.3.2 2D-SIMULATION

a) Test G1 (Fr = 0.1)

The simulated velocity distribution indicates that there is a zone towards the end of the curved section where the velocities are higher on the outside of the bend than on the inside. It is also noted that there are some places near the end of the straight section and at the beginning of the curved section where the simulated velocity distribution indicates higher velocities on the inside of the curve. This is in disagreement with the results from the laboratory experiments and is not as expected (see Appendix C: Figure C-1).

The simulated water levels show good agreement with laboratory work. The elevated water levels on the outside of the curved section can clearly be seen from Figure C-2 (see Appendix C).

b) Test G2 (Fr = 0.3)

The simulated velocity distribution (see Figure 11-4) for this scenario is in good agreement with the laboratory experiments. Approximately halfway through the curved section higher velocities developed on the outside of the bend with the highest velocities near the end of the curved section on the outside of the bend. However, there is still a zone at the beginning of the curved section where higher velocities are present on the inside of the bend contrary to the laboratory experiments.

Figure C-4 (see Appendix C) indicates that the simulated water levels were as expected, higher on the outside of the bend.

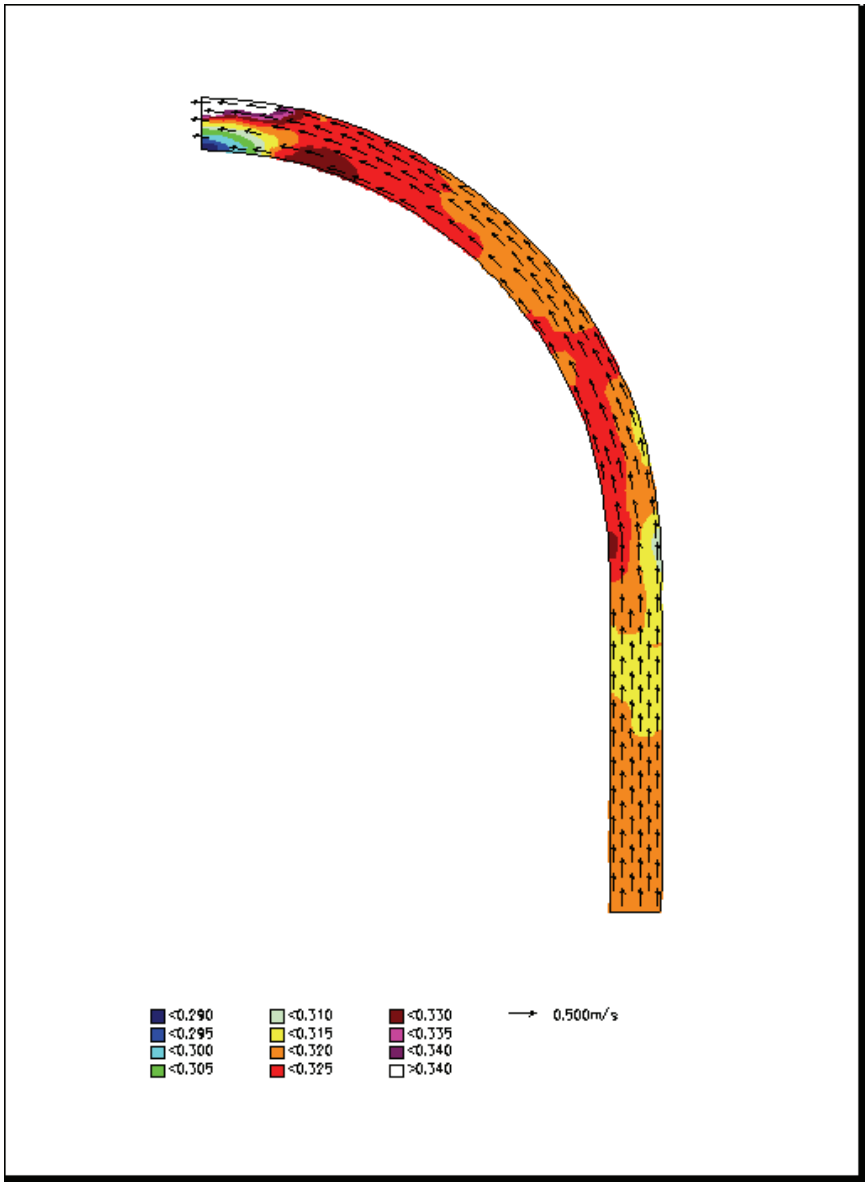

Figure 11-4 Test G2-Simulated velocity distribution in the horizontal plane

c) Test G3 (Fr = 0.5)

The simulated velocity distributions and water levels were in total disagreement with the laboratory experiments. The velocities seem to increase in the downstream direction throughout the straight and curved section. It is therefore the opinion of the authors that the simulation time was too short and therefore the velocities were not fully developed when the simulation was stopped (see Appendix C: Figures C-5 to C-6).

11.3 MIKE 21C (SEDIMENT DYNAMICS)

11.3.1 DESCRIPTION OF MODEL

For the computational modelling, the two-dimensional model MIKE 21C, developed by the DHI Water and Environment (DHI, 2003), was used. MIKE 21 is a software package for simulating free-surface flows, water quality, sediment transport and waves in rivers, lakes, estuaries, bays, coastal seas and other water bodies. In particular MIKE 21C, a special module developed to simulate river morphology, was used. MIKE 21C is based on a curvilinear grid, and hydrodynamics, sediment transport and river morphology can be simulated, with modules to describe:

- Flow hydrodynamics – water levels and flow velocities are computed over a curvilinear or rectangular grid.
- Helical flow (secondary currents).
- Sediment transport – based on various model types, capable of graded sediment transport computations.
- Alluvial resistance due to bed material and bed forms.
- Scour and deposition – large-scale movement of bed material is computed and the effect of supply limited sediment layers can be incorporated.
- Bank erosion and planform changes – bank lines as well as the curvilinear grid can be updated.

The bed slope effect on the sediment transport is very important and is incorporated into MIKE 21C as a transverse and longitudinal component.

The model has the following characteristics:

- It solves the 2D Saint-Venant equations

$$\frac{\partial p}{\partial t}+\frac{\partial (p^2/h)}{\partial x}+\frac{\partial (pq/h)}{\partial y}+\frac{gp\sqrt{p^2+q^2}}{C^2h^2}+gh\frac{\partial s}{\partial x}=h\frac{\partial}{\partial x}\left(E\frac{\partial (p/h)}{\partial x}\right)+h\frac{\partial}{\partial y}\left(E\frac{\partial (p/h)}{\partial y}\right)$$
$$\frac{\partial q}{\partial t}+\frac{\partial (pq/h)}{\partial x}+\frac{\partial (q^2/h)}{\partial y}+\frac{gq\sqrt{p^2+q^2}}{C^2h^2}+gh\frac{\partial s}{\partial y}=h\frac{\partial}{\partial x}\left(E\frac{\partial (q/h)}{\partial x}\right)+h\frac{\partial}{\partial y}\left(E\frac{\partial (q/h)}{\partial y}\right)$$
$$\frac{\partial h}{\partial t}+\frac{\partial p}{\partial x}+\frac{\partial q}{\partial y}=0 \qquad (11\text{-}4)$$

- Dynamic acceleration, spatial acceleration, bed friction, water level gradients and horizontal shear.
- The flow is assumed to be friction dominated, so the eddy viscosity is set to a small value.
- Transformed to curvilinear coordinates, solved as scalar equations (avoid grid curvature terms).
- The model can simulate both cohesive and non-cohesive sediment transport. Most of the sediment transported during floods in sand bedded rivers consists of silt and clay, (about 70 %). In this research, however, limiting sand diversion was of importance and therefore cohesive sediment was not simulated.
- Cohesive sediment model: Pseudo-3D model, convection by a modified flux field

Advection-dispersion equation:

$$\frac{\partial hc}{\partial t}+\frac{\partial p'c}{\partial x}+\frac{\partial q'c}{\partial y}=\frac{\partial}{\partial x}\left(hD_{xx}\frac{\partial c}{\partial x}\right)+\frac{\partial}{\partial y}\left(hD_{yy}\frac{\partial c}{\partial y}\right)+E-D \qquad (11\text{-}5)$$

Advection is with a modified flux field:

$$\begin{pmatrix}p'\\q'\end{pmatrix}=\alpha_{01}\begin{pmatrix}p\\q\end{pmatrix}+\alpha_{02}\frac{h}{R}\begin{pmatrix}-q\\p\end{pmatrix} \qquad (11\text{-}6)$$

- R: Streamline curvature
- α_{01}, α_{02}: Streamwise and transverse modifications
- α_{01} and α_{02} are functions of the distributions of momentum and sediment (profile functions).
- α_{01}: the sediment is usually located where the flow velocity is smaller than the depth-averaged. α_{01} always smaller than or equal to unity; reduced streamwise convection. α_{01} changes the magnitude of the flux.
- α_{02}: streamline curvature driven secondary flow (helical flow). The modification by α_{02} is perpendicular to the flow direction. α_{02} changes the direction of the flux (turns towards the local center of curvature). Refer to Figures 11-5 and 11-6.

$$\alpha_{01} = \int_0^1 p_1(z)\phi_0(z)dz$$

$$a_{02} = \int_0^1 p_2(z)\phi_0(z)dz$$

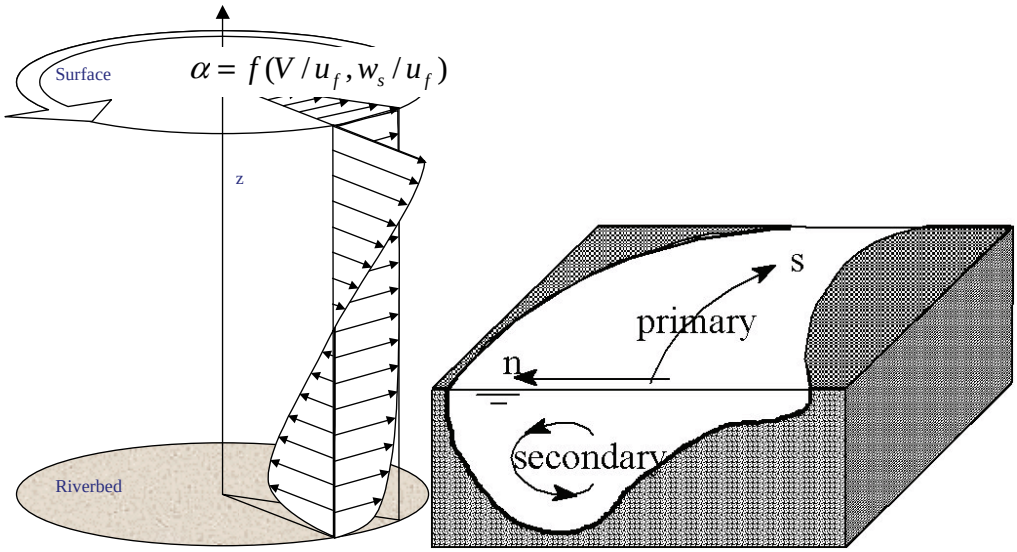

Figure 11-5 Profile functions in pseudo 3D model

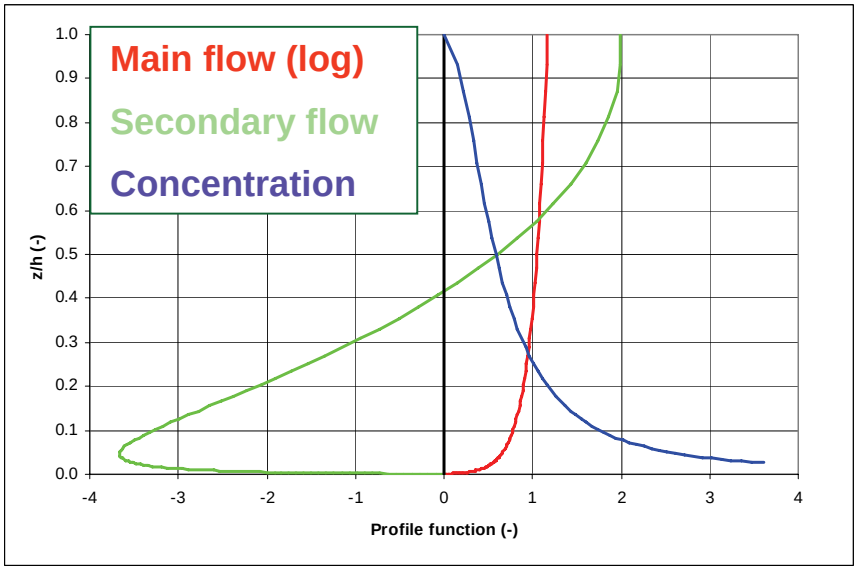

Figure 11-6 Vertical flow and concentration distribution

The benefit of this model over fully 3D models for river analysis is high accuracy in results in relatively short computer time required. For example a 3 year simulation of a 20 km river takes about 3 h. This will however vary depending on the selected grid and time step.

11.3.2 SEDIMENT SIMULATIONS OF LABORATORY CANAL

The parameters used in the simulation are shown in Table 11-2.

Table 11-2 Mike21C properties for 0.3m channel

Mike21C parameter	Description	Value assigned
Modelling period	Length of simulation	8 hours
Timestep	Length of calculation iteration	0.4 seconds
Boundaries	Water levels and discharges	Q = 0.0102 m^3/s H = 0.1 m
d_{50} of sediment	Size of sediment	0.12 mm
Transport mode	Type of sediment movement	Both bed and suspended sediment
Transport formulation	Theory behind sediment movement	Engelund and Fredsøe
Horizontal eddy viscosity (ν)	Velocity or flux based viscosity	0.03 m^2/s
Manning n value	Roughness of channel	0.045 $s/m^{1/3}$
Threshold for drying and flooding	Water depth at which model begins calculating the hydrodynamics for that point	0.01 m

Figure 11-7 shows the result of a Mike21C simulation of the laboratory tests. It is clearly evident that the measured bed profiles and the simulated one only vaguely resemble each other. The reason for the discrepancy is that the model was unable to accurately simulate the sluice gate at

the end of the channel. This problem can be remedied by adding another straight section downstream of the bend, which adds stability to the simulated water flows.

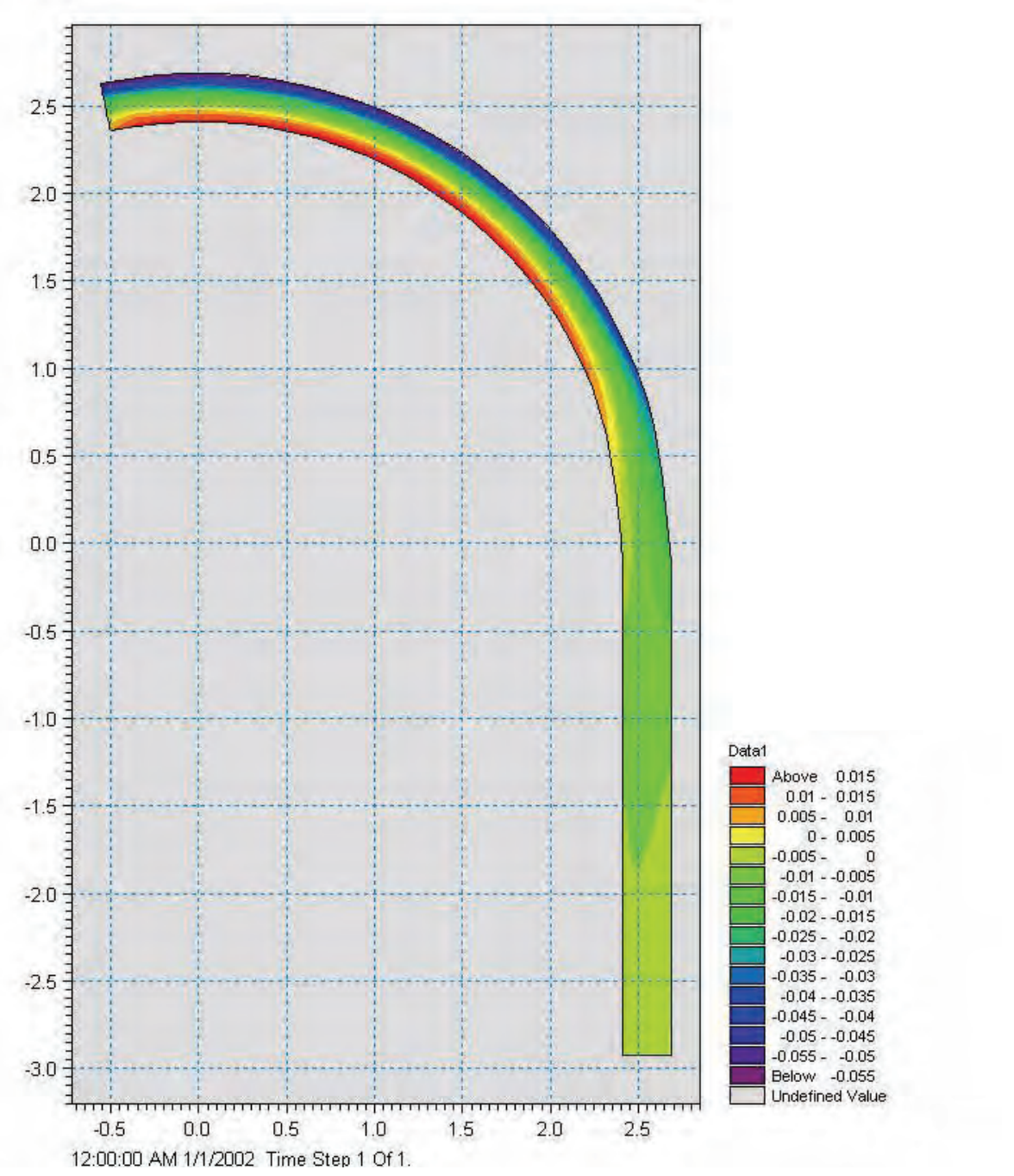

Figure 11-7 Model simulation of test run for 0.3m wide channel

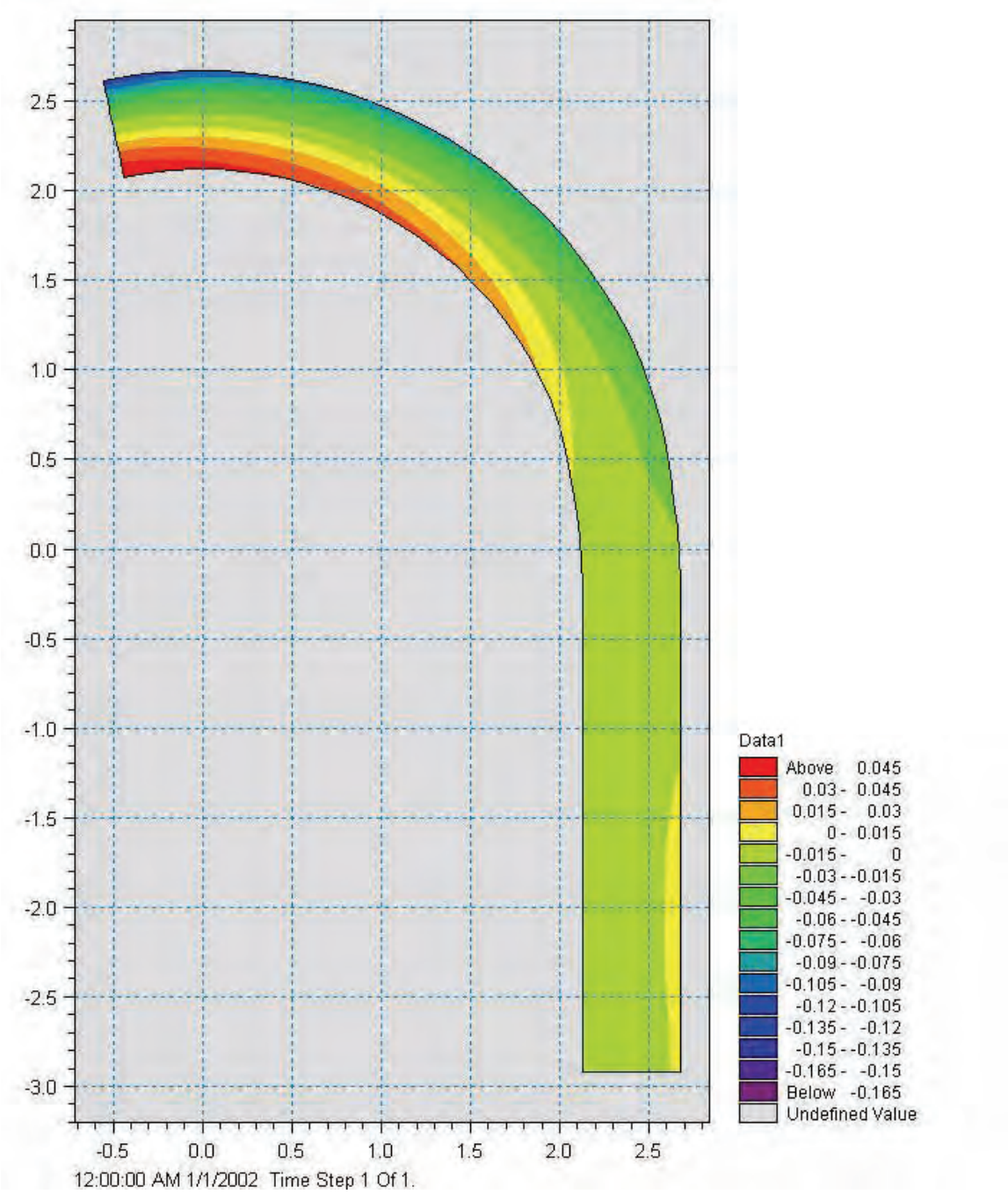

Figure 11-8 Model simulation of test run for 0.6 m wide channel

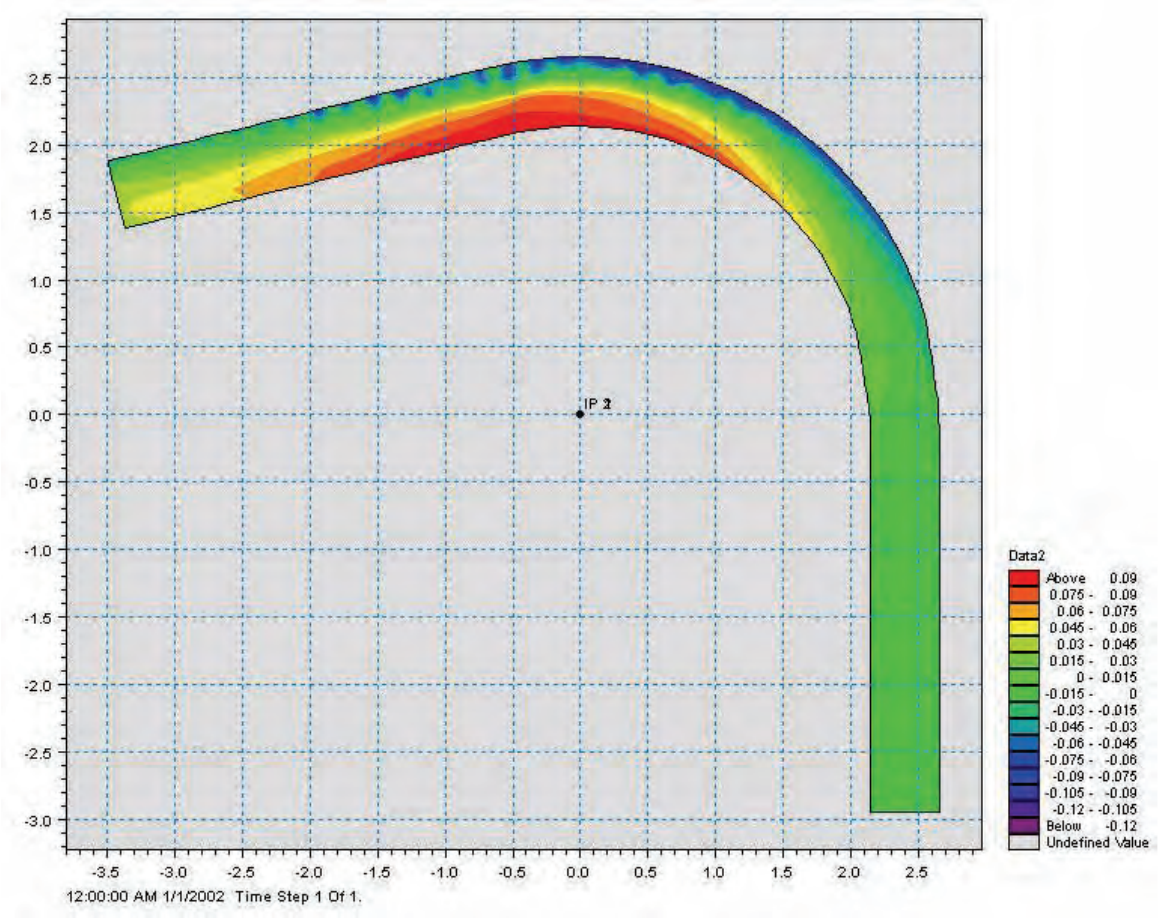

Figure 11-9 Simulation of longer channel

Figure 11-8 shows another attempt to simulate the bed profile with Mike21C. The same Mike21C parameters that were used for the 0.3m simulations were used here apart from the different discharge. It is evident however, that the same problem as for the 300mm channel was experienced. The solution to this is shown in Figure 11-9. The channel was extended beyond the sluice gate in the laboratory model. The thought behind this was that the straight section would behave much like a sluice gate, at least to the extent that it would dam water.

As can be seen, the extra straight channel had the desired effect. The scour position corresponds with that of the laboratory test and the hole closes up as it moves downstream as was observed in the measured profile. The deepest scour hole achieved during the simulation is 0.132m below the

original bed level. Hence, the simulation produced an accurate prediction of the observed bed levels.

11.3.3 TYPICAL RIVER BEND MATHEMATICAL MODELLING

In order to determine the behaviour of river bends with a movable bed, a sinusoidal channel was set up. A few characteristics of the channel were also changed from test to test to find out what effect they would have on the scour. Such aspects include the sinuosity, sediment size and lastly channel width.

Figure 11-10 shows a grid that was set up for a 70m wide bed width channel with a sinuosity of 1.24. This means that the length of the centreline of the sinusoidal part of the channel is 1.24 times longer than a straight line joining the ends of the sin curve. Note that an extra straight channel was added before and after the main channel. This was done so as to add stability to the simulation.

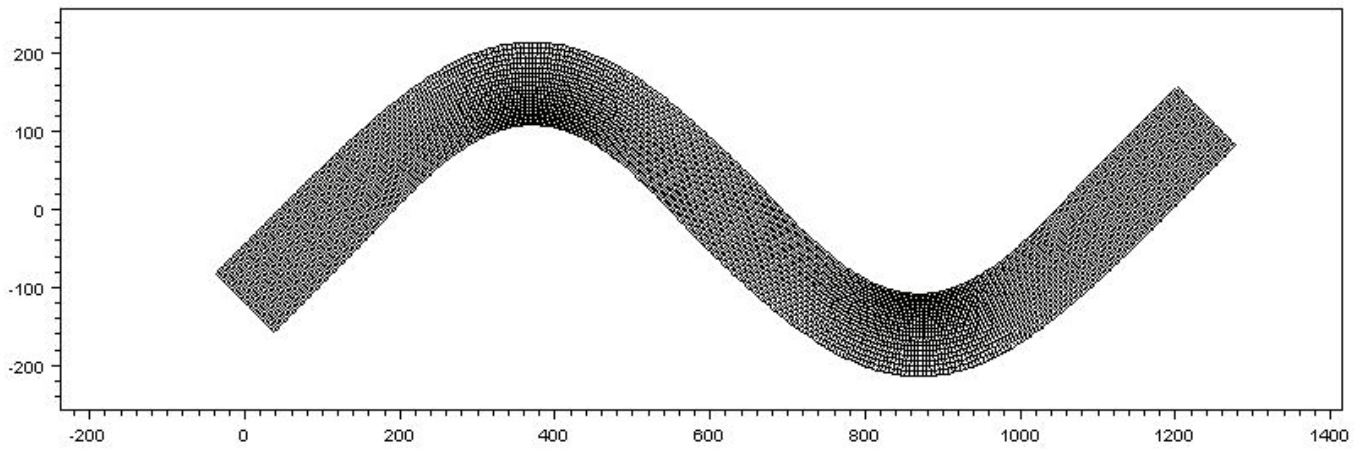

Figure 11-10 Sin1.24 grid (grid cell size 4x4m)

The grid was then given a trapezoidal cross section 80m wide top width and 5m deep with bank slopes of 45 degrees. The uniform downstream gradient was taken as 0.003 in each case and the

Manning roughness value was taken as n = 0.045. The downstream boundary water level was calculated for the discharge chosen to provide uniform flow conditions in the channel.

The following table shows some of the more important parameters that were used in Mike21C for these simulations.

Table 11-3 Mike21C parameters for sinusoidal channels

Mike21C parameter	Description	Value assigned
Modelling period	Length of simulation	11 hours
Timestep	Length of calculation iteration	5 seconds
Boundaries	Water levels and discharges	Vary from test to test
d_{50} of sediment	Size of sediment	Either 0.5mm or 1mm
Transport mode	Type of sediment movement	Both bed and suspended sediment
Transport formulation	Theory behind sediment movement	Engelund and Fredsøe
Horizontal eddy viscosity (ν)	Velocity or flux based viscosity	0.03 m^2/s
Manning n value	Roughness of channel	0.045 $s/m^{1/3}$
Threshold for drying and flooding	Water depth at which model begins calculating the hydrodynamics for that point	0.1 m

11.3.3.1 SIMULATION 1

A 70m wide channel with a sinuosity of 1.24 was assigned a sediment size of 0.5mm. A discharge of 300m^3/s was put through the channel which resulted in a water depth of 2.04m. This discharge relates to a 1:10 year recurrence interval flood for the size of the river based on regime theory. After a simulated time of 11 hours the bed level changes shown in Figure 11-11 occurred.

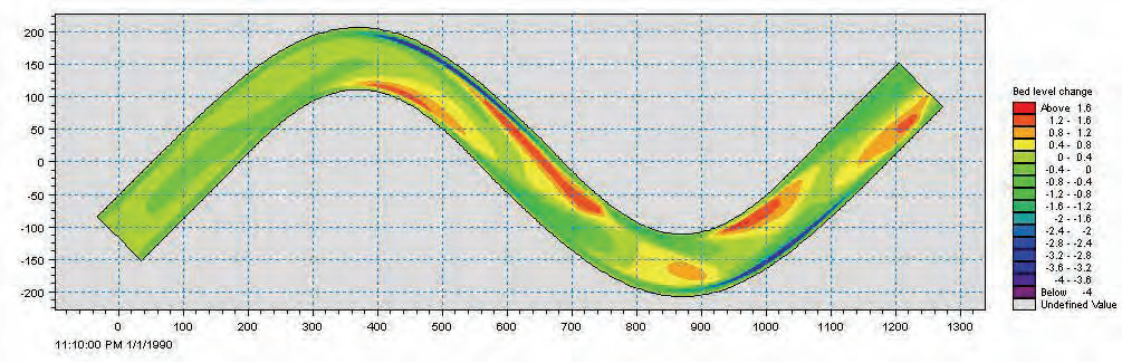

Figure 11-11 Simulated bed level changes: Sin 1.24 Q=300m^3/s d=0.5mm

The deepest scour hole present is 4.31m deep. It occurred downstream of the vertex of the curve roughly two breadths after the upstream intersection point. Many sand banks also formed due to the large amount of sediment that was scoured out at the bends. The sandbanks also indicate that the first bend does not influence the scour observed in the second bend. This fact can be more readily seen in Figure 11-12. It shows the helical flow intensity in the channel and it is clear that almost no secondary flows exist in the middle part between the two curves.

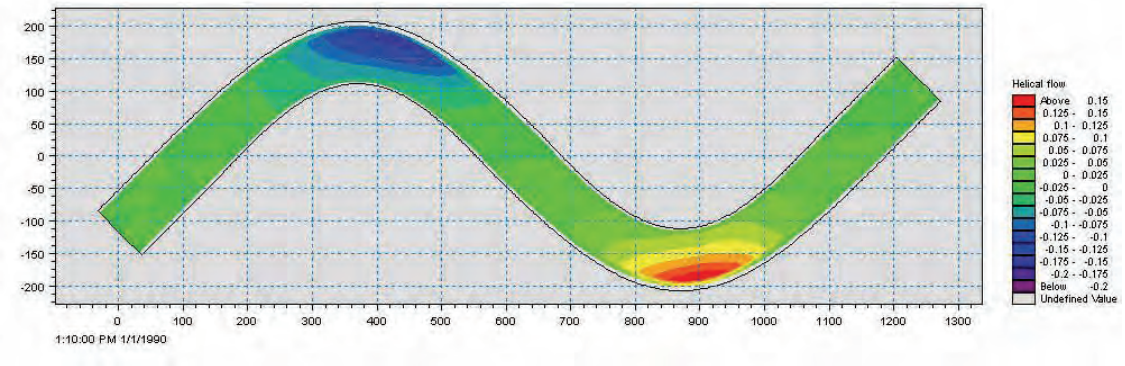

Figure 11-12 Helical flow intensity for sin 1.24 channel

In a three dimensional hydrodynamic model only set-up in Delft 3D, the same simulation was repeated to investigate the spiral flow patterns around the river bend. The simulation result is shown in Figures 11-13 to 11-15. Although the 3D simulation provides detailed information, the bed morphology changes the hydraulics considerably in the 2D simulations carried out with Mike 21 C and it is therefore important to have a sediment transport module in the simulations.

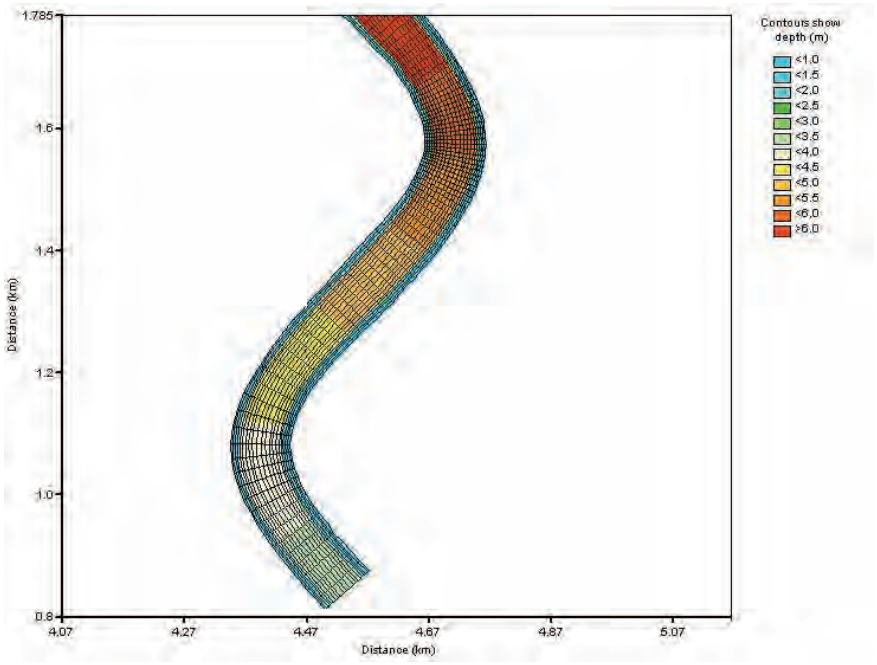

Figure 11-13 3D Model bed layout (sinuosity 1.24, 80 m wide)

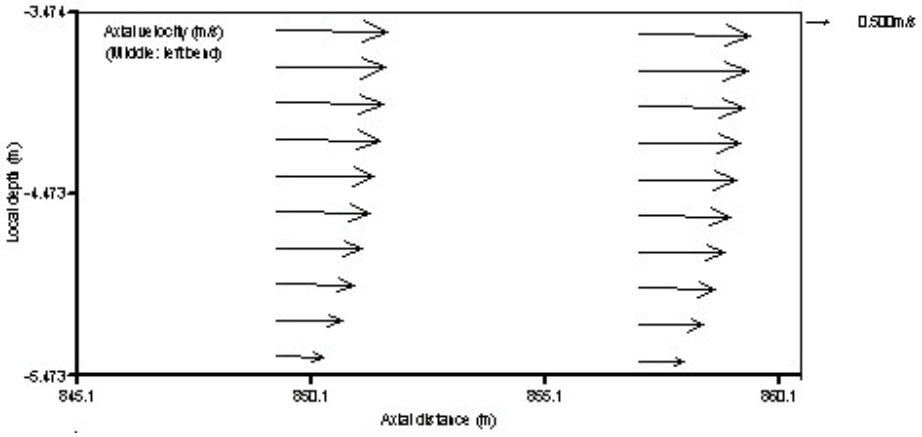

Figure 11-14 3D Model velocity vectors in bed cross-section (Axial velocity)

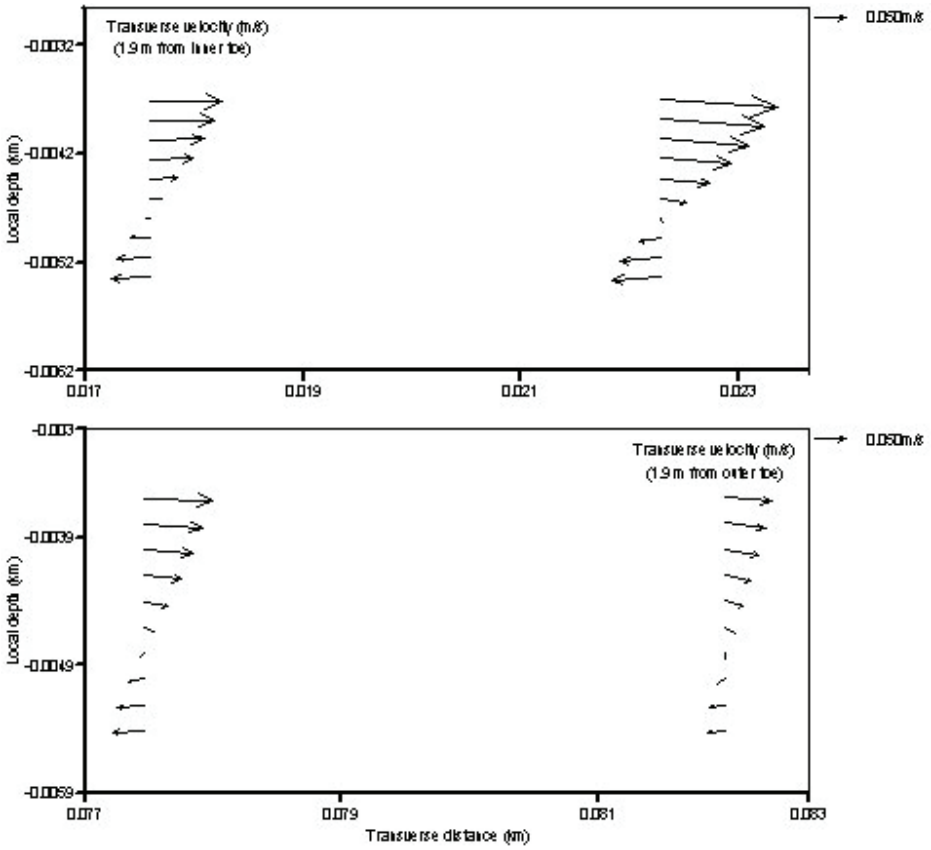

Figure 11-15 3D Model velocity vectors in bed cross-section (Transverse velocity)

11.3.3.2 SIMULATION 2

In this simulation the sinuosity was decreased to 1.1 as can be seen from the notably shorter channel. The channel width is still 70m, the discharge was 300m^3/s and the sediment size was 0.5mm. After 11 hours the deepest scour occurred in the usual place, just after the vertex of the curve to a depth of 3.69m (Figure 11-16).

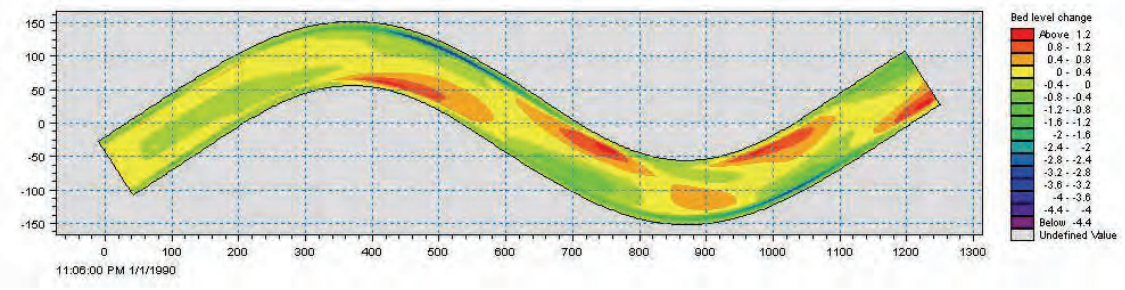

Figure 11-16 Simulated bed level changes: Sin1.1 Q=300m^3/s d=0.5mm

11.3.3.3 SIMULATION 3

In simulation 3 the sinuosity was taken as 1.4. A discharge of 300m^3/s was used together with a sediment size of 0.5mm. The width was kept at 70m. In this instance a scour hole of 4.53m formed. The result of the simulation is shown in Figure 11-17.

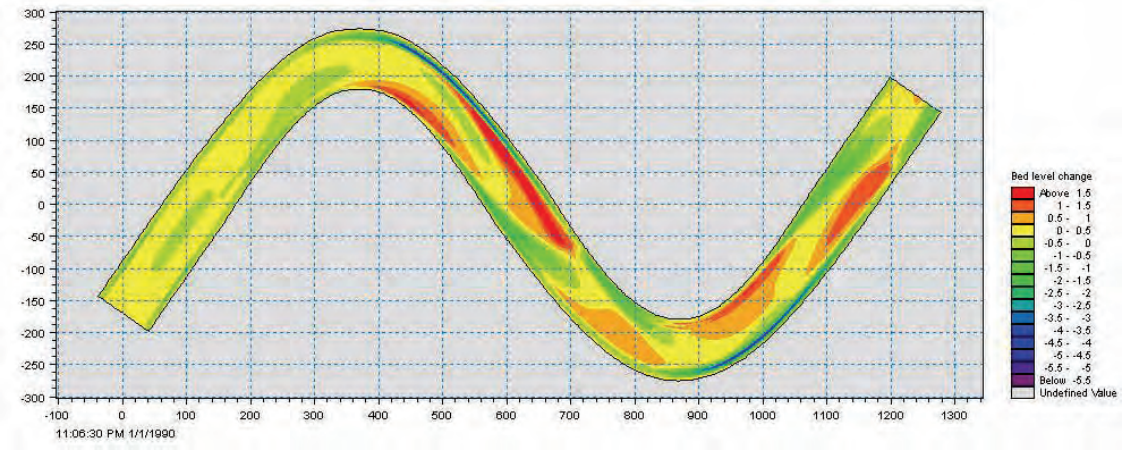

Figure 11-17 Simulated bed level changes: Sin 1.4 Q=300m^3/s d=0.5mmm

11.3.3.4 SIMULATIONS 4 TO 12

Several more simulations were conducted to ascertain what effect a smaller width as well as a larger sediment size would have on the depth of scour. The smaller width was chosen as 20m and the larger sediment size was 1mm. The 1:10 year recurrence interval flood for the 20m wide river was determined to be 20m^3/s.

The simulated maximum scour depths are shown in Table 11-4 and Figure 11-18. The scour depths are deeper with smaller sediment sizes as can be expected. The scour depths increase with increasing sinuosity both in the 20m and 70m wide channels. The 70m wide channel scour depths are also considerably deeper than those of the 20m wide channel.

Table 11-4 Simulated maximum scour depths (m)

Sinuosity	B = 20m (Q = 20m^3/s)		B = 70m (Q = 300m^3/s)	
	d = 0.5mm	d = 1mm	d = 0.5mm	d = 1mm
Sin 1.1	0.24	0.11	3.69	1.34
Sin 1.24	0.43	0.18	4.31	2.77
Sin 1.4	0.71	0.27	4.53	3.68

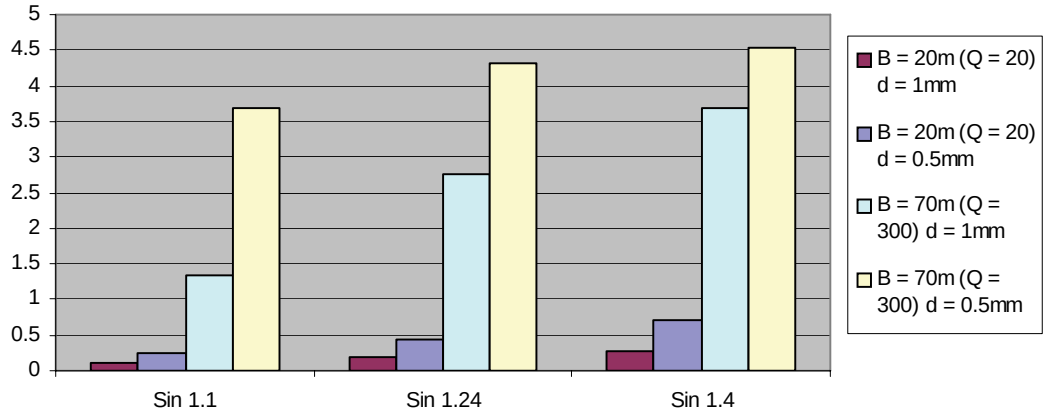

Figure 11-18 Simulated maximum scour depths (m)

Figure 11-19 to Figure 11-21 show the results of some of the simulations. The change in bed levels is depicted and as can be seen, the depth of the scour holes changes considerably from simulation to simulation. The position of the scour holes also changes with channel width as well as sinuosity but not with change in sediment size.

The positions of the various scour holes on the many different channels calls for a look at the accuracy of certain empirical models claiming to predict the scour position.

The method of Raudkivi (1993) has already been mentioned earlier. It states that the deepest scour hole will form two breadths away from the upstream axis intercept point. It was found previously that the 0.3m channel width sediment related tests corresponded very well with this method. The 0.6m channel, however, did not conform to this method. The scour hole formed further downstream from where it was predicted.

A similar verdict exists for the sinusoidal channels. The 70m wide channels formed their deepest scour holes where the Raudkivi predicted. For the 20m channels this did not concur. Their scour holes were to be found further downstream.

The method of Chen, using equation 7-10 in Section 9.3.1.2 also does not produce reliable predictions. Not one of the calculated values for the location of deepest scour was where the deepest scour was observed.

Certain trends can however be identified. By inspecting the figures of all the sediment related tests that were conducted it can be seen that the wider a channel is, the further downstream from the curve apex the deepest scour will be observed.

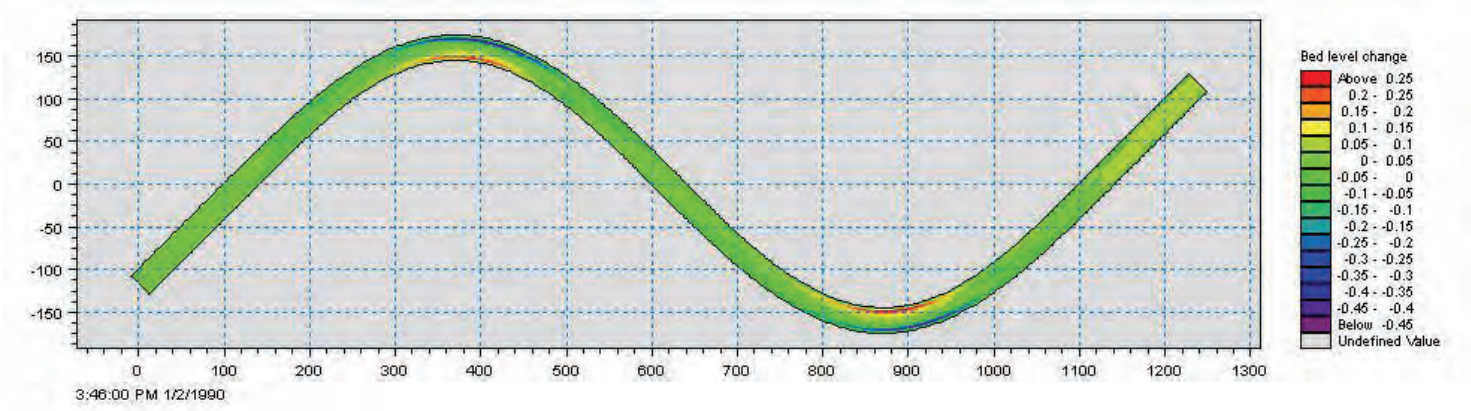

Figure 11-19 Bed level change Sin1.24 20m wide channel (sediment = 0.5mm)

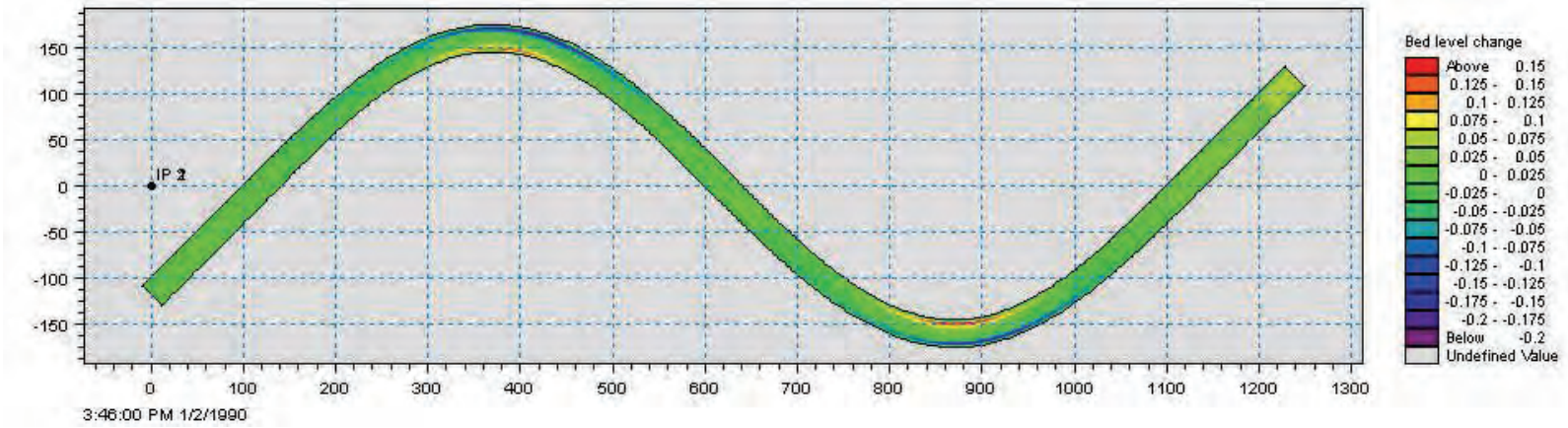

Figure 11-20 Bed level change Sin1.24 20m wide channel (sediment = 1mm)

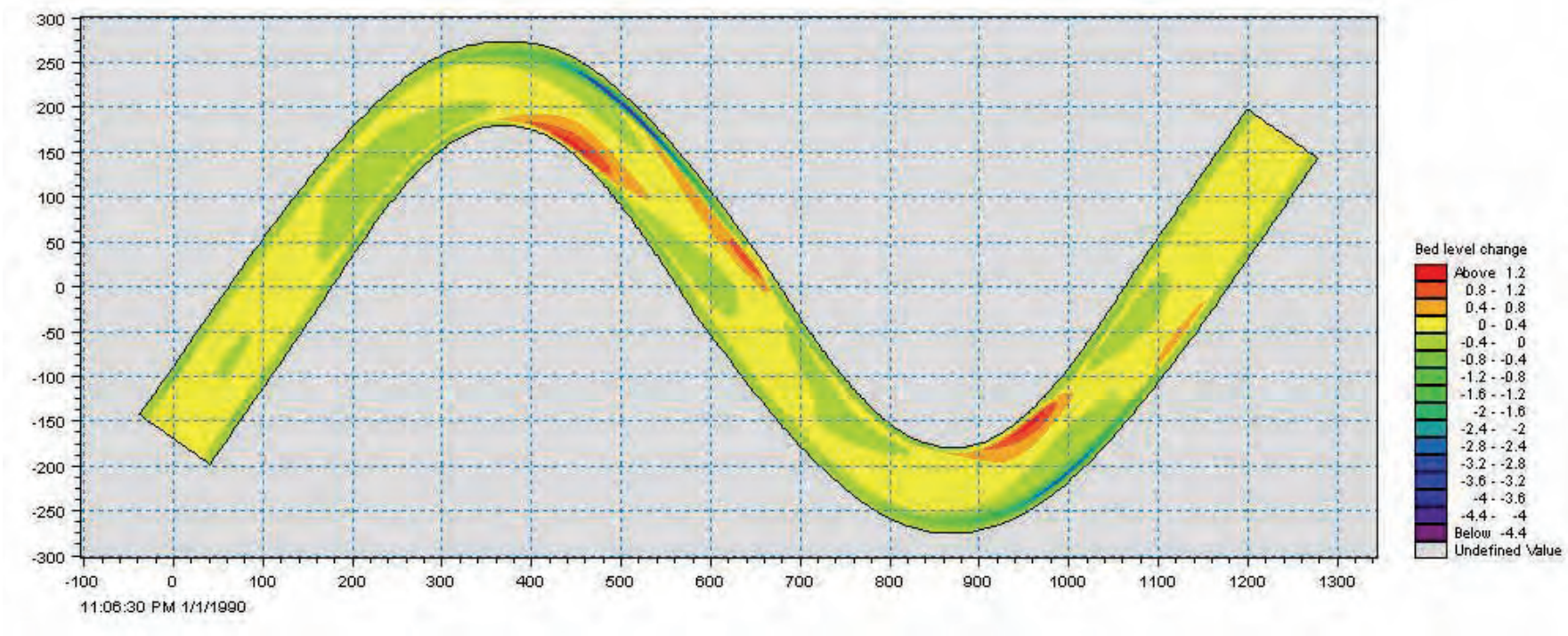

Figure 11-21 Bed level change Sin1.4 70m wide channel (sediment = 1mm)

11.4 DIVERSION ORIENTATION

This section concerns the investigation into the effect that the orientation of a diversion structure would have on the spiral flow and creation of a deep scour hole zone at the intake.

11.4.1 DIVERSION ANGLE

The diversion angle can play a major role in the depth of scour that will take place at the tip of the diversion structure. Common sense dictates that a structure that makes a small angle between itself and the general stream direction would have a gentler effect on the stream than would a structure with a large angle. This is precisely what was observed in the experiments carried out in this study.

11.4.2 LABORATORY ORIENTATION TESTS AND MODELLING

A 2m by 10m flume was used to model the angled diversion structures. The tank was filled with a 0.15m layer of 0.12mm sand around a vertical plank which was used to represent the diversion structure. The first plank was placed at an angle of 45 degrees to the bank, the second at 30 degrees and the third at 15 degrees. Care was taken to make sure that the constriction that the water underwent during each test was the same for every test and that the level of sand was identical in each case.

A v-notch weir was used at the upstream end of the tank to ensure that the flows for each test were the same ($Q = 0.0309 m^3/s$). A sluice gate downstream of the plank was utilised to control the water level in the tank, which was taken as 0.076m above the initial level of sand. Water was added slowly from downstream and upstream, to fill the flume to the required flow depth before each test was started. Figure 11-22 and Figure 11-23 show the original setup of the experiment for the 45 degree groyne.

Figure 11-22 45 degree groyne with level sand before test

Figure 11-23 45 degree groyne with level water

After the tests were completed, Mike21C simulations of the experiments were conducted with varying degrees of success. There were initial problems in setting up the grid for the simulations but once these were solved the program predicted the positions of scour and sedimentation satisfactorily. The simulated dimensions of these scour holes and sand banks, however, are not as accurate as expected. This could be due to the inaccuracy of the sediment transport equation used by the model and the fact that large dunes formed in the experiment which cannot be simulated by the mathematical model.

Some of the important Mike21C model parameters for the experiments are given in Table 11-5 below:

Table 11-5 Mike21C parameters for groyne experiments

Mike21C parameter	Description	Value assigned
Modelling period	Length of simulation	2.5 hours
Timestep	Length of calculation iteration	0.1 seconds
Boundaries	Water levels and discharges	Discharge = 0.0306 m^3/s Downstream water level at gate = 0.05m
d_{50} of sediment	Size of sediment	0.12 mm
Transport mode	Type of sediment movement	Both bed and suspended sediment
Transport formulation	Theory behind sediment movement	Engelund and Fredsøe
Horizontal eddy viscosity (ν)	Velocity or flux based viscosity	0 m^2/s
Manning n value	Roughness of channel	Calibrated for each test
Threshold for drying and flooding	Water depth at which model begins calculating the hydrodynamics for that point	0.001 m
Grid spacing	Size of grid cell	0.1m by 0.1m

11.4.2.1 GROYNE SIMULATION 1 (15 DEGREES)

As was expected, the 15 degree experiment did not scour out or deposit a great amount of material. The test was allowed to run for 3.5hours and thereafter a maximum scour hole depth of 0.0588m was observed. The deposited sand bank downstream of the diversion reached a height of 0.0573m above the original sand level. The measured bed topography is depicted in Figure 11. It shows the change in bed level measured in meters. The red "steps" represent the groyne/diversion structure. The many undulations that are visible in Figure 11-24 are dunes that formed in the bed.

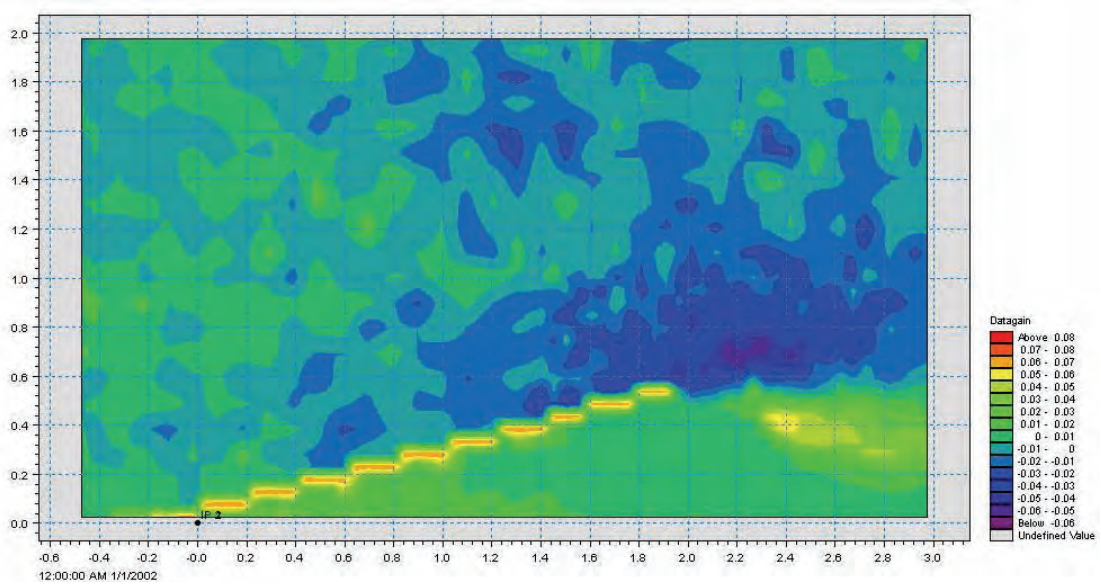

Figure 11-24 Observed bed level changes with the 15 degree groyne experiment

The deepest scour hole formed downstream in line with the groyne, with a prominent sand bank forming just to the right of it. Figure 11-25 and Figure 11-26 show the bed forms created by the 15 degree groyne.

Figure 11-25 15 degree groyne

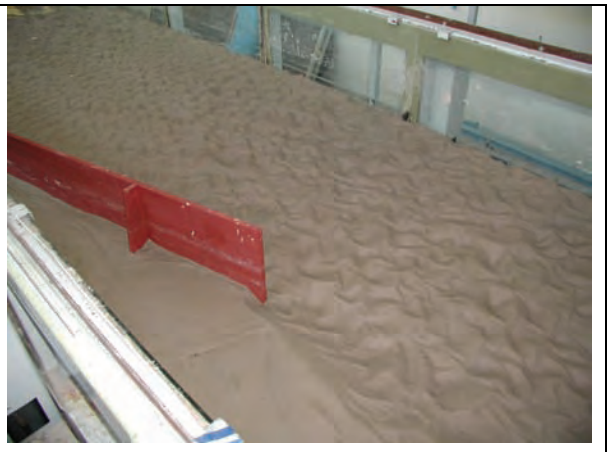

Figure 11-26 15 degree groyne

The result of the computer simulation of the 15 degree groyne is given in Figure 11-27. Water levels were measured during the test and these were used to determine the Manning roughness of the channel. In this case the Manning 'n' value was found to be equal to 0.0196. The locations of the changes in bed level correspond with those measured in the experiment. The maximum depth of scour achieved is 0.0494m and the sand bank reached a height of 0.0284m. Both the depth of scour and height of deposition are very near the observed values.

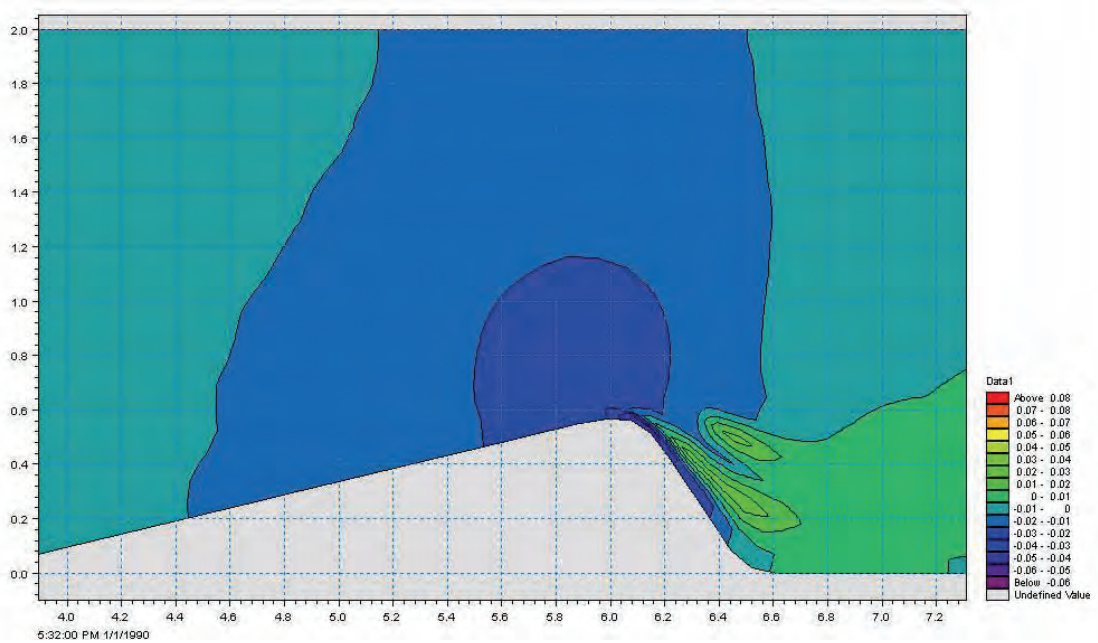

Figure 11-27 15 degree groyne simulation

11.4.2.2 GROYNE SIMULATION 2 (30 DEGREES)

The 30 degree groyne washed out a bigger hole than the previous experiment. After 3.5 hours the deepest scour depth observed was 0.0779m and a sand bank 0.0535m high formed. They occurred in similar positions to the other tests: downstream in line with the groyne that formed them. The 30 degree experiment survey is shown in Figure 11-28 Figure 11-29 and Figure 11-30 show the observed scour patterns.

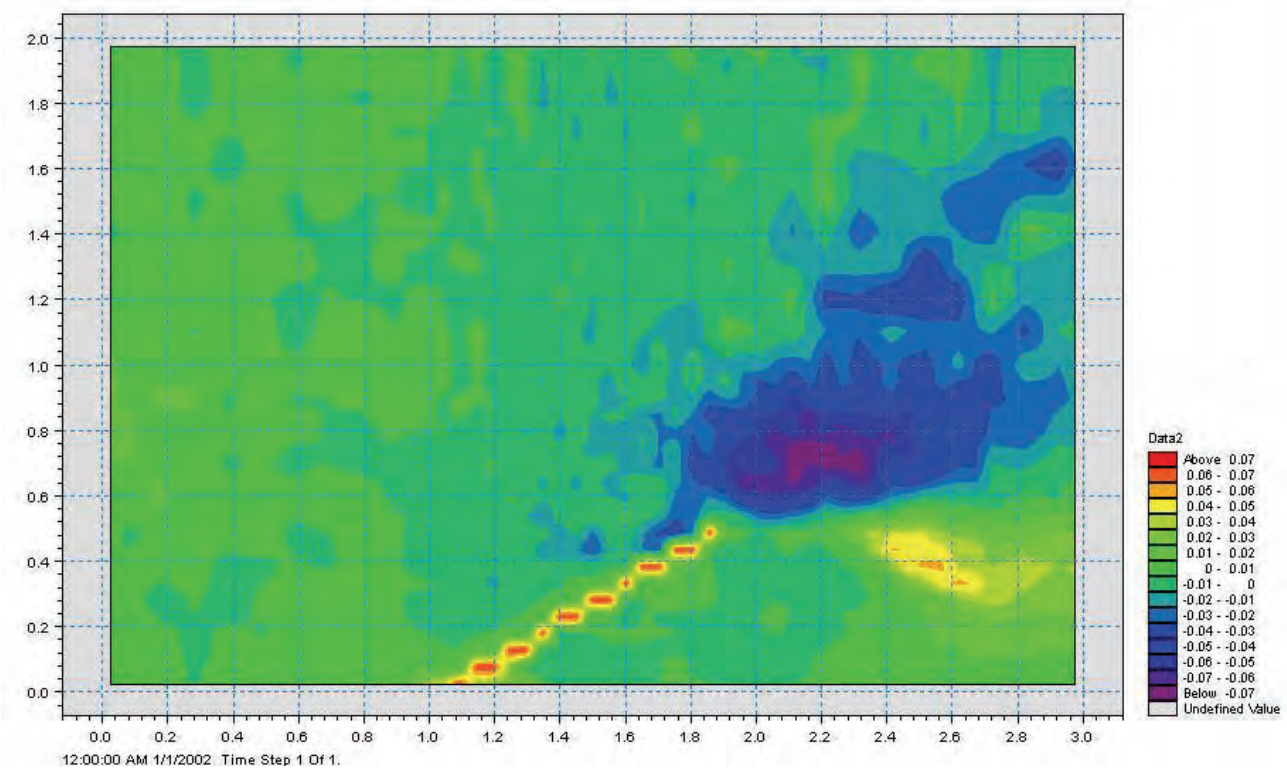

Figure 11-28 Observed bed level changes with the 30 degree groyne experiment

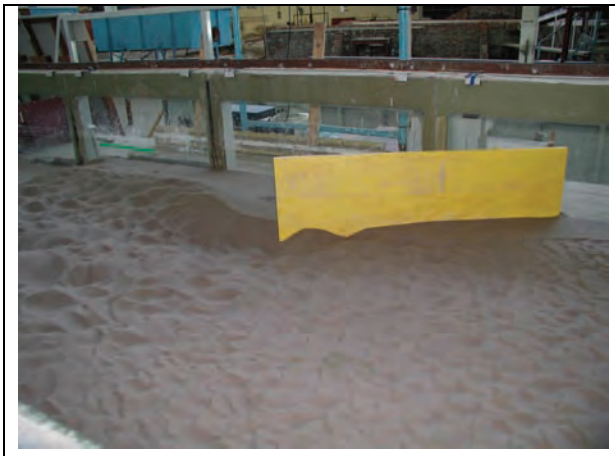

Figure 11-29 30 degree groyne

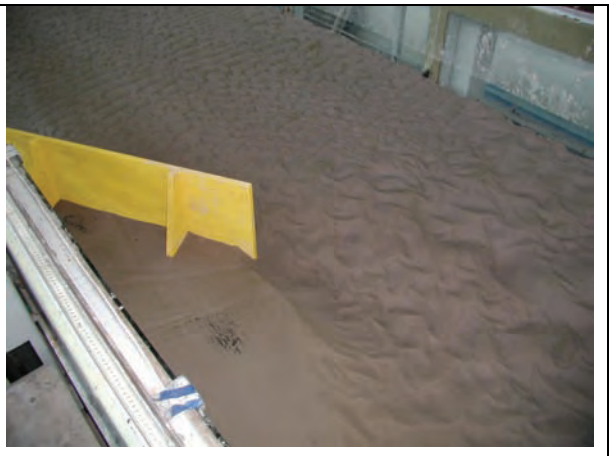

Figure 11-30 30 degree groyne

The simulation of the 30 degree groyne is given Figure 11-11. The positions are once again reliable, yet the depths predicted fall below the measured ones. Maximum predicted depth is 0.037m whilst the sand bank height is 0.024m. The calculated Manning 'n' value was 0.025.

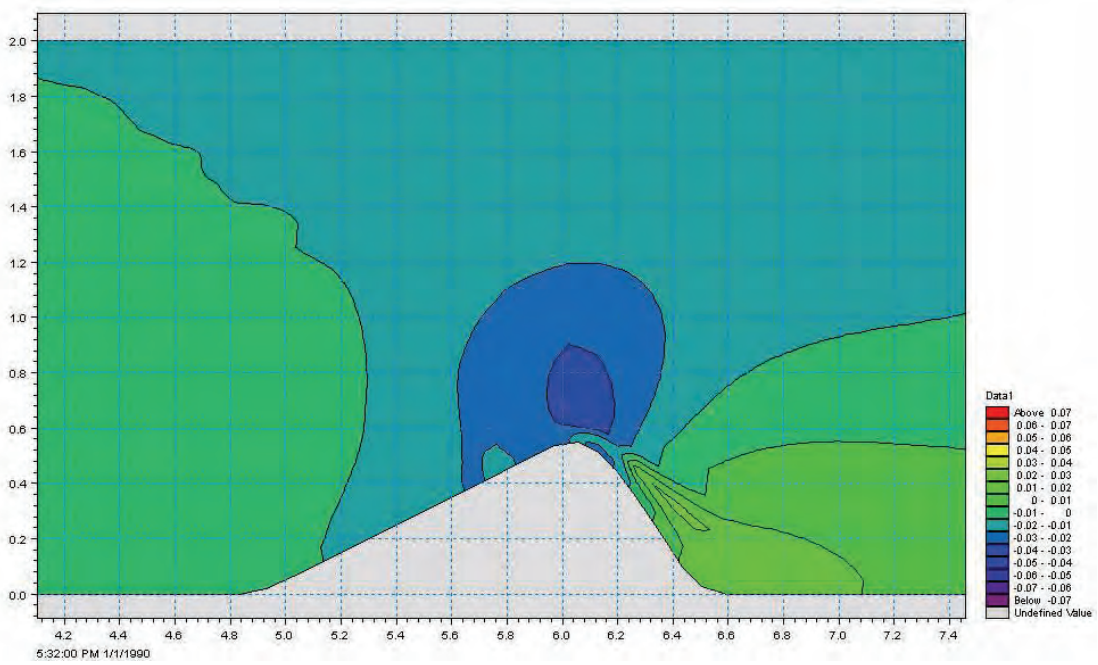

Figure 11-31 30 degree groyne simulation

11.4.2.3 GROYNE SIMULATION 3 (45 DEGREES)

The 45 degree diversion groyne caused the most sudden concentration of flow out of all the tests. It is therefore expected that the scour hole would be the biggest of all three tests. It formed in the now familiar position where the concentrated flow from upstream started making small vortex eddies when it encounters the slower moving water behind the groyne. Figure 11-32 shows the observed change in bed level in meters after 3.5hours with bed forms and scour holes clearly visible.

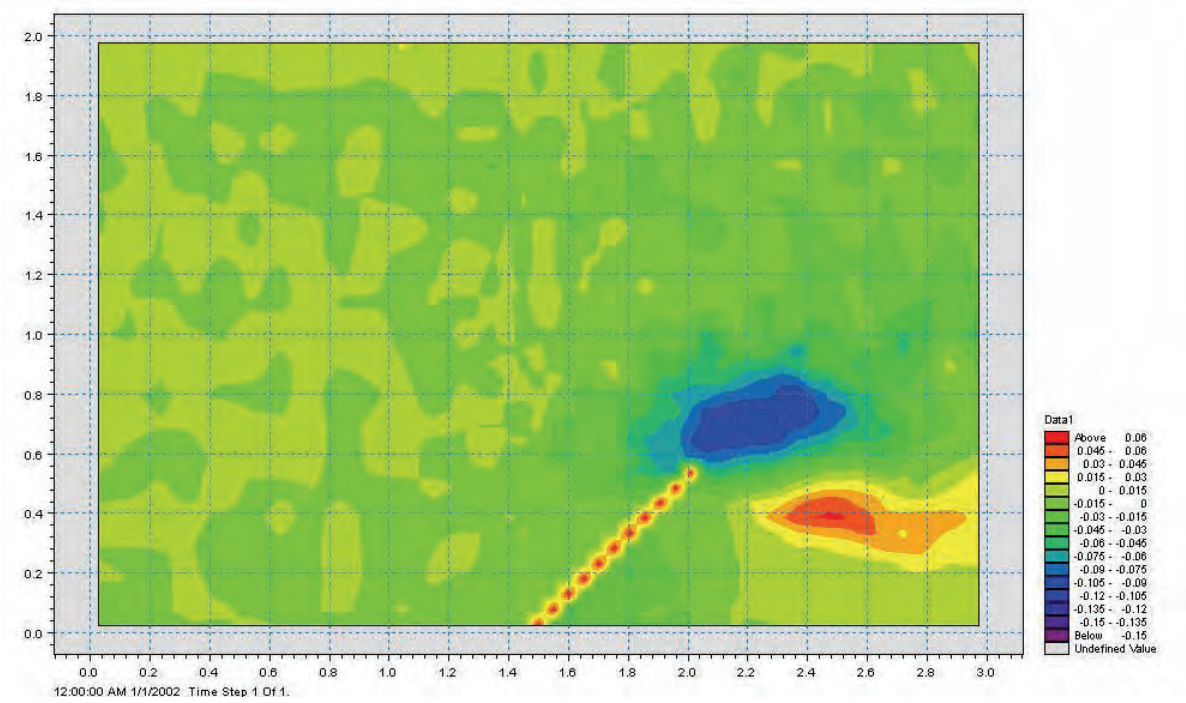

Figure 11-32 Observed bed level changes with the 45 degree groyne experiment

The deepest hole that formed was 0.119m deep and the sand bank rose up to a level of 0.0618m. Scour patterns are shown in Figure 11-33 and Figure 11-34.

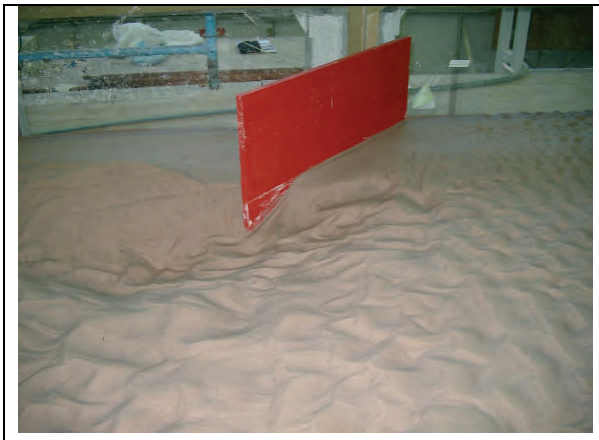

Figure 11-33 45 degree groyne

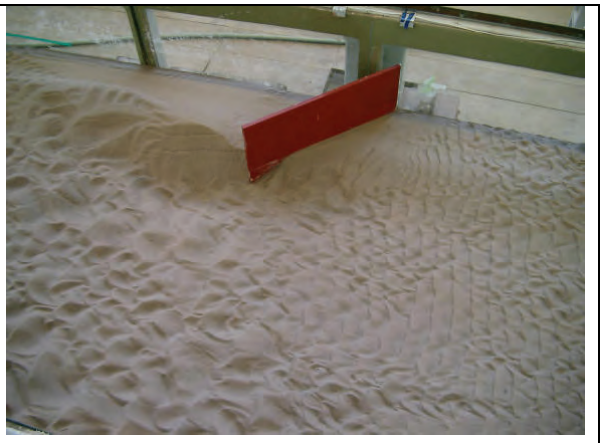

Figure 11-34 45 degree groyne

A simulation of the experiment above is shown in Figure 11-35. A Manning 'n' value of 0.031 was used. The position of the scour hole is most satisfactory. Its depth however, is as before, too shallow. The depth simulated is 0.0673m. The sand bank (of height 0.0617m) exhibits a behaviour that did not occur in the previous two simulations: it split into multiple units. Such an outcome was not observed during the experiment itself, thus one is led to believe that further refinement of the model setup and grid is possible.

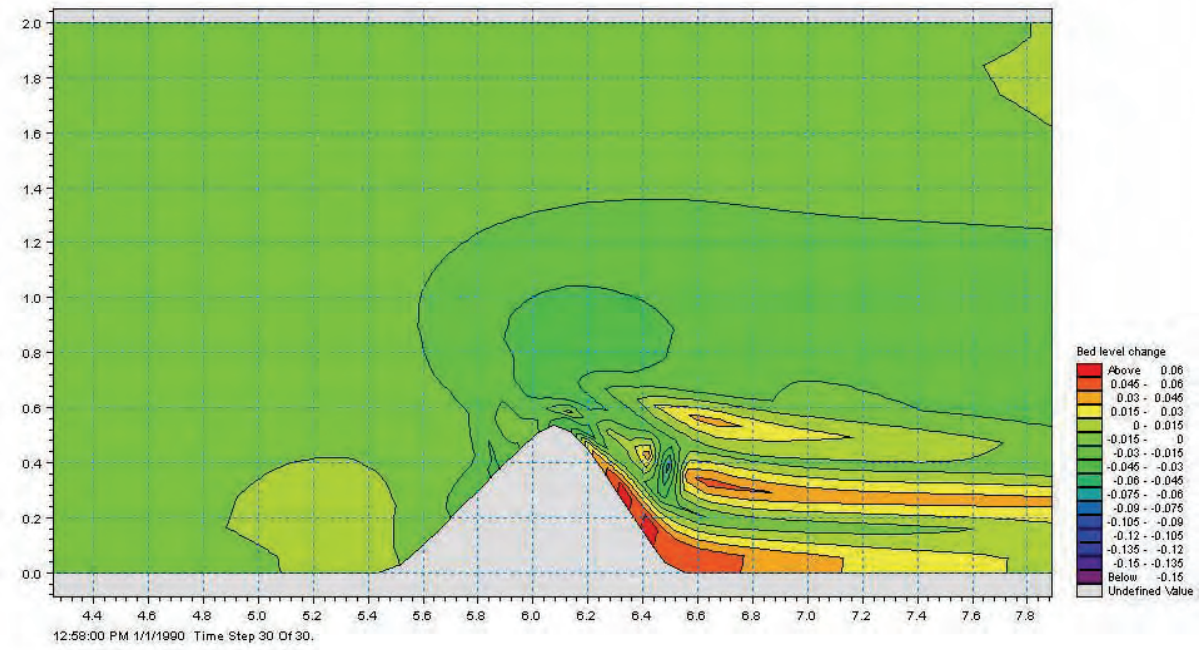

Figure 11-35 45 degree groyne simulation

11.4.2.4 CONCLUSIONS FOR DIVERSION STRUCTURE EXPERIMENTS

It was hoped that the groyne structure would induce erosion along its entire length; so as to assist in keeping the abstraction works sediment free. This, as can be seen from the experiments, did not occur. The majority of the erosion scour took place at the nose point of the diversion structure. If such a structure is however placed in a bend in a river, it could possibly help with the generation of spiral flow. The next section investigates such a scenario.

11.4.3 RIVER BEND WITH DIVERSION STRUCTURE SIMULATION

In the end it is attempted to combine the scour properties of a diversion structure with those of a river bend. Such an attempted simulation is shown in Figure -36.

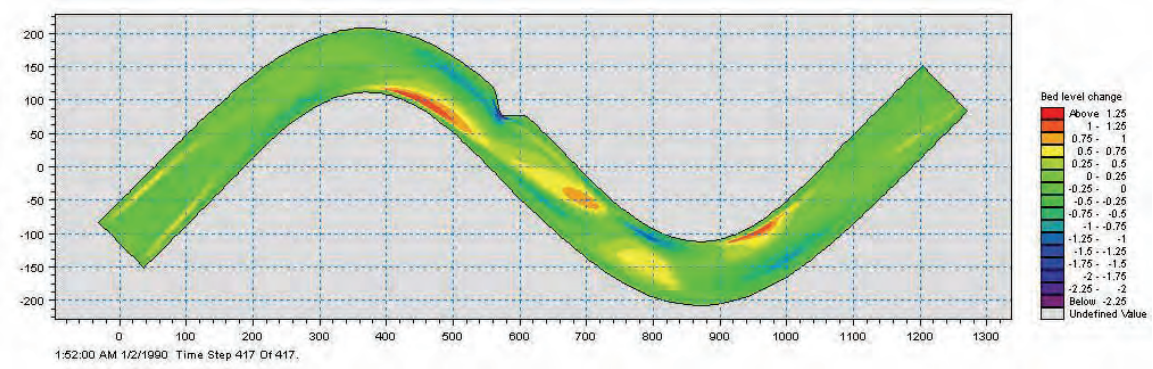

Figure 11-36 Bed level change simulation of 70m wide channel with groyne (Sin 1.24, 45 groyne, Q = 300m^3/s, d = 0.5mm)

A 45 degree groyne was placed in the approximate position of largest scour formed without a groyne. The deepest scour hole formed, as expected, at the point of largest contraction at the point of the groyne with a simulated depth of 2.1m. This is not as deep as the original 70m wide sin1.24 channel without a groyne where the maximum simulated scour depth was found to be 4.31m. The most likely reason is evident from Figure 11-37 which shows a close-up of the structure in the bend.

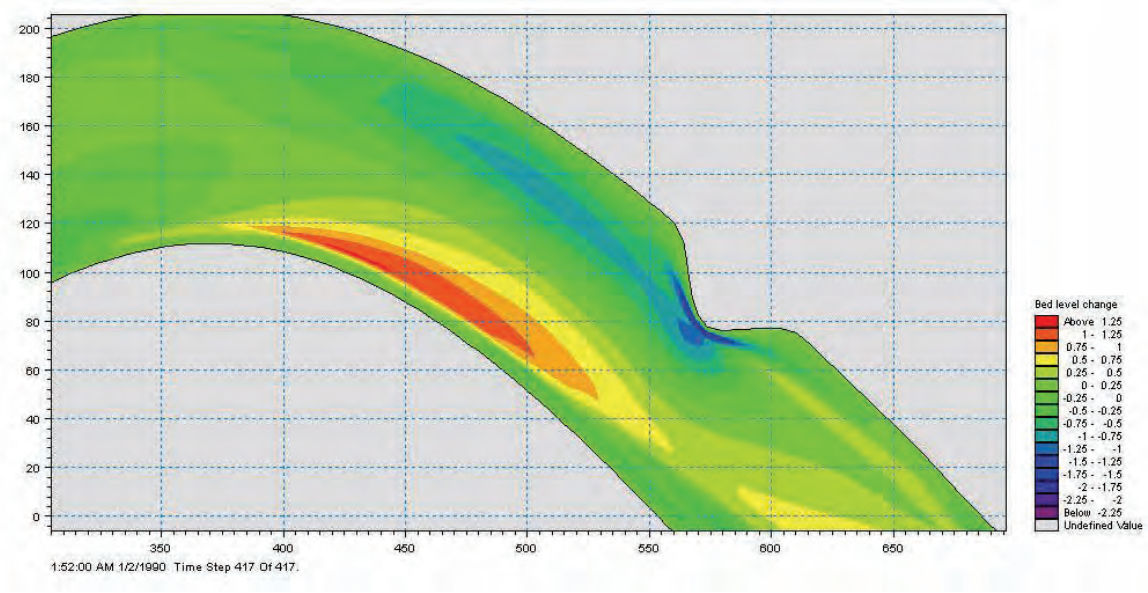

Figure 11-37 Close up of 45 degree groyne

The natural scour holes that form due to the secondary currents in a river bend are present; they are, however not as pronounced as before. The cause is that the groyne inhibits the full development of the secondary currents. This is however, not of great concern. What is important is that a scour hole formed next to the groyne structure, which is most beneficial for the withdrawal of water there.

11.5 DIVERSION STRUCTURE WITH BROAD CRESTED WEIR

Another model test was conducted to determine the influence of a weir on the scour caused by a diversion structure. The same flume used for the previous tests was used. A 30 degree groyne was chosen and a 200mm high broad crested weir was constructed at the maximum constriction of the groyne.

It was attempted to create the same conditions as for the previous tests: in other words, a discharge of 0.031m^3/s and a water depth of 0.076m. The discharge for the model run was measured as 0.034m^3/s and a water depth of 0.06m. The experiment is depicted in Figure 11-38.

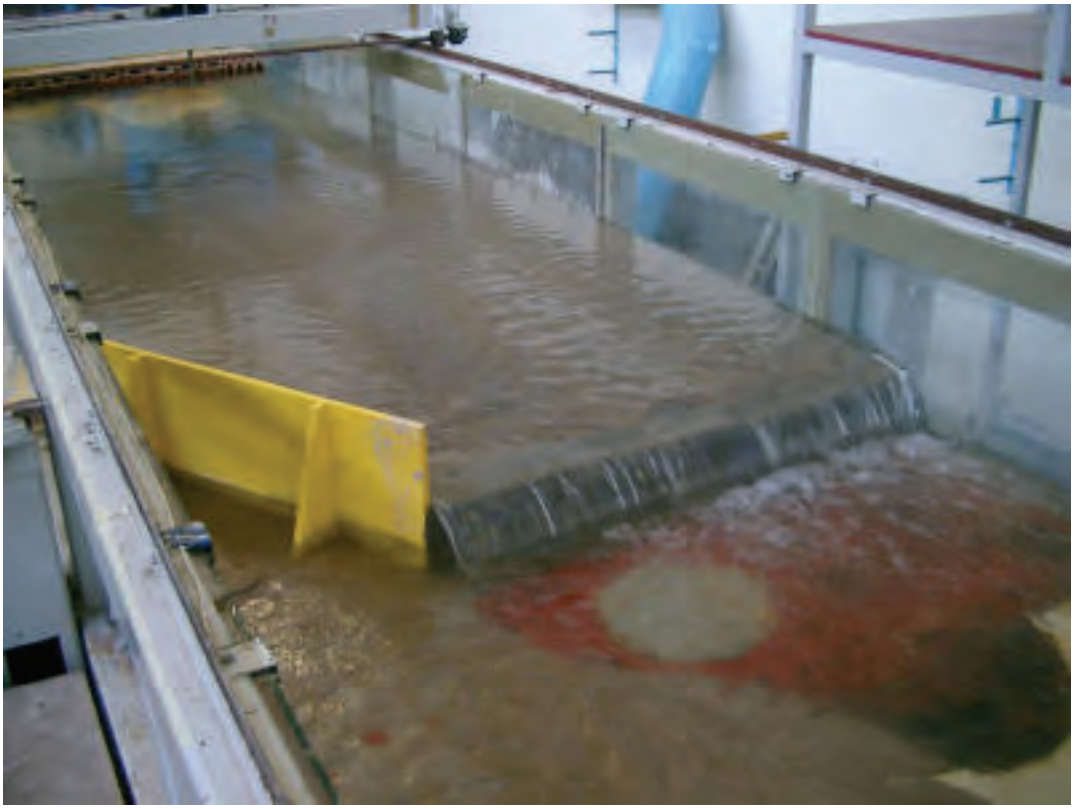

Figure 11-38 Thirty degree groyne and weir

In the initial run of the test a level layer of sand was placed behind the weir and groyne to a height of 70mm below the crest of the weir. It was found, however that at this depth almost no change in sediment levels. Hence, the layer of sand was increased to be level with that of the weir crest.

11.5.1 TEST RESULTS

The test was allowed to run for a period of four hours in which a great deal of sediment was moved. As expected, the greatest amount of scour took place next to the weir itself as can be seen in Figure 11-39.

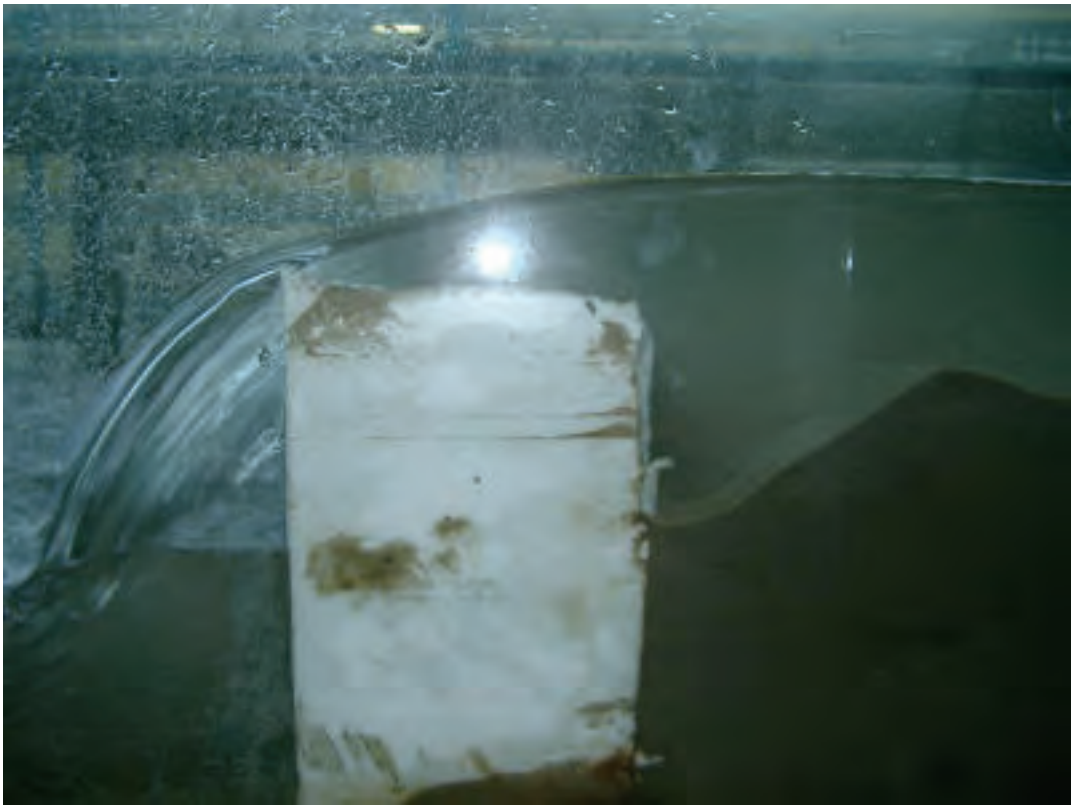

Figure 11-39 Side view of weir

What wasn't expected however are the distinct troughs that formed on both sides of the channel. This phenomenon can best be viewed by looking at the plot of the measured depths shown in Figure 11-40 as well as Figure 11-41. The deepest through forming next to the groyne.

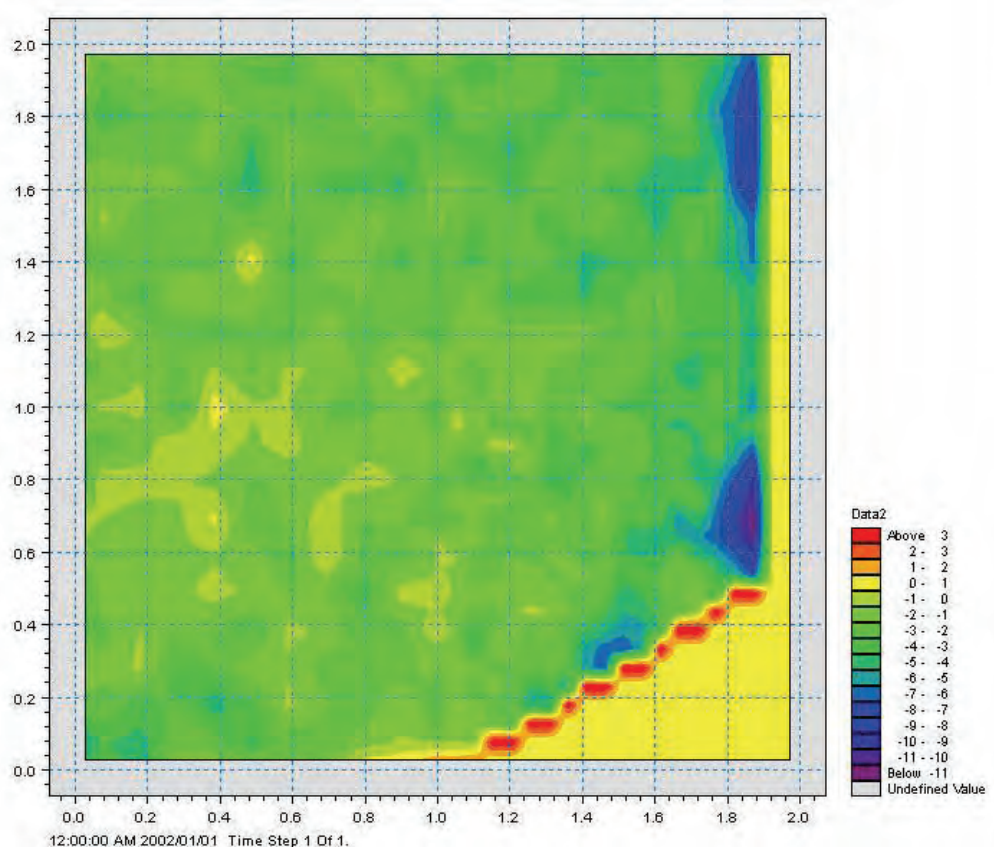

Figure 11-40 Change in bed level after test run

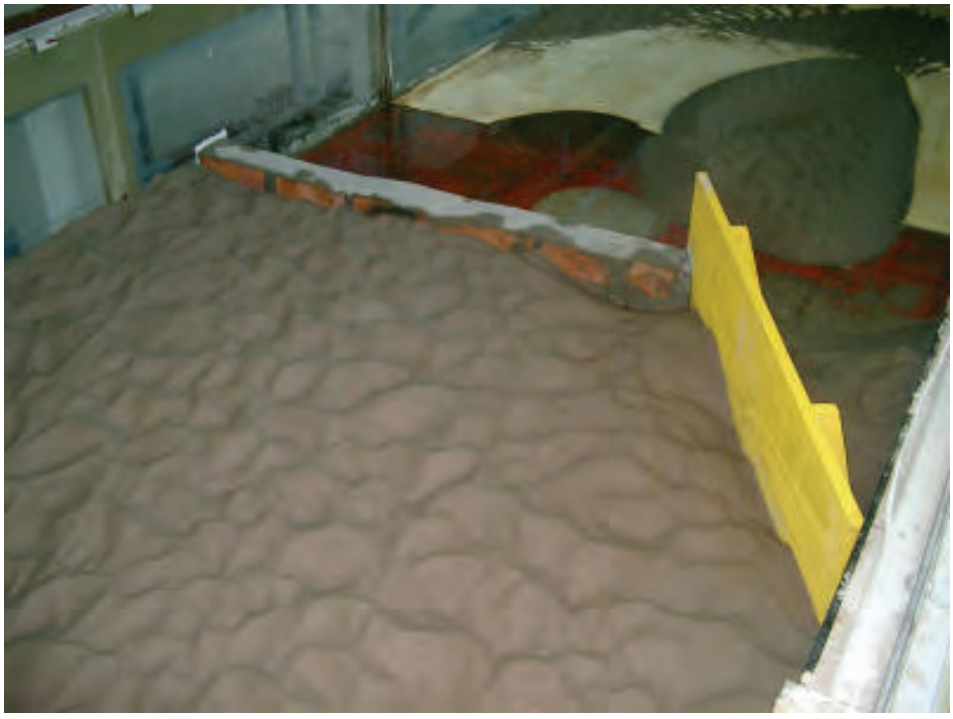

Figure 11-41 Bed forms after test run

The maximum depth that was measured afterwards was 115.3mm below the weir crest level, which is a great deal deeper than the previous tests without the weir. It is clear that the weir is responsible for the large amount of turbulence and secondary currents that takes place. It must also be noted however, that the average velocity for the weir test was slightly higher than that for the other tests, which would have a marked influence on scour.

11.5.2 GROYNE AND WEIR SIMULATIONS

Although it was expected that Mike21C would have difficulty in simulating the weir structure together with the large 3 dimensional currents that go along with it, an attempt was made resulting in the following:

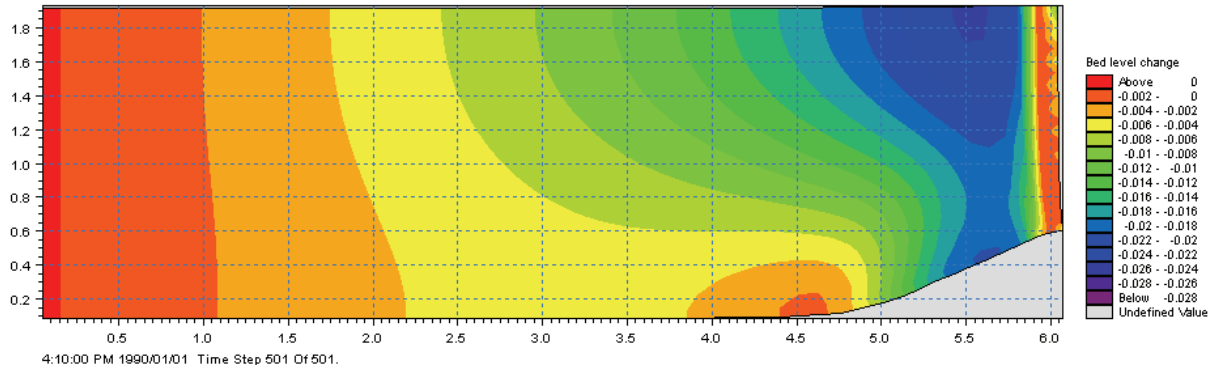

Figure 11-42 Mike21C simulation of bed level change with weir

The simulation succeeded in creating the two troughs found in the test run, however the deeper trough is found away from the groyne. Its depth is only 0.024m, vastly less than the measured values. This is most likely due to the lack of the three-dimensional currents in the model.

11.6 ANALYSIS OF MATHEMATICAL MODEL SIMULATION RESULTS

11.6.1 MODELLING OF HYDRODYNAMICS

The three-dimensional simulation results in higher velocities being indicated on the outside of the bend from approximately halfway through the bend with the maximum velocity being

near the end of the curved section. Higher velocities are also found closer to the inside of the bend in the region near the end of the straight section and the beginning of the curved section. A typical simulated velocity distribution is presented in Figure 11-43(b). This is essentially the same as were obtained from the laboratory experiments (see Figure 11-43(a)). Figure 11-43 (a) is not to scale (n.t.s) whereas Figure 11-43 (b) is to scale. From Figure 11-43 it can be seen that the simulated flow pattern is in good agreement with the observed flow pattern. Figure 11-44 is an enlarged view of the observed and simulated flow patterns in the curved section. The zone of the maximum velocity is at 5.19 m near the outside of the bend. The velocity distribution obtained from the two-dimensional simulation indicates higher velocities on the outside of the bend only develop at the very end of the curved section.

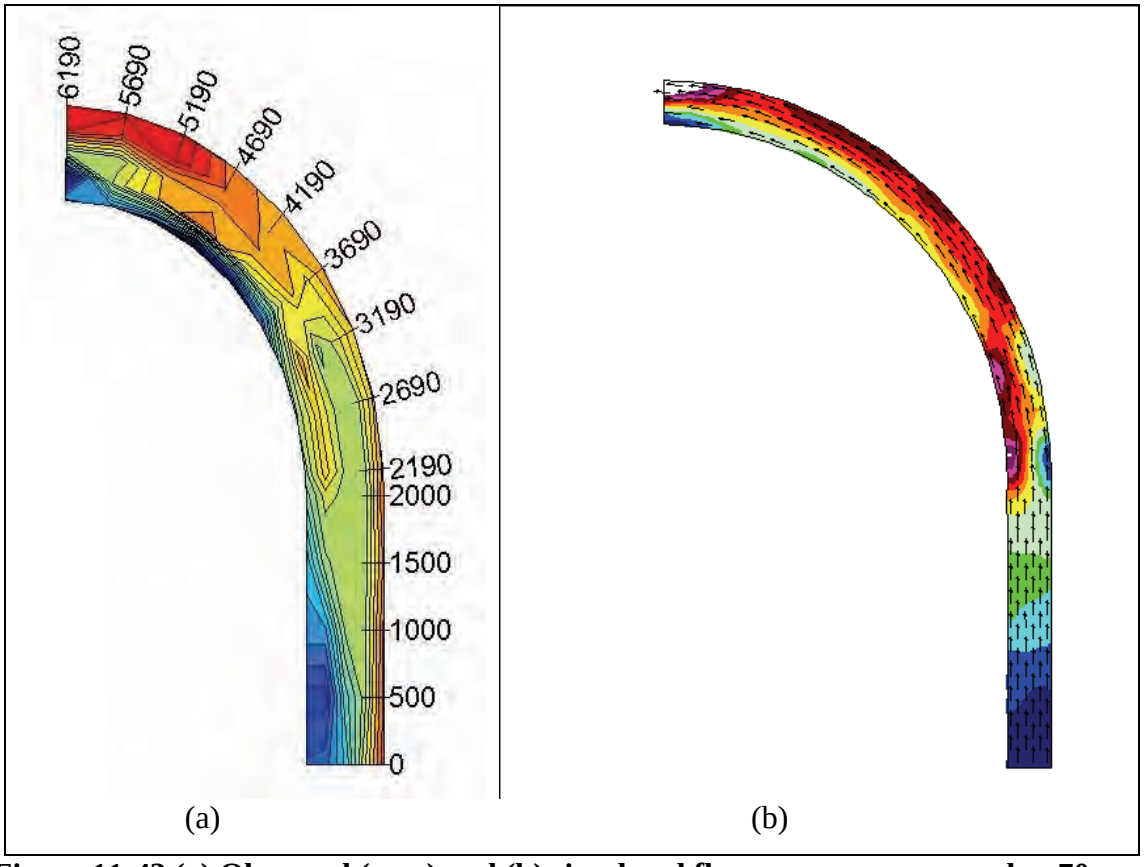

Figure 11-43 (a) Observed (n.t.s) and (b) simulated flow patterns measured at 70 mm above the bed (r_c/w =8.5 ,fr =0.5) (For legend refer to Figure 11-44)

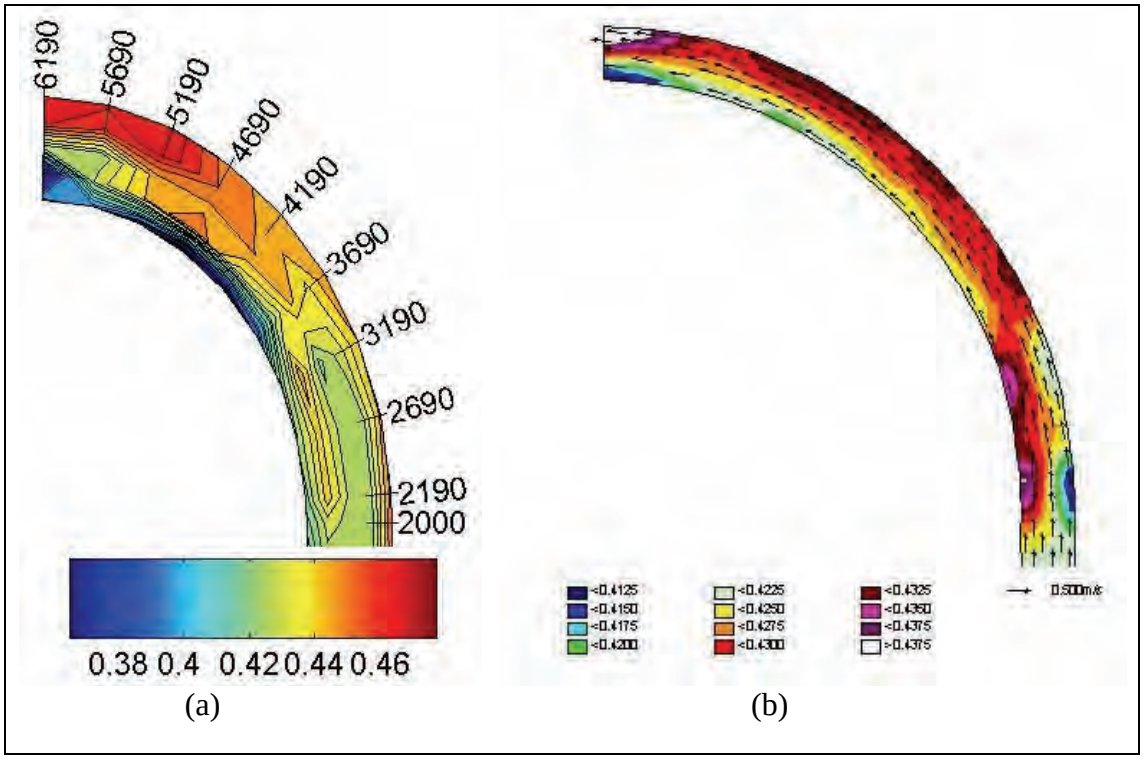

Figure 11-44 Enlarged view of the observed (a) and simulated (b) flow patterns in the curved section measured at 70 mm above the bed (r_c/w =8.5 ,fr =0.5)

The simulated water levels are also in good agreement with the observed water levels. The super elevation of the water level on the outside of the bend is more evident in the case of the three dimensional simulation than for the two dimensional simulation.

In summary, it was found that the three-dimensional hydrodynamic model simulations result in a velocity distribution and simulated water levels that are in good agreement with those obtained from the laboratory experiments. The simulations with a Froude number of 0.3 and 0.5 were also in better agreement with the laboratory results than the simulation with a Froude number of 0.1.

11.6.2 MODELLING OF SEDIMENT DYNAMICS

A curvilinear grid that resembles a flow net of the river was set-up and at each of the nodes of this grid a value is then assigned, usually representing height. In other words the bathymetry of a river can be accurately incorporated. The grid was set-up to represent the points where the sediment levels were measured.

Several other parameters can be adjusted in the model of which some are more important than others. Some of the more important parameters include discharge into the channel, water depth at the end of the channel, eddy viscosity, resistance (Chezy or Manning) and sediment grain size, among many others. Those mentioned parameters were seen to have the greatest effect on the simulations.

Initial simulation problems were remedied by the addition of a straight section downstream of the sluice gate. The addition of the straight section acted in some way as a sluice gate that allowed the water levels to be simulated more accurately, that in return produced results that are in good agreement with the measured sediment levels of the laboratory experiment.

Figure 11-45 (a) shows the measured sediment bed level changes with (b) being the simulated sediment level changes for Test A5 with r_c/w=8.5 and fr=0.3. In general the simulation is in good agreement with the measured sediment levels with the centre of the scour zone corresponding along the outside of the bend. However, the simulated sediment levels indicate a much smaller scour zone in comparison with the measured bed profile and earlier deposition is noted on the inside of the bend. A possible reason for this difference may be due to Engelund and Fredsoe sediment transport formula that was selected for the simulations and due to the fact that the sediment transport formula was not calibrated on the measured data from the laboratory.

It can be concluded that the three-dimensional hydrodynamics of the channel can be well-imitated with the two-dimensional depth averaged model (2DH) as well as the sediment dynamics of the curved section. Therefore this model can be applied with greater reliability in field conditions. The advantages of the 2DH model to simulate field conditions lies in the significantly shorter simulation times for the often large models especially if a long term analysis is carried out that is longer than 6 months with rivers being longer than say 10 km.

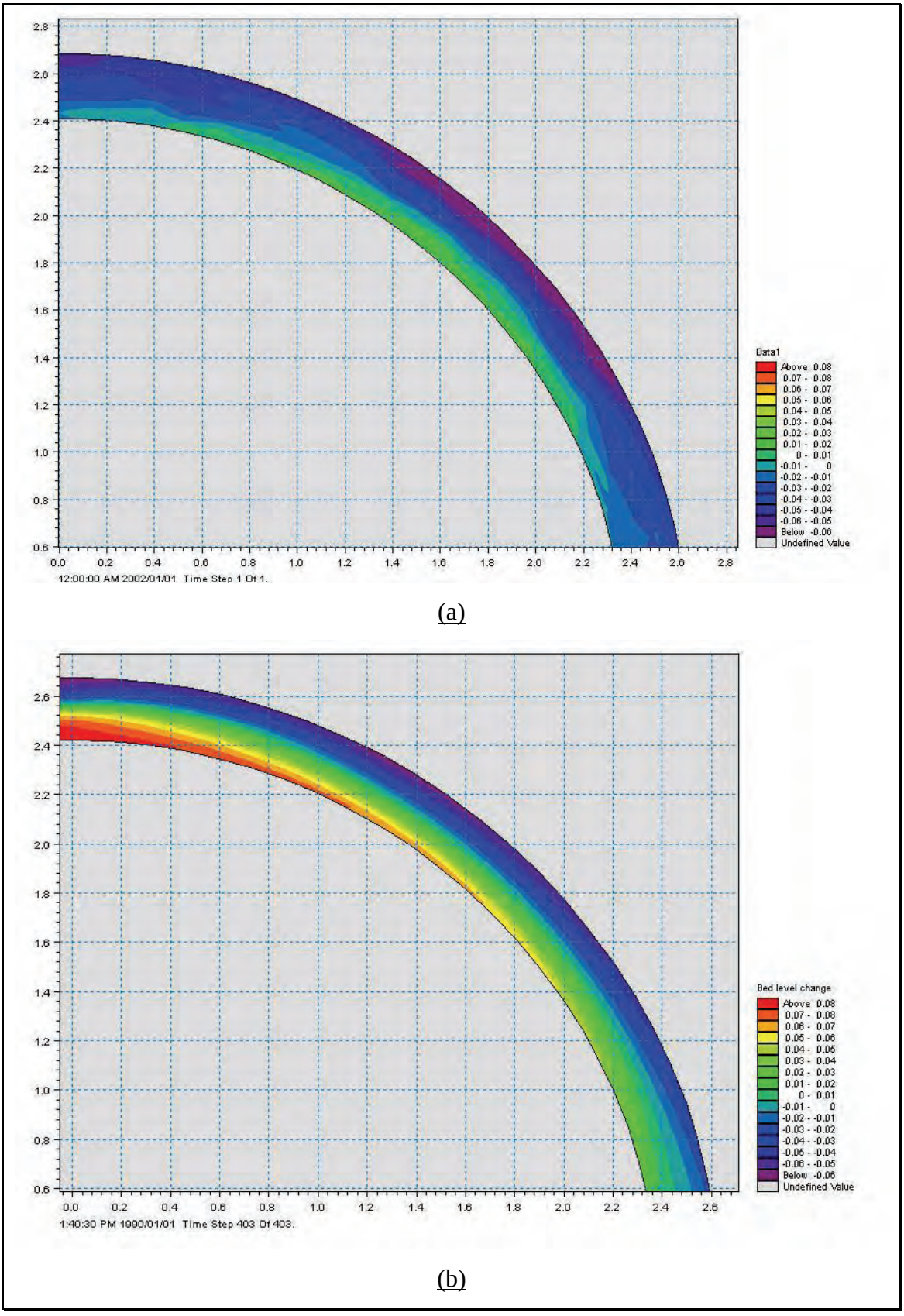

Figure 11-45 (a) Measured and (b) Simulated sediment bed level changes (r_c/w=8.5, fr=0.3)

12 CONCLUSIONS

The semi-arid conditions in South Africa create highly variable flows and sediment load variations are large, which makes the design of river diversion works very complex. Furthermore the sediment transported during floods is relatively fine and the sediment concentrations high. Methods developed in Western Europe for example to control sediment extraction are less effective in South Africa due to the different climatic conditions and sediment characteristics.

A review of various diversion control measures to limit sediment diversion was carried out. Most international diversion layouts focus on river bend flow to exclude coarse sediment. Several South African case studies were also reviewed and the conclusion was made that allowance has to be made in the design of control measures for fine sediment entering the diversion. This can be done by using canals that can be flushed through gates under gravity, by selecting pumps that can handle solids and/or by using a sand-silt trap or settler.

The hydraulics of secondary flow currents at a river bend that creates a deep scour hole at the outside of the bend was investigated in this study to determine the best location of diversion works to limit sediment diversion. Laboratory tests of a 0.3 m wide and a 0.6 m wide rectangular channel, with various radii, flows and flow depths, and with movable bed conditions, were carried out. These test results were analysed and also used for mathematical model (3D and 2D) calibration, in order to apply the model for river simulations with more confidence. The movable bed conditions observed in the laboratory could be simulated accurately by moving the mathematic model boundary further downstream so that it does not interfere with the bend hydraulics. The three-dimensional simulation of the DELFT 3D mathematical model provided good simulations of the laboratory experiments (see Figure 12-1). The simulations of the sediment dynamics with Mike21C (2DH) provided results that are in good agreement with the measured sediment levels (see Figure 12-2).

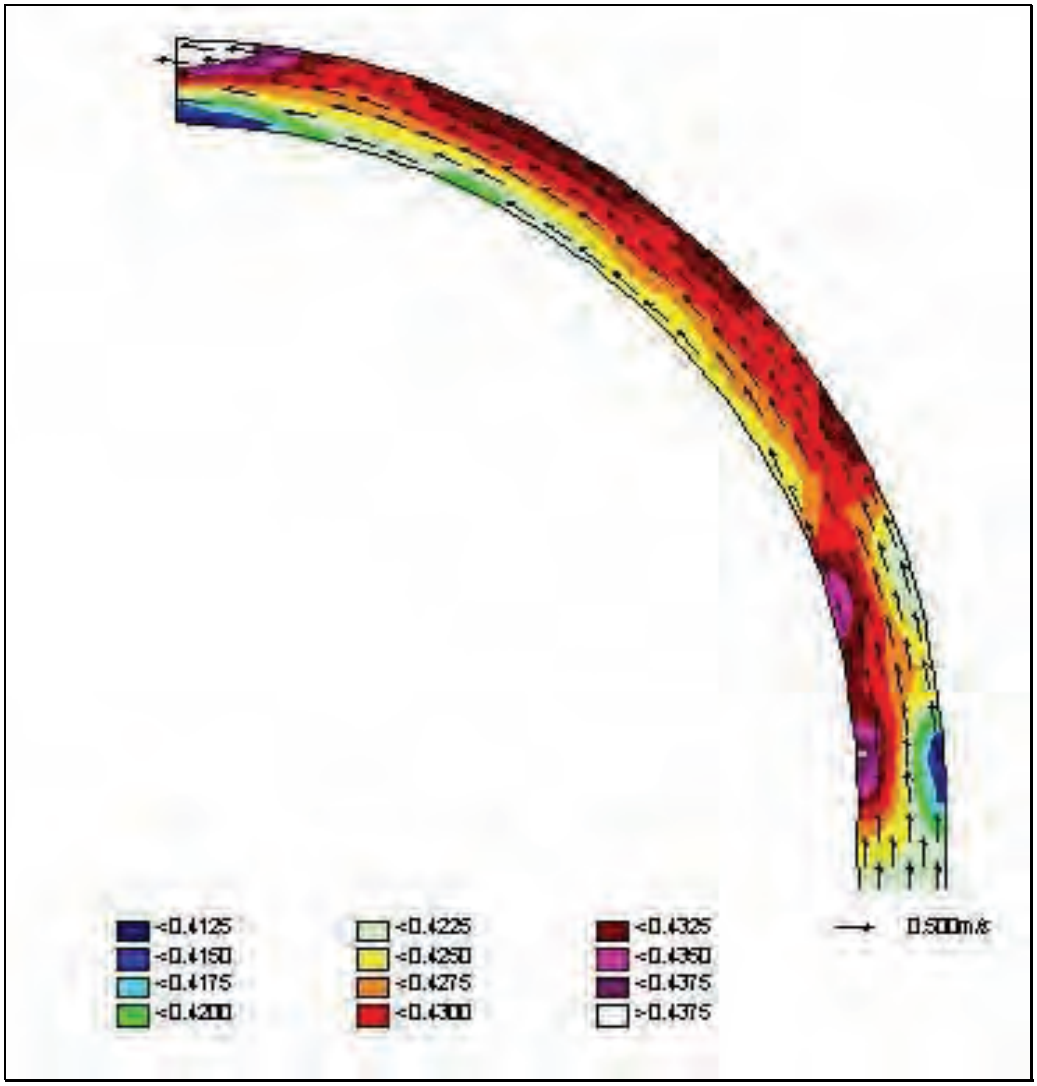

Figure 12-1 Simulated flow pattern in the curved section

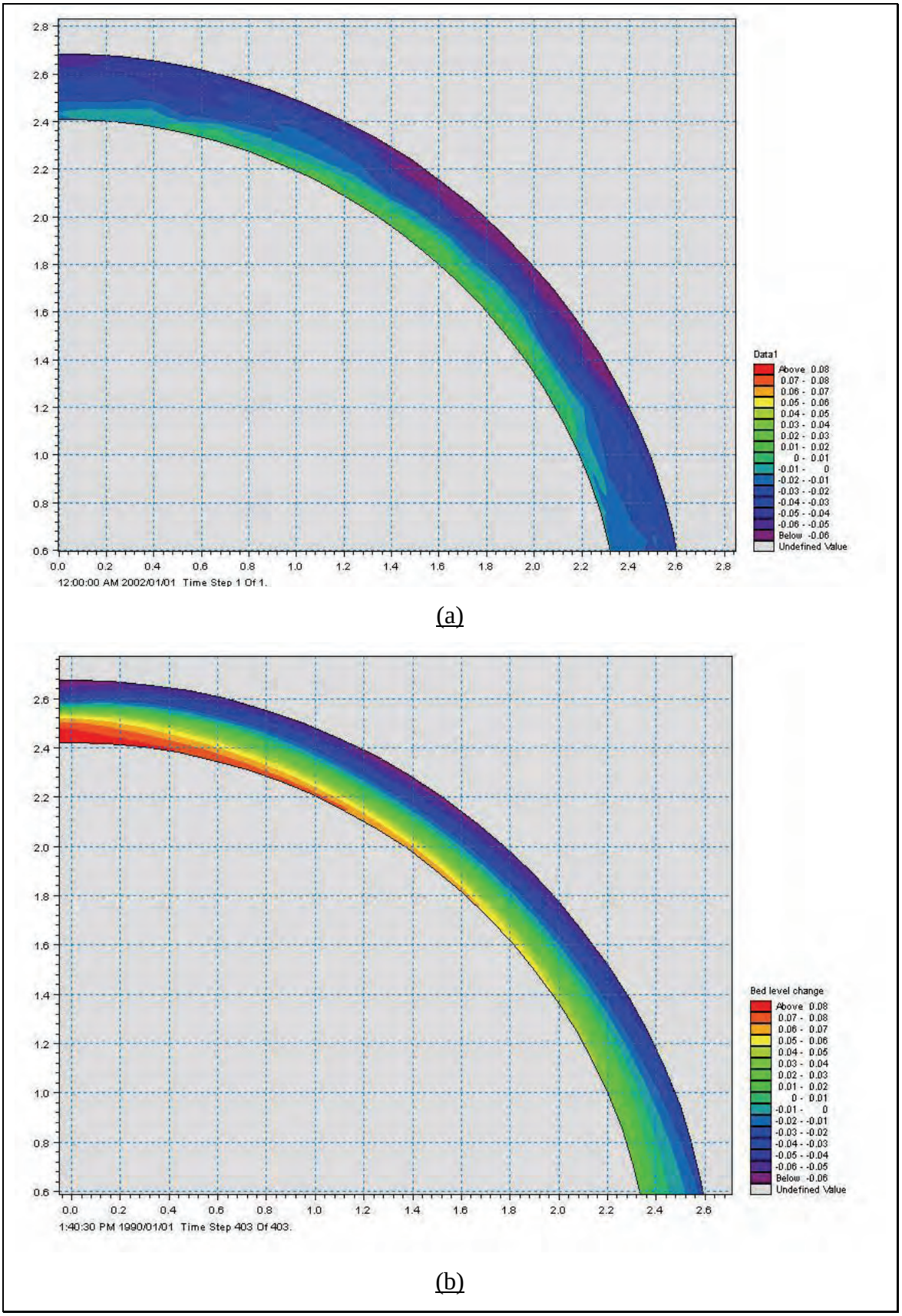

Figure 12-2 (a) Measured and (b) Simulated sediment bed level changes (m)

It is well-evident that the diverted discharge ratio (DDR) increases with an increase in the diversion angle while it decreases with an increase in Froude number. The velocity distribution obtained with a Froude number of 0.3 and 0.5 is also more favourable than those obtained with a Froude number of 0.1 since the bend effect is more prominent. This is in agreement with *Avery (1989)* who suggested a Froude number of 0.5-0.8 in the main curved channel. An important conclusion from the tests is that the diversion does not influence the secondary flow patterns (for the range of DDR's tested) and that the maximum velocity zone stayed in the same location as in the tests without a diversion.

In summary, the recommended approach to determine the optimum diversion location is by applying Table 8-1 (*SC and CHES, 1992)* which is applicable on a wide range of hydraulic conditions. The two-dimensional depth averaged model (2DH) can be used with great reliability to simulate the hydrodynamics of the channel as well as to predict scour patterns in the curved section. The results from these simulations are in good agreement with the data obtained from the laboratory experiments.

The optimum diversion location was determined in a laboratory canal by assessing the location of the maximum measured velocity.

The velocity distributions obtained from the measured data can be summarised as follows:

In the horizontal plane a fairly uniform velocity distribution is obtained in the first part of the straight section. Towards the end of the straight section the maximum velocity moves slightly towards the inside of the bend. The maximum velocity then gradually shifts towards the outside of the bend and reaches the outside of the bend between 3.19 m and 3.69 m. Further downstream it remains near the outside of the bend up to the end of the measurements (see Figure 12-3). The horizontal velocity distribution as described above is in good agreement with that described by *Bridge and Jarvis (1982)* and *Bridge (1983).*

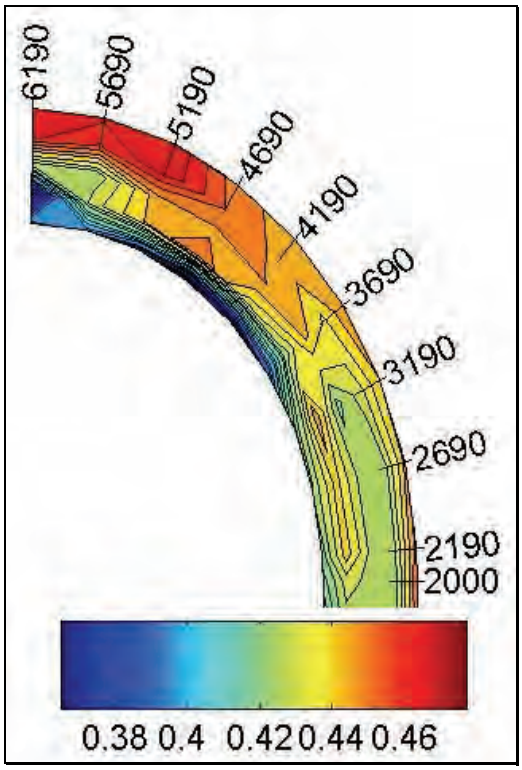

Figure 12-3 Flow pattern in the curved section (n.t.s)

In the vertical plane the general tendency is that the maximum velocity dives towards the bottom while moving towards the outside of the bend in the downstream direction. This is in good agreement with *Lee, Yu and Hsieh (1990)*. The vertical velocity distribution can be characterised by the following:

i) The measured velocity at 70 mm from the bottom (*V70*) has a decreasing tendency near the inside of the bend.

ii) In the centre of the bend all the measured velocities show an increasing tendency.

iii) Near the outside of the bend the measured velocity at 30 mm from the bottom (*V30*) shows an increasing tendency.

iv) The locations of the turning points where *V30>V50, V30>V70* and *V50>V70* stay relatively constant near the inside of the bend but move in the downstream direction with an increase in Froude numbers.

v) The locations of the turning points where *V30>V50, V30>V70* and *V50>V70* move downstream near the inside and outside of the bend with an increase in the radius of curvature ratio (r_c/w).

vi) The range of the location of the turning points increase on the inside and outside of the bend for an increase in the radius of curvature

The location of the maximum velocity was found to be relative constant with varying Froude number, whilst moving in the downstream direction with an increase in the radius of curvature-to-width ratio (r_c/w).

Mathematical model simulations of river bends with 20 m and 70 m width trapezoidal channels, a bed slope of 1:333, range of steady flows, sediment sizes and different sinuosity of the channel were carried out.

The development of secondary flow can be predicted with equation 7-16 *(Raudkivi, 1993)* and equation 7-18 *(Rozovskii, 1961)* with a constant of 1.97. A radius of curvature-to-width ratio (r_c/w) smaller than 14.6 is required to ensure that the secondary flow can develop fully in a bend according to Figure 12-4 *(Raudkivi, 1993)*. From this figure it is noted that the secondary flow was not fully developed for the range of tests with r_c/w=15.2, applying the principles of *Raudkivi (1993).*

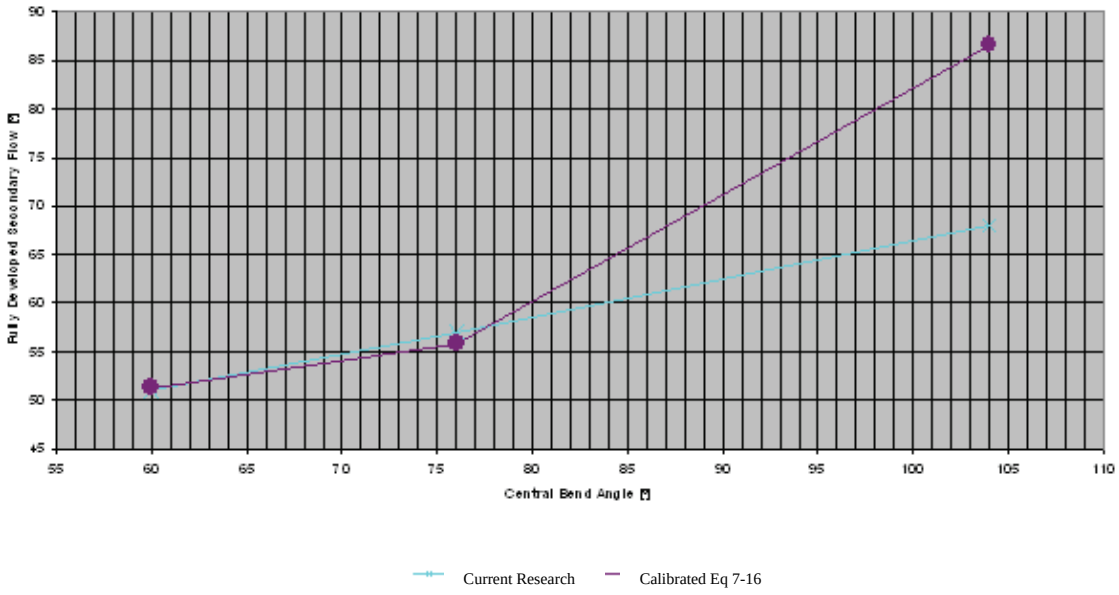

Figure 12-4 Fully developed secondary flow

The optimum diversion location from the current research is in good agreement with the recommended diversion location of Table 8-1 *(SC and CHES, 1992)* (see Figure 12-5). Applying Figure 8-4 *(Raudkivi, 1993)* to the data of the current research resulted in the diversion location being 8.8 times (not 2 as Raudkivi proposed) the width of the channel downstream of the intersection of the upstream axis with the outer bank. Equation 8-1 *(SC and CHES, 1992)* was calibrated on the data of the current research with a constant of 1.71.

The diversion location can also be predicted where the diversion location is expressed as a ratio of the diversion location and the central bend angle in relation to the radius of curvature-to-width ratio (r_c/w), as derived in this research.

It is recommended that Table 8-1 (*SC and CHES, 1992)* be used in predicting the optimum diversion location that covers a wide range of radius of curvature-to-width ratios (r_c/w) and hydraulic conditions. The empirical relationships by *SC and CHES (1992)* (Equation 8-1) and *Raudkivi (1993)* (Figure 8-3) were found to be only applicable on specific hydraulic conditions and cannot be applied generally. Wherever possible, however, physical or mathematical modelling should be carried out to position river abstraction works.

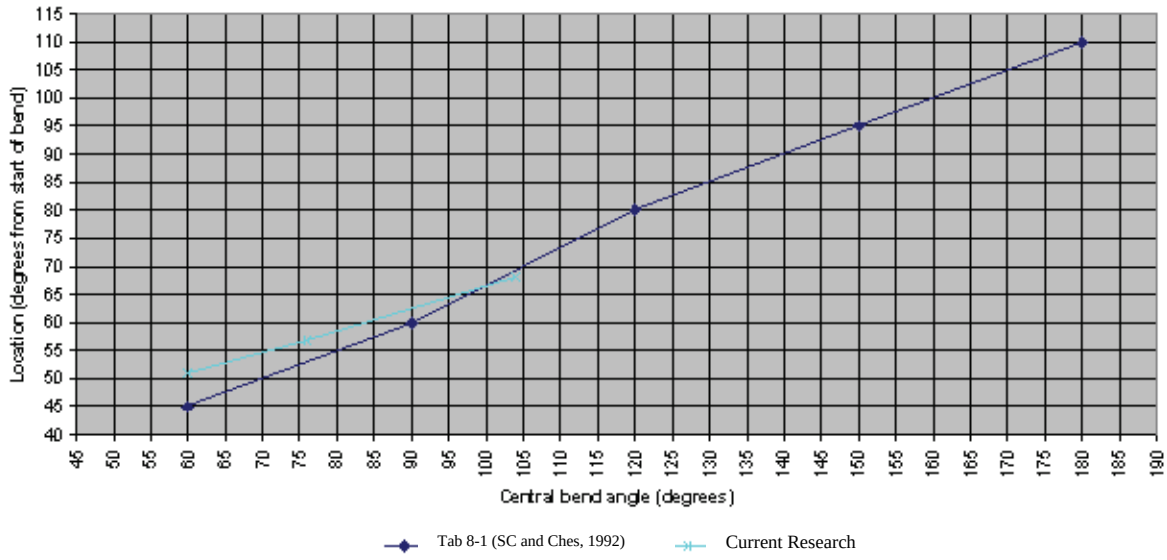

Figure 12-5 Relation between the optimum diversion location and the central bend angle

The results show that that with a wider channel the deepest scour hole forms further downstream. Higher sinuosity also created deeper scour holes.

Laboratory tests were also carried out on the orientation of the diversion works to induce spiral flow along the intake wall. Most of the scour was found at the downstream end of the wall and it was the deepest in the channel with the most sudden contraction, with the diversion wall forming a 45 degree angle with the flow. 2D mathematical model simulations of the movable bed in the flume was carried out with the scour hole position predicted accurately. Further simulations were carried out with a diversion positioned in a river bend and deep scour was found against the structure, but the diversion structure actually inhibits the full development of spiral flow and scour around the river bend.

Mathematical models can be used to determine river bend fluvial processes for the location of diversion works. It was found that empirical rules to determine the deepest scour hole position on a bend are not reliable.

Field tests were carried out at the Lebalelo pumpstation on the Olifants River during 2003. The gravel trap and pump canals were flushed and sediment concentrations recorded. The canals flushed quickly and effectively due to large gates and steep gradients in the canals. The sediment concentrations of flushed water was extremely high, but the duration very short.

A review of sand abstraction systems indicated that they often have a low yield (lower than the design and reducing with time), flood damage is a high risk, as is clogging of screens and pipes by biological fouling. When backwash systems are installed and operated on a daily basis, the performance of the systems are better than of systems that are not backwashed. Backwashing removes fine sediment and associated biological fouling. Backwash systems using air and water seem to be effective.

Guidelines for the design of river abstraction works to control sedimentation have been prepared as a separate document and gives practical guidance on several aspects such as: weir and energy dissipation design, flushing of canals, pump sump design, inclusion of fishways, etc.

13 RECOMMENDATIONS

It is recommended that the design of a river abstraction works is based on the design guidelines reviewed and developed in this study. The following are some of the key aspects to consider:

- Assess river stability from aerial photos.
- Consider low flow conditions and flood flows and the variability in sediment loads. The environmental flow requirement must be released downstream during low flow periods and the diversion must operate during floods.
- Locate the diversion on the outside curve of a river bend to limit coarse sediment diversion and to scour a deep pool at the intake during floods, which should still be present during low flow periods.
- Use a mathematical model or physical hydraulic model to simulate the sediment dynamics to select the best position and orientation of the diversion at important abstraction works.
- Fine sediment will enter the diversion, therefore allow for flushing under gravity back to the river. Even the pump canals can be flushed.
- A gravel trap should be provided upstream of the pump/diversion canals.
- Robust pumps, preferably submersible, should be selected to handle the coarse sediments.

The following aspect could be researched in future:

- The ecological impact of sediment flushing from the abstraction works with field measurements

14 REFERENCES

Ahmad, M. (1973). Cited in Vanoni

Apmann, R.P. (1972). Cited in Nwachukwu, B.A. (1973).

Avery, P. (ed.) (1982). The problems of sedimentation modelling with particular reference to river intake models. Int. Conf. On the Hydraulic Modelling of Civil Engineering Structures, Coventry, England, pp. 167-180.

Avery, P. (1989). Sediment control at intakes – a design guide. BHRA (The Fluid Engineering Centre), England.

Bagnold, R.A. (1960). Cited in Vanoni

Bathurst, J.C. (1979). Secondary flow and shear stress at river bends. Journ. of the Hydr Proc ASCE (New York). Vol 105, No 10, pp. 1277 – 1295.

Blench, T. (1969). Mobile-Bed Fluviology. The University of Alberta Press, Canada

Bosman, D.E. et al, (2003). An investigation into the removal of sediments from water intakes on rivers by means of jet-type dredge pumps. WRC Report No. 1187/1/02.

Bouvard, M. (1992). Mobile Barrages and Intakes on Sediment Transporting Rivers. A.A. Balkema, Brookfield.

Bridge, I.S and Jarvis, J. (1982). Cited in Lee, H.Y. and Ho, H.Y. (1988).

Bridge, J.S. (1977). Cited in Bridge (1983).

Bridge, J.S. (1983). Flow and Sedimentary Processes in River Bends: Comparison of Field Observations and Theory. Proc. Conf.on River Meandering, New Orleans, New York, pp.857-872.

Bridge, J.S. and Jarvis, J. (1982). The dynamics of a river bend: a study of flow and sedimentary processes. Sedimentology (Amsterdam). Vol. 29, No 4, pp. 499 – 541.

Bulle, H. (1926). Cited in Hufferd, J.A., Watkins, J.S. (1972)

Cecen, M.K. (1988). Reduction of Sediment Entrainment: Its Trapping and Flushing. Water Resources Publications, USA, Littleton, pp. 398-425. (Mahmood editor)

Chang, H.C. (1983). Energy expenditure in curved open channels. Journ. of Hydr.

Eng, Vol 109, No 7, pp. 1012 – 1022.

Chatley, H. (1931). Cited in Nwachukwu, B.A. (1973).

Chen, G.X. and Shen, H.W. (1983). River Curvature-Width Ratio Effect on Shear Stress. Proc. Conf.on River Meandering, New Orleans, New York, pp.687-699.

Chien et al. (1987). Cited in Lee, H.Y., Yu, W.S. and Hsieh, K.C. (1990).

Choudhary, U.K. and Narasimhan, D. (1977). Flow in 180 Degrees Open Channel Rigid Boundary Bends. Journal of the Hydr Proc ASCE (New York), Vol 103, No 6, pp 651 – 657.

Chow, V.T. (1959). Open-channel hydraulics, McGraw-Hill Book Co. INC, London.

Christian, H.E. (1988). Streambank Erosion and Bank Stabilization. Reduction of Sediment Entrainment: Its Trapping and Flushing. Water Resources Publications, USA, Littleton, pp. 450-471. (Mahmood editor)

DHI. (2003). MIKE 21C Reference Manual.

De Vriend, H.J. and Struiksma, N. (1983). Flow and Bed Deformation in River Bends. Proc. Conf.on River Meandering, New Orleans, New York, pp.810-828.

Featherston, R.E. and Nalluri, C. (1995). Civil Engineering Hydraulics, Blackwell Science, London.

Francis, J.R.D and Asfari, A.F. (1971). Cited in Chen, G.X. and Shen, H.W. (1983).

friedkin (1945). Cited in Shen

Habermaas, F. (1935). Cited in Shen

Henderson, F.M. (1967). Open Channel Flow. The Macmillan Company, New York.

Hufferd, J.A., Watkins, J.S. (1972a). Chapter V: Sediment Control Methods: C. Control of sediment in Canals. Am. Soc. Civ Engrs Task Committee for the Preparation of the Manual of Sedimentation, USA, New York.

Hussein, A.S.A and Smith, K.V.H. (1986). Flow and bed deviation angle in curved open channels. Journ. of Hydr. Res. (Delft; Netherlands). Vol. 24, No. 2, pp. 93 – 108.

Jackson, R.G. (1975). Cited in Chen, G.X. and Shen, H.W. (1983).

Joglekar, D.V., Gotankar, S.T. and Kulkarni, P.K. (1951). Cited in Hufferd, J.A., Watkins, J.S. (1972).

Kalkwijk, J.P. and De Vriend, H.J. (1980). Computation of the flow in shallow river bends. Journ. of Hydr. Research. Vol 18, No. 4, pp. 327 – 342.

Khalid, S.A. (1964). Cited in Chen, G.X. and Shen, H.W. (1983).

Lacey (1929). Cited in Raudkivi

Lacey (1930). Cited in Nwachukwu, B.A. (1973).

Lane, E.W. (1955). Cited in Shen

Lee and Yu (1990). Cited in Lee, H.Y., Yu, W.S. and Hsieh, K.C. (1990).

Lee, H.Y., Yu, W.S. and Hsieh, K.C. (1990). Flow Characteristics of Sand-Silt River Bend. Int. conf. of Physical Modelling of Transport and Dispersion, Massachusetts, USA, pp.11B.19-11B.24.

Leliavsky, S. (1965). Irrigation Engineering: Syphons, Weirs and Locks. Chapman and Hall Ltd, London

Liu, X. et al. (1982). Cited in Tan, Y

Mandouh, A.N. and Townsend, R.D. (1979). Shear-stress distributions in stable channel bends. Journ. of the Hydr Proc ASCE (New York). Vol 105, No 10, pp. 1233 – 1245.

Minikin, R.C.R. (1920). Practical River and Canal Engineering. Bedford Court Mansions, London

Mosoyi, E. (1965). Cited in Shen

Muller, R. (1955). Cited in Cecen

Müller, R. (1943). Theorecische frundlagen der Fluss- und Wildbachverbauungen (Theoretical principles for regulation of rivers and torrents). Eidgenössische Technische Hochschule, Zürich, Mitteilungen der Versuchsanstalt für Wasserbau und Erdbau, no.4.

Nelson, J.M. and Smith, J.D. (1989). Cited in Yalin

Nwachukwu, B.A. (1973). Laboratory Study of Scour at Channel Bends. Proc. of First Canadian Hydraulics Conf, Edmonton, Canada, pp.144-164.

Odgaard, A.J. (1986). Cited in Baird, D.C. and Achterberg, D.C. (1989).

Okoye, K.G. (1989). Mean Flow Structure in Model Alluvial Channel Bends. Proc. of Tech. Session B: Fluvial Hydraulic, IAHR 23rd Congress, Ottawa, pp.B-81–B-90.

Raudkivi, A.J. (1993). Sedimentation: Exclusion and removal of sediment from diverted water. A.A. Balkema, Brookfield.

Ripley, H.C. (1927). Relation of depth to curvature of channels. Transactions, ASCE, vol.90, pp.207-238.

Rooseboom, A.R. (1992). Sediment transport in rivers and reservoirs. Water Research Commission Report.

Rooseboom, A.R. and Mülke. (1982).

Rouse, H. (1950). Cited in Varshney, D.V. (1977).

Rouse. H. (1937). Engineering Hydraulics. John Wiley & Sons, New York, 707p.

Rozovskii, I.L. (1957). Cited in Shen

Rozovskii, I.L. (1961). Cited in Chang, H.C. (1983).

Rozovskii, J.L. (1962). Cited in Yalin

Rozovski, I.L. (1963). Cited in Bathurst, J.C. (1979).

Rzhanitsyn, N.A. (1960). Cited in Shen

SC (Sediment Committee) and CHES. (1992). Sedimentation Handbook. Environment Science Press, Beijing (in Chinese)

Scheurelin, H. (1984). Die Wasserentnahme aus geschiebeführenden Flüssen, Ernst and Sohn, Berlin, Germany. (In German)

Sharma,H.D.,Varshney, D.V. and Tiagi, S.S. (1973). Cited in Varshney, D.V. (1977).

Shen, H.W. (1971). River Mechanichs: Volume 2, Shen, USA

Shukry, A. (1950). Cited in Chow

Simons, D.B. (1971). Cited in Baird, D.C. and Achterberg, D.C. (1989).

Snell, E.F.A. (1994). The Design of River Intakes to minimise Abstraction of Sediment. Proc. Conf. Fifty Years of Water Engineering in South Africa. A Tribute to Prof Des Midgley, Johannesburg, South Africa, pp.467-500.

Tan, Y. (1996). Design of silt related hydraulic structures, Int conf on Reservoir Sedimentation

Thompson, J. (1876). [Cited in Vanoni]

Thorn and Hey (1979). Cited in Bridge, J.S. and Jarvis, J. (1982).

Tyagi, A.K. (1967). Cited in Varshney, D.V. (1977).

United States Bureau of Reclamation (1959). Cited in Vanoni

Vanoni, V.A. (1977). Sedimentation Engineering. Am. Soc. Civ Engrs Task Committee for the Preparation of the Manual of Sedimentation, USA, New York.

Varshney, D.V. (1977). Scour around Bends in Alluvial Channels. Journ. of the Institution of Engineering (India). Vol 58, No CI2 & CI3, pp.91 – 98.

Varshney, D.V. and Garde, R.J. (1975). Cited in Chen, G.X. and Shen, H.W. (1983).

WL Delft Hydraulics. (2003). Delft 3 User Manual.

Walton. (1963).

Yalin, M.S. (1992). River Mechanics. Pergamon Press, New York

Yen, B.C. (1965). Cited in Varshney, D.V. (1977).

Yen, C and Lee, K. T. (1995). Bed topography and sediment sorting in channel bend with unsteady flow. Journ. of Hydr. Eng. Vol. 121, No. 8, pp. 591 – 599.